FINAL REPORT ~ FHWA-OK-20-06

EVALUATING THE PERFORMANCE OF EXISTING REINFORCEMENT FOR OKLAHOMA BRIDGES

David Darwin, Ph.D., P.E.
Matthew O'Reilly, Ph.D., P.E.
Pooya Vosough Grayli, Ph.D. Candidate

Department of Civil, Environmental & Architectural Engineering
The University of Kansas
Lawrence, Kansas

Julie Ann Hartell, Ph.D.

Department of Construction Science
Texas A&M University
College Station, Texas

November 2020

OKLAHOMA
Transportation

The Oklahoma Department of Transportation (ODOT) ensures that no person or groups of persons shall, on the grounds of race, color, sex, religion, national origin, age, disability, retaliation or genetic information, be excluded from participation in, be denied the benefits of, or be otherwise subjected to discrimination under any and all programs, services, or activities administered by ODOT, its recipients, sub-recipients, and contractors. To request an accommodation please contact the ADA Coordinator at 405-521-4140 or the Oklahoma Relay Service at 1-800-722-0353. If you have any ADA or Title VI questions email ODOT-ada-titlevi@odot.org.

EVALUATING THE PERFORMANCE OF EXISTING REINFORCEMENT FOR OKLAHOMA BRIDGES

FINAL REPORT ~ FHWA-OK-20-06
ODOT SP&R ITEM NUMBER 2281

Submitted to:
Office of Research and Implementation
Oklahoma Department of Transportation

Submitted by:
David Darwin, Ph.D., P.E.
Matthew O'Reilly, Ph.D., P.E.
Pooya Vosough Grayli, Ph.D. Candidate
Department of Civil, Environmental & Architectural Engineering
The University of Kansas

Julie Ann Hartell, Ph.D.
Department of Construction Science
Texas A&M University

November 2020

TECHNICAL REPORT DOCUMENTATION PAGE

1. REPORT NO. FHWA-OK-20-06	2. GOVERNMENT ACCESSION NO.	3. RECIPIENT'S CATALOG NO.
4. TITLE AND SUBTITLE EVALUATING THE PERFORMANCE OF EXISTING REINFORCEMENT FOR OKLAHOMA BRIDGES		5. REPORT DATE Nov 2020
		6. PERFORMING ORGANIZATION CODE
7. AUTHOR(S) David Darwin, Matthew O'Reilly, Pooya Vosough Grayli, and Julie Ann Hartell		8. PERFORMING ORGANIZATION REPORT SM Report No. 146
9. PERFORMING ORGANIZATION NAME AND ADDRESS University of Kansas Center for Research, Inc. 2585 Irving Hill Road Lawrence, Kansas 66045-7563		10. WORK UNIT NO.
		11. CONTRACT OR GRANT NO. ODOT SPR Item Number 2281
12. SPONSORING AGENCY NAME AND ADDRESS Oklahoma Department of Transportation Office of Research and Implementation 200 N.E. 21st Street, Room G18 Oklahoma City, OK 73105		13. TYPE OF REPORT AND PERIOD COVERED Final Report Oct 2017 - Oct 2020
		14. SPONSORING AGENCY CODE

15. SUPPLEMENTARY NOTES
Click here to enter text.

16. ABSTRACT

This study evaluated the corrosion resistance of conventional, epoxy-coated, galvanized ASTM A767 and A1094 reinforcement, and ASTM A1035 reinforcement using the rapid macrocell, Southern Exposure, and cracked beam tests. Coated bars were evaluated with coatings in both an undamaged condition and with damage simulating that which would occur during handling and placing. Selected epoxy-coated bars were exposed to an accelerated weathering program under ultraviolet light, simulating outdoor exposure. Galvanized reinforcement is evaluated after bending, was well as straight. Two waterproofing admixtures, Ipanex and Xypex, were also evaluated. Field observations of an in-service bridge deck on I-35 over Chikaskia River containing A1035 reinforcement with Ipanex were conducted, and deck panels containing conventional and epoxy-coated reinforcement from a bridge on I -35 over Cow Creek were evaluated. Costs over a 100-year design life were estimated for all systems studied.

ECR exhibited much greater corrosion resistance than conventional reinforcement, even after simulating damage from handling and placing; however, simulated UV exposure equivalent to as low of 1.2 months of exposure significantly reduced the effectiveness of the coating. Both A767 and A1094 reinforcement exhibited better corrosion resistance than conventional reinforcement as well, but corrosion rates on both types of galvanized reinforcement increased when the bars were bent. Xypex was effective at reducing the corrosion rate of conventional reinforcement, but not A1035 reinforcement; Ipanex had no effect on either type of reinforcement. Over a 100-year design life, ECR, galvanized reinforcement, and A1035 reinforcement are all cost-effective solutions.

17. KEY WORDS	18. DISTRIBUTION STATEMENT		
Concrete, chlorides, corrosion, epoxy-coated reinforcement, galvanized reinforcement	No restrictions. This publication is available from the Office of Research and Implementation, Oklahoma DOT.		
19. SECURITY CLASSIF. (OF THIS REPORT) Unclassified	20. SECURITY CLASSIF. (OF THIS PAGE) Unclassified	21. NO. OF PAGES 194	22. PRICE N/A

Form DOT F 1700.7 (08/72)

SI* (MODERN METRIC) CONVERSION FACTORS

APPROXIMATE CONVERSIONS TO SI UNITS

SYMBOL	WHEN YOU KNOW	MULTIPLY BY	TO FIND	SYMBOL
		LENGTH		
in	inches	25.4	millimeters	mm
ft	feet	0.305	meters	m
yd	yards	0.914	meters	m
mi	miles	1.61	kilometers	km
		AREA		
in^2	square inches	645.2	square millimeters	mm^2
ft^2	square feet	0.093	square meters	m^2
yd^2	square yard	0.836	square meters	m^2
ac	acres	0.405	hectares	ha
mi^2	square miles	2.59	square kilometers	km^2
		VOLUME		
fl oz	fluid ounces	29.57	milliliters	mL
gal	gallons	3.785	liters	L
ft^3	cubic feet	0.028	cubic meters	m^3
yd^3	cubic yards	0.765	cubic meters	m^3
		NOTE: volumes greater than 1000 L shall be shown in m^3		
		MASS		
oz	ounces	28.35	grams	g
lb	pounds	0.454	kilograms	kg
T	short tons (2000 lb)	0.907	megagrams (or "metric ton")	Mg (or "t")
		TEMPERATURE (exact degrees)		
°F	Fahrenheit	5 (F-32)/9 or (F-32)/1.8	Celsius	°C
		ILLUMINATION		
fc	foot-candles	10.76	lux	lx
fl	foot-Lamberts	3.426	candela/m^2	cd/m^2
		FORCE and PRESSURE or STRESS		
lbf	poundforce	4.45	newtons	N
lbf/in^2	poundforce per square inch	6.89	kilopascals	kPa

APPROXIMATE CONVERSIONS FROM SI UNITS

SYMBOL	WHEN YOU KNOW	MULTIPLY BY	TO FIND	SYMBOL
		LENGTH		
mm	millimeters	0.039	inches	in
m	meters	3.28	feet	ft
m	meters	1.09	yards	yd
km	kilometers	0.621	miles	mi
		AREA		
mm^2	square millimeters	0.0016	square inches	in^2
m^2	square meters	10.764	square feet	ft^2
m^2	square meters	1.195	square yards	yd^2
ha	hectares	2.47	acres	ac
km^2	square kilometers	0.386	square miles	mi^2
		VOLUME		
mL	milliliters	0.034	fluid ounces	fl oz
L	liters	0.264	gallons	gal
m^3	cubic meters	35.314	cubic feet	ft^3
m^3	cubic meters	1.307	cubic yards	yd^3
		MASS		
g	grams	0.035	ounces	oz
kg	kilograms	2.202	pounds	lb
Mg (or "t")	megagrams (or "metric ton")	1.103	short tons (2000 lb)	T
		TEMPERATURE (exact degrees)		
°C	Celsius	1.8C+32	Fahrenheit	°F
		ILLUMINATION		
lx	lux	0.0929	foot-candles	fc
cd/m^2	candela/m^2	0.2919	foot-Lamberts	fl
		FORCE and PRESSURE or STRESS		
N	newtons	0.225	poundforce	lbf
kPa	kilopascals	0.145	poundforce per square inch	lbf/in^2

ACKNOWLEDGEMENTS:

This study was supported by the Oklahoma Department of Transportation (ODOT SP&R Item Number 2281). Additional material support was provided by Commercial Metals Company, the Concrete Reinforcing Steel Institute, Midwest Concrete Materials, Cement Chemistry Systems LP, and Xypex Chemical Corporation. Walter Peters, P.E. of ODOT provided data bridge construction costs in Oklahoma.

TABLE OF CONTENTS

LIST OF FIGURES

LIST OF TABLES

CHAPTER 1: INTRODUCTION

The ever-increasing use of deicing salts poses results in a constant threat to transportation infrastructure, particularly bridge deck components, due to corrosion of the reinforcing steel in concrete structures. For over forty years, the preferred method of corrosion protection of reinforced concrete bridge decks has been the use of epoxy-coated reinforcement (ECR). This system is not without its flaws, however; ECR is prone to damage from handling, construction, and exposure to the environment, and early failures of some structures with ECR have been documented. These shortcomings have led some state DOT's, such as Virginia and Florida, to abandon the use of ECR in favor of other corrosion protection systems, such as stainless steel, corrosion-inhibiting admixtures, and galvanized reinforcement. The majority of states, however, still use ECR due to its low initial cost and good performance in the overwhelming majority of structures. As more is learned about existing corrosion protection systems and new corrosion protection systems enter the market, there is a need to predict the design life and cost effectiveness of these systems to determine if ECR remains the most effective means of extending the life of bridge decks.

1.1 Objectives

The objectives of this study are as follows:

1) Evaluate the corrosion resistance of conventional, galvanized, ChromX, and epoxy-coated reinforcement in the lab.
   i) Compare the performance of continuous hot-dip galvanized reinforcement (ASTM A1094) with that of conventional galvanized reinforcement (A767)
   ii) Evaluate the performance of conventional and ChromX (A1035) reinforcement with and without the use of waterproofing admixtures (Ipanex and Xypex)
   iii) Evaluate the corrosion resistance of ECR after simulating unprotected outdoor exposure to ultraviolet (UV) light.
2) Conduct evaluations of field panels removed from the Cow Creek bridge on I-35 and the in-service bridge deck over the Chikaskia River, also on I-35.
3) Conduct a cost analysis for a 100-year design life for each of the systems in this study.

1.2 Previous Work

1.2.1 Corrosion Mechanisms in Concrete

The cost of corrosion has been a large and growing problem in the U.S. highway system for decades. Nearly 20 years ago, the direct annual cost of corrosion damage in bridges was estimated to be $8.3 billion (Koch et al. 2002), a number that has continued to grow. Indirect costs are estimated to be more than ten times this value (Koch et al. 2002). This cost justifies a significant investment in corrosion control, either by preventing or slowing the penetration of water, oxygen, carbon dioxide, and salt into the concrete or by using reinforcement that is more resistant to corrosion.

Conventional reinforcement in uncontaminated concrete will not corrode, because of the formation of a protective barrier, known as a passive layer, in the high-pH environment of concrete. This passive layer can be disrupted, however, as the result of carbonation of the concrete or chloride ingress. Carbonation disrupts formation of the passive layer on steel

reinforcing bars embedded in concrete by decreasing the pH of the concrete pore solution. A pH below 11.5 is generally regarded as the threshold for disruption of the passive layer on conventional reinforcing steel (Verbeck 1975, Poursaee 2016). Increased concrete quality and cover has resulted in carbonation becoming less of a threat on most bridge decks.

Chlorides can also break down the passive layer on reinforcing steel, even in highly-alkaline concrete, by reacting with iron in the passive layer to form a Fe-Cl complex. The Fe-Cl complex reacts with water to form ferric oxides (rust), releasing the chloride ions to react with other ferrous ions, a process which causes depletion of the passive layer. A minimum quantity of chlorides is required to attack the passive layer in this manner; this quantity is known as the critical chloride corrosion threshold, and it is dependent on the type of reinforcing steel as well as the pH of the surrounding concrete. Chloride-induced corrosion is the principal cause of corrosion in most bridge decks; in many cases, the critical chloride corrosion threshold for conventional reinforcement can be reached after the first winter (Lindquist et al. 2006).

The initiation of corrosion does not mark the end of the useable life for a bridge deck; rather, corrosion must continue for some time before repair or replacement is needed. The corrosion products of steel occupy several times the volume of the solid metal (Broomfield 2003). As a reinforcing bar corrodes, the corrosion products build up around the bar and induce tensile stresses in the surrounding concrete. When sufficient corrosion products have built up, the concrete over the bar cracks or spalls. The amount of corrosion required to crack the concrete depends on the reinforcing bar diameter, concrete cover, and extent of corrosion–localized corrosion requires far greater corrosion losses to crack concrete than generalized corrosion (Torres-Acosta and Sagues 2004, O'Reilly et al. 2011). The corrosion loss required to crack concrete is generally low, however; conventional reinforcement in a typical bridge deck only requires about 2 mils (50 μm) of corrosion loss to cause a crack to occur.

1.2.2 Corrosion Protection Systems

Corrosion protection systems aim to extend the life of reinforced concrete structures through one or more of the following mechanisms:

- Slowing the rate at which chlorides, water, and carbon dioxide penetrate through the concrete.
- Increasing the critical chloride corrosion threshold of the reinforcement.
- Slowing the corrosion rate after initiation of corrosion.
- Increasing the corrosion loss required to crack concrete.

Previous work on the corrosion protection systems in this study is summarized below.

1.2.2.1 Epoxy-Coated Reinforcement (ECR)

Epoxy-coated reinforcement (ECR) was first used in a bridge deck in the 1970's, and today is by far the most common corrosion-resistant reinforcement. Epoxy coatings provide a barrier to oxygen and moisture and protect the steel from chlorides, resulting in a relatively inexpensive and cost-effective corrosion protection system. ECR does require special handling, and the coating is prone to damage in the field, but even in the damaged state ECR exhibits corrosion losses two orders of magnitude less than that of conventional reinforcement. (Weyers, Pyc, and Sprinkel 1998, Draper et al. 2006, Darwin et al. 2011, O'Reilly et al. 2011, Poursaee 2016).

Although ECR has been successfully used in countless structures, some reports of poor performance exist. In the late 80's, cracking and spalling was observed five to seven years in bridge piers constructed in the Florida Keys using first generation epoxy-coated reinforcement. The ECR used in these bridges was of a much lower quality than what is currently available; that coupled with poor construction practices resulted in significant corrosion in four out of the five major bridges it was used in (Broomfield 2003, Poursaee 2016), leading Florida to discontinue the use of ECR. With modern coatings and good construction practices, the vast majority of states continue to use ECR with success.

Although significant research has been conducted on the effect of physical damage on the corrosion resistance of ECR, comparatively little research is available on the effect of ultraviolet (UV) light exposure. UV light is known to cause degradation of epoxies and other polymers (Cetiner et al. 2000, Kotnarowska 1999). UV exposure causes fading, strength loss, brittleness, and cracking of the material, and can reduce the ability of the epoxy coating ability to provide corrosion protection. Cetiner et al. (2000) exposed pipeline epoxy coatings (which are generally thicker and more durable than those used on reinforcement) to natural sunlight for up to two years and noted significant degradation of the coating after 15 months. Recent research by Kamde and Pillai (2020) evaluated epoxy-coated reinforcement in mortar after one month of UV exposure and concluded that UV exposure can decrease the design life of structures with epoxy-coated steel reinforcing bars by about 70%. Kamde and Pillai recommended that epoxy-coated steel reinforcing bars be exposed to sunlight no more than one month. Currently, ASTM A775 and ASTM D3963 require protection for ECR stored outdoors for longer than two months.

1.2.2.2 Galvanized Reinforcement

The use of galvanized reinforcement predates that of ECR. To date, however, it remains far less commonly used than epoxy coatings as a corrosion protection system. Galvanized (zinc) coatings can sacrificially protect steel reinforcing bars since zinc is thermodynamically more active than iron; the zinc coating also acts as a barrier to moisture and chlorides. Galvanized coatings are more damage resistant than ECR and continue to provide sacrificial protection to the underlying steel, even if damaged.

Hot-dip galvanizing, covered under ASTM A767, is the most common galvanizing method for reinforcing steel. The process involves immersing treated steel in a bath of molten zinc at a temperature of 440 °C to 460 °C, where metallurgical reactions occur between the steel and the zinc. The coating that remains on the steel after it cools has an external bright layer of pure zinc and internal layers of iron-zinc alloys linked to the base steel. These iron-zinc compounds are brittle and may crack in bending.

Studies of the corrosion performance of A767 reinforcing bars show mixed results, especially when highly alkaline pore solutions were used. Darwin et al. (2009) found that the average critical chloride corrosion threshold for A767 reinforcement was about 1.6 times the threshold of conventional steel, but that A767 reinforcement also exhibited a much larger range in performance, with some A767 specimens behaving similarly to conventional bars. A study by Treadaway et al. (1989) examined conventional and A767 reinforcement and found that slabs cast with galvanized reinforcement exhibited significantly more cracking than slabs cast with conventional steel. Other researchers have found that A767 reinforcement is effective in the presence of carbonation and may be used in structures exposed to carbonation or mild contamination with chlorides, such as cladding panels and coastal buildings (Andrade and

Macias 1988, Broomfield 2003, Darwin et al. 2009, Bertolini et al. 2013, Poursaee 2016).

An alternate method, known as continuous galvanizing, has recently been introduced and is covered under ASTM A1094. Continuous galvanizing produces a more flexible coating that is marketed as allowing the bars to be bent after fabrication without damaging the corrosion protection provided to the underlying steel. The coating on A1094 bars is mostly zinc and does not exhibit the intermetallic iron-zinc layers found on A767 reinforcement. Limited research on A1094 coatings is available. A recent study by Ogunsanya (2017) found that A767 bars showed lower corrosion rates than continuous galvanized bars; however, the continuous galvanized coating evaluated in the study was an early prototype version that exhibited poor quality control and uneven coating thickness.

The corrosion products of zinc are less expansive than that of iron, suggesting both A767 and A1094 reinforcement would require greater corrosion losses to crack concrete. O'Reilly et al. (2018) evaluated conventional and galvanized (A767) reinforcement in laboratory specimens with concrete cover ranging from 0.5 to 2 in. and found that A767 reinforcement required twice the corrosion loss to crack concrete compared to conventional reinforcement.

1.2.2.3 A1035 (ChromX) Reinforcement

ASTM A1035 microcomposite steel reinforcement is a chromium alloy reinforcing steel. MMFX Steel Corporation of America introduced this type of reinforcing steel bar, which comes in nominal chromium contents of ~2% (Type CL), ~4% (Type CM), or ~9% (Type CS), as a high strength reinforcement and a less expensive alternative to stainless steel. A1035 reinforcement typically exhibits higher yield strengths (100 and 120 ksi) than conventional reinforcement, and in some cases can offer cost savings relative to conventional reinforcement due to the need for reduced steel. The addition of chromium also increases the corrosion resistance of the steel. Prior studies by Ji, Darwin, and Browning (2005) found that the critical chloride corrosion threshold of A1035 reinforcement is approximately four times higher than that of conventional steel. Gong et al. (2002) and Darwin et al. (2002) found that A1035 reinforcement exhibits corrosion rates one-third to two-thirds those of conventional bars; however, they also noted A1035 reinforcement exhibited poorer corrosion resistance than damaged ECR. They did not recommend the use of A1035 reinforcement unless used along with a supplementary corrosion protection system.

Reinforcement spacing in bridge decks is typically governed by factors other than strength; therefore, the higher yield strength of A1035 reinforcement cannot be used to advantage. Nevertheless, A1035 reinforcement has been used in over 1000 bridge decks in 40 states, both alone and with corrosion inhibitors (see Section 1.2.2.4). To date, these decks are performing well, although the vast majority represent relatively new construction.

1.2.2.3 Corrosion Inhibiting and Waterproofing Admixtures

Many concrete admixtures have been developed with the aim of delaying corrosion initiation or slowing the corrosion rate after initiation. Some admixtures directly impact the corrosion process, either by strengthening the passive layer of the reinforcement or by binding with chlorides before they reach the reinforcement. These admixtures can be considered corrosion-inhibiting admixtures and include calcium nitrite and various organic inhibitors. Waterproofing admixtures, on the other hand, do not directly impact the chemistry of the corrosion process, but rather slow the rate at which moisture and chlorides migrate through the

concrete. This can indirectly delay the time to corrosion initiation as well as slow the corrosion rate after initiation.

Two waterproofing admixtures were examined as part of this study–Ipanex and Xypex. Ipanex is an inorganic admixture that gives the hydrated cement paste in concrete a finer microstructure (Cement Chemistry Systems 2016). Xypex reacts with byproducts of cement hydration to form non-soluble crystals in concrete pores in the presence of water (Xypex 2020). Both products claim to reduce the permeability and increase the durability of concrete over time- the manufacturers of Xypex, in particular, note that it can take several months for the crystals to form.

Overall, there are few studies evaluating the corrosion performance of Ipanex or Xypex, as their primary markets are well linings and similar unreinforced concrete applications. Hisey (2004) found that Ipanex did not have any effects on hardened concrete properties, nor did it have any significant effects on the corrosion performance of reinforcing bars in the concrete; the effect of Ipanex on the permeability of concrete was not evaluated. Another study conducted by the Iowa Department of Transportation found no significant benefits of the use of Ipanex on the permeability, chloride resistance, or strength of concrete (Engle 1999).

1.3 Scope

This study will achieve the objectives outlined in Section 1.1 by evaluating conventional, epoxy-coated, A767, A1094, and A1035 reinforcement in the laboratory tests described in Section 2.2. Field observations of an in-service bridge deck containing A1035 reinforcement with Ipanex were conducted, as described in Section 2.3, and deck panels containing conventional and epoxy-coated reinforcement from a bridge over Cow Creek were evaluated, as described in Section 2.4. The results from the laboratory data (Chapter 3) and prior field results are used to conduct a 100-year design life cost analysis in Chapter 4.

CHAPTER 2: EXPERIMENTAL WORK

This chapter describes the corrosion protection systems evaluated in this study and the materials and experimental methods used. The crack survey performed on an in-service bridge on I-35 over the Chikaskia River is described. The investigation and analysis of deck panels taken from a bridge over Cow Creek, one of the first decks constructed with epoxy-coated reinforcement in Oklahoma, is also discussed.

2.1 Materials

2.1.1 Reinforcement

Tests were performed on No. 5 ASTM A775 epoxy-coated reinforcement (ECR), ASTM A767 and A1094 galvanized bars, and ASTM A1035 Type CS bars with 9% chromium. Three heats of ASTM A615 conventional reinforcement were also evaluated. Identified as Conv. A, B, and C, the conventional bars were used to produce the ECR, A767, and A1094 reinforcing bars, respectively. Initial test results led to an expansion of the scope of work to further investigate the effect of UV exposure. As insufficient ECR remained from the original heat of steel, a second heat of epoxy-coated bars (ECR 2) was used for some of these additional macrocell tests. As delivered, some of the A767 bars had limited regions with poor or no coating, and exhibited exposed steel and surface rusting (Figure 2.1); these bars were discarded. The bars were, otherwise, in good condition. The steel chemistry of the bars used in this study is shown in Table 2.1.

Figure 2.1: Lack of coating and exposed steel on A767 reinforcement. Bars with damaged coatings are not used in tests.

Table 2.1: Steel Chemistry

Material	C%	Mn%	P%	S%	Si%	Cu%	Ni%	Cr%	V%	Mo%	Sn%	N_2%
Conv-A (ECR)	0.42	0.72	0.011	0.039	0.21	0.22	0.13	0.3	0.001	0.021	0.006	-
Conv-B (A767)*	-	-	-	-	-	-	-	-	-	-	-	-
Conv-A (A1094)*	-	-	-	-	-	-	-	-	-	-	-	-
ECR2	0.03	1.23	0.012	0.038	0.26	0.33	0.09	0.17	-	0.023	0.009	0.013
A1035 (ChrōmX)	0.09	0.59	0.012	0.017	0.39	0.18	0.09	9.36	0.019	0.02	0.008	0.01

*Data not provided

Most bars were evaluated in the as-received condition. Selected ECR bars were also exposed to UV exposure under Cycle 1 of ASTM G154, which consists of alternating cycles of 8 hours of UV exposure at an irradiance of 0.89 W/(m^2 × nm) and a temperature of 60 °C, followed by four hours of condensation (with no UV) at 50 °C. ECR was exposed to these cycles for between 100 and 1000 hours; 1000 hours of exposure under these conditions is regarded as equivalent to one year of unprotected outdoor exposure (Fedor and Brennan 2011). ASTM D3963 requires ECR to be protected from sunlight if left outdoors for longer than two months. Figure 2.2 shows ECR bars before and after 1000 hours of UV exposure. Significant discoloration of the coating is visible after exposure to UV.

All coated bars were evaluated without and with damage to the coating, the latter simulating the effects of handling and placement of concrete. A767 and A1094 bars were also evaluated after bending the bars 180°. Damage and bending procedures are described in Section 2.2.

Figure 2.2: ECR before (top) and after (bottom) UV exposure.

2.1.2 Concrete

The concrete mixture proportions used in this study are detailed in Table 2.2 and are representative of those typically used in bridge decks. The concrete has a 0.45 water-cement ratio, a target slump of 3 ± ½ in., a target air content of 6 ± 1%, and a target 28-day compressive strength of 4000 psi. Two waterproofing admixtures, Ipanex and Xypex, were also investigated as part of this study. For mixtures containing Ipanex and Xypex, the admixtures were added at a dosage of 75 oz/yd^3 and 6 lb/yd^3 respectively, following manufacturer's recommendations.

A total of fifteen batches of concrete were cast. Two of the batches contained Ipanex and another two contained Xypex. The remaining eleven batches were used to cast the specimens without inhibitor, with no more than one specimen with a given type or reinforcement per batch.

Table 2.2: Mixture proportions for lab and field specimens based on SSD aggregate

Cement lb/yd^3	Water lb/yd^3	Coarse Aggregate lb/yd^3	Fine Aggregate lb/yd^3	Air-Entraining Agent oz/yd^3
598	269	1484	1435	8.5-9.5

The materials used in the concrete mixtures were:

Cement – Type I/II Ash-grove portland cement.

Water – Municipal tap water from the city of Lawrence.

Fine Aggregate – Kansas River sand. Bulk specific gravity (SSD) = 2.62, absorption (dry) = 0.8%, fineness modulus = 2.51.

Coarse Aggregate – Crushed limestone from Midwest Concrete Materials. Nominal maximum size = 0.75 in. (19 mm), bulk specific gravity (SSD) = 2.58, absorption = 2.3%, unit weight = 95.9 lb/ft^3 (1534 kg/m^3).

Air-Entraining Agent – Daravair 1400, a saponified rosin-based air-entraining agent manufactured by W. R. Grace.

2.2 Test Methods

This section outlines the laboratory test methods used to evaluate the corrosion protection systems in this study. Three test methods were used; the rapid macrocell test, the Southern Exposure test, and the cracked beam test.

2.2.1 Rapid Macrocell Test

The rapid macrocell test exposes steel reinforcing bars directly to a simulated concrete environment with chloride contamination and is outlined in Annexes A1 and A2 of ASTM A955/A955M-19. The rapid macrocell test is shown in Figure 2.3. A single rapid macrocell specimen consists of an anode and a cathode. The test uses two containers, each filled to a depth of 3 in. with a simulated pore solution. Sodium chloride (NaCl) is added to the pore solution in the container with the anode, where corrosion is induced, to produce a 15% (6.04 molal ion) sodium chloride solution (NaCl) to simulate chloride-contaminated concrete; the cathode has pore solution with no chlorides. One liter of pore solution consists of 974.8g of distilled water, 18.81g of potassium hydroxide (KOH), and 17.87g of sodium hydroxide (NaOH). Air is bubbled into the cathode solution to remove carbon dioxide, ensuring an adequate supply of oxygen required for the cathodic reaction. Deionized water is added to the containers as needed to maintain a constant volume of the solution. The solutions are changed every five weeks to limit the effects of carbonation. The anode and cathode are electrically connected across a 10-ohm resistor. A potassium chloride (KCl) salt bridge provides an ionic connection between the anode and the cathode (Figure 2.3).

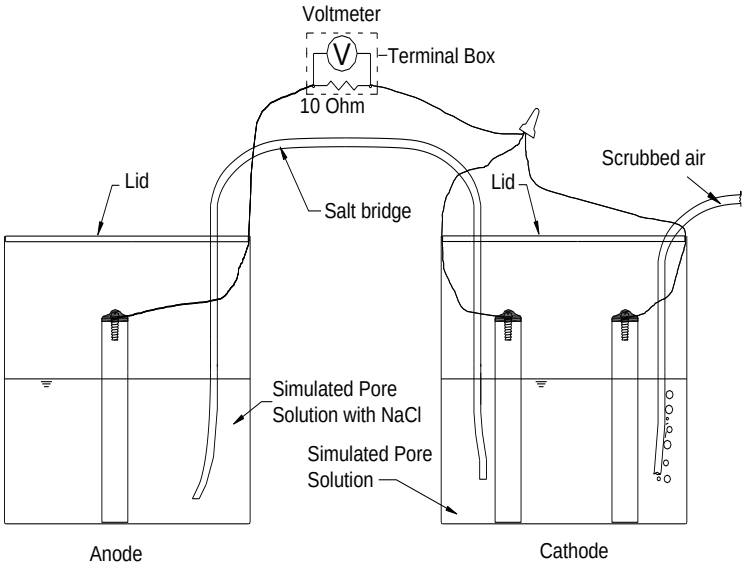

Figure 2.3: Rapid macrocell test.

A modified rapid macrocell specimen is used for bent anode bars to determine the effect of field fabrication on the corrosion resistance of coated reinforcement, as shown in Figure 2.4. The modified rapid macrocell consists of a single anode bar, bent around a 3.75-in. diameter pin and submerged to a depth of 1.75 in. in simulated pore solution with salt. The cathode consists of four No. 5 reinforcing bars submerged to a depth of 3 in. The change in the solution depth at the anode and number of cathode bars is used to keep the ratio of anode bar area to cathode bar area the same as in the standard macrocell test. The test is otherwise identical to the standard macrocell test.

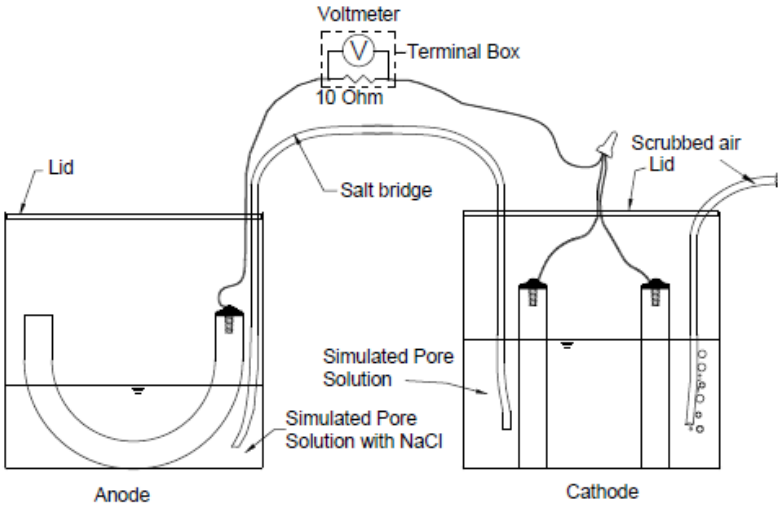

Figure 2.4: Rapid macrocell test for bent anode bar. Note: Four bars are present in the cathode.

2.2.1.1 Fabrication

For the rapid macrocell test, reinforcing bars are cut to a length of 5 in. with a band saw. One end of each bar is drilled and tapped to receive a 3/8-in. long stainless steel screw with 10-24 threading. For coated reinforcing bars (ECR or galvanized) with intentional damage, the

coating is penetrated to a depth of 15 mils with a 0.125-in. diameter four-flute drill bit using a milling machine. Two holes are placed on each side of the bar approximately 1 in. and 2 in. from the bottom. The coating is not penetrated on bent bars. Bare and galvanized bars are soaked in acetone for a minimum of two hours and cleaned to remove any oil. Epoxy-coated bars are cleaned with warm soapy water, rinsed, and allowed to dry. Bars are inspected before the test to ensure there are no unintentional perforations in the coating of bars used as the anode. 16-gauge wire leads are connected to the test bars using a 10-24 × 3/8-in. stainless steel screw. Multiple coats of epoxy are applied to the electrical connection to protect it from corrosion. Vinyl caps filled with epoxy are applied to the end of coated specimens to protect the cut end from corrosion. Bars are placed upright in the plastic containers and pore solution added to a depth of 3 in. or 1.75 in. in containers holding a bent anode. Bars are connected to a terminal box at the start of testing.

2.2.1.2 Rapid Macrocell Test Procedure

The rapid macrocell test is a 15-week test. Corrosion rate and corrosion potential measurements are taken daily for the first week and weekly thereafter. The exposed area of the anode bar is used to calculate the corrosion rate, which is calculated based on the voltage drop measured across the 10-ohm resistor using Faraday's equation.

$$\text{Rate} = K \frac{V\ m}{n\ F\ D\ R\ A} \tag{2.1}$$

where the rate is given in μm/yr,

K = conversion factor = $31.5 \cdot 10^4$ amp·μm ·sec/μA·cm·yr

V = measured voltage drop across resistor, millivolts

m = atomic weight of the metal (for iron, m = 55.8 g/mol; for zinc, m = 65.4 g/mol)

n = number of ion equivalents exchanged (for iron and zinc, n = 2 equivalents)

F = Faraday's constant = 96485 coulombs/equivalent

D = density of the metal, g/cm^3 (for iron, D = 7.87 g/cm^3; for zinc, D = 7.14 g/cm^3)

R = resistance of resistor, ohms = 10 ohms for the test

A = surface area of anode exposed to solution

In some cases, the corrosion rate may appear to be negative. This negative corrosion rate does not indicate negative corrosion; it is rather caused by minor differences in the oxidation rate between the single anode bar and the cathode bars.

Determining the corrosion rate by taking voltage readings across the 10-ohm resistor (referred to as the macrocell corrosion rate) has the potential to miss localized corrosion, where the current flow between the anodic and cathodic reactions does not pass through the resistor placed between test bars. To capture both localized and general corrosion (referred to as the total corrosion rate) linear polarization resistance (LPR) tests are performed every 3 weeks. In addition, the corrosion potential is measured at both the anode and cathode using a silver-silver chloride electrode. Potential readings are converted to an equivalent copper-copper sulfate

electrode (CSE) for presentation.

2.2.2 Southern Exposure and Cracked Beam Tests

Southern Exposure (SE) and cracked beam (CB) tests evaluate concrete in uncracked and cracked concrete, respectively. The specimens undergo alternative cycles of wetting (exposure to a 15% salt solution) and drying. Southern Exposure specimens (Figure 2.5) consist of 12 × 12 × 7 in. blocks. Twelve-inch long No. 5 reinforcing bars are cast in the specimen in two mats. The top and bottom mats consist of two and four bars, respectively, each with 1-in. clear cover to the horizontal surfaces. The bars in the top and bottom mats are electrically connected through a terminal box across a 10-ohm resistor to allow for the macrocell corrosion rate measurements. A 0.75-in. deep concrete dam is integrally cast with the specimen to contain the ponded salt solution. Southern Exposure tests represent conditions in uncracked reinforced concrete. A modified Southern Exposure specimen was also used to allow for bent bars to be tested (Figure 2.6).

Cracked beam specimens (Figure 2.7) are half the width of the Southern Exposure specimens, measuring 12 × 6 × 7 in. The top mat consists of a single No. 5 bar; the bottom mat consists of two No. 5 bars. Prior to fabrication, a 12-mil thick × 6-in. long stainless steel shim is placed in the mold in direct contact with the top reinforcing bar. The shim is removed 12-24 hours after casting. This results in direct infiltration of chlorides at the beginning of the test.

Both the Southern Exposure and cracked beam tests are 96 weeks in duration. As in the rapid macrocell tests, the epoxy-coated and galvanized bars are evaluated using specimens with the epoxy or zinc intact and with the epoxy coating or zinc coating penetrated, in this case by ten $^{1}/_{8}$-in. (3-mm) diameter holes to simulate defects or damage.

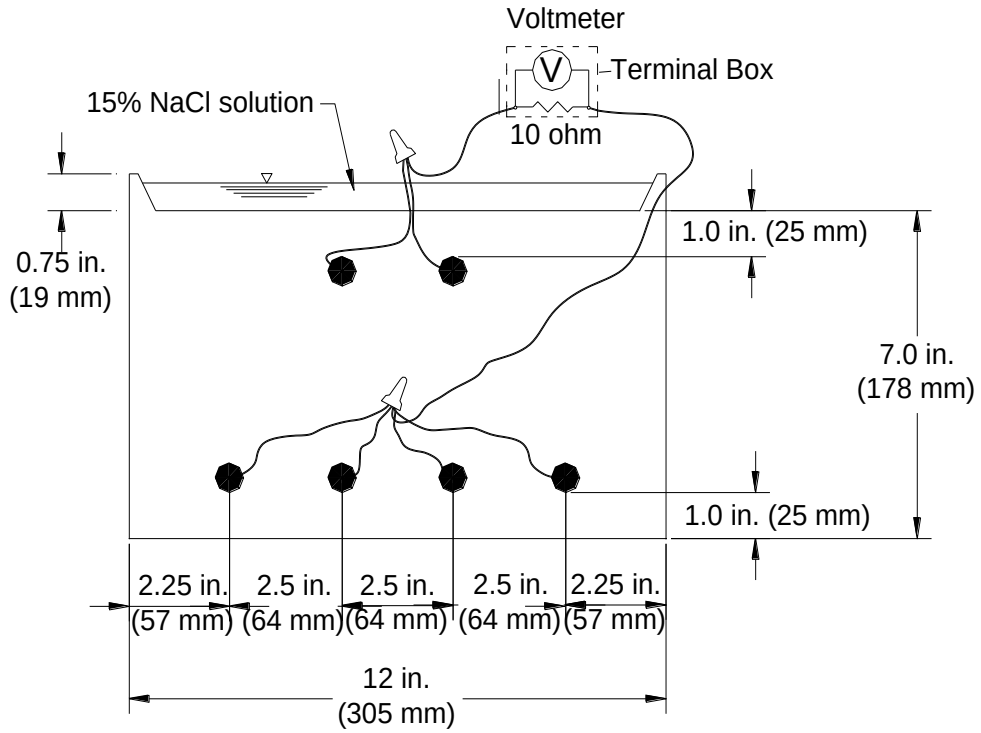

Figure 2.5: End view of Southern Exposure (SE) specimen.

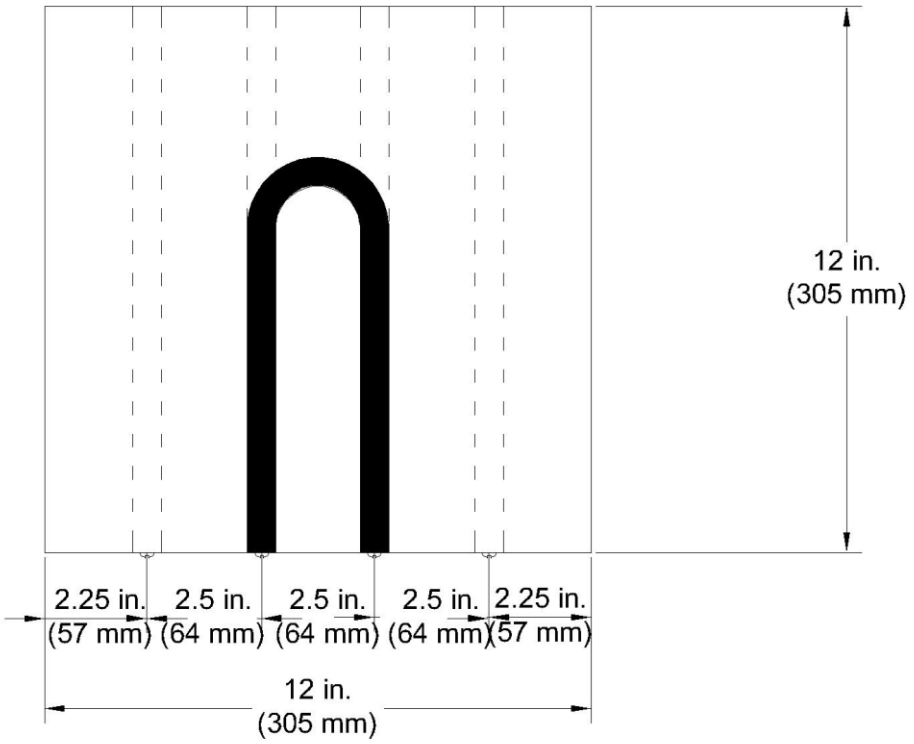

Figure 2.6: Plan view of Southern Exposure specimen with a bent anode bar.

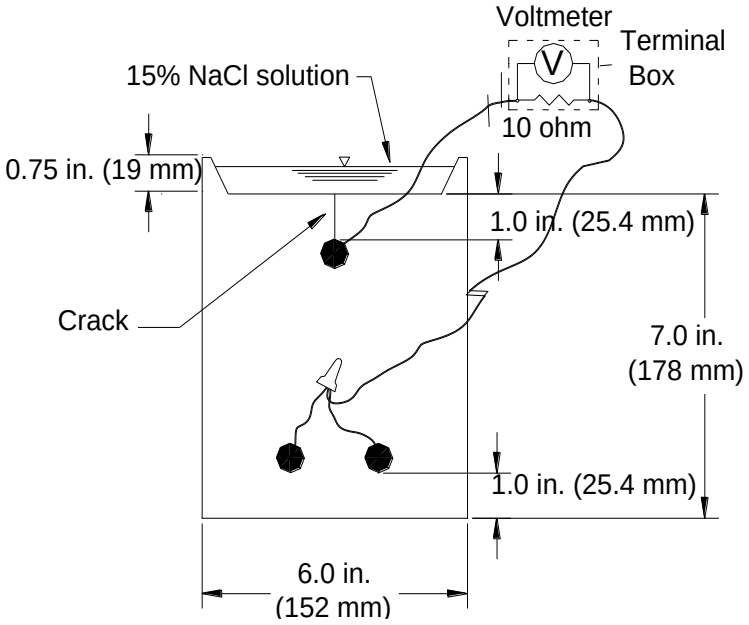

Figure 2.7: Cracked beam (CB) specimen.

2.2.2.1 Fabrication

Specimen fabrication for Southern Exposure and cracked beam specimens is as follows:

1. Reinforcing bars are cut to 12 in. with a band saw. Bars that are to be bent are cut to a length of 15 in. Epoxy-coated bars are covered with padding for protection against unintentional damage during machining.

2. Both ends of each bar are drilled and tapped to a 3/8 in. depth with 10-24 threading.

3. For coated reinforcing bars (ECR or galvanized) with intentional damage, the coating is penetrated to a depth of 15 mils with a 0.125-in. diameter four-flute drill bit using a milling machine. Five holes are placed on each side of the bar approximately 2 in. apart. The coating is not penetrated on bent bars.

4. Epoxy-coated bars are cleaned with warm soapy water, rinsed, and allowed to dry. Bare bars are soaked in acetone for a minimum of two hours and scrubbed to remove any oil.

5. The forms are assembled, and the reinforcement is attached. Reinforcing bars with penetrations in the coating are aligned so that the holes face the top and bottom of the specimen. Forms and reinforcement are held in place using 10-24 threaded stainless-steel machine screws.

6. Specimens are cast in an inverted position in two layers, with each layer consolidated using a 0.75- in. diameter vibrator. The free surface of the concrete (the bottom of the specimen as they are cast upside-down) is finished with a trowel.

7. Specimens are cured for 24 hours at room temperature. A plastic cover is used to minimize evaporation. Stainless steel shims are removed from cracked beam specimens after 12-24 hours, when the concrete has set.

8. Formwork is removed after 24 hours.

9. Specimens are cured for an additional two days in a plastic bag containing deionized water, then air-cured for 25 days.

10. Prior to test initiation, wire leads are connected to the test bars using 10-24 × 3/8-in. stainless steel screws. Epoxy coating is applied to the vertical sides of the specimens and the top surface of the dams, while the top and bottom surfaces of the specimens are left uncoated.

11. The two mats of steel are connected to the terminal box. Specimens are left connected across the 10-ohm resistor, except when readings are taken. Specimens are placed on 2 × 2 studs to allow air flow under the specimens. Tests begin 28 days after casting.

2.2.2.2 Test Procedure

The Southern Exposure and cracked beam tests are subjected to alternate cycles of ponding and drying. The test begins with 12 weeks of ponding and drying, followed by 12 weeks of ponding, for a total of 24 weeks. This exposure regime is then repeated for the duration of the test. The tests conclude after 96 weeks. The procedures are described below.

Ponding and Drying Cycles:

A 15% NaCl solution is ponded on the surface of the specimens. The temperature is

maintained at 72 ± 3° F. SE specimens receive 600 mL of solution; CB specimens receive 300 mL. The specimens are covered with plastic sheeting during ponding to minimize evaporation. Readings are taken on day 4. After the readings are completed, the specimens are vacuumed to remove the salt solution, and a heat tent is placed over the specimens. The tent maintains the specimens at 100 ± 3° F for three days. The tent is then removed, and the specimens are again ponded with the NaCl solution to start the second week of testing. Ponding and drying cycles continue for 12 weeks.

Ponding Cycle:

After 12 weeks of ponding and drying, specimens are ponded for 12 weeks with the 15% NaCl solution and covered with plastic sheeting. The NaCl solution remains on the specimens throughout the 12 weeks at 72 ± 3° F. Readings continue to be taken on a weekly basis. Deionized water is added to maintain the desired solution depth on the specimens during this time. After 12 weeks, the specimens are again subjected to the weekly ponding and drying cycles.

Corrosion rate and corrosion potential measurements are taken weekly; (LPR) polarization resistance measurements are taken every four weeks. The voltage drop between anode and cathode is recorded and used to calculate corrosion rate using Faraday's equation and Ohm's law, as described in Section 2.2.1.2. Following the measurement of the voltage drop, the electrical connection is interrupted to measure corrosion potentials. The specimens remain disconnected for a minimum of two hours before measuring corrosion potentials and taking the LPR readings. Potentials are measured with respect to a silver-silver chloride electrode and converted to an equivalent copper-copper sulfate electrode (CSE) value for presentation.

2.2.3 Chloride Sampling of Test Specimens

2.2.3.1 Chloride Sampling

Upon the initiation of corrosion, Southern Exposure specimens are drilled to obtain chloride samples at the level of the top mat of steel (anode). Cracked beam specimens are not sampled for chlorides, because the simulated crack allows direct infiltration of the salt solution. For conventional reinforcement, corrosion initiation is marked by voltage drops that signify macrocell corrosion rates above 0.3 µm/yr and top-mat corrosion potentials more negative than –0.350 V with respect to a CSE as per ASTM C876. For coated bars, corrosion initiation is marked by sudden voltage drops, which are often smaller than those signifying corrosion in conventional reinforcement.

2.2.3.2 Chloride Sampling Procedure

Chloride sampling is performed after all corrosion measurements are taken for an SE specimen. Prior to sampling, the specimen is cleaned on all four sides with tap water and soap. Afterwards, the specimens are rinsed with deionized water. After drying, the specimens are marked for drilling so that the top of the drill bit is level with the top of the top mat of steel (Figure 2.8). Samples are obtained from the sides of the specimen, perpendicular to the steel bars, with a 0.25-in. masonry drill bit. Three samples are taken from each side of the specimen for a total of six samples.

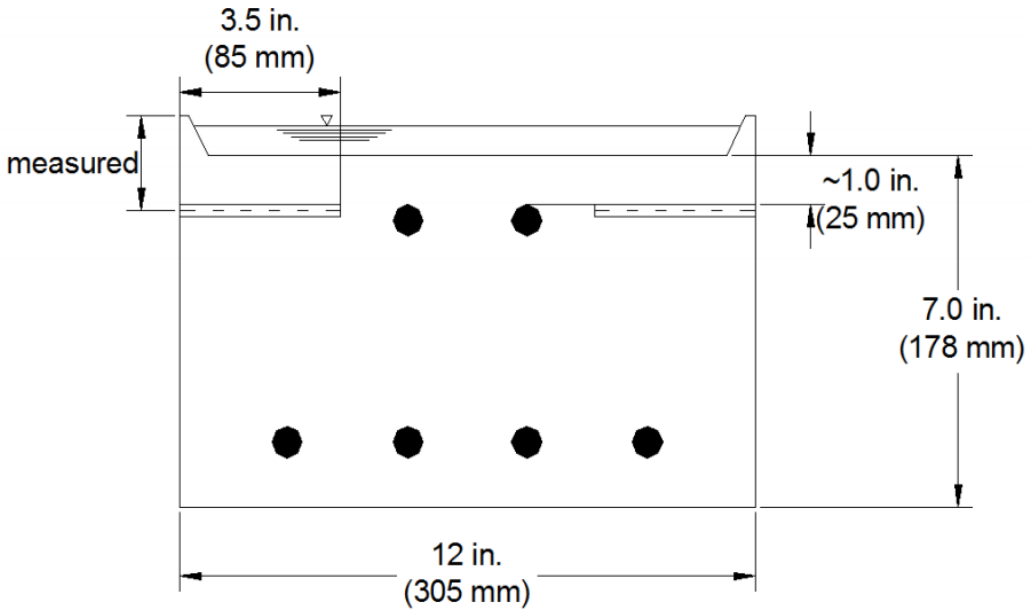

Figure 2.8: Southern Exposure chloride sampling.

For each sample site, a 0.5-in. deep hole is initially drilled. The resulting powder is then removed and discarded. The drill bit is then rinsed with deionized water, re-inserted, and used to penetrate to a depth of 3.5 in. This sample is collected in a plastic bag and labeled for analysis. Each sample provides approximately four grams of material. The drill bit is rinsed with distilled water between specimens. The holes left from drilling are filled with clay, and the specimen is reconnected for continued testing.

Chloride Analysis

Concrete samples are analyzed for water-soluble chloride content in accordance with ASTM C1218 (Standard Test Method for Water-Soluble Chloride in Mortar and Concrete). Each concrete sample is boiled in distilled water to free any water-soluble chlorides. Solutions rest for a minimum of 24 hours after boiling and are then filtered. The solution is acidified with nitric acid and then titrated with silver nitrate ($AgNO_3$). The potential with respect to a chloride sensitive electrode is measured throughout titration. For an incremental addition of silver nitrate, the change in potential with respect to each endpoint is indicated by an inflection point of the potential-volume curve. The endpoint is indicated by the greatest change in potential for a given incremental addition of silver nitrate. This procedure gives the chloride concentration in terms of percent chloride by mass of the sample. In this study, values are presented in lb/yd^3 by multiplying by the unit weight of concrete, taken as 3786 lb/yd^3.

2.2.4 End of Life and Autopsy

All specimens (rapid macrocell, Southern Exposure, and cracked beam) are photographed upon completion of the test. For specimens in the rapid macrocell test, protective caps on coated bars are removed and the specimens are inspected for under-the-cap corrosion. A disbondment test is conducted on ECR specimens with intentional damage. A sharp utility knife is used to cut through the epoxy at 45° forming an “X” at the intentional hole. The coating is then peeled back until the coating will no longer peel back. If the disbondment extends more

than 0.5 in. (12 mm) beyond the hole, the coating is considered to have undergone total disbondment. A 0.01-in. (0.254-mm) transparent grid is used to measure the disbonded area. Specimens with total disbondment are assigned a disbonded area of 1.05 in.^{2}, equivalent to a square extending 0.5 in. on all sides from the edges of the damage site.

2.2.5 Laboratory Test Program

Table 2.3 shows the test program in this study. Conv. A, B, and C bars are the conventional steel used in the ECR, A767, and A1094 reinforcing bars, respectively, and the -ND and -Bent modifiers indicate undamaged and bent bars, respectively. For ECR bars with UV exposure, the number following the -UV indicator indicated the number of hours of exposure. To allow for additional investigation into the effect of UV exposure on epoxy coatings, some of the ECR bars exposed to ultraviolet light came from a second heat of steel; ECR designations are labeled to reflect the two different heats of reinforcement used (ECR and ECR2). ECR2 bars were only evaluated in the rapid macrocell test. Bench-scale specimens containing A1035 and Conv.-B reinforcing bars were also used to study the effects of Ipanex and Xypex.

2.3 Chikaskia River Bridge Survey

The deck on the Chikaskia River bridge on I-35 in northern Oklahoma was chosen for evaluation as part of this study. This bridge is reinforced with A1035 bars and the concrete contains Ipanex, a combination that was chosen as an alternative to the stainless steel reinforcement originally proposed for the deck. A direct electrical connection to the reinforcement is not available, so a visual survey was conducted to evaluate the deck for cracking, spalling, and corrosion-induced damage.

The survey method follows that developed by Darwin et al. (2016). Surveys are performed on dry bridge decks, with mostly sunny conditions and an air temperature of at least 60°F (16°C) at the time of surveying. A scaled drawing of the bridge deck is used to record cracking and damage. The drawing is produced at a scale of 1 in. = 10 ft; a similarly scaled 5 ft × 5 ft grid is placed underneath the deck plan to aid in accurate placement of cracks on the drawing. At the start of the survey, two surveyors draw a 5 ft × 5 ft grid on the bridge deck using chalk or lumber crayons, matching the grid on the drawing. Surveyors mark any cracks they can see while bending at waist height. When surveyors see a crack, they may bend closer and trace the crack to its end, including portions of the same crack that cannot be seen from waist height. If the surveyors see another crack while tracing a crack, they do not mark it unless it is also visible when bending from waist height. At least two surveyors inspect each section of the bridge. This method results in consistent crack survey results between surveys (Lindquist et al. 2005, 2008). After cracks are marked on the bridge, another surveyor draws the marked cracks on the scaled bridge plan. Crack densities are calculated for the bridge deck by scanning the marked plan into AutoCAD. Damage, other than cracking, is also noted during the survey.

Table 2.3: Laboratory Test Program – Number of Test Specimens

Reinforcement	Macrocell	Southern Exposure (SE)	Cracked Beam (CB)
Conv-A	6	6	6
Conv-B	6	4	4
Conv-C	6	3	3
ECR*	6	4	4
ECR2 *	5	-	-
ECR-ND	6	3	3
ECR2-ND	6	-	-
ECR-UV-1000*	12	3	3
ECR-UV-500*	6	-	-
ECR-UV-250*	6	-	-
ECR2-UV-1000*	5	-	-
ECR2-UV-200*	6	-	-
ECR2-UV-100*	6	-	-
ECR1-UV-1000-ND	6	3	3
ECR-Bent	6	-	-
A767*	6	6	6
A767-ND	6	6	6
A767-Bent	6	6	-
A1094*	6	6	6
A1094-ND	6	6	6
A1094-Bent	6	6	-
A1035	6	6	6
Conv-B-Ipanex	-	6	6
A1035-Ipanex	-	6	6
Conv-B-Xypex	-	6	6
A1035-Xypex	-	6	6

*Damaged bars in rapid macrocell specimens have four $^{1}/_{8}$-in. diameter holes in the coating (two on each side). Damaged bars in the cracked beam and Southern Exposure specimens have 10 $^{1}/_{8}$-in. diameter holes (5 on each side).

2.4 Cow Creek Deck Panel Analysis

As part of this study, deck panels were removed during demolition of the Cow Creek bridge were analyzed. The Cow Creek bridge was a reinforced concrete bridge deck on I-35 near Perry, Oklahoma passing over Cow Creek, NBIS #14495, constructed in 1979. The southbound lanes were constructed with conventional reinforcement, and the northbound lanes were constructed with epoxy-coated reinforcement. The deck with conventional reinforcement had received a silane treatment and a 1.5-in. thick concrete overlay to extend its service life. The panels varied in thickness from 8 to 9 in., with dimensions of roughly 5 by 7 ft. Clear

concrete cover to both top and bottom transverse reinforcement, as measured from core samples, was approximately 2 in. A total of ten panels were removed from the bridges during demolition; six with epoxy-coated reinforcement and four with conventional reinforcement. The location of these panels is shown in Figures 2.9 and 2.10 for panels containing ECR and conventional reinforcement, respectively. Of the ten panels, three each from the decks with epoxy-coated (X1, X2, and X3) and conventional reinforcement (#1, #2, #3) were selected for analysis. Each panel was marked with a 1 ft × 1 ft grid to aid in collection of data.

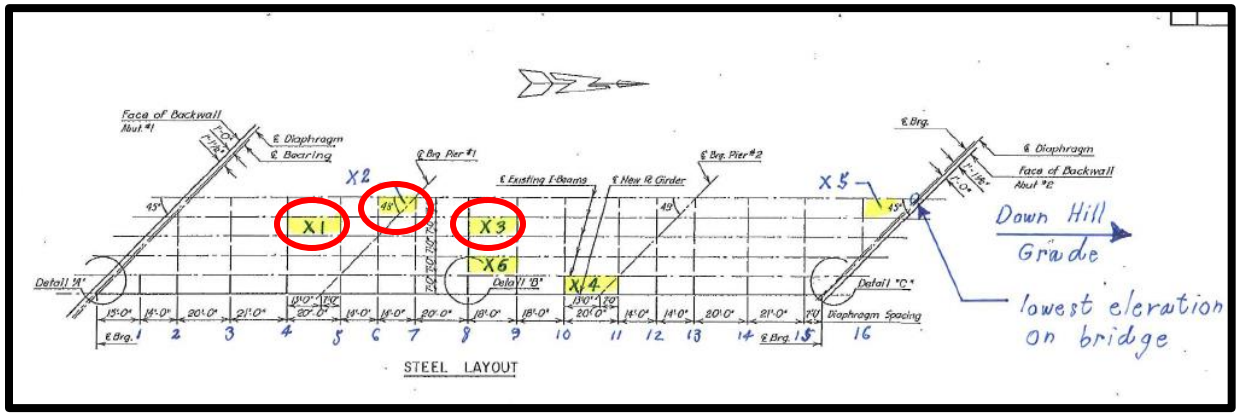

Figure 2.9: Panel locations-ECR. Analyzed panels are circled in red.

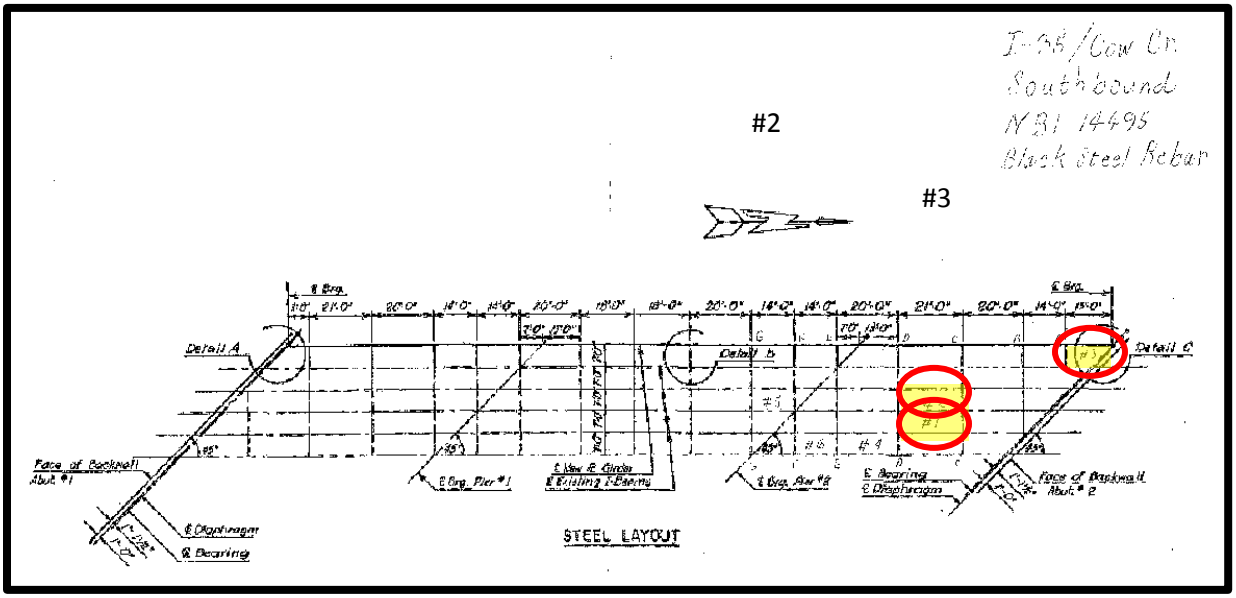

Figure 2.10: Panel locations-conventional reinforcement. Analyzed panels are circled in red.

2.4.1 Test Program for Cow Creek Deck Panels

2.4.1.1 Visual Condition Survey

A visual condition survey was completed for each slab following the guidelines of ACI 364.1 and ACI 201.1R-08. The survey focused on factors related to corrosion and durability, such as transverse cracks, spalls, severe scaling, bug holes, and shrinkage cracking. Cracking was documented using the crack survey procedure outlined in Section 2.3. These features were mapped using chalk on the concrete surface and recorded via an overhead photo.

2.4.1.2 Strength Testing

Prior to determining the compressive strength of the concrete, 1-ft square regions were marked on the panels. The panels were first tested using a rebound hammer and the pulse-echo technique. The rebound hammer was used to measure surface hardness in accordance with ASTM C805. Ten measurements were taken within each 1-ft square region and averaged. A pulse-echo survey was performed in accordance with ASTM C597, with a total of three readings per slab.

The compressive strength of the concrete was evaluated using 2.6 × 5 in. cores, taken and tested in accordance with ASTM C42. The cores were all conditioned in the lab after being taken from the slabs and were vacuum saturated for 24 hours prior to testing. Testing was performed on three cores sampled from the same 1-ft square region. Regions were selected based on results from the surface hardness survey. Two cores were tested only for strength, while the third was subjected to loading and unloading to determine the modulus of elasticity in accordance with ASTM C469 prior to loading to failure. The surface hardness and pulse echo readings were correlated with the compressive strengths.

2.4.1.3 Half-Cell Potential Survey

Half-cell potential measurements were taken for the top longitudinal and transverse bars in each deck panel. Potentials were taken on a 2 in. square grid using a copper/copper sulfate electrode (CSE) with an electrical connection to the reinforcement. Values were obtained over the full slab surface and reported in a contour map.

2.4.1.4 Electrical Resistivity Testing

Electrical resistivity provides an indirect measurement of the permeability of concrete. Bulk resistivity testing was conducted with a GIATEC RCON2. The test measures the voltage drop across a concrete core under a 1kHz AC current. Two measurements per core (different from the cores used to evaluate strength) were collected and averaged.

2.4.1.5 Ultrasonic Pulse Velocity

Ultrasonic pulse velocity (UPV) provides a measure of concrete quality and can detect internal defects and degradation. Direct transmission UPV measurements were taken on cores obtained from each panel. Due to the small core size, it was optimal to use a higher frequency and so all testing was done with 150 kHz transducers.

2.4.1.6 Colorimetric Testing of Cores

Colorimetric testing involves the application of a special indicator dye or chemical to establish the quantity or extent of some substance in concrete. In this study, colorimetric testing was used to establish the depth of carbonation, chloride ingress, and silane treatment. Four-inch diameter cores were collected from different locations on each deck panel, some of which included locations with severe cracks or cores taken directly above reinforcing steel. Locations were chosen as to provide a range of concrete quality, including areas both with and without cracking, spalling, and other signs of deterioration. Each core was split lengthwise following the procedures in ASTM C496 to expose the inside of the core for testing.

The depth of chloride penetration was determined using a 0.1M silver nitrate ($AgNO_3$) indicator, commonly used in field applications. This solution was applied to the inside surface

(surface exposed by splitting) of the cores. In the presence of chlorides, the silver nitrate will precipitate out, leaving a visible white discoloration. The depth of discoloration was measured at four locations along the radial axis of the on an inside surface of the core, avoiding large aggregates. The recorded value was the mean of these four measurements.

The carbonation depth on each core was determined using thymolphthalein. On concrete above a pH of about 10.5, thymolphthalein will turn dark blue. This color fades below a pH of 10.5, and thymolphthalein will exhibit no color below a pH of 9.3. This corresponds with severe carbonation in concrete. Application and measurement of carbonation depth proceeded in the same manner as chloride penetration.

The presence of a hydrophobic agent such as silane was tested by measurement of the depth of absorption for a water-based dye into the concrete surface. Prior to testing for carbonation depth and chloride penetration depth, the cores were placed in bins containing a dark dye for 30 minutes, then removed and measured for penetration depth. The presence of silane or a similar agent would inhibit absorption into the concrete.

2.4.1.7 Linear Polarization Resistance (LPR)

Linear polarization resistance (LPR) measurements were taken on the top and bottom mats of reinforcement for two panels with conventional reinforcement and two panels with ECR. Panels were wetted prior to testing, but were not fully saturated.

CHAPTER 3: RESULTS

This chapter presents the results of the rapid macrocell, Southern Exposure, and cracked beam tests, as well as the Chikaskia River crack survey and evaluations of the Cow Creek deck panels. For the corrosion tests, the average corrosion rates, losses, potentials, and critical chloride corrosion thresholds are presented for each of the systems in this study. Results from individual specimens are presented in Appendix A.

3.1 Rapid Macrocell Test

The rapid macrocell test was used to evaluate conventional, epoxy-coated, galvanized, and A1035 (ChromX) reinforcement. Coated bars were evaluated both undamaged (-ND) and with 4 0.125-in. diameter holes in the coating, simulating damage that occurs during handling and placement of reinforcement on a job site. Epoxy-coated reinforcement (ECR) was also evaluated after being subjected for different periods to ultraviolet (UV) light, simulating outdoor storage, and galvanized bars were evaluated with a 180-degree bend.

3.1.1 Macrocell Corrosion Rates and Potentials

3.1.1.1 Conventional Reinforcement

Figure 3.1 shows the average corrosion rates in the rapid macrocell test for the three heats of conventional reinforcement evaluated in this study. Conv-A, Conv-B, and Conv-C refer to the heats of conventional reinforcement coated with epoxy (ASTM A775) and the two types of galvanized reinforcement (ASTM A767 and A1094), respectively. For the first 10 weeks of testing, the Conv-A bars exhibited corrosion rates that were lower (generally in the range of 10-20 µm/yr) than those observed for Conv-B or Conv-C (generally in the range of 20-35 µm/yr). After week 10, however, the corrosion rates of Conv-B and Conv-C decreased sharply, and all three heats of steel exhibited similar corrosion rates through the last five weeks of testing.

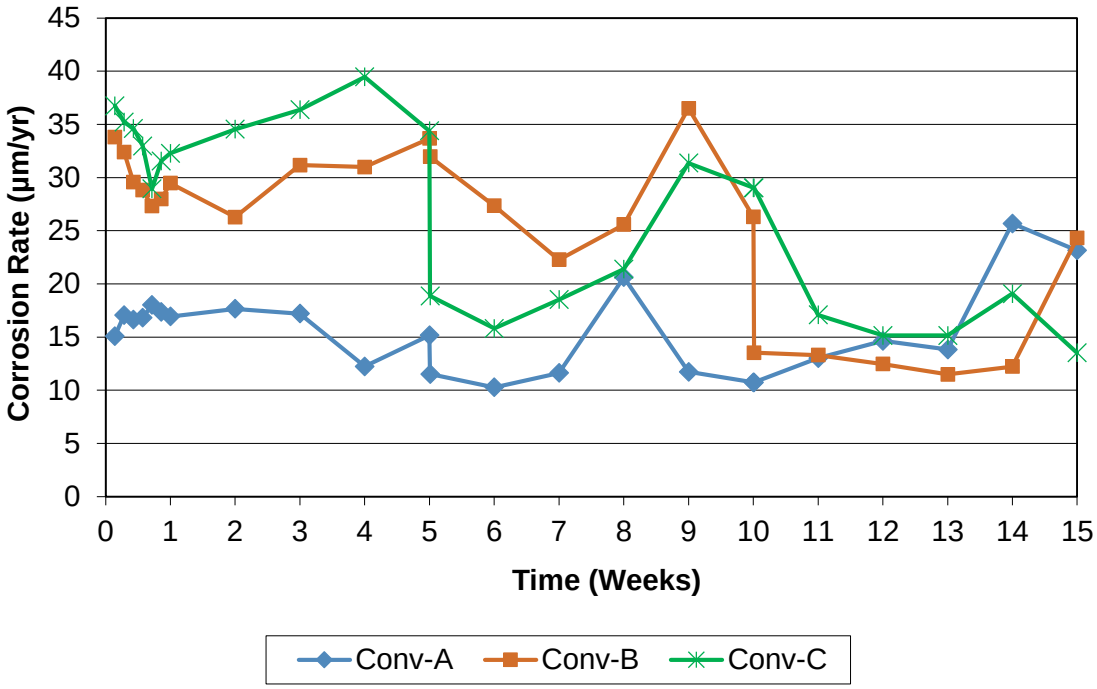

Figure 3.1: Rapid Macrocell Test. Average corrosion rate vs. time. Corrosion rate based on total bar area of conventional reinforcement.

Figure 3.2 shows the average corrosion potentials versus a copper/copper sulfate electrode (CSE) for the three heats of conventional reinforcement evaluated in this study. All three heats of steel consistently exhibited a potential of approximately –0.600 V versus CSE throughout testing, indicating active corrosion.

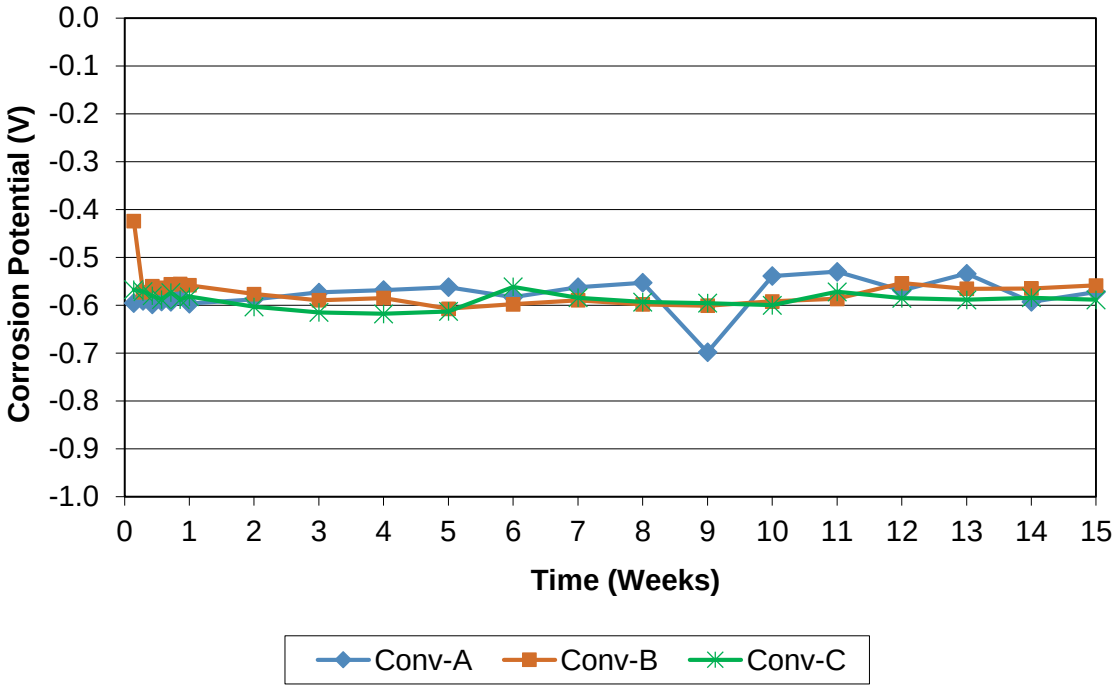

Figure 3.2: Rapid Macrocell Test. Average corrosion potential of conventional reinforcement vs. time.

3.1.1.2 Epoxy-Coated Reinforcement

Figure 3.3 shows the average corrosion rates based on total bar area for epoxy-coated reinforcement (ECR) with and without damage and 1000 hours of exposure to ultraviolet (UV) light, simulating one year of outdoor exposure. Throughout the test, ECR with UV exposure exhibited a corrosion rate several times higher than that of ECR without UV exposure, indicating that extended UV exposure significantly reduces the corrosion resistance of ECR. Even in the absence of simulated damage, UV-exposed ECR (ECR-UV-1000-ND) exhibited a positive corrosion rate for approximately half the testing period, whereas undamaged ECR without UV exposure (ECR-ND) showed no corrosion activity.

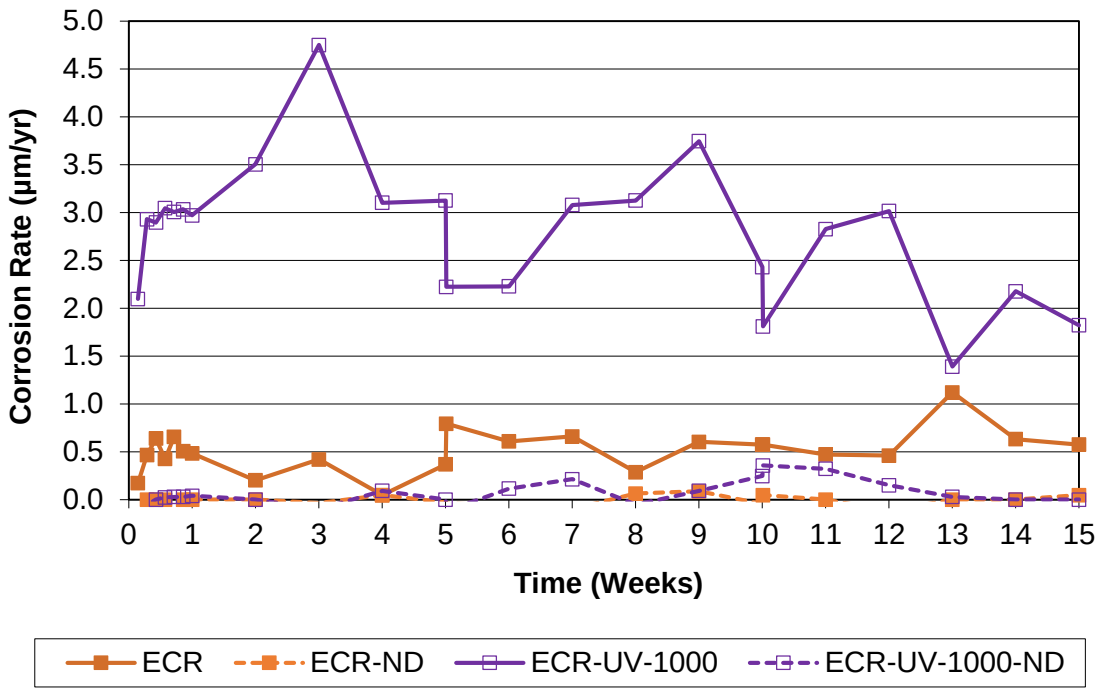

Figure 3.3: Rapid Macrocell Test. Average corrosion rate vs. time. Corrosion rate based on total bar area of damaged and undamaged ECR

To further evaluate the effect of UV exposure on ECR, additional rapid macrocell tests were performed after exposing damaged ECR bars to between 100 and 1000 hours of UV light. Figure 3.4 shows the average corrosion rates based on total area for ECR and ECR2 for different periods of UV exposure. Two heats of steel were used for this expanded study; ECR2 indicates the bars were from the second heat of steel. Figure 3.4 shows the average corrosion rates based on total area for ECR and ECR2 for different periods of UV exposure. A second series of specimens of ECR with 1000 hours of UV exposure was also evaluated; this series is referred to as ECR-UV-1000 (b) in the figure. As shown in the figure, while bars with 250 hours or less of UV exposure tended to exhibit lower corrosion rates than bars with 500 or 1000 hours of UV exposure, UV exposure as low as 100 hours (equivalent to 1.2 months of outdoor exposure) resulted in corrosion rates several times that of unexposed ECR.

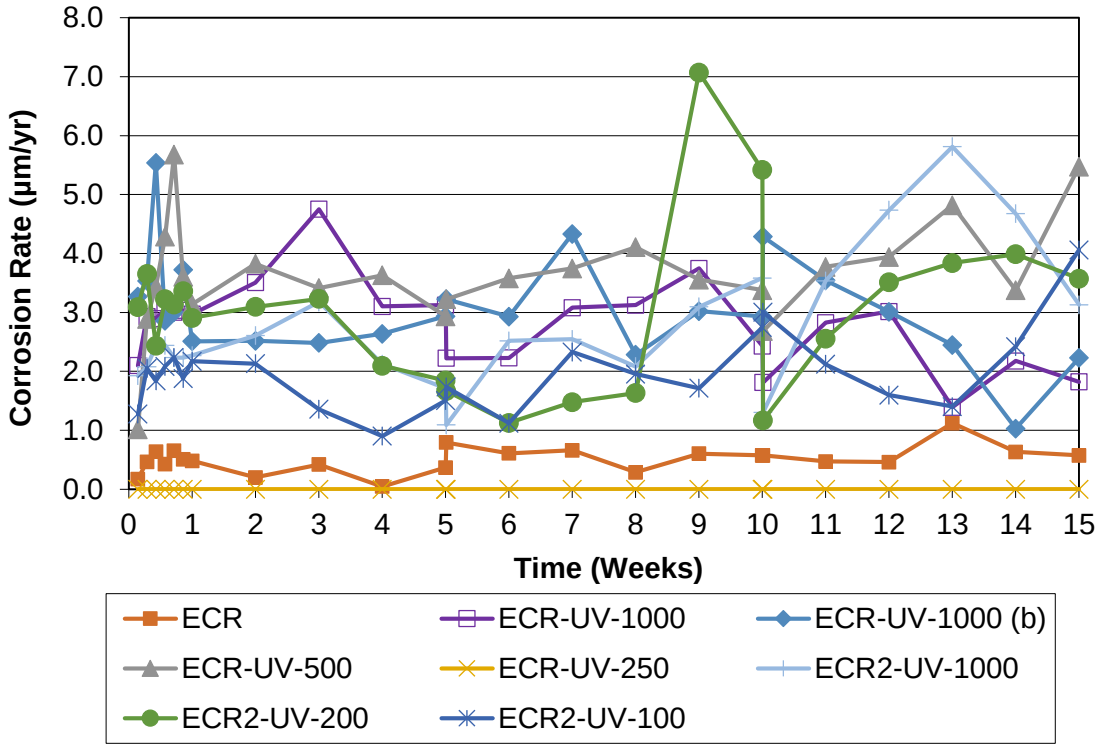

Figure 3.4: Rapid Macrocell Test. Average corrosion rate vs. time. Corrosion rate based on total bar area of ECR and ECR2 after different periods of UV exposure.

Figure 3.5 shows the average corrosion potentials for epoxy-coated reinforcement (ECR) with and without damage and 1000 hours of UV exposure. Note that corrosion potentials for ECR-ND specimens were unable to be obtained, as the undamaged coating prevented an ionic connection from forming between the reference electrode and the steel. For the first six weeks of testing, ECR-UV-1000 specimens exhibited an average corrosion potential approximately 0.1 V to 0.2 V more negative than other specimens. After week 6, the corrosion potential of ECR-UV-1000 became somewhat more positive; all specimens exhibited an average corrosion potential between –0.48 V and –0.60 V for the remainder of the test.

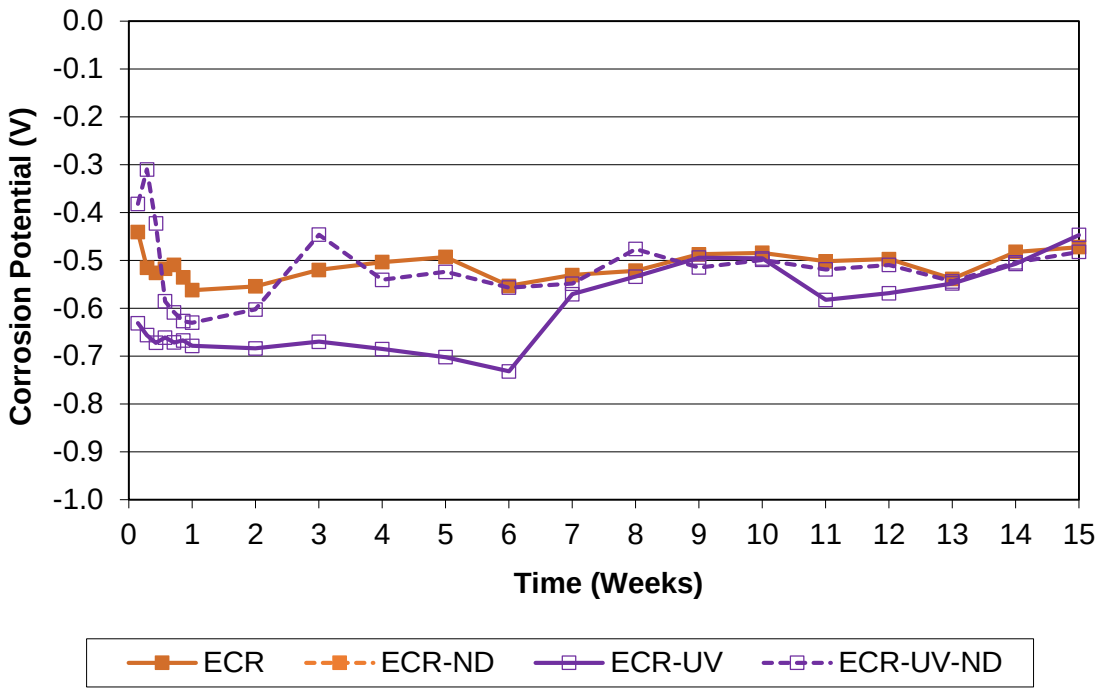

Figure 3.5: Rapid Macrocell Test. Average corrosion potentials of damaged and undamaged ECR vs. time

Figure 3.6 shows the average corrosion potentials for ECR and ECR2 after different periods of UV exposure. Regardless of the amount of exposure, ECR specimens with any amount of UV exposure exhibited corrosion potentials up to 0.2 V more negative than those exhibited by ECR with no UV exposure during testing. No correlation between amount of UV exposure and corrosion potential was observed.

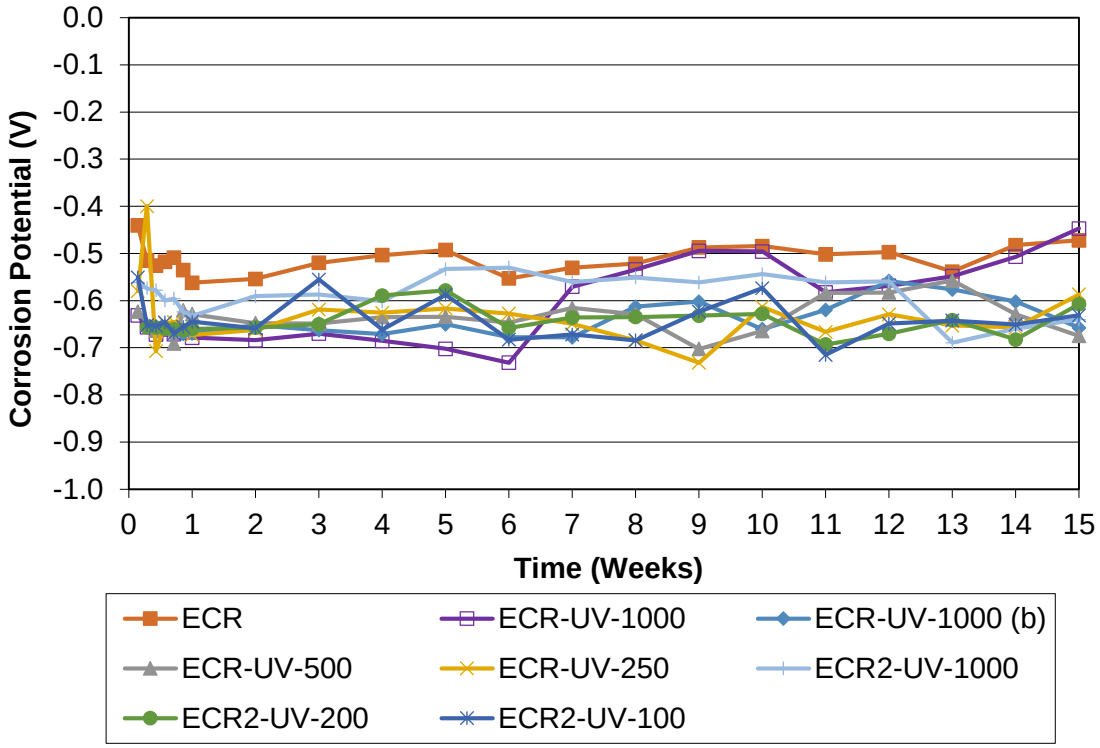

Figure 3.6: Rapid Macrocell Test. Average corrosion potentials of ECR and ECR2 after different periods of UV exposure vs. time.

3.1.1.3 Galvanized Reinforcement

Figure 3.7 shows the average corrosion rates based on total area for A767 and A1094 galvanized reinforcement. Conventional reinforcement (representing the average of the three heats of conventional reinforcement used in this study) is shown for reference. Both A767 and A1094 reinforcement exhibited very high corrosion rates throughout testing, particularly in the first three weeks. This behavior is not unexpected; the rapid macrocell test places reinforcement in a higher pH environment than is found in concrete, and the liquid environment can interfere with the formation of the crystalline passive layer that would normally protect zinc in concrete. The behavior in the rapid macrocell test should not, therefore, be taken as representative of the behavior of galvanized reinforcement in concrete.

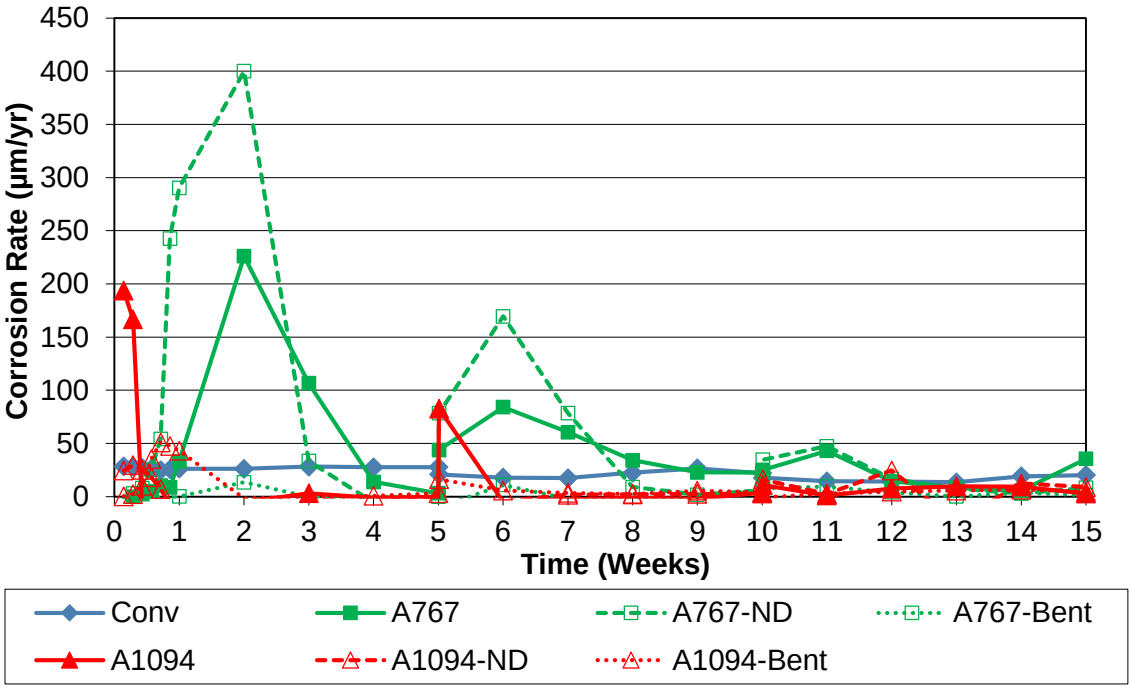

Figure 3.7: Rapid Macrocell Test. Average corrosion rate vs. time. Corrosion rate based on total bar area of A767 and A1094 galvanized reinforcement.

Figure 3.8 shows the average corrosion potentials for A767 and A1094 galvanized reinforcement. Both A767 and A1094 reinforcement exhibited very negative corrosion potentials at the start of testing, corresponding with the high initial corrosion rates. This behavior is expected, as zinc is a more corrosively active metal than iron. The corrosion potential for specimens with A1094 reinforcement increased to between –0.4 V and –0.6 V within the first two weeks of testing and remained there for the remainder of the test. The corrosion potential for specimens with A767 reinforcement increased to around –0.4 V by week 4. Unlike A1094 reinforcement, the corrosion potential of A767 reinforcement decreased after the solution changes at weeks 5 and 10; the potential returned to around –0.4 V within two weeks of the solution change. For both types of reinforcement, no significant differences were observed between damaged, undamaged, and bent reinforcement.

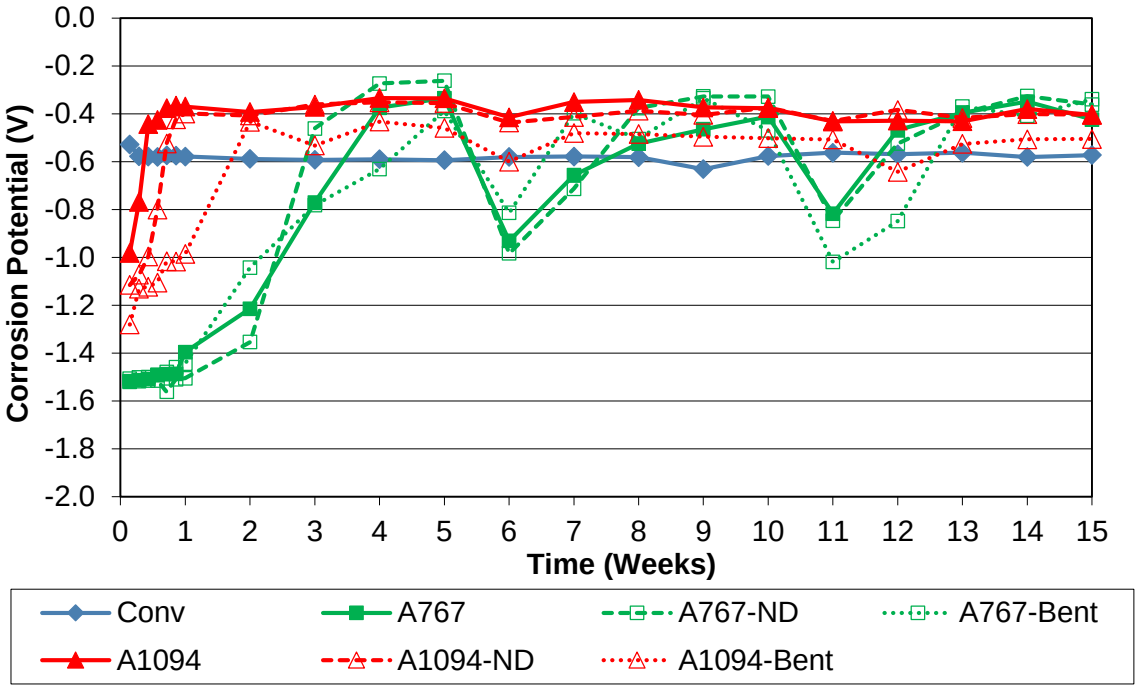

Figure 3.8: Rapid Macrocell Test. Average corrosion potentials of A767 and A1094 galvanized reinforcement vs. time.

3.1.1.4 A1035 (ChromX) Reinforcement

Figure 3.9 shows the average corrosion rate based on total bar area for A1035 Type CS reinforcement. Conventional reinforcement (representing the average of the three heats of conventional reinforcement used in this study) is shown for reference. Other than a spike in corrosion rate after the solution change on week 5, A1035 reinforcement exhibited a corrosion rate similar to that of conventional reinforcement. This matches the behavior of A1035 reinforcement observed in prior studies (Farshadfar et al 2017).

Figure 3.10 shows the average corrosion potential for A1035 Type CS reinforcement. A1035 reinforcement exhibited a slightly more positive potential than conventional reinforcement throughout the test.

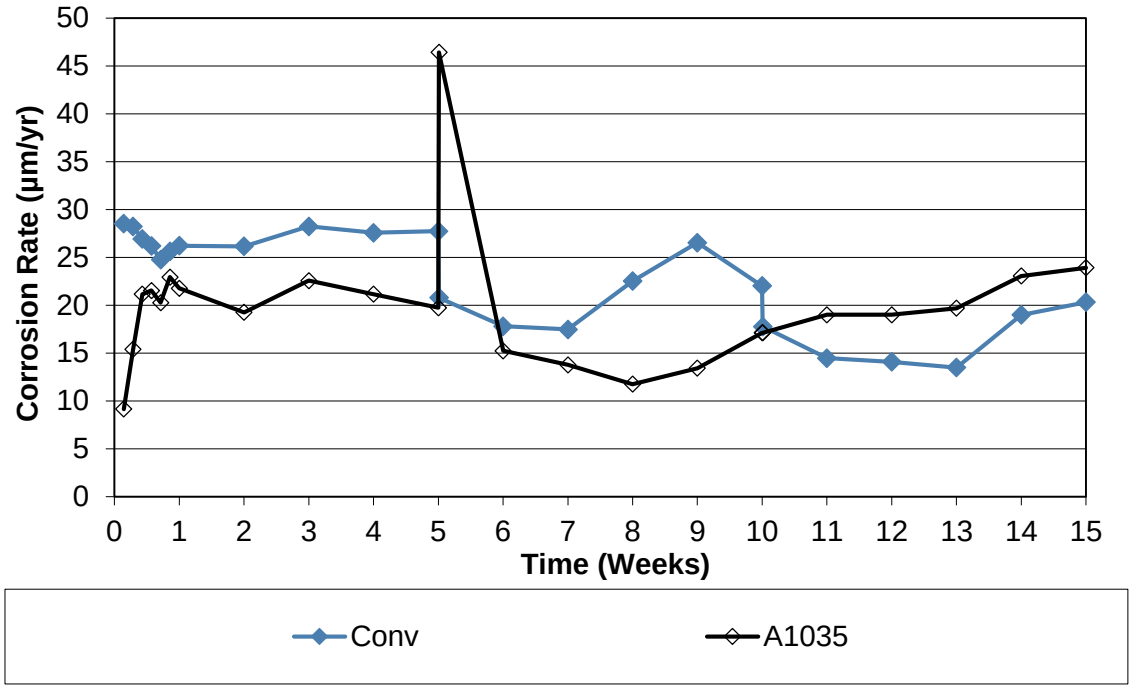

Figure 3.9: Rapid Macrocell Test. Average corrosion rate vs. time. Corrosion rate based on total bar area of A1035 reinforcement.

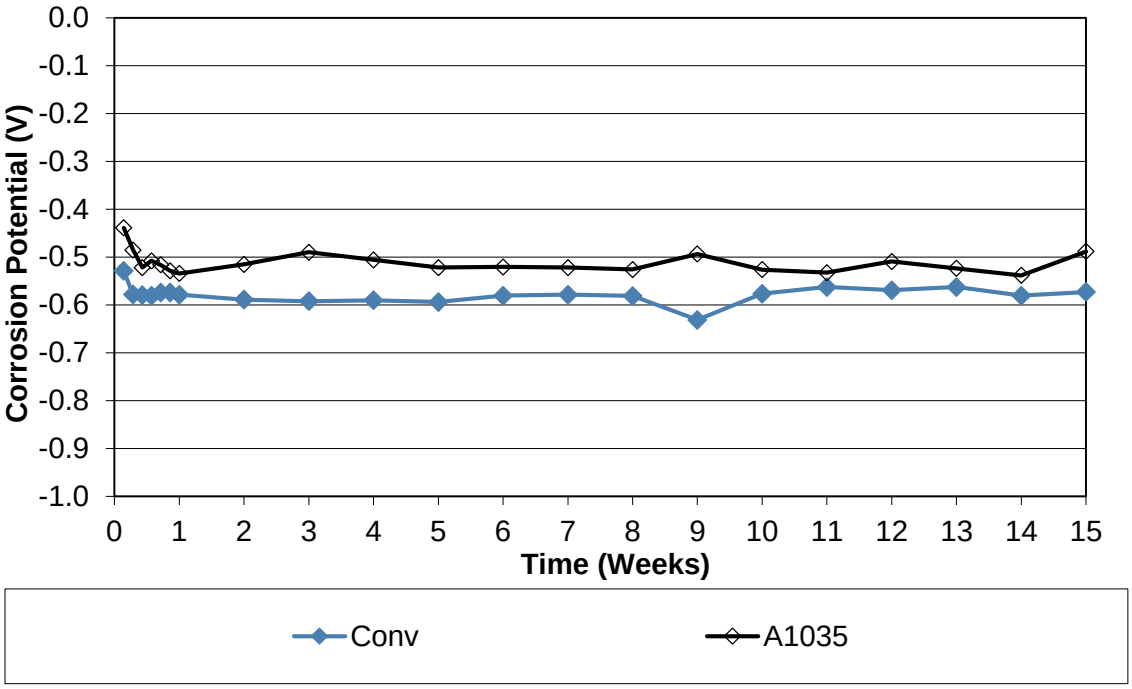

Figure 3.10: Rapid Macrocell Test. Average corrosion potentials of conventional and A1035 reinforcement vs. time.

3.1.2 Corrosion Losses at End of Testing

Table 3.1 shows the macrocell corrosion losses based on total area at the end of testing for all specimens in the rapid macrocell test. To determine the statistical significance of the differences in corrosion losses between corrosion protection systems, a two-tailed Student's t-test is used. Student's t-test is a method of statistical analysis that compares the means and variances of two data sets to determine the probability, *p*, that any differences between the two datasets could have arisen by chance; that is, differences in the mean values are due to the natural variability of the test program, not differences in the effectiveness of the corrosion protection systems. In this study, a value of 0.20 is used as the maximum threshold for statistical significance. Results for all Student's t-test comparisons are presented in Appendix B.

Individual conventional reinforcement specimens exhibited losses at the end of testing between 1.77 µm and 9.49 µm, with Conv-A bars (average loss of 3.97 µm) generally exhibiting lower losses than Conv-B or Conv-C bars (average losses of 6.98 and 7.17 µm, respectively), a difference that is statistically significant ($p < 0.02$). The losses of the Conv-A bars are low compared to those observed in earlier tests (Ji et al. 2005). The difference in corrosion losses between Conv-B and Conv-C is not statistically significant. ECR without UV exposure exhibited losses between 0.006 and 0.433 µm based on total area–two orders of magnitude lower than conventional reinforcement. UV exposure resulted in increased losses relative to ECR without UV damage, including losses over 2 µm for two specimens. In all cases, the differences in losses between specimens with and without UV exposure were statistically significant. Undamaged ECR showed no significant losses.

Both A767 and A1094 reinforcement exhibited significant variations in losses at the end of testing. As discussed earlier, the high pH liquid environment of the rapid macrocell test prevents a stable protective layer from forming on the zinc, resulting in active corrosion on both the bar in salt solution and the bars in pore solution without salt. This activity may not be captured by the macrocell corrosion losses, which are based on the current flow between the bar in salt solution and the bars in pore solution without salt.

A1035 reinforcement exhibited an average loss of 5.32 µm, greater than that observed for Conv-A ($p = 0.142$), and less than Conv-B or Conv-C ($p < 0.113$). The performance of A1035 reinforcement in the rapid macrocell test can therefore be considered comparable to that observed for conventional reinforcement.

Table 3.1: Rapid Macrocell Test-Macrocell Corrosion Losses based on Total Area at End of Testing (μm)

	Corrosion Loss						Average Loss	Std. Dev
	1	2	3	4	5	6		
Conv-A	2.64	6.52	3.48	1.77	4.53	4.88	3.97	1.70
Conv-B	7.20	6.60	8.60	9.47	6.25	3.73	6.98	2.00
Conv-C	9.49	7.28	5.74	6.14	6.42	7.96	7.17	1.39
ECR	0.106	0.433	0.059	0.006	0.278	0.006	0.15	0.172
ECR-ND	-0.002	-0.010	0.005	-0.010	0.016	-0.019	0.00	0.012
ECR-UV-1000	0.584	0.689	0.815	1.21	0.871	0.802	0.83	0.212
ECR-UV-1000 (b)	1.06	0.483	0.752	1.04	0.712	0.770	0.80	0.216
ECR-UV-500	1.32	1.15	0.932	1.06	1.30	0.786	1.09	0.211
ECR-UV-250	0.728	0.527	0.889	0.243	0.425	0.391	0.53	0.237
ECR2-UV-1000	2.65	0.257	0.326	0.201	0.532	-	0.79	1.04
ECR2-UV-200	0.965	0.557	0.674	0.717	2.02	0.542	0.91	0.563
ECR2-UV-100	0.913	0.536	0.440	0.403	0.573	0.505	0.56	0.183
ECR-UV-1000-ND	-0.005	-0.006	-0.001	0.059	0.085	-0.007	0.02	0.041
A767	10.76	14.02	6.65	22.49	17.27	8.07	13.21	5.98
A767-Bent	0.257	0.576	2.078	0.604	0.096	1.337	0.82	0.748
A767-ND	8.72	16.12	10.07	23.42	19.87	20.77	16.49	5.99
A1094	3.88	-2.05	0.350	1.57	3.37	0.140	1.21	2.21
A1094-Bent	2.62	1.49	1.73	0.604	0.528	1.60	1.43	0.780
A1094-ND	-0.184	-0.189	1.95	-0.021	-1.03	2.20	0.45	1.31
A1035	5.47	4.42	6.04	5.27	3.68	7.05	5.32	1.184

- No specimen

The values shown in Table 3.1 treat the corrosion losses as if they were uniformly distributed over the total surface area of the bar exposed to the simulated pore solution with salt. While this is a reasonably accurate assumption for uncoated and galvanized reinforcement, it does not capture the corrosion behavior of epoxy-coated reinforcement, where corrosion is concentrated near the damaged area on the coating, referred to as the exposed area. Table 3.2 presents the macrocell corrosion losses based on exposed area for damaged ECR. (The theoretical exposed area for undamaged ECR is 0, hence, corrosion losses based on exposed area are not presented for these specimens). ECR without UV exposure exhibited the lowest average losses based on exposed area, 18.7 μm. As discussed previously, any amount of UV exposure resulted in losses several times those observed on ECR without UV exposure, with average losses ranging from 67.4 to 138 μm. For all ECR specimens, the losses based on exposed area were several times greater than the losses exhibited by conventional reinforcement based on total area.

Table 3.2: Rapid Macrocell Test-Macrocell Corrosion Losses based on Exposed Area at End of Testing (μm)

	Corrosion Loss						Average Loss	Std. Dev
	1	2	3	4	5	6		
ECR	13.4	54.7	7.45	0.751	35.1	0.751	18.7	21.7
ECR-UV-1000	73.7	87.0	102.9	152.3	110.0	101.3	104.5	26.8
ECR-UV-1000 (b)	133.3	61.0	95.0	131.0	89.9	97.3	101.2	27.3
ECR-UV-500	167.1	145.8	117.7	133.7	164.4	99.2	138.0	26.6
ECR-UV-250	91.9	66.5	112.3	30.7	53.7	49.3	67.4	29.9
ECR2-UV-1000	334.4	32.4	41.2	25.3	67.2	-	100.1	131.9
ECR2-UV-200	121.8	70.3	85.1	90.5	254.8	68.4	115.2	71.1
ECR2-UV-100	115.2	67.6	55.6	50.8	72.3	63.8	70.9	23.1

- No specimen

Table 3.3 shows the total corrosion losses based on total area at 15 weeks obtained from the LPR measurements. These losses capture the macrocell losses obtained by voltage drop readings as well as localized corrosion on the bar. As expected, total losses are greater than macrocell losses; the trends observed on total losses, however, generally follow those observed in macrocell losses. Conventional reinforcement exhibited losses between 7.71 and 38.7 μm, with the Conv-A bars generally exhibiting lower losses than the Conv-B or Conv-C bars. In all cases, differences in losses between heats of conventional reinforcement were statistically significant ($p < 0.165$). For conventional reinforcement, total losses were two to three times macrocell losses. Damaged ECR exhibited losses between 0.054 and 0.606 μm, with UV exposure significantly increasing losses. Damaged ECR with UV exposure exhibited total corrosion losses 2 to 10 times higher than damaged ECR with no UV exposure. With the exception of ECR and ECR2-UV-100 ($p = 0.348$), the difference in losses between ECR with and without UV exposure was statistically significant. For most ECR specimens, total losses were 1.3 to 2.8 times the macrocell losses. Undamaged ECR showed no significant losses.

Both the A767 and A1094 bars exhibited losses regardless of damage to the coating; however, A767 reinforcement exhibited significantly higher losses than A1094 reinforcement, a difference that is statistically significant ($p < 0.04$). Damaged and bent A767 reinforcement exhibited average total losses of 687 and 1000 μm, compared to undamaged A767, which exhibited an average total loss of 105 μm. A1094 reinforcement exhibited average total losses two orders of magnitude lower, ranging from 3.34 to 7.37 μm. This should not be taken as a superior resistance to chlorides, but rather as a resistance to high-pH environments. For A767 reinforcement, total losses were two orders of magnitude larger than macrocell losses; for A1094 reinforcement, total losses were five to ten times larger than macrocell losses. As expected, the sacrificial behavior of the zinc resulted in more localized corrosion than observed for conventional reinforcement.

A1035 reinforcement exhibited average total losses between 2.45 μm and 5.82 μm, about one-third to one-fifth the losses observed on conventional reinforcement, a difference that is statistically significant ($p < 0.008$). This is in contrast to the observations from macrocell corrosion losses, where the corrosion losses of A1035 and conventional reinforcement were comparable.

Table 3.4 shows the total corrosion losses at 15 weeks based on exposed area obtained from the LPR measurements. Damaged ECR with UV exposure exhibited corrosion losses 2 to 10 times higher than damaged ECR with no UV exposure, with losses as high as 1934 µm based on exposed area. For most ECR specimens, total losses were 1.3 to 2.8 times those observed with macrocell losses.

Table 3.3: Rapid Macrocell Test-Total Corrosion Losses based on Total Area at End of Testing obtained from LPR measurements (µm)

	Corrosion Loss						Average Loss	Std. Dev
	1	2	3	4	5	6		
Conv-A	7.71	12.9	7.90	9.42	11.8	8.89	9.77	2.13
Conv-B	12.4	11.0	12.0	38.7	14.0	30.4	19.8	11.8
Conv-C	15.2	13.9	10.6	11.3	11.3	12.4	12.4	1.76
ECR	0.149	0.998	0.054	0.257	0.606	-	0.413	0.388
ECR-ND	0.000	0.000	0.000	0.081	0.000	0.000	0.014	0.033
ECR-UV-1000	1.87	15.32	1.37	2.85	2.83	2.04	4.38	5.39
ECR-UV-1000 (b)	2.54	1.91	2.00	2.78	1.64	2.06	2.15	0.424
ECR-UV-500	1.92	1.81	3.03	3.81	0.57	1.41	2.09	1.16
ECR-UV-250	0.652	1.14	2.56	0.691	0.691	0.451	1.03	0.781
ECR2-UV-1000	0.787	0.916	0.951	1.593	1.171	-	1.08	0.32
ECR2-UV-200	0.782	0.353	1.08	0.454	0.462	1.852	0.830	0.568
ECR2-UV-100	2.294	0.187	0.113	0.887	0.520	0.801	0.800	0.796
ECR-UV-1000-ND	0.005	0.663	0.020	0.313	0.573	0.052	0.271	0.293
A767	774.1	36.0	1068.0	779.0	534.9	930.1	687.0	365.3
A767-Bent	47.5	75.8	93.8	152.0	114.9	147.2	105.2	40.9
A767-ND	709.7	687.2	797.5	350.6	388.1	3068.7	1000.3	1029.5
A1094	6.81	2.32	7.06	5.39	10.84	8.02	6.74	2.82
A1094-Bent	7.20	20.77	3.25	1.24	8.35	3.41	7.37	7.08
A1094-ND	2.09	2.03	5.56	2.03	2.08	6.25	3.34	2.00
A1035	2.79	2.45	3.84	3.73	4.41	5.82	3.84	1.208

- No specimen

Table 3.4: Rapid Macrocell Test-Total Corrosion Losses based on Exposed Area at End of Testing obtained from LPR measurements (µm)

	Corrosion Loss						Average Loss	Std. Dev
	1	2	3	4	5	6		
ECR	18.8	126.0	6.8	32.5	76.5	_	52.1	49.0
ECR-UV-1000	236.6	1934.6	172.5	359.5	356.8	257.2	552.9	680.8
ECR-UV-1000 (b)	320.4	240.8	251.9	350.7	206.9	259.7	271.7	53.5
ECR-UV-500	241.9	228.0	382.9	480.5	71.7	178.4	263.9	146.4
ECR-UV-250	82.3	143.4	322.7	87.2	87.2	56.9	130.0	98.6
ECR2-UV-1000	99.3	115.6	120.0	201.1	147.9	_	136.8	40.0
ECR2-UV-200	98.7	44.5	136.2	57.4	58.3	233.8	104.8	71.7
ECR2-UV-100	289.6	23.6	14.2	112.0	65.7	101.2	101.0	100.5

- No specimen

3.1.3 End of Test Photos and Disbondment Results

Figure 3.11 shows specimen Conv-B-5 after 15 weeks of testing, and is representative of all Conv specimens in the rapid macrocell test. Significant corrosion products are visible on the anode bar (the bar in salt solution), particularly at and above the 3-in. waterline. No corrosion products were observed on the cathode bars (the bars in pore solution without salt).

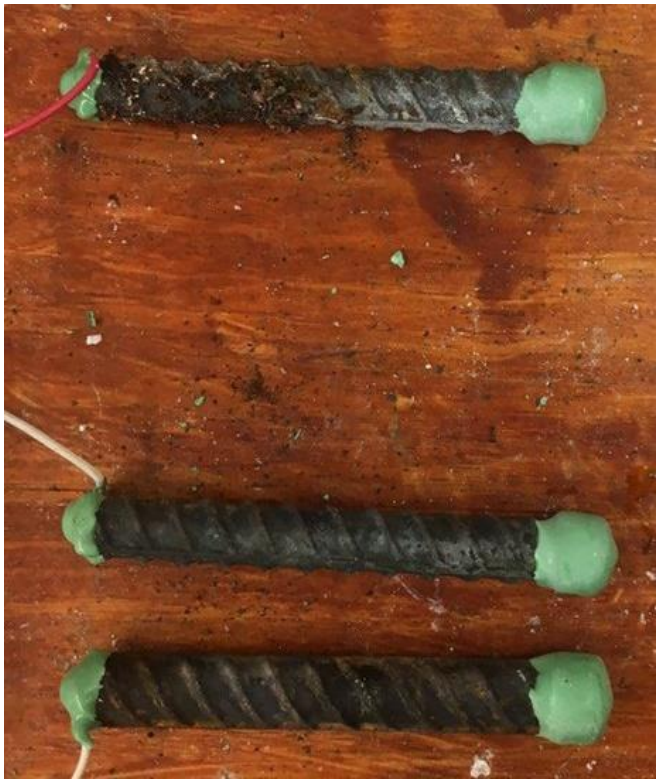

Figure 3.11: Rapid Macrocell Test. Specimen Conv-B-5 anode bar (top) and cathode bars (bottom)

Figure 3.12 shows specimen ECR-2 after 15 weeks of testing. As observed on most damaged ECR specimens, some of the damage sites on the anode bar showed signs of rust, and other damage sites appeared clean. No blistering or other distress was visible in the undamaged portions of the coating.

All damaged ECR bars underwent a disbondment test after testing, as described in Chapter 2. Figure 3.13 shows specimen ECR-2 after the disbondment test. As shown in the figure, a significant portion of the coating disbonded from the underlying metal, both at sites with and without visible corrosion at the hole. Full disbondment results are described later in this section (Table 3.5).

Figure 3.12: Rapid Macrocell Test. Specimen ECR-2 anode bar (top) and cathode bars (bottom)

Figure 3.13: Rapid Macrocell Test. Specimen ECR-2 anode bar after disbondment test

Figures 3.14 and 3.15 show specimen ECR-UV-1000-4 after 15 weeks of testing, before and after the disbondment test. Corrosion products were visible at all damage sites, and the coating readily disbonded. Discoloration of the ECR from the UV exposure was observed on all bars exposed to UV light, but no other distress was observed on the coating. Similar trends

were noted on bars with lower periods of UV exposure (Figures 3.16 through 3.18). For undamaged ECR both with and without UV exposure, no disbondment was observed on any of the bars (Figure 3.19).

Figure 3.14: Rapid Macrocell Test. Specimen ECR-UV-1000-4 anode bar (top) and cathode bars (bottom)

Figure 3.15: Rapid Macrocell Test. Specimen ECR-UV-1000-4 anode bar after disbondment test

Figure 3.16: Rapid Macrocell Test. Specimen ECR-UV-500-5 anode bar after disbondment test

Figure 3.17: Rapid Macrocell Test. Specimen ECR2-UV-200-3 anode bar after disbondment test

Figure 3.18: Rapid Macrocell Test. Specimen ECR2-UV-100-4 anode bar after disbondment test

Figure 3.19: Rapid Macrocell Test. Specimen ECR-ND-6 anode bar after disbondment test

Table 3.5 summarizes the measured disbonded area on the ECR specimens at the end of testing. As described in Chapter 2, disbondment that extended more than 0.5 in. from the intentional damage site in all directions was classified as total disbondment and was assigned a disbonded area of 1.05 in.^{2} As shown in the table, damaged ECR not exposed to UV light exhibited a relatively low amount of disbondment, averaging 0.057 in.^{2}; any amount of UV exposure resulted in significant increases in disbondment, often by an order of magnitude compared to the specimens with no UV exposure. For the ECR2 specimens, disbondment appeared to increase as the amount of UV exposure increased; this trend was not observed on the first heat of ECR bars. Undamaged ECR, both with and without UV exposure, did not exhibit disbondment.

Figures 3.20 and 3.21 show A767 and A1094 reinforcement after 15 weeks of testing and are representative of all galvanized bars in this study. Heavy corrosion was observed on both the anode and cathode bars. This suggests corrosion was due to the high pH of the macrocell pore solution, and not solely due to chloride exposure. The rapid macrocell test results should, therefore, not be considered as representative of the performance of galvanized reinforcement in the concrete.

Table 3.5: Rapid Macrocell Test-Measured Disbondment (in.^{2}) at End of Testing

	Specimen						
	1	**2**	**3**	**4**	**5**	**6**	**Average**
ECR	0.0475	0.1025	0.0375	-	0.155	-	0.057
ECR-ND	-	-	-	-	-	-	0.000
ECR-UV-1000	0.168	0.253	0.388	0.293	0.303	0.240	0.274
ECR-UV-1000 (b)	0.300	0.430	0.725	0.305	0.250	0.300	0.385
ECR-UV-500	0.640	0.298	0.238	0.670	0.205	0.315	0.394
ECR-UV-250	0.613	0.498	0.840	0.565	0.195	0.190	0.483
ECR2-UV-1000	1.05	1.05	0.708	1.05	1.05	1.05	0.993
ECR2-UV-200	0.585	0.225	1.05	0.593	0.235	1.05	0.623
ECR2-UV-100	0.643	0.058	0.070	0.605	0.163	0.175	0.285
ECR-UV-1000-ND	-	-	-	-	-	-	0.000

Figure 3.20: Rapid Macrocell Test. Specimen A767-1 anode bar (top) and cathode bars (bottom)

Figure 3.21: Rapid Macrocell Test. Specimen A1094-4 anode bar (top) and cathode bars (bottom)

Figure 3.22 shows specimen A1035-6 after 15 weeks of testing, and is representative of all A1035 specimens in the rapid macrocell test. Significant corrosion products are visible on the anode bar, particularly at and above the 3-in. waterline. No corrosion products were observed on the cathode bars.

Figure 3.22: Rapid Macrocell Test. Specimen A1035-6 anode bar (top) and cathode bars (bottom)

3.2 Southern Exposure and Cracked Beam Tests

The Southern Exposure and cracked beam tests were used to evaluate conventional, epoxy-coated, galvanized, and A1035 (ChromX) reinforcement. Coated bars were evaluated in both the undamaged condition (-ND) and with ten 0.125-in. diameter holes in the coating, simulating damage that occurs during handling and placement of reinforcement on a job site. Epoxy-coated reinforcement (ECR) was also evaluated after 1000 hours of UV exposure, simulating outdoor storage, and galvanized bars were evaluated with a 180-degree bend. In addition, the effects of Ipanex and Xypex, two waterproofing admixtures, were studied in conjunction with conventional and A1035 reinforcement.

3.2.1 Macrocell Corrosion Rates and Potentials

3.2.1.1 Conventional Reinforcement

Figure 3.23 shows the average macrocell corrosion rates based on total bar area in the Southern Exposure test for the three heats of conventional reinforcement evaluated in this study. For all three heats of steel, the average corrosion rate gradually increased through the first 30 weeks of testing before leveling off. After 24 weeks, Conv-A exhibited corrosion rates that were lower (generally in the range of 2-4 µm/yr) than those observed on Conv-B or Conv-C (generally in the range of 6-10 µm/yr). These rates were one-third to one-fifth the rates observed in the rapid macrocell test.

In the cracked beam test (Figure 3.24), both Conv-A and Conv-C exhibited corrosion rates near 15 µm/yr at the start of testing, dropping to 5 µm/yr by week 40 and remaining in the 5-10 µm/yr range for the duration of testing. Conv-B exhibited greater corrosion rates, starting near 25 µm/yr, and dropping to the 10-15 µm/yr range after week 40. All specimens exhibited the greatest corrosion rate at the start of testing; the corrosion rate gradually decreased as corrosion products filled the crack and inhibited the ingress of additional oxygen and chlorides.

In the cracked beam test, two specimens with Conv-B reinforcement, Conv-B-3 and Conv-B-4, exhibited enough corrosion to crack the concrete (Figure 3.25). These specimens were removed from testing early, at weeks 49 and 67, respectively.

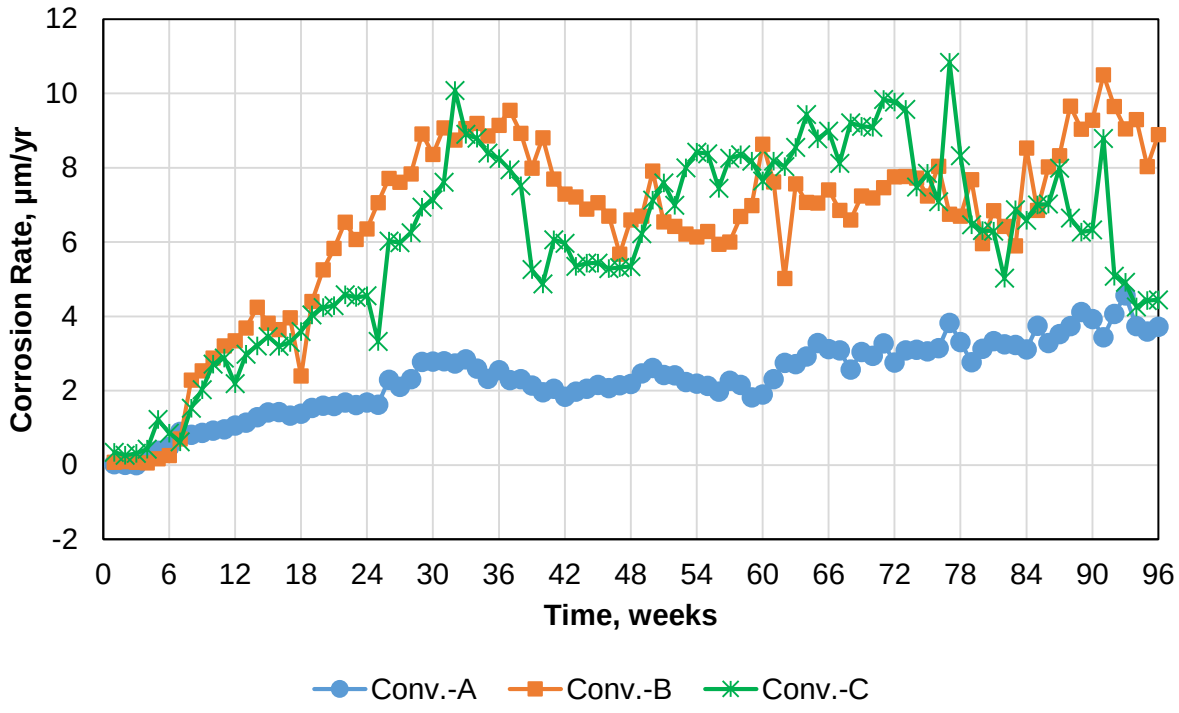

Figure 3.23: Southern Exposure test. Average macrocell corrosion rate vs. time. Corrosion rate based on total bar area of conventional reinforcement.

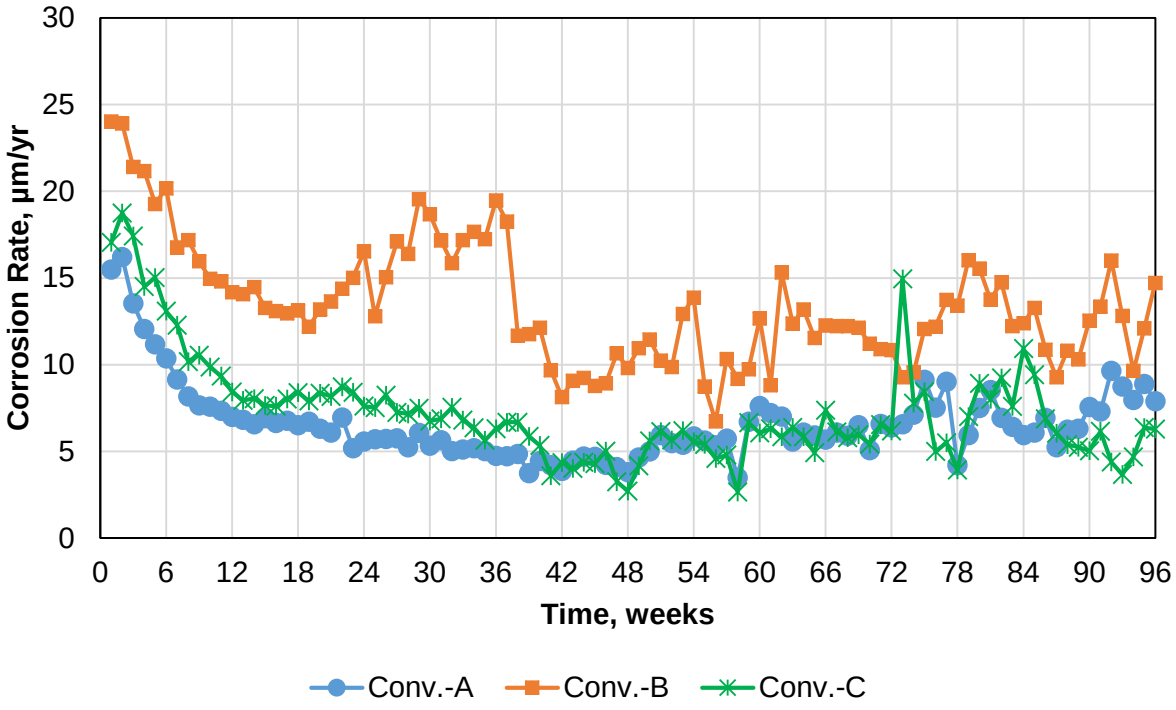

Figure 3.24: Cracked beam test. Average macrocell corrosion rate vs. time. Corrosion rate based on total bar area of conventional reinforcement.

Figure 3.25: Cracked beam test. Cracking of concrete in specimen Conv-B-3.

Figures 3.26 and 3.27 show the average corrosion potentials versus a copper/copper sulfate electrode (CSE) for the three heats of conventional reinforcement under the Southern Exposure and cracked beam tests, respectively. At the initiation of the Southern Exposure test (Figure 3.26), all three heats of steel exhibited a corrosion potential of approximately –0.200 V vs. CSE, indicating a >90% probability of no corrosion per ASTM C876. As corrosion initiated, the corrosion potential became more negative, reaching values between –0.450 V and –0.600 V by week 48 and remaining there for the remainder of the test. Throughout the duration of the cracked beam test (Figure 3.27), all three heats of steel exhibited corrosion potentials more negative than –0.400 V, indicating >90% probability of active corrosion per ASTM C876.

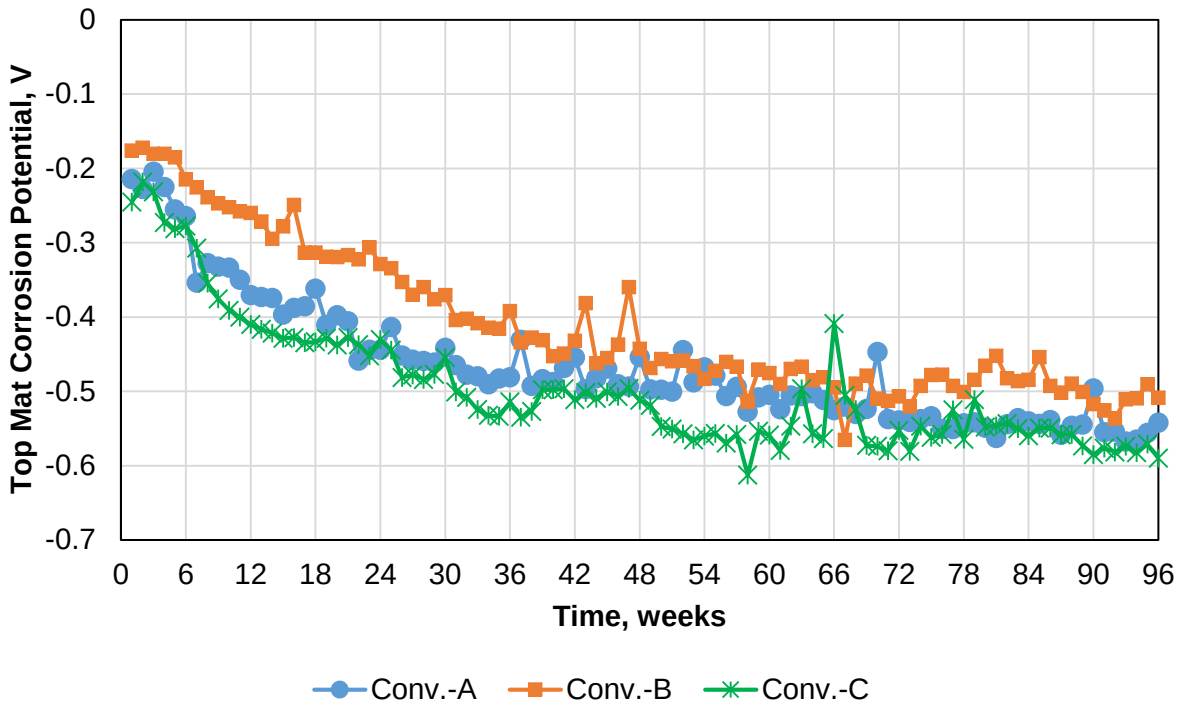

Figure 3.26: Southern Exposure test. Average corrosion potentials of conventional reinforcement vs. time.

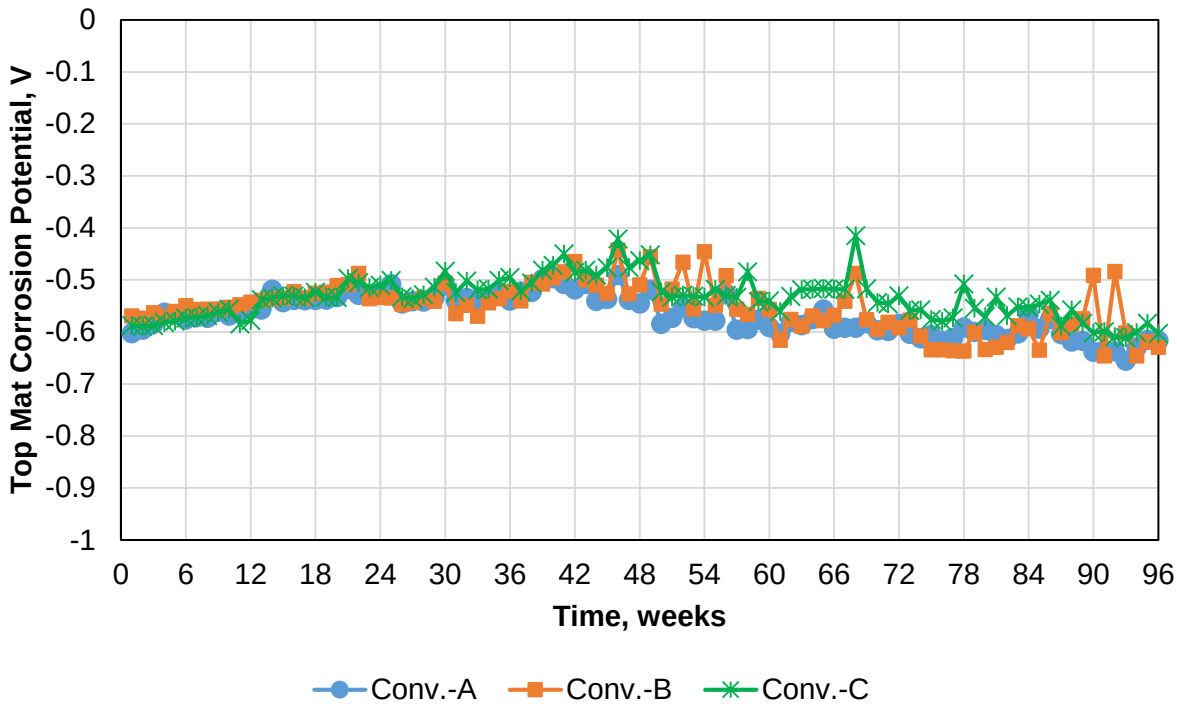

Figure 3.27: Cracked beam test. Average corrosion potentials of conventional reinforcement vs. time.

3.2.1.2 Epoxy-Coated Reinforcement (ECR)

Figures 3.28 and 3.29 show the average macrocell corrosion rate based on total bar area for specimens with damaged epoxy-coated reinforcement in the Southern Exposure and cracked beam tests, respectively. In the Southern Exposure test, damaged ECR with no UV exposure exhibited no corrosion activity through 30 weeks of testing. After 30 weeks, the corrosion rate periodically jumped to as high as 0.2 µm/yr for limited periods of time before returning to 0. Damaged ECR with 1000 hours of UV exposure exhibited corrosion at an earlier age than damaged ECR with no UV exposure. Damaged ECR with UV exposure started showing corrosion activity after 24 weeks; after week 48, corrosion rates were consistently above 0.3 µm/yr, peaking at over 0.6 µm/yr. Undamaged ECR exhibited no significant corrosion. In the cracked beam test, damaged ECR with UV exposure exhibited corrosion from the start of testing, quickly exceeding and an average value of 2 µm/yr. After week 20, the corrosion activity of ECR-UV-1000 declined, to around 1 µm/yr by week 32, where it remained for the remainder of testing. Damaged ECR without UV exposure also exhibited corrosion activity from the start of testing, but at much lower rates–0.1 to 0.2 µm/yr. Undamaged ECR with UV exposure exhibited corrosion rates in the range of 0.1 to 0.2 µm/yr for the first 72 weeks of testing–comparable to damaged ECR without UV exposure. After week 72, however, the corrosion rate of ECR-UV-ND-1000 began to increase, with spikes in corrosion rate as high as 0.8 µm/yr. Undamaged ECR without UV exposure only exhibited isolated single-week spikes of corrosion activity.

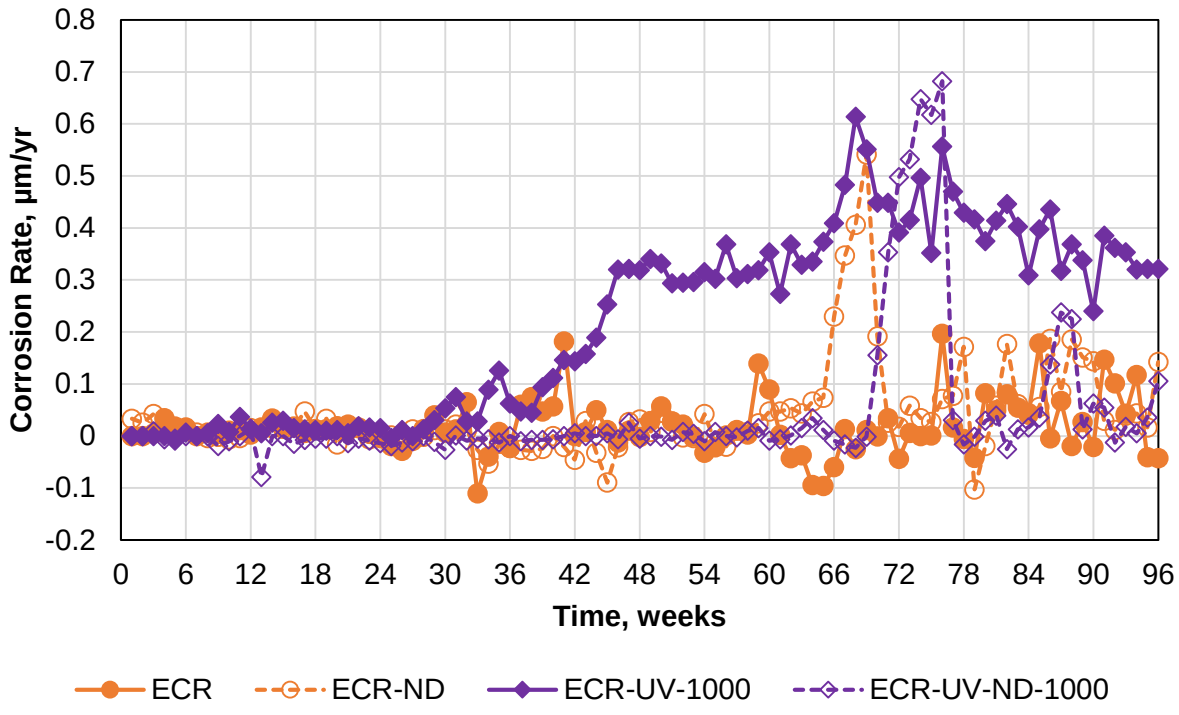

Figure 3.28: Southern Exposure test. Average macrocell corrosion rate vs. time. Corrosion rate based on total bar area of epoxy-coated reinforcement.

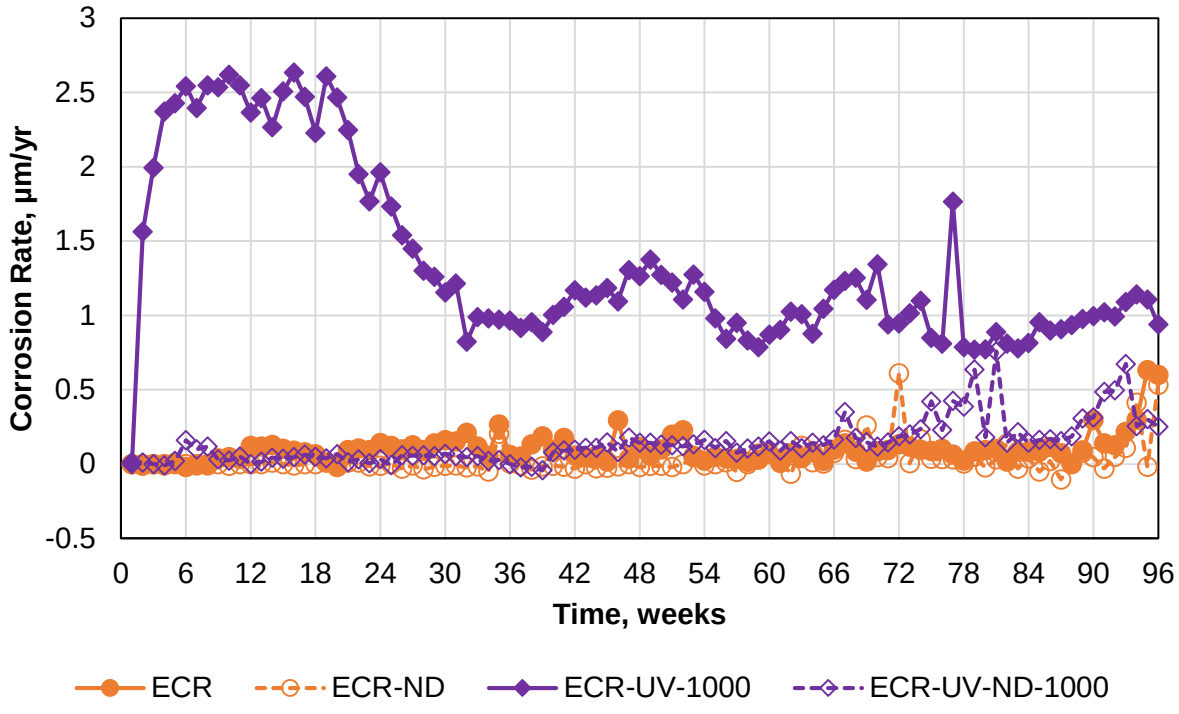

Figure 3.29: Cracked beam test. Average macrocell corrosion rate vs. time. Corrosion rate based on total bar area of epoxy-coated reinforcement.

Figures 3.30 and 3.31 show the average corrosion potentials with respect to a CSE for specimens with epoxy-coated reinforcement in the Southern Exposure and cracked beam tests, respectively. In the Southern Exposure test, ECR and ECR-ND specimens exhibited an average potential of –0.25 and –0.35 V, respectively, at the start of testing. Potentials for both series of specimens approached –0.3 V by week 30 and generally remained around –0.3 V for the duration of testing. ECR with UV exposure-both with and without damage-exhibited potentials more positive than –0.2 V for the first 18 weeks of testing. After week 18, ECR-UV-1000 specimens exhibited a gradual decline in potential, followed by a more drastic drop in corrosion potential around week 42, corresponding with the time the corrosion rate on these specimens increased. After week 48, ECR-UV-1000 specimens exhibited a corrosion potential more negative than –0.400 V, more negative than any other ECR specimens. ECR-UV-ND-1000 specimens exhibited potentials that gradually became more negative, approaching –0.3 V by the end of testing.

In the cracked beam test (Figure 3.31), specimens generally exhibited corrosion potentials that remained approximately constant after the first few weeks of testing. Specimens with UV exposure consistently exhibited more negative potentials than specimens without UV exposure. Damaged ECR with 1000 hours of UV exposure consistently exhibited the most negative potentials, around –0.6 V. Damaged ECR without UV exposure exhibited potentials around –0.2 V early in testing; the potential rapidly dropped to –0.5 V after week 6 before recovering to between –0.3 and –0.4 V. Undamaged ECR with UV exposure exhibited potentials between –0.4 and –0.5 V, whereas undamaged ECR with UV exposure generally exhibited potentials between –0.2 and –0.3 V.

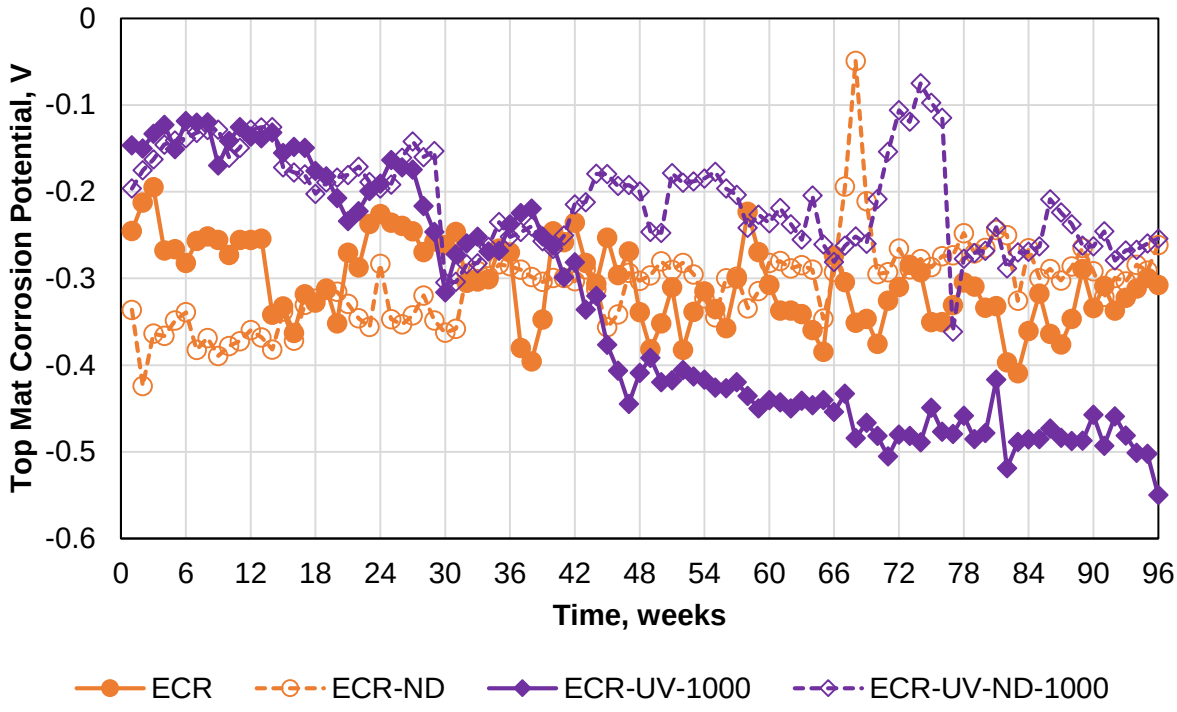

Figure 3.30: Southern Exposure test. Average corrosion potentials of epoxy-coated reinforcement vs. time.

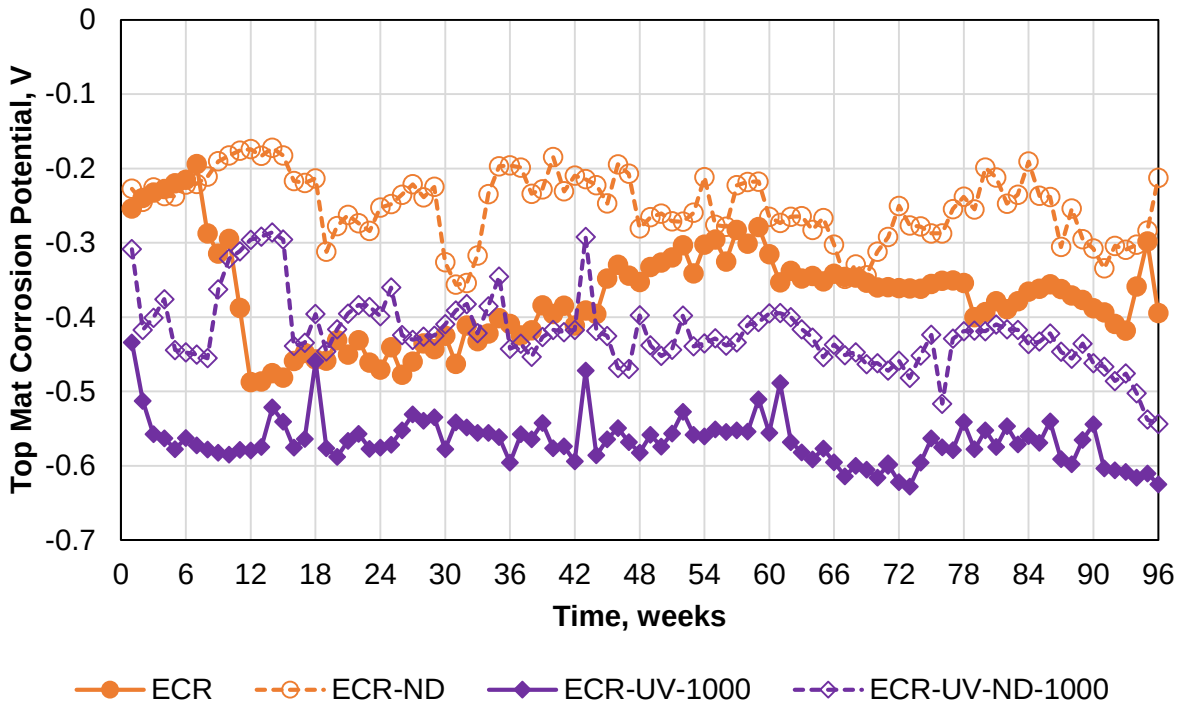

Figure 3.31: Cracked beam test. Average corrosion potentials of epoxy-coated reinforcement vs. time.

3.2.1.3 Galvanized Reinforcement

Figures 3.32 and 3.33 show the average macrocell corrosion rates based on total area for A767 and A1094 galvanized reinforcement in the Southern Exposure and cracked beam tests, respectively. Conventional reinforcement (representing the average of the three heats of conventional reinforcement used in this study) is shown for reference. In the Southern Exposure test, both A767 and A1094 reinforcement exhibited some corrosion activity early in the test, with corrosion rates generally in the range of 1 to 2 µm/yr. By week 30, the corrosion rate of all specimens had dropped to 0 or became negative, indicating corrosion activity on the bottom mat as well as the top mat of steel. A767 reinforcement began exhibiting corrosion activity again around week 54, with corrosion rates again in the range of 1 to 2 µm/yr. A1094 reinforcement exhibited some corrosion activity around week 78, with rates generally less than 1 µm/yr. No difference in behavior was noted between damaged, undamaged, and bent specimens. For all galvanized bars, corrosion rates after week 20 were much lower than for conventional reinforcement.

In the cracked beam test, all galvanized bars exhibited very high corrosion activity in the first few weeks of testing, with initial corrosion rates between 15 and 20 µm/yr. Corrosion rates rapidly dropped to less than 4 µm/yr by week 10, and gradually decreased to 1 to 2 µm/yr by week 40. Corrosion rates for A767 reinforcement began to increase after week 42, reaching as high as 5 µm/yr, while corrosion rates on A1094 reinforcement increased after week 70. Corrosion rates for galvanized bars were one-third to one-fourth that of conventional reinforcement. It should be noted, however, that the A767 reinforcement used Conv-B reinforcement as a base layer, which exhibited much greater corrosion activity than the Conv-C

reinforcement used by the A1094 reinforcement, so the differences in behavior between the two types of galvanized reinforcement may not be due to differences in the coating–particularly for the damaged bars where the underlying steel was exposed.

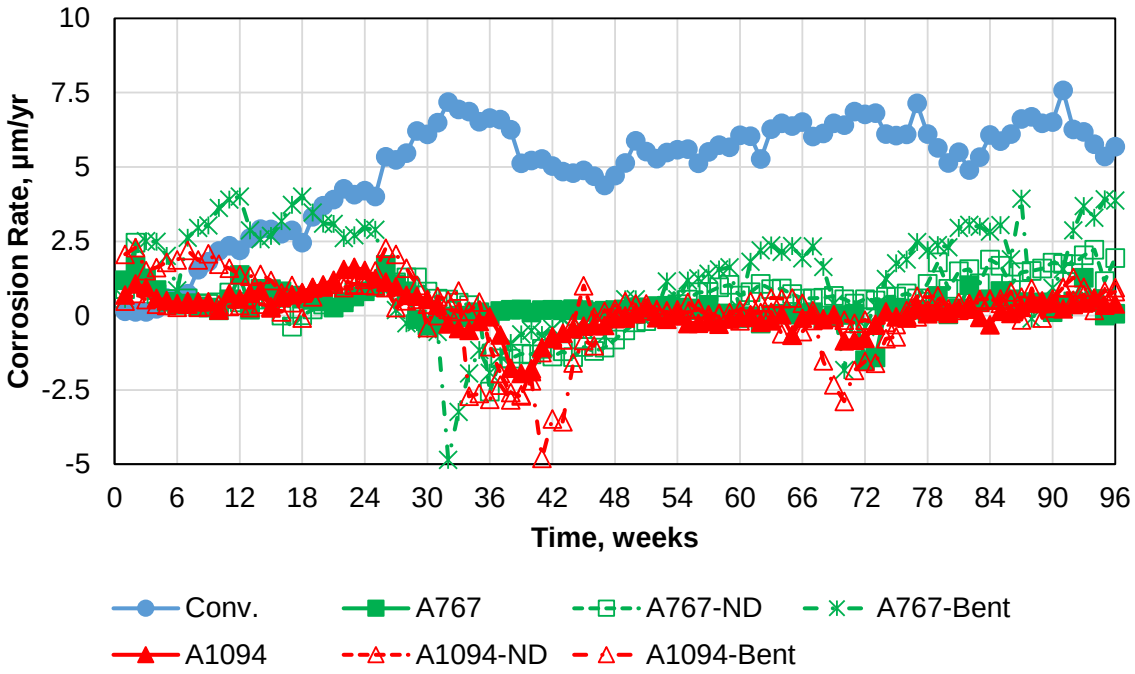

Figure 3.32: Southern Exposure test. Average macrocell corrosion rate vs. time. Corrosion rate based on total bar area of conventional, A767, and A1094 reinforcement.

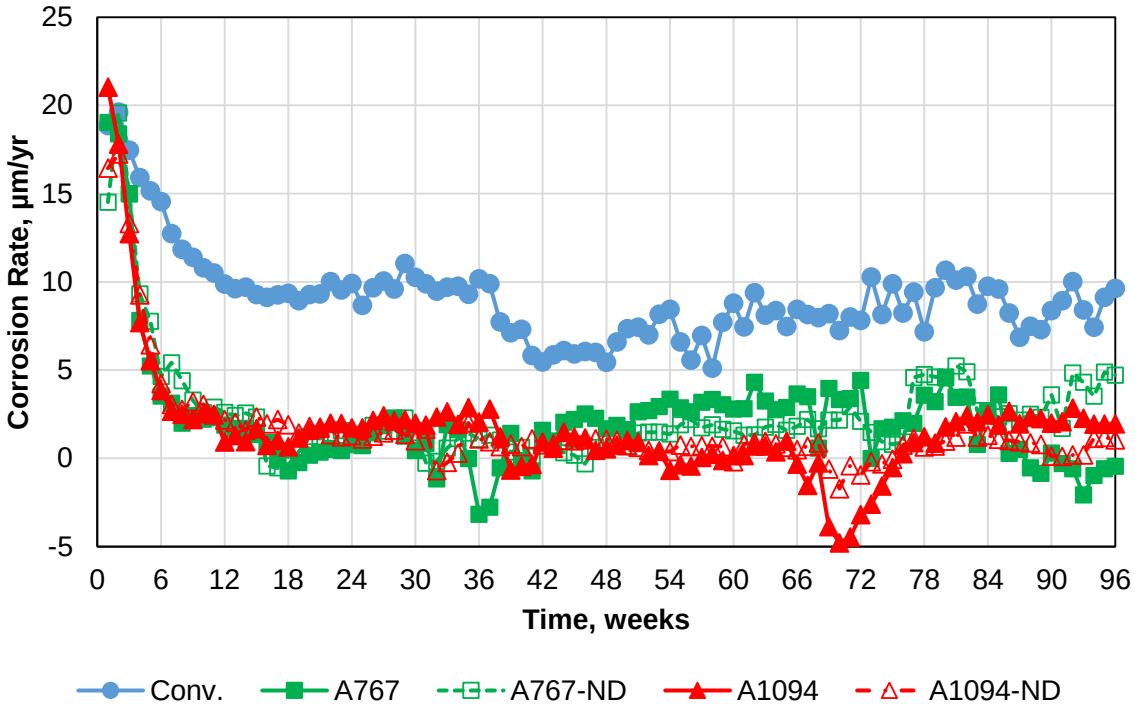

Figure 3.33: Cracked beam test. Average macrocell corrosion rate vs. time. Corrosion rate based on total bar area of conventional, A767, and A1094 reinforcement.

Figures 3.34 and 3.35 show the average corrosion potentials versus a CSE for A767 and A1094 galvanized reinforcement in the Southern Exposure and cracked beam tests, respectively. In the Southern Exposure test, damaged and undamaged A767 had an initial potential around –0.5 V, while damaged and undamaged A1094 had an initial potential around –0.7 V. The potentials for A767 and A1094 gradually increased over the first 30 weeks (reaching –0.4 and –0.5 V, respectively), then remained approximately constant. A767 reinforcement exhibited a drop in potential after 72 weeks in the Southern Exposure test; other specimens with galvanized reinforcement exhibited stable potentials. In the cracked beam test, damaged and undamaged A767 had an initial potential around –0.8 V, while damaged and undamaged A1094 had an initial potential around –1.0 V. The potentials for A767 and A1094 gradually increased over the first 18 weeks (reaching –0.5 and –0.6 V, respectively), then remained approximately constant.

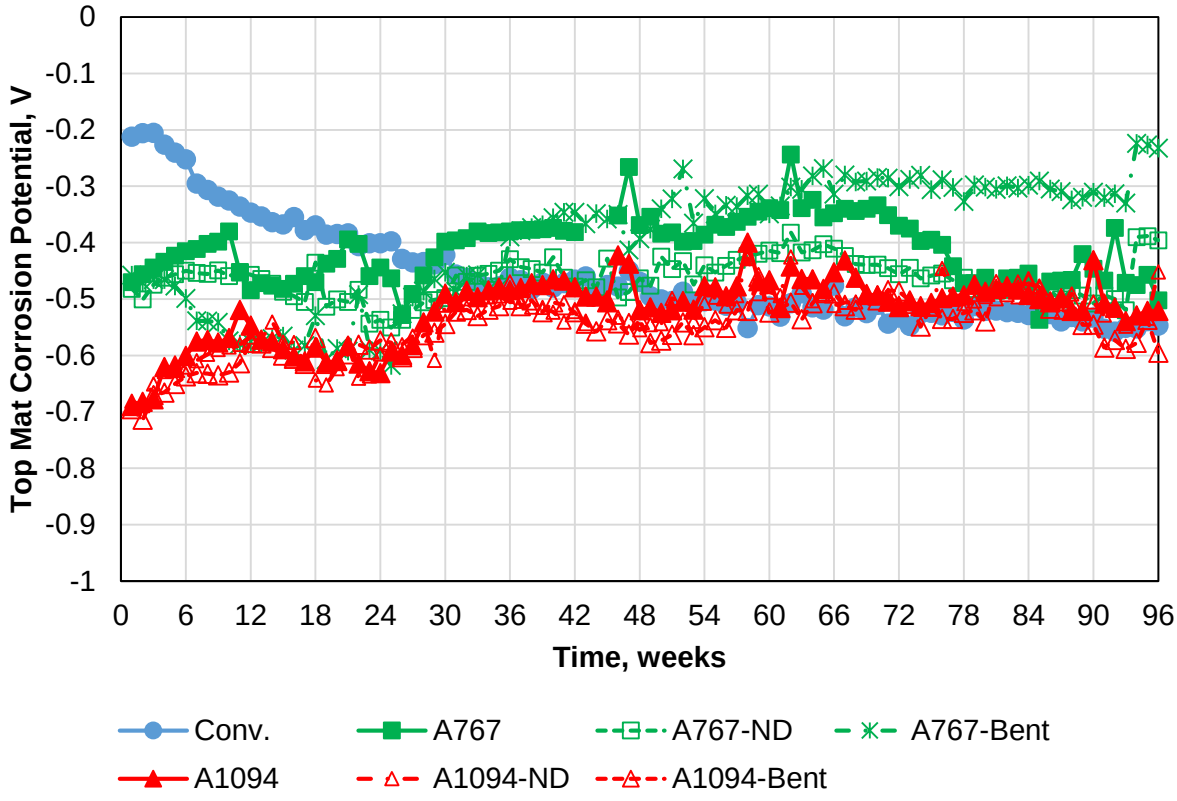

Figure 3.34: Southern Exposure test. Average corrosion potentials of conventional, A767, and A1094 reinforcement vs. time.

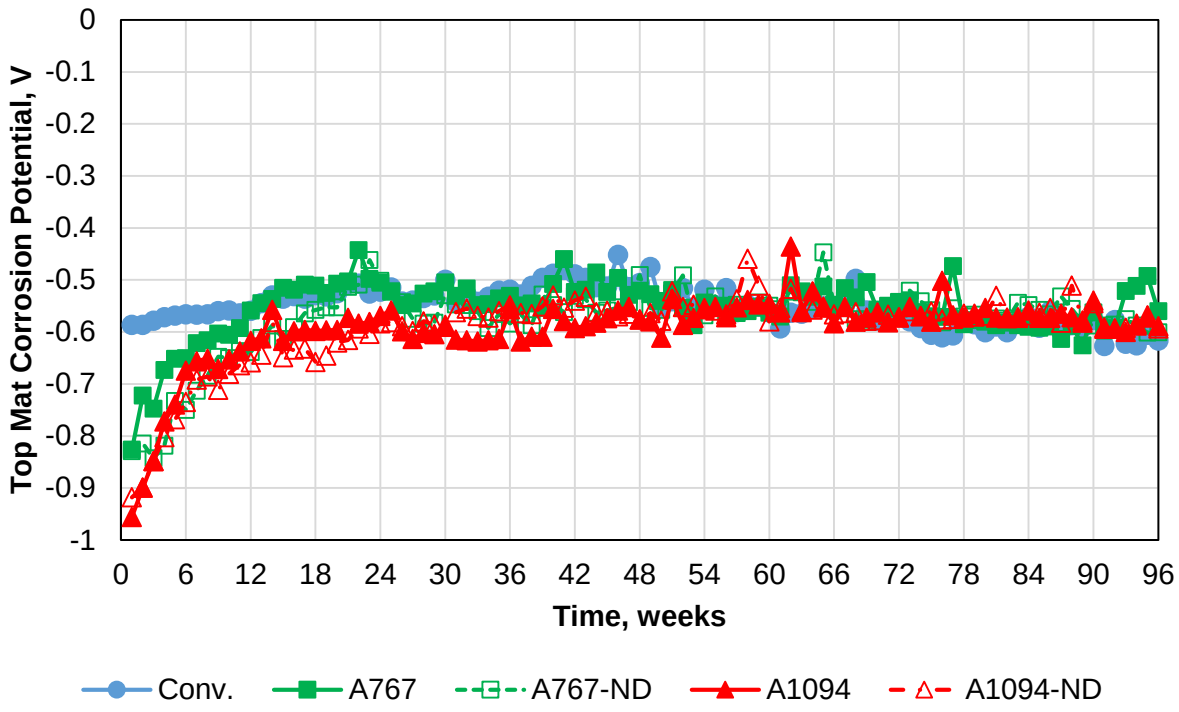

Figure 3.35: Cracked beam test. Average corrosion potentials of conventional, A767, and A1094 reinforcement vs. time.

3.2.1.4 A1035 (ChromX) Reinforcement, Ipanex, and Xypex

Figures 3.36 and 3.37 show the average macrocell corrosion rates based on total bar area for conventional and A1035 (ChromX) reinforcement in the Southern Exposure and cracked beam tests, respectively. Results are presented for bars in concrete with and without Ipanex and Xypex. Of the three heats of conventional reinforcement, only Conv-B was evaluated with the two admixtures. In both tests, A1035 reinforcement exhibited significantly lower corrosion rates than conventional reinforcement, ranging from approximately one-fifth to one-half the corrosion rate of conventional reinforcement. In the Southern Exposure test, A1035 reinforcement exhibited corrosion rates less than 2 µm/yr throughout testing, whereas Conv-B reinforcement exhibited rates as high as 10 µm/yr. In the cracked beam test, A1035 reinforcement exhibited corrosion rates less than 5 µm/yr throughout testing, whereas Conv-B reinforcement exhibited rates as high as 25 µm/yr early in testing, with rates in the 10-15 µm/yr range later in the test. This is in contrast to the results from the rapid macrocell test, where A1035 reinforcement exhibited corrosion rates comparable to that of conventional reinforcement. The behavior of A1035 reinforcement in concrete is considered more representative of field performance than that in the rapid macrocell test.

The addition of Ipanex did not significantly alter the corrosion rate of either conventional or A1035 reinforcement in the Southern Exposure and cracked beam tests. In the cracked beam test, four specimens with conventional reinforcement and Ipanex cracked due to excessive corrosion and had to be removed from testing prior to 96 weeks (Conv-B-Ipanex-1 at week 55, Conv-B-Ipanex-2 at week 77, Conv-B-Ipanex-4 at week 81, and Conv-B-Ipanex-5 at week 80). Specimens with conventional reinforcement and Xypex, however, exhibited lower corrosion

rates than conventional reinforcement by itself, particularly after 18 weeks of testing. In the Southern Exposure test, specimens with conventional reinforcement with Xypex exhibited a maximum average macrocell corrosion rate of 6 µm/yr, with an average corrosion rate around 4 µm/yr. Without Xypex, the corrosion rates of conventional reinforcement exhibited a maximum corrosion rate of 10 µm/yr and an average rate in the 6-8 µm/yr range after week 24. In the cracked beam test, specimens with conventional reinforcement with Xypex exhibited a maximum corrosion rate of 10 µm/yr after week 18, with an average corrosion rate around 6 µm/yr. Without Xypex, the corrosion rates of conventional reinforcement exhibited a maximum corrosion rate of 20 µm/yr and an average rate in the 10-15 µm/yr range after week 24. Xypex claims to reduce the permeability of concrete over time by filling the concrete pores, which, if true, may explain the improved relative performance later in testing.

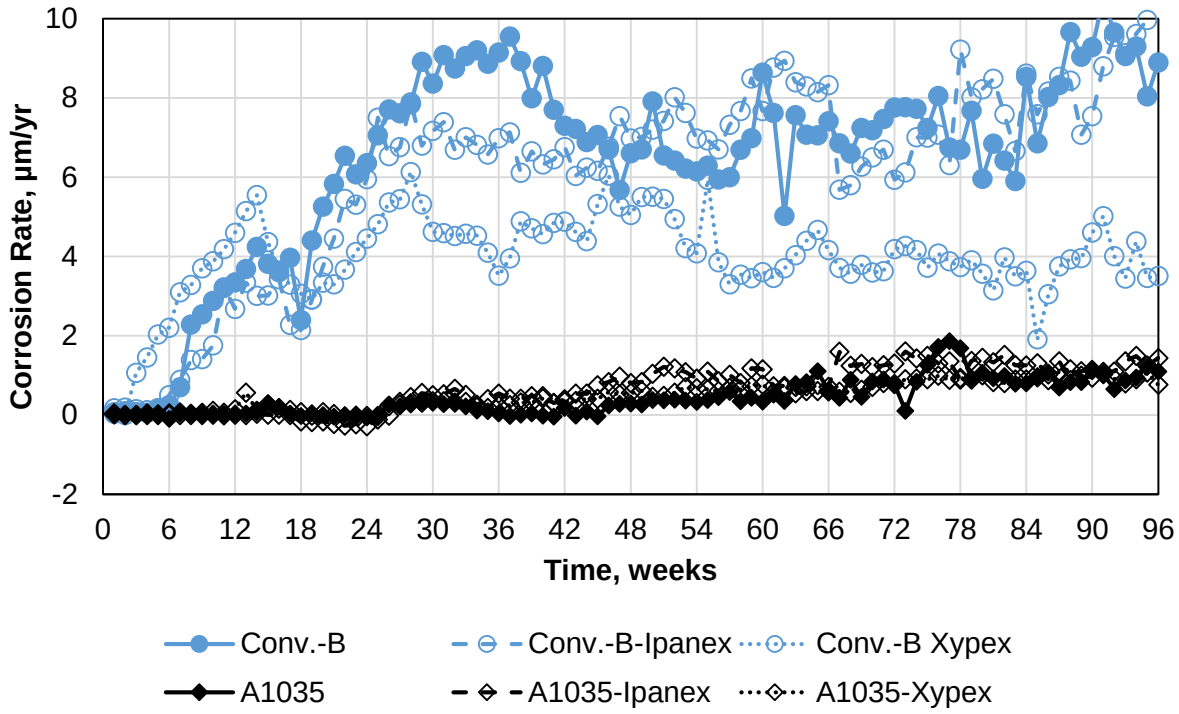

Figure 3.36: Southern Exposure test. Average macrocell corrosion rate vs. time. Corrosion rate based on total bar area of Conv-B and A1035 reinforcement with and without Ipanex and Xypex.

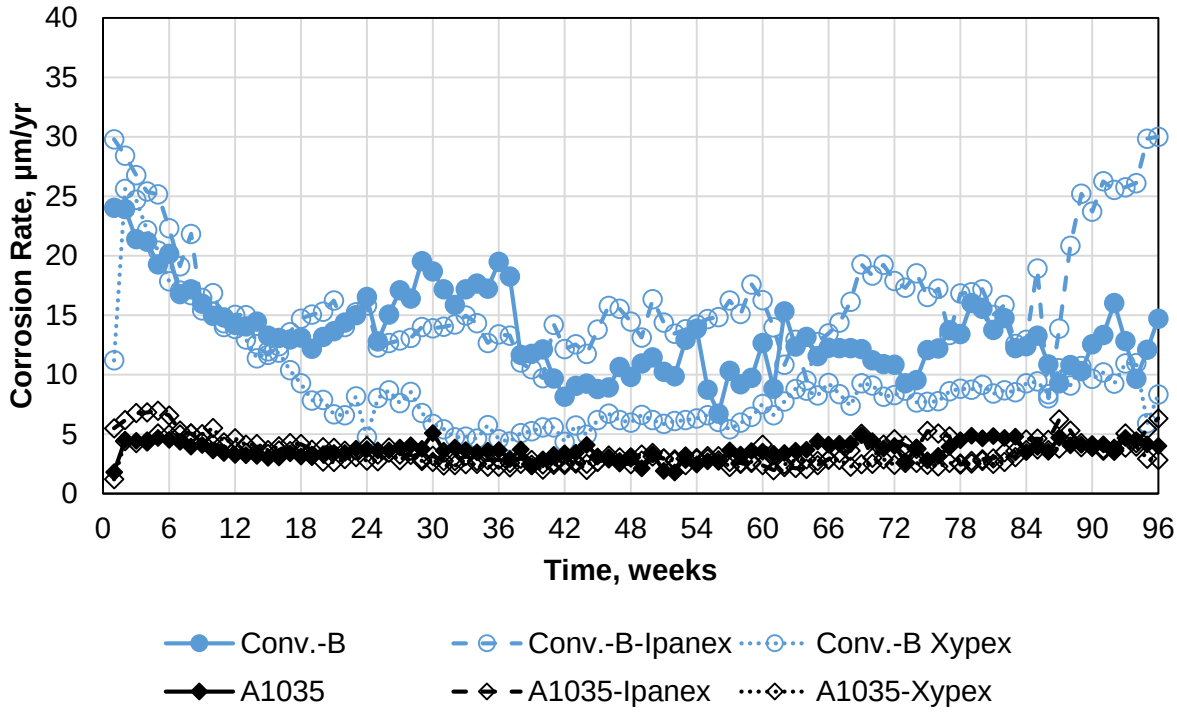

Figure 3.37: Cracked beam test. Average macrocell corrosion rate vs. time. Corrosion rate based on total bar area of Conv-B and A1035 reinforcement with and without Ipanex and Xypex

Figures 3.38 and 3.39 show the average corrosion potentials for conventional and A1035 reinforcement in the Southern Exposure and cracked beam tests, respectively. Results are presented for bars in concrete with and without Ipanex and Xypex. In both tests, conventional reinforcement exhibited a potential approximately –0.1 V more negative than A1035 reinforcement for most of the test. In the Southern Exposure test, all specimens started testing with a potential of approximately –0.2 V; potentials dropped as specimens initiated corrosion, with conventional and A1035 reinforcement reaching potentials of –0.4 and –0.3 V, respectively, by week 30. Potentials for both specimens decreased by another –0.1 V by week 96. In the cracked beam test, specimens exhibited a consistent corrosion potential throughout the test, with A1035 reinforcement exhibiting a potential around –0.5 V and Conv-B reinforcement exhibiting a potential around –0.6 V. Neither admixture had a significant effect on corrosion potential.

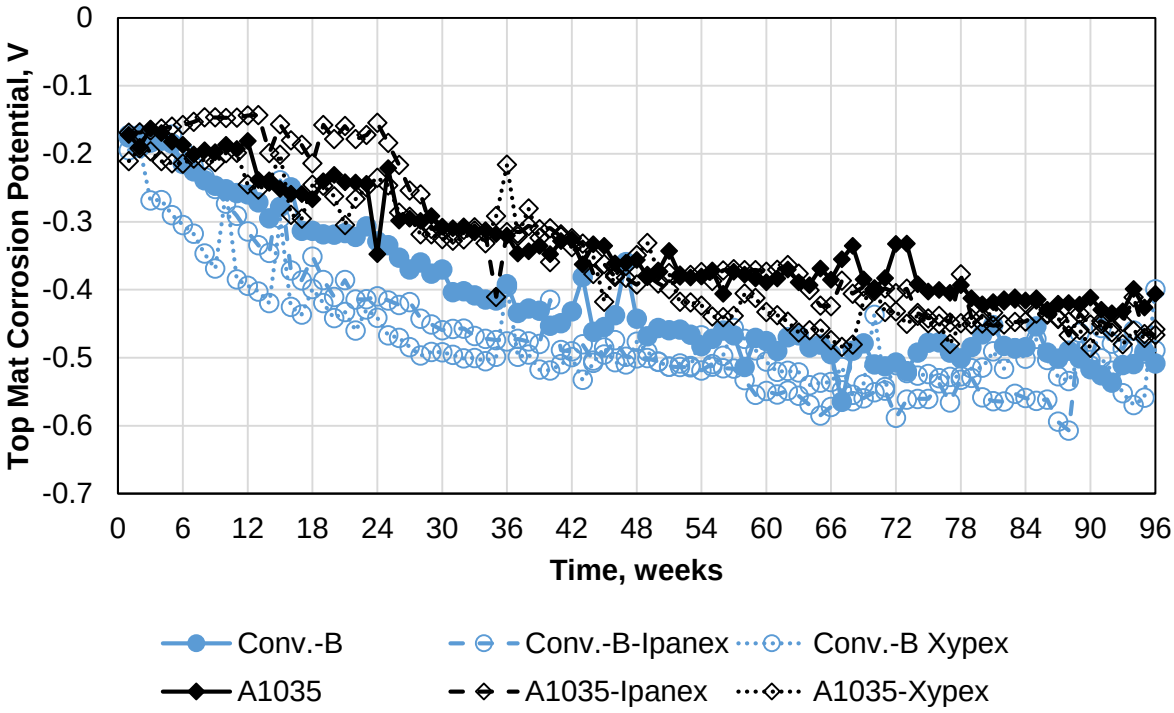

Figure 3.38: Southern Exposure test. Average corrosion potentials of Conv-B and A1035 reinforcement with and without Ipanex and Xypex vs. time.

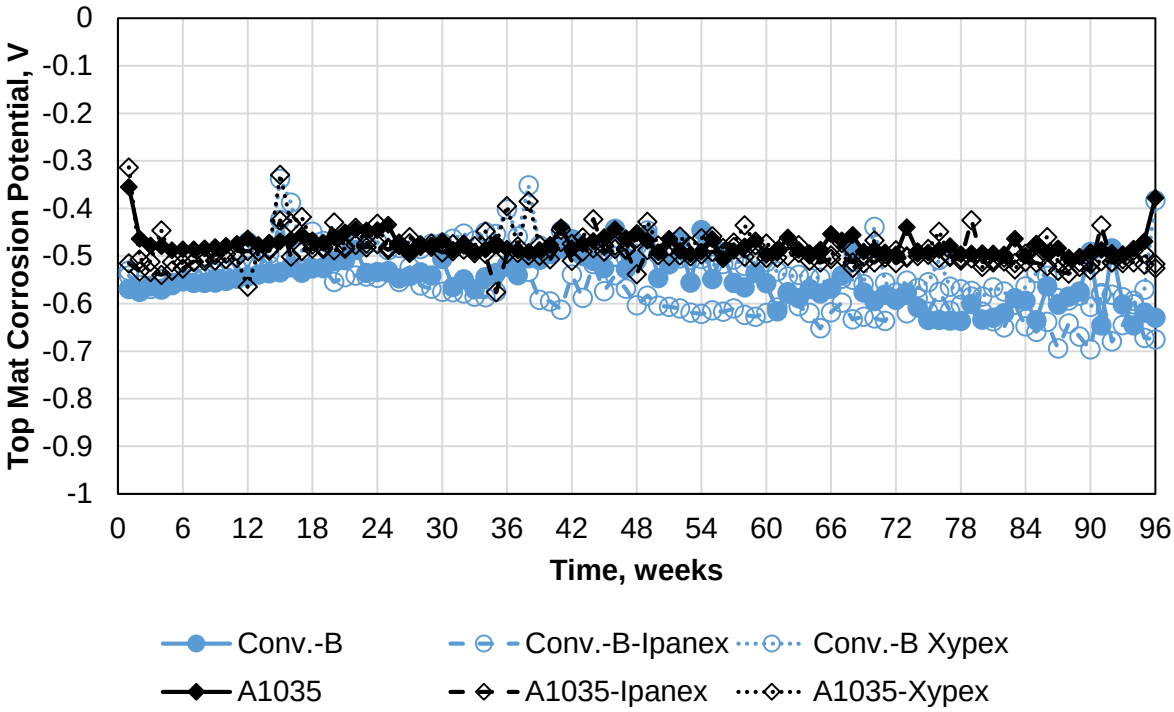

Figure 3.39: Cracked beam test. Average corrosion potentials of Conv-B and A1035 reinforcement with and without Ipanex and Xypex vs. time.

3.2.2 Initiation Age and Chloride Thresholds

Table 3.6 shows the age at corrosion initiation and average critical chloride corrosion threshold (CCCT) for specimens in the Southern Exposure test. Initiation was not tracked in the cracked beam test, as the crack provides a direct path for chlorides to reach the reinforcing steel. As shown in the table, most specimens with conventional reinforcement initiated corrosion within the first 10 weeks of testing. Conv-B exhibited an average CCCT of 0.65 lb/yd^3, much lower than the CCCT values for Conv-A or Conv-C (1.36 and 1.54 lb/yd^3, respectively), a difference that was statistically significant ($p < 0.161$).

Epoxy-coated reinforcement exhibited a much longer time to initiation than conventional reinforcement-45 weeks, at an average CCCT of 2.36 lb/yd^3; the differences in both time and chloride threshold between ECR and conventional reinforcement were statistically significant. Even with 1000 hours of UV exposure, ECR exhibited an average time to corrosion initiation of 33 weeks, over 3 times longer than conventional reinforcement ($p < 0.022$). Undamaged ECR did not exhibit corrosion, and only one specimen with undamaged ECR and UV exposure initiated corrosion, at 68 weeks.

All specimens with galvanized reinforcement (both A767 and A1094) exhibited corrosion activity early in the test as passivation of the zinc layer occurred. This passivation occurred on both the top and bottom mats of steel, resulting in individual corrosion rate readings that would jump erratically from week to week depending on the relative activity of bars in the top and bottom mats. Initiation for these specimens was defined as a sustained positive corrosion rate after the initial passivation period. This allowed the point of corrosion initiation to be determined retroactively, but made timely detection of corrosion initiation difficult. As such, many of the specimens could not be sampled at the time of initiation and a single initiation value, representing the average of all accurately obtained samples for a given bar type, is presented.

A767 and A1094 reinforcement exhibited a large variation in initiation age; average ages at initiation ranged from 42 to 58.2 weeks, with no statistically significant difference between A767 and A1094 specimens. Bending or damaging the coating had no statistically significant impact the initiation age of either bar type, and the critical chloride corrosion thresholds for the two bar types were similar, 1.37 and 1.58 lb/yd^3 for A767 and A1094 reinforcement, respectively. This difference between chloride thresholds is also not statistically significant.

A1035 reinforcement exhibited an average initiation age of 33.4 weeks, 3 to 5 times the initiation age of the conventional reinforcement in this study ($p < 0.011$), but less than that of ECR ($p = 0.215$, just above the threshold for significance). The critical chloride corrosion threshold, 3.37 lb/yd^3, was also greater than that of conventional reinforcement, with a difference that is statistically significant ($p < 0.143$).

The addition of Ipanex or Xypex had no statistically significant effect on the initiation age or critical chloride corrosion threshold of either conventional or A1035 reinforcement.

Table 3.6: Southern Exposure Test-Average Age and Chloride Content at Corrosion Initiation

	Initiation Age, Weeks						Average Age	Chloride Content at Initiation, lb/yd^3	Standard Deviation
	1	2	3	4	5	6			
Conv-A	8	13	5	23	6	4	9.8	1.36	0.880
Conv-B	5	7	12	10	***	***	8.5	0.65	0.198
Conv-C	8	5	5	***	***	***	6.0	1.54	0.088
ECR	55	*	40	40	***	***	45.0	2.577	0.958
ECR-ND	-	-	-	***	***	***	-	-	-
ECR-UV-1000	24	48	28	***	***	***	33.3	**	-
ECR-UV-1000-ND	68	-	-	***	***	***	68.0	**	-
A767	23	26	62	82	17	64	45.7		
A767-ND	56	76	26	48	64	47	52.8	1.37	0.092
A767-Bent	57	80	79	40	56	37	58.2		
A1094	67	81	*	43	45	40	55.2		
A1094-ND	18	83	37	23	62	*	44.6	1.58	0.686
A1094-Bent	*	*	17	59	35	57	42.0		
A1035	28	18	46	47	28	**	33.4	3.37	1.86
A1035-Ipanex	74	28	32	44	26	28	38.7	2.00	0.497
A1035-Xypex	46	52	16	15	37	26	32.0	3.42	2.26
Conv-B-Ipanex	11	15	8	12	8	7	10.2	0.86	1.26
Conv-B-Xypex	10	5	7	4	4	5	5.8	0.82	0.649

*Specimen excluded due to corrosion at electrical connection

**Initiation missed

***No specimen

- No initiation

3.2.3 Corrosion Losses at End of Testing

Table 3.7 shows the macrocell corrosion losses (based on voltage drop) for specimens in the Southern Exposure test. Corrosion losses were obtained by integrating the weekly corrosion rate measurements over time. Among specimens with conventional reinforcement, Conv.-A exhibited the lowest average losses at 96 weeks, 4.29 µm; the difference between Conv-A and the other two heats of steel was statistically significant ($p < 0.011$). Conv-B and Conv-C exhibited similar average losses at 96 weeks, 11.9 and 11.2 µm, respectively. Among ECR specimens, only damaged ECR with UV exposure exhibited significant losses, 0.404 µm based on total area and 77.6 µm based on exposed area (Table 3.8), much greater than any other type of ECR tested; the differences are statistically significant ($p < 0.085$).

Among specimens with galvanized reinforcement, a wide variation in losses was observed. As previously described, the passivation of both the top and bottom mats of steel

resulted in significant fluctuations in corrosion activity. Specimens with bent A767 bars exhibited losses an order of magnitude greater than the other A767 specimens and all A1094 specimens; when comparing the losses of bent A767 to other galvanized bars the differences were statistically significant ($p < 0.184$) for all cases except for the comparison with undamaged A767 ($p = 0.214$).

A1035 reinforcement exhibited losses of 0.890 µm at the end of testing, one-fifth to one-tenth that of conventional reinforcement, but an order of magnitude greater than ECR specimens (with the exception of ECR-UV-1000); these differences are statistically significant. This is in contrast to results in the rapid macrocell test, where A1035 reinforcement exhibited losses similar to that of conventional reinforcement. In the Southern Exposure test, the addition of Ipanex or Xypex had little effect on the corrosion loss of A1035 reinforcement. The addition of Ipanex also had little effect the average corrosion loss for Conv-B reinforcement, although the addition of Xypex resulted in a 40% reduction in corrosion loss for Conv-B reinforcement, a difference that is statistically significant ($p = 0.064$).

Table 3.7: Southern Exposure Test-Macrocell Corrosion Loss Based on Total Area at End of Testing

	Corrosion Loss (µm)-Total Area						Average Loss	Std. Dev
	1	2	3	4	5	6		
Conv-A	7.95	4.06	2.90	2.51	4.58	3.72	4.29	1.95
Conv-B	10.5	17.8	5.44	13.7			11.9	5.24
Conv-C	9.90	10.1	13.5				11.2	2.03
ECR	0.034	-0.090	0.020	0.160			0.031	0.102
ECR-ND	0.155	0.106	-0.013				0.083	0.086
ECR-UV-1000	0.573	0.214	0.425				0.404	0.181
ECR-UV-1000-ND	0.272	-0.031	0.003				0.081	0.166
A767	-0.109	-0.462	1.307	0.598	-0.010	0.893	0.370	0.674
A767-ND	2.11	0.405	1.273	-0.599	1.12	1.55	0.977	0.953
A767-Bent	1.90	-0.759	-0.077	4.01	3.68	6.56	2.55	2.75
A1094	-0.565	0.309	0.319	-0.759	-0.229	1.02	0.016	0.661
A1094-ND	0.504	-1.83	0.836	0.272	0.838	1.13	0.292	1.08
A1094-Bent	2.21	-4.78	-1.41	2.28	1.42	1.88	0.266	2.83
A1035	0.05	1.11	1.37	-0.06	1.98	*	0.890	0.877
A1035-Ipanex	0.10	1.99	0.72	1.07	2.27	1.39	1.26	0.805
A1035-Xypex	0.45	0.79	0.34	0.53	0.94	2.46	0.916	0.789
Conv-B-Ipanex	15.8	10.1	6.03**	11.3	13.9	9.70	12.2	2.58
Conv-B-Xypex	6.65	6.53	7.35	2.46	9.16	8.30	6.74	2.32

*Specimen exhibited early corrosion at the electrical connection with the bar

**Terminated early due to cracking of concrete (week 90)

Table 3.8: Southern Exposure Test-Macrocell Corrosion Loss Based on Exposed Area at End of Testing

	Corrosion Loss (µm)-Exposed Area						Average Loss	Std. Dev
	1	2	3	4	5	6		
ECR	6.61	-17.3	3.77	30.6			5.93	19.6
ECR-UV-1000	110.1	41.0	81.7				77.6	34.7

Tables 3.9 and 3.10 show the macrocell corrosion losses (based on voltage drop) for specimens in the cracked beam test based on total and exposed area, respectively. In the cracked beam test, several specimens with Conv-B reinforcement cracked due to excessive corrosion losses; the age of removal for these specimens is shown in Table 3.11. The average corrosion loss for Conv-B specimens only includes those specimens that reached 96 weeks. Among specimens with conventional reinforcement, Conv-A and Conv-C exhibited the lowest average losses at 96 weeks, 12.2 and 12.9 µm, respectively, a difference that is not statistically significant. Conv-B exhibited much higher average losses than the other two heats of steel, 20.3 µm ($p < 0.186$). Furthermore, testing on Conv-B-3 and Conv-B-4 was terminated early due to cracking. Among the ECR specimens, damaged ECR with UV exposure exhibited the greatest losses, 2.47 µm based on total area and 474 µm based on exposed area (Table 3.10), far greater than damaged ECR without UV exposure ($p = 0.004$). ECR and ECR-UV-1000-ND exhibited losses based on total bar area of 0.183 and 0.265 µm, respectively. No losses were observed for the ECR-ND specimens.

Among individual specimens with galvanized reinforcement, a wide variation of losses was observed, as occurred for Southern Exposure specimens. The A767 specimens exhibited slightly greater losses than A1094 specimens, although these differences are not statistically significant ($p > 0.35$).

A1035 reinforcement exhibited losses of 6.47 µm at the end of testing, one-half to one-third that of conventional reinforcement ($p < 0.033$), but an order of magnitude greater than most ECR specimens ($p < 0.102$). The addition of Ipanex or Xypex did not improve the corrosion resistance of A1035 reinforcement in the cracked beam test ($p > 0.514$). The addition of Ipanex also did not significantly change the average corrosion loss for Conv-B reinforcement, although the addition of Xypex did result in a 70% reduction in corrosion loss for Conv-B reinforcement ($p = 0.016$)–a much greater reduction than was observed in the Southern Exposure test, suggesting that Xypex may have partially sealed the crack, as claimed by the manufacturer, or reduced the porosity of the concrete, limiting access of oxygen and moisture to the cathode (lower mat) bars.

Table 3.9: Cracked Beam Test-Macrocell Corrosion Loss Based on Total Area at End of Testing

	Corrosion Loss (µm)-Total Area						Average Loss	Std. Dev
	1	2	3	4	5	6		
Conv-A	14.9	14.1	13.1	16.8	5.90	8.21	12.2	4.20
Conv-B	9.7	27.4	15.6**	28.7**			18.6	12.5
Conv-C	9.21	15.2	14.4				12.9	3.24
ECR	0.000	0.292	0.467	-0.028			0.183	0.238
ECR-ND	-0.135	0.025	0.101				-0.003	0.121
ECR-UV-1000	3.49	2.18	1.75				2.47	0.905
ECR-UV-1000-ND	0.080	0.717	-0.002				0.265	0.394
A767	0.638	4.21	2.71	-1.18	9.35	8.18	3.99	4.15
A767-ND	1.32	8.81	2.20	6.98	6.51	2.29	4.69	3.13
A1094	3.60	6.12	3.10	-2.65	3.71	4.04	2.99	2.95
A1094-ND	2.78	4.59	2.36	1.99	2.02	4.00	2.96	1.09
A1035	12.9	3.79	7.36	3.19	5.98	5.57	6.47	3.51
A1035-Ipanex	6.24	6.16	4.88	5.98	10.2	6.99	6.74	1.84
A1035-Xypex	5.05	5.92	5.81	9.07	2.98	7.09	5.99	2.04
Conv-B-Ipanex	16.8**	25.2**	32.2	18.8**	24.9**	19.0	25.6	9.34
Conv-B-Xypex	5.92	5.81	9.07	2.98	7.09	5.99	6.14	1.98

**Terminated early due to cracking of concrete (See Table 3.11)

Table 3.10: Cracked Beam Test-Macrocell Corrosion Loss Based on Exposed Area at End of Testing

	Corrosion Loss (µm)-Exposed Area						Average Loss	Std. Dev
	1	2	3	4	5	6		
ECR	0.028	56.1	89.6	-5.5			35.1	45.8
ECR-UV-1000	669.3	418.1	335.6				474.3	173.8

Table 3.11: Cracked Beam Test-Early Termination

Specimen	Termination Age (weeks)
Conv-B-3	49
Conv-B-4	67
Conv-B-Ipanex-1	55
Conv-B-Ipanex-2	77
Conv-B-Ipanex-4	81
Conv-B-Ipanex-5	80

Table 3.12 shows the total corrosion losses (based on LPR) for specimens in the Southern Exposure test. The trends are similar to those observed for these specimens for the macrocell corrosion losses based on voltage drop, although the total losses are higher than the macrocell losses. For conventional reinforcement, Conv-A again had the lowest losses (9.88 µm), although Conv-C exhibited greater total losses (18.0 µm) than Conv-B (14.3 µm); these differences are statistically significant ($p < 0.125$). Damaged ECR with UV exposure exhibited the greatest losses of the ECR specimens, averaging 0.897 µm based on total area, far greater than damaged ECR without UV exposure ($p = 0.022$). Damaged ECR with no UV exposure exhibited lower losses than undamaged ECR; this result is likely erroneous and the difference is not statistically significant.

Among galvanized specimens, there was generally no statistically significant difference between the A767 and A1094 specimens. For both types of galvanized bars, however, bent bars did exhibit higher total losses than straight bars, with differences that are statistically significant ($p < 0.151$). These losses are on the same order as those observed for conventional reinforcement. Using total losses, as opposed to losses based on macrocell corrosion rates, is useful because it removes the effects of corrosion of the bars in the bottom mat of steel, which, as described, tends to reduce macrocell current. These observations suggest potential issues with damage to the coating during bending and the need to patch or repair any damage that may occur.

A1035 reinforcement exhibited total average losses of 3.34 µm, one-third to one-sixth that of conventional reinforcement ($p < 0.009$). The addition of Ipanex or Xypex had no statistically significant effect on total corrosion losses when paired with A1035 reinforcement ($p > 0.796$). As was the case for macrocell corrosion losses, the addition of neither Ipanex nor Xypex resulted in a statistically significant difference in corrosion loss for conventional reinforcement in the Southern Exposure test ($p > 0.252$).

Table 3.12: Southern Exposure Test-Total Corrosion Loss Based on Total Area at End of Testing

	Corrosion Loss (µm)-Total Area						Average Loss	Std. Dev
	1	2	3	4	5	6		
Conv-A	9.50	13.0	11.3	3.76	11.5	10.2	9.88	3.23
Conv-B	11.8	17.8	11.7	15.8			14.3	3.01
Conv-C	18.5	15.8	19.6				18.0	1.98
ECR	0.094	0.050	0.086	0.037			0.067	0.028
ECR-ND	0.305	0.045	0.016				0.122	0.159
ECR-UV-1000	1.502	0.586	0.602				0.897	0.524
ECR-UV-1000-ND	0.031	0.172	0.161				0.121	0.078
A767	19.7	4.11	8.70	5.68	2.72	13.5	9.06	6.46
A767-ND	5.41	5.08	5.84	2.50	10.34	8.02	6.20	2.69
A767-Bent	16.3	9.19	4.66	16.1	30.1	20.0	16.05	8.81
A1094	15.4	6.13	5.17	3.11	2.72	14.2	7.79	5.59
A1094-ND	6.45	7.44	3.43	2.01	17.5	7.17	7.33	5.42
A1094-Bent	18.3	4.13	5.50	15.5	19.0	17.5	13.34	6.72
A1035	2.54	3.03	0.35	1.93	8.86	*	3.34	3.24
A1035-Ipanex	1.06	5.44	3.24	1.95	4.13	1.81	2.94	1.65
A1035-Xypex	2.73	2.79	1.98	2.34	2.54	7.97	3.39	2.26
Conv-B-Ipanex	19.2	12.1	10.1**	15.3	18.3	11.9	14.5	3.74
Conv-B-Xypex	17.6	18.4	8.33	22.5	17.5	23.3	17.9	5.33

**Terminated early due to cracking of concrete (Week 90)

Table 3.13 shows the total corrosion losses (based on LPR) for specimens in the cracked beam test. As was the case for the Southern Exposure specimens, trends generally match those observed for the macrocell corrosion losses, with total losses being higher than macrocell losses. For conventional reinforcement, Conv-B had the highest losses of the three heats of steel (42.0 µm), with Conv-A and Conv-C exhibiting total losses of 36.6 and 27.4 µm, respectively, although only the difference in loss between Conv-B and Conv-C was found to be statistically significant. Damaged ECR with UV exposure exhibited the greatest losses of the ECR specimens, averaging 6.09 µm based on total area, an order of magnitude higher than any other condition of ECR evaluated ($p < 0.0008$). Damaged ECR without UV exposure exhibited similar losses to undamaged ECR with UV exposure, and undamaged ECR without UV exposure exhibited negligible losses.

Among galvanized specimens, there was no statistically significant difference between A767 and A1094 specimens ($p > 0.451$). Losses for all types of bar tested were about 20 µm.

A1035 reinforcement exhibited total losses of 13.7 µm, one-half to one-third those of conventional reinforcement ($p < 0.019$). The addition of Xypex did not result in a statistically difference in total corrosion losses when paired with A1035 reinforcement, while the addition of

Ipanex resulted in increased losses (p = 0.004). As was the case for the macrocell corrosion losses, the addition of Ipanex did not have a statistically significant effect on corrosion loss for conventional reinforcement in the cracked beam test (p = 0.547), but the addition of Xypex resulted in a 44% reduction in total losses ($p = 4 \times 10^{-6}$).

Table 3.13: Cracked Beam Test-Total Corrosion Loss Based on Total Area at End of Testing

	Corrosion Loss (µm)-Total Area						Average Loss	Std. Dev
	1	2	3	4	5	6		
Conv-A	47.6	38.9	44.3	27.3	38.2	23.4	36.6	9.49
Conv-B	39.9	44.1	27.7**	28.3**			42.0	3.0
Conv-C	22.5	38.9	20.8				27.4	10.0
ECR	0.034	0.611	1.005	0.107			0.439	0.456
ECR-ND	0.007	0.024	0.007				0.013	0.010
ECR-UV-1000	4.940	6.761	6.582				6.09	1.004
ECR-UV-1000-ND	0.244	0.917	0.163				0.441	0.414
A767	15.2	23.4	28.3	8.74	18.2	34.0	21.3	9.14
A767-ND	19.8	21.4	6.28	21.8	27.4	24.2	20.2	7.29
A1094	14.2	33.5	12.7	13.0	19.1	26.9	19.9	8.55
A1094-ND	17.6	19.5	14.3	12.6	25.0	18.3	17.9	4.34
A1035	16.8	14.8	14.5	11.2	18.0	6.76	13.7	4.10
A1035-Ipanex	22.1	21.9	18.7	17.5	25.6	20.8	21.1	2.84
A1035-Xypex	12.5	18.7	15.2	15.2	15.3	12.9	15.0	2.25
Conv-B-Ipanex	22.4**	48.8**	50.6	28.8**	30.6**	40.9	45.8	6.9
Conv-B-Xypex	23.2	22.6	24.5	22.3	22.7	24.2	23.3	0.91

**Terminated early due to cracking of concrete (See Table 3.11)

3.2.4 End of Test Photos and Disbondment Results

Figure 3.40 shows the bars from Southern Exposure specimen Conv-C-1 after 96 weeks of testing, and is representative of all conventional reinforcement in the Southern Exposure test. As shown in the photo, moderate amounts of corrosion are visible on both bars from the top mat of steel, although corrosion did not cover the entirety of both bars. This corrosion was frequently sufficient to cause staining on the surface of the specimen (Figure 3.41). No corrosion products were visible on the bars from the bottom mat of steel.

Figure 3.40: Southern Exposure test. Specimen Conv-C-1 after 96 weeks of testing. Top mat (top) and bottom mat (bottom).

Figure 3.41: Southern Exposure test. Surface staining on specimen with conventional reinforcement.

Figure 3.42 shows the bars from cracked beam specimen Conv-B-4 after 96 weeks of testing, and is representative of all conventional reinforcement. Moderate to heavy amounts of corrosion are visible on the top mat of steel, with some pitting and deeper localized corrosion occurring, particularly in the region directly under the 6-in. simulated crack. As was the case with Southern Exposure specimens, most cracked beam specimens with conventional reinforcement exhibited staining on the surface (Figure 3.43). Light or no corrosion products were visible on the bars from the bottom mat of steel.

Figure 3.42: Cracked beam test. Specimen Conv-B-4 after 96 weeks of testing. Top mat (top) and bottom mat (bottom).

Figure 3.43: Cracked beam test. Surface staining on specimen with conventional reinforcement.

Figure 3.44 shows the bars from Southern Exposure specimen ECR-2 after 96 weeks of testing, and is representative of all damaged ECR. As shown in the photo, minimal amounts of corrosion damage are visible; corrosion was typically limited to small amounts at the damage sites in the epoxy. No significant disbondment was observed on any Southern Exposure

specimen (Figure 3.45). Figure 3.46 shows undamaged ECR specimen ECR-ND-2 after 96 weeks of testing. No corrosion was observed on any ECR-ND specimen in the Southern Exposure test.

Figure 3.44: Southern Exposure test. Specimen ECR-2 after 96 weeks of testing. Top mat (top) and bottom mat (bottom).

Figure 3.45: Southern Exposure test. Top bar of specimen ECR-1 after disbondment test.

Figure 3.46: Southern Exposure test. Specimen ECR-ND-2 after 96 weeks of testing. Top mat (top) and bottom mat (bottom).

Figure 3.47 shows the bars from cracked beam specimen ECR-3 after 96 weeks of testing, and is representative of all damaged ECR. Minimal amounts of corrosion damage are visible on damaged ECR specimens; corrosion was limited to small amounts at the damage sites in the top mat of steel. Unlike the bars in the Southern Exposure test, damaged ECR bars exhibited significant disbondment after exposure in the cracked beam test; corrosion had spread underneath the undamaged portions of the coating (Figure 3.48)

Figure 3.47: Cracked beam test. Specimen ECR-3 after 96 weeks of testing. Top mat (top) and bottom mat (bottom).

Figure 3.48: Cracked beam test. Top bar of specimen ECR-2 after disbondment test.

Figures 3.49 and 3.50 show photos of undamaged ECR after 96 weeks of testing in the cracked beam test. Two of the undamaged ECR specimens showed no visible corrosion (Figure 3.49); however, specimen ECR-ND-1 showed some rust buildup at an unnoticed holiday in the coating (Figure 3.50).

Figure 3.49: Cracked beam test. Specimen ECR-ND-2 after 96 weeks of testing. Top mat (top) and bottom mat (bottom).

Figure 3.50: Top bar of cracked beam test. Specimen ECR-ND-1 after 96 weeks of testing.

Figure 3.51 shows the bars from Southern Exposure specimen ECR-UV-1000-1 after 96 weeks of testing, and is representative of all ECR-UV-1000 specimens. Much larger amounts of corrosion damage are visible than was the case for damaged ECR specimens without UV exposure. Damaged ECR bars exhibited significant disbondment after exposure, and for most bars, the entire coating could be easily removed (Figure 3.52)

Figure 3.51: Southern Exposure test. Specimen ECR-UV-1000-1 after 96 weeks of testing. Top mat (top) and bottom mat (bottom).

Figure 3.52: Southern Exposure test. Top bar of specimen ECR-UV-1000-1 after disbondment test.

Figure 3.53 shows the bars from cracked beam specimen ECR-UV-1000-ND-1 after 96 weeks of testing, and is representative of all ECR-UV-1000-ND specimens. Minimal to no corrosion damage was observed on the bars, but discoloration from the UV exposure was visible.

Figure 3.53: Southern Exposure test. Specimen ECR-UV-1000-ND-1 after 96 weeks of testing. Top mat (top) and bottom mat (bottom).

Figure 3.54 shows the bars from cracked beam specimen ECR-UV-1000-1 after 96 weeks of testing, and is representative of all ECR-UV-1000 specimens. Much larger amounts of corrosion damage are visible than was the case for damaged ECR specimens without UV exposure; blistering and cracking of the coating was observed on all top bars. Damaged ECR bars exhibited significant disbondment after exposure, and in every bar evaluated the entire coating could be easily removed (Figure 3.55)

Figure 3.54: Cracked beam test. Specimen ECR-UV-1000-2 after 96 weeks of testing. Top mat (top) and bottom mat (bottom).

Figure 3.55: Cracked beam test. Top bar of specimen ECR-UV-1000-2 after disbondment test.

Figure 3.56 shows the bars from cracked beam specimen ECR-UV-1000-ND-1 after 96 weeks of testing, and is representative of all ECR-UV-1000-ND specimens. As was the case for Southern Exposure specimens, minimal to no corrosion damage was observed on the bars, but discoloration from the UV exposure was visible.

Figure 3.56: Cracked beam test. Specimen ECR-UV-1000-ND-1 after 96 weeks of testing. Top mat (top) and bottom mat (bottom).

Tables 3.14 and 3.15 summarize the measured disbonded area on each damaged ECR specimen from the Southern Exposure and cracked beam tests, respectively, at the end of testing. As described in Chapter 2, disbondment that extended more than 0.5 in. from the intentional damage site in all directions is classified as total disbondment and is assigned a disbonded area of 1.05 in.^{2} In the Southern Exposure test (Table 3.14), damaged ECR without UV exposure exhibited no disbondment, whereas ECR with UV exposure exhibited total disbondment on two out of three specimens and large amounts of disbondment on the third specimen, for an average disbonded area of 0.902 in.^{2}. Disbondment tests were not performed on undamaged specimens. In the cracked beam test (Table 3.15), both ECR and ECR-UV-1000 bars exhibited greater disbondment than in the Southern Exposure test, with two out of four ECR bars and all ECR-UV-1000 bars exhibiting total disbondment. Average disbonded areas for ECR and ECR-UV-1000 bars were 0.902 in.^{2} and 0.902 in.^{2}, respectively.

Table 3.14: Southern Exposure Test-Measured Disbondment (in.^{2}) At End of Testing

	Specimen				Average
	1	2	3	4	
ECR	0	0	0	0	0
ECR-ND	-	-	-	-	-
ECR-UV-1000	1.050	1.050	0.605	-	0.902
ECR-UV-1000-ND	-	-	-	-	-

Table 3.15: Cracked Beam Test-Measured Disbondment (in.^{2}) At End of Testing

	Specimen				Average
	1	2	3	4	
ECR	0.375	1.05	1.05	0.63	0.776
ECR-ND	-	-	-	-	-
ECR-UV-1000	1.050	1.050	1.050	-	1.05
ECR-UV-1000-ND	-	-	-	-	-

Figure 3.57 shows the bars from Southern Exposure specimen A767-3 after 96 weeks of testing. The top mat of steel exhibited moderate amounts of corrosion (heavy in places) with both zinc corrosion products (white) and steel corrosion products (orange-brown) visible. Corrosion was uneven, with the coating intact in several places but the underlying intermetallic layers visible in others. On several A767 specimens, corrosion was also present on the bottom bars (Figure 3.58), explaining the “negative” corrosion loss observed on some A767 specimens.

Figure 3.57: Southern Exposure test. Specimen A767-3 after 96 weeks of testing. Top mat (top) and bottom mat (bottom).

Figure 3.58: Southern Exposure test. Specimen A767-2 after 96 weeks of testing. Top mat (top) and bottom mat (bottom). Corrosion on bottom mat circled.

Figure 3.59 shows the bars from cracked beam specimen A767-3 after 96 weeks of testing. As observed for the Southern Exposure specimens, the top mat of steel exhibited moderate amounts of corrosion (heavy in places) with both zinc corrosion products (white) and steel corrosion products (orange-brown) visible. Fewer white zinc corrosion products were visible on the bottom bars, with isolated areas of steel corrosion products visible.

Figure 3.59: Cracked beam test. Specimen A767-3 after 96 weeks of testing. Top mat (top) and bottom mat (bottom).

Figure 3.60 shows the bars from Southern Exposure specimen A1094-4 after 96 weeks of testing. The top mat of steel exhibited moderate to heavy corrosion with both zinc corrosion products (white) and steel corrosion products (orange-brown) visible. As for the A767 specimens, corrosion was uneven, with undisturbed zinc adjacent to exposed underlying intermetallic layers. As observed on the A767 specimens, corrosion was also present on the bottom mat on some specimens, explaining the “negative” corrosion losses observed on these specimens.

Figure 3.60: Southern Exposure test. Specimen A1094-4 after 96 weeks of testing. Top mat (top) and bottom mat (bottom).

Figure 3.61 shows the bars from cracked beam specimen A1094-6 after 96 weeks of testing. The top mat of steel exhibited moderate amounts of corrosion with both zinc corrosion products (white) and steel corrosion products (orange-brown) visible. Again, limited amounts of zinc corrosion products were observed on the bottom mat.

Figure 3.61: Cracked beam test. Specimen A1094-6 after 96 weeks of testing. Top mat (top) and bottom mat (bottom).

Figures 3.62 and 3.63 show bent A767 and A1094 bars, respectively from the Southern Exposure test. For both types of bar, corrosion products were observed on the top of the bar both at and away from the bend. As discussed based on total corrosion losses, the presence of the bend resulted in a statistically significant increase in corrosion when compared to straight bars.

Figure 3.62: Southern Exposure test. Specimen A767-b-2 after 96 weeks of testing. Top mat (top) and bottom mat (bottom).

Figure 3.63: Southern Exposure test. Specimen A1094-b-2 after 96 weeks of testing. Top mat (top) and bottom mat (bottom).

Figure 3.64 shows the bars from Southern Exposure specimen A1035-5 after 96 weeks of testing. Light to moderate amounts of corrosion are visible on portions of both bars from the top mat of steel. No corrosion products were visible on the bars from the bottom mat of steel. A1035 bars in concrete with Ipanex (Figure 3.65) and Xypex (Figure 3.66) did appear to have less corrosion than A1035 with no admixture. Given that overall losses were similar between A1035 specimens with and without Ipanex or Xypex, it is possible the reduced permeability of the concrete resulted in more localized corrosion on the bars.

Figure 3.64: Southern Exposure test. Specimen A1035-5 after 96 weeks of testing. Top mat (top) and bottom mat (bottom).

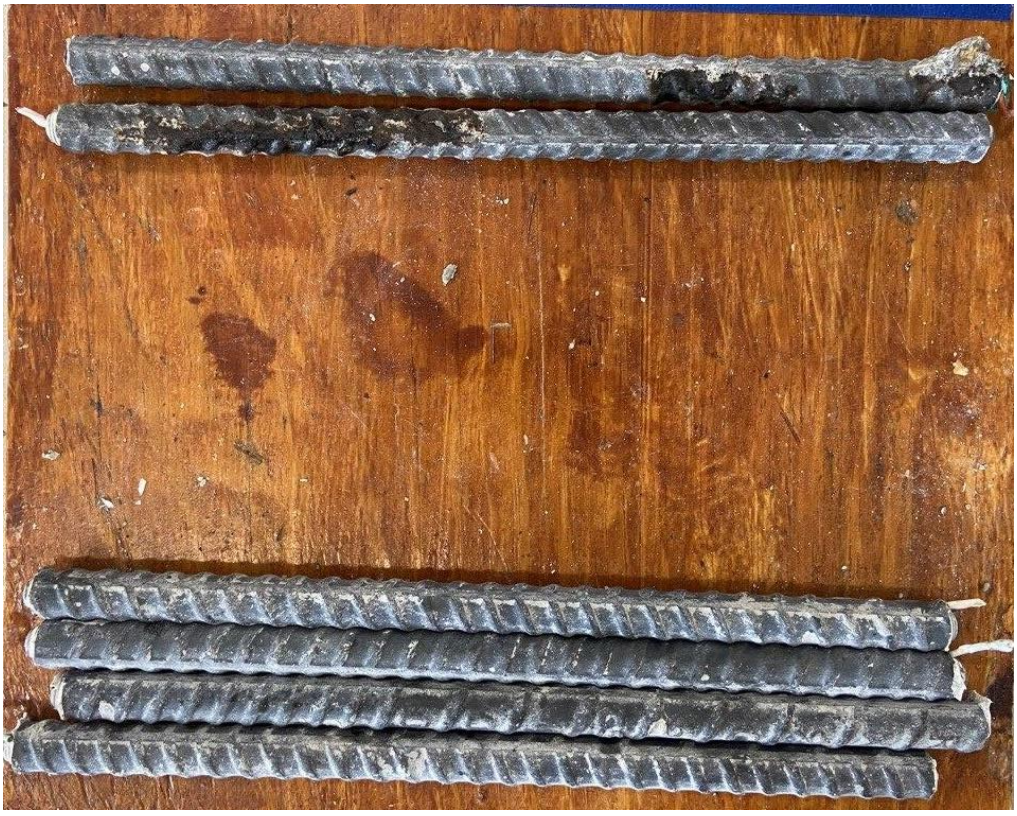

Figure 3.65: Southern Exposure test. Specimen A1035-Ipanex-2 after 96 weeks of testing. Top mat (top) and bottom mat (bottom).

Figure 3.66: Southern Exposure test. Specimen A1035-Xypex-1 after 96 weeks of testing. Top mat (top) and bottom mat (bottom).

Figure 3.67 shows the bars from cracked beam specimen A1035-1 after 96 weeks of testing. Light to moderate amounts of corrosion are visible on both bars from the top mat of steel, significantly less than observed on conventional reinforcement in the cracked beam test. Corrosion was concentrated in the region immediately under the 6-in. simulated crack in the specimen. A1035 bars in concrete with Ipanex (Figure 3.68) and Xypex (Figure 3.69) exhibited similar behavior, with the corrosion products predominantly in the region under the simulated crack.

Figure 3.67: Cracked beam test. Specimen A1035-1 after 96 weeks of testing. Top mat (top) and bottom mat (bottom).

Figure 3.68: Cracked beam test. Specimen A1035-Ipanex-6 after 96 weeks of testing. Top mat (top) and bottom mat (bottom).

Figure 3.69: Cracked beam test. Specimen A1035-Xypex-2 after 96 weeks of testing. Top mat (top) and bottom mat (bottom).

3.3 Chikaskia River Bridge Survey

Figure 3.70 shows the results of the bridge survey of the Chikaskia River bridge, performed on May 29, 2018. This bridge contains a combination of A1035 reinforcement and concrete containing Ipanex dosed at 13.8 oz per 100 lb of cementitious material. Due to time

constraints, the crack survey was only performed on the right lane and shoulder of the northbound I-35 bridge over the Chickaskia River. Extensive cracking was observed over the entire bridge deck (Figure 3.70), with an average crack density of 2.715 m/m^2, an order of magnitude greater than what is typically observed on a bridge deck made with low-cracking high-performance concrete after 10 years (the latest available data) (Darwin et al. 2016). No staining was noted on the bridge deck, indicating that these cracks had not yet resulted in corrosion observable at the surface after 15 years. It should be noted that based on the predicted design life for A1035 reinforcement (Section 4.1.2), corrosion-induced cracking would not be expected at this age.

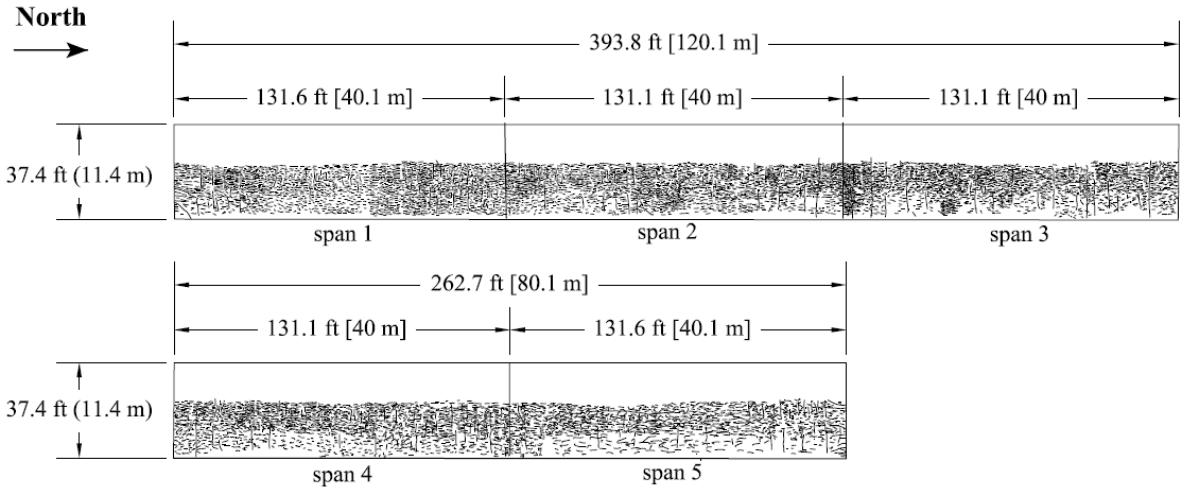

Bridge Number: 26415
Bridge Location: NB I-35 Over Chikaskia River
Construction Date: 2003
Crack Survey Date: 5/29/2018
NOTE Only right shoulder and lane surveyed (22 ft width)

Bridge Length: 656.8 ft (200.2 m)
Bridge Width: 37.4 ft (11.4 m)
Skew: 0°
Number of Spans: 5
Span 1: 131.6 ft (40.1 m)
Span 2: 131.1 ft (40 m)
Span 3: 131.1 ft (40 m)
Span 4: 131.1 ft (40 m)
Span 5: 131.6 ft (40.1 m)
Number of Placements: 1

Bridge Age: 180 Months
Crack Density: 2.715m/m^2
Span 1: 2.387 m/m^2
Span 2: 3.354 m/m^2
Span 3: 2.890 m/m^2
Span 4: 2.624 m/m^2
Span 5: 2.322 m/m^2

Figure 3.70: Crack survey of Northbound I-35 on the Chickaskia River. Note: survey not performed on the left lane.

3.4 Cow Creek Deck Panel Analysis

3.4.1 Visual Condition Survey

Figures 3.71 and 3.72 show deck panels with conventional and epoxy-coated reinforcement, respectively, and are representative of all panels in this study. In the figures, damage and degradation are noted. All panels exhibited moderate transverse cracking, with crack densities ranging from 0.14 to 0.26 m/m^2 for panels with conventional reinforcement and from 0.13 to 0.23 m/m^2 for panels with epoxy-coated reinforcement. These values *are* in the

range for bridge decks made with low-cracking high-performance concrete after 10 years (Darwin et al. 2016). All slabs also exhibited areas of scaling or other surface deterioration.

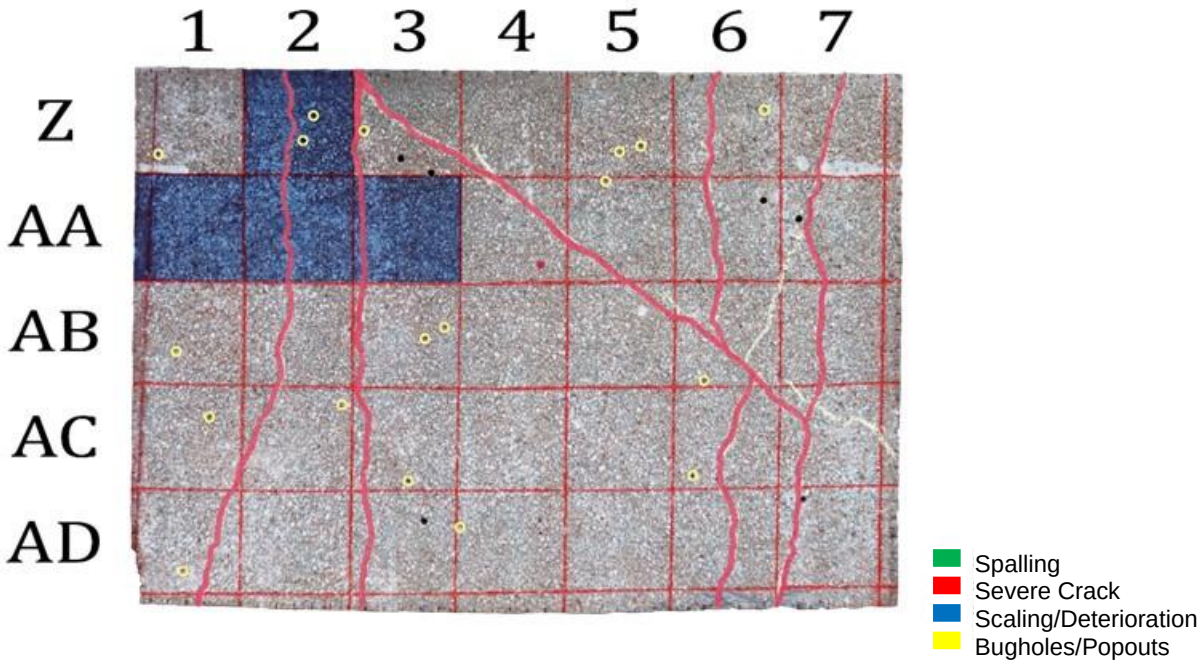

Figure 3.71: Cow Creek deck panel with conventional reinforcement.

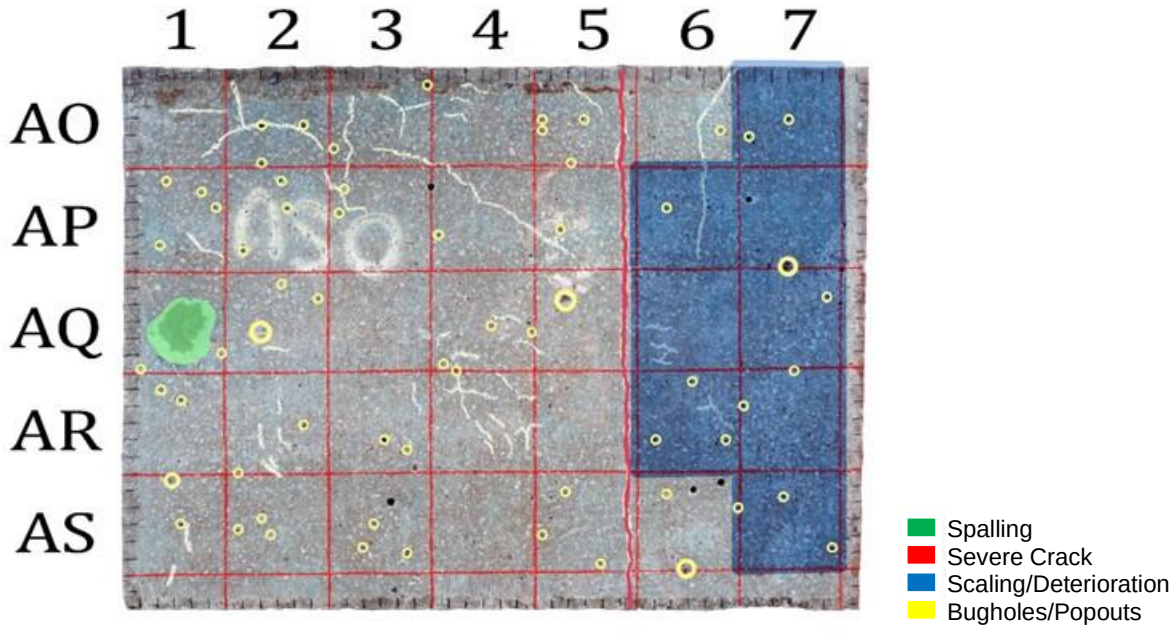

Figure 3.72: Cow Creek deck panel with epoxy-coated reinforcement.

3.4.2 Strength Testing

Figures 3.73 and 3.74 show the rebound readings (rebound hammer) for one panel each with conventional reinforcement and ECR, respectively, and are representative of the panels analyzed in this study. As shown in the figures, some variation in hardness was observed over the surface of each panel. Panels with conventional reinforcement (and an overlay) generally exhibited surface hardness readings in the 30's or 40's, whereas panels with epoxy-coated reinforcement (and no overlay) generally exhibited surface hardness readings in the 50's or 60's. The differences are due to the differences in properties between the overlay (Figure 3.73) and the original deck (Figure 3.74). As will be shown in Section 3.4.6, carbonation of the concrete in ECR panels (with no overlay) may have contributed to the increased surface hardness.

	1	2	3	4	5	6	7
A	**37**	**38**	**34**	**37**	**37**	**40**	**38**
B	**37**	**41**	**35**	**37**	**33**	**32**	**35**
C	**34**	**33**	**33**	**35**	**34**	**32**	**36**
D	**33**	**36**	**36**	**35**	**40**	**30**	**34**
E	**39**	**36**	**36**	**36**	**41**	**36**	**34**

Figure 3.73: Rebound readings for Cow Creek deck panel with conventional reinforcement.

	1	2	3	4	5	6	7
A	**52**	**51**	**52**	**53**	**53**	**57**	**52**
B	**52**	**54**	**51**	**51**	**53**	**56**	**51**
C	**55**	**57**	**52**	**54**	**59**	**55**	**54**
D	**58**	**55**	**54**	**53**	**53**	**52**	**52**
E	**51**	**52**	**50**	**52**	**52**	**53**	**53**

Figure 3.74: Rebound readings for Cow Creek deck panel with ECR.

Figures 3.75 and 3.76 show the results from compressive strength testing of cores taken from panels with conventional and ECR, respectively. For the panels from the bridge deck with conventional reinforcement, the strength of the overlay was measured separately from the remainder of the core. For panels with conventional reinforcement, average compressive strengths ranged from 3400 to 4900 psi, with the strength of the overlay being slightly weaker than the strength of the underlying concrete in one case and about 500 psi greater in the other two cases. Panels with ECR exhibited strengths between 4000 and 4900 psi.

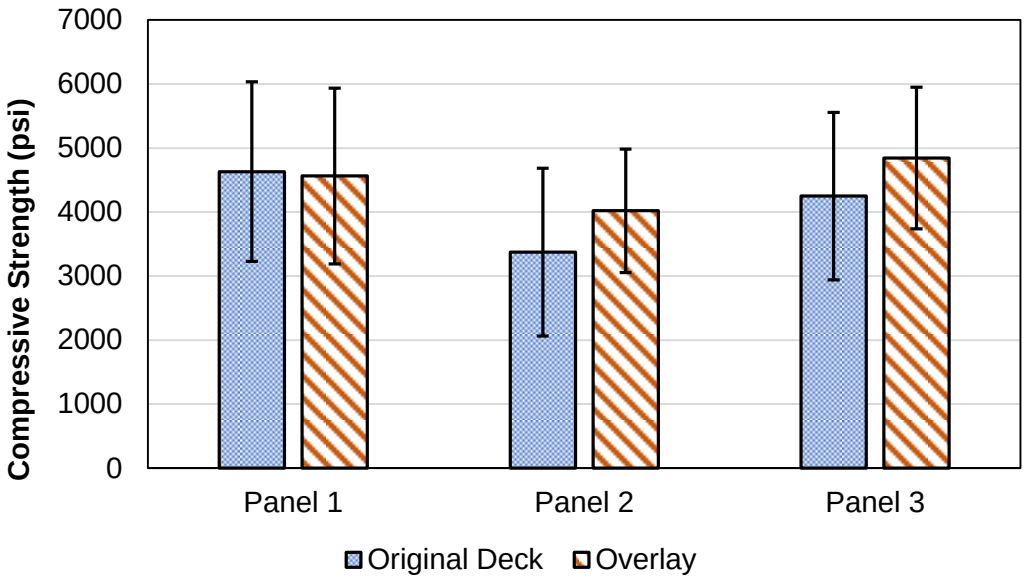

Figure 3.75: Average compressive strength (psi) for cores taken from Cow Creek deck panels with conventional reinforcement.

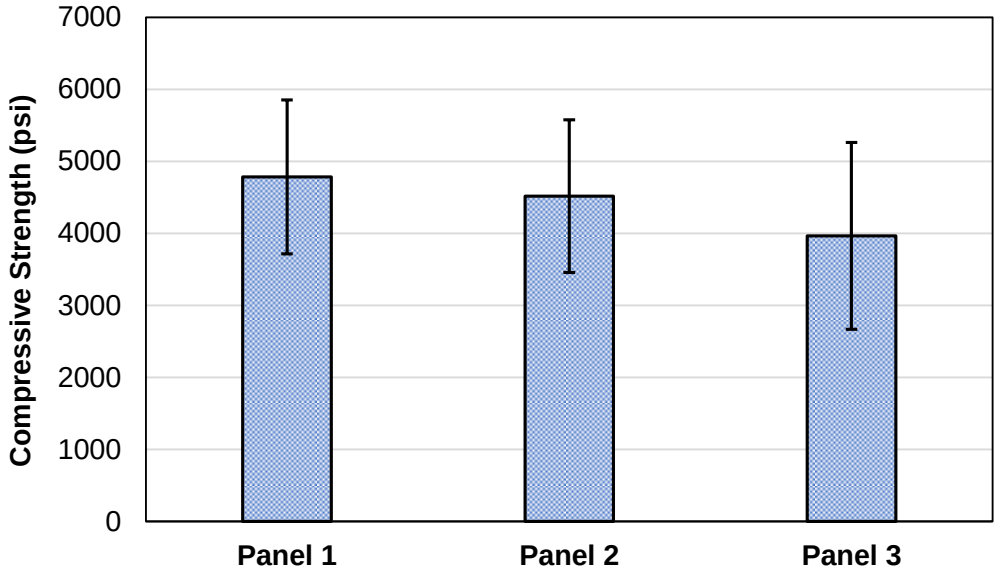

Figure 3.76: Average compressive strength (psi) for cores taken from Cow Creek deck panels with ECR.

3.4.3 Half-Cell Potential

Figures 3.77 and 3.78 show the half-cell potential contour plots for the top longitudinal and transverse reinforcement, respectively, from one of the Cow Creek deck panels with conventional reinforcement. Similar results were obtained for all three slabs evaluated. Half-cell potentials were generally low, ranging from –50 to –400 mV vs. CSE, with areas of more negative potential (indicating a greater likelihood of corrosion) noted on all slabs. Generally,

areas of more negative potential occurred at crack locations, although not all cracks caused a drop in potential.

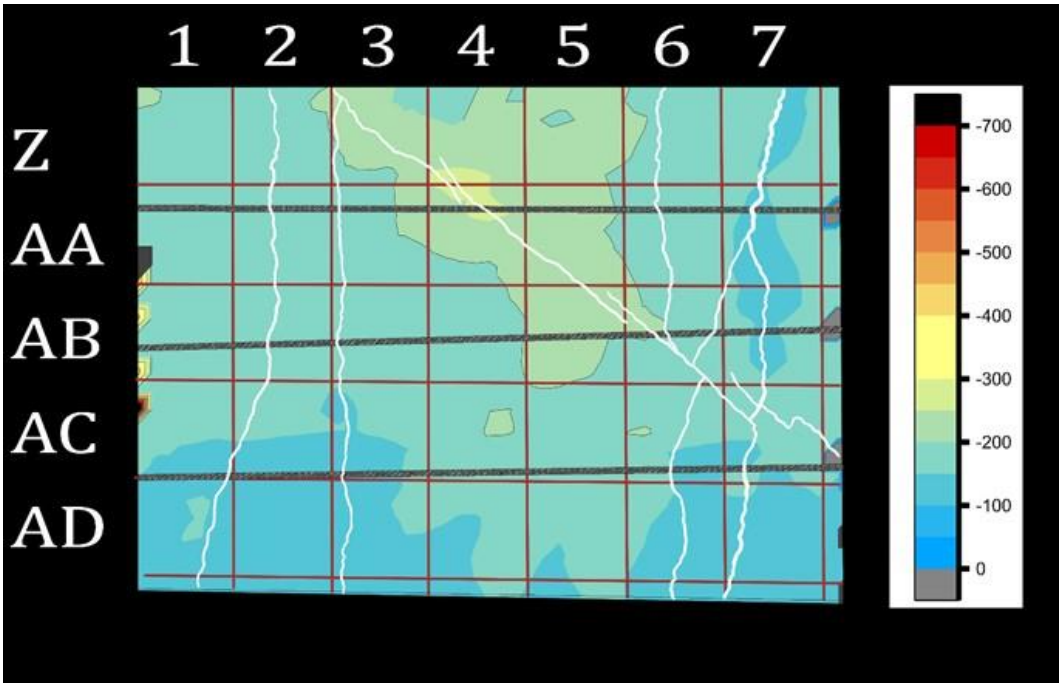

Figure 3.77: Half-cell potential in millivolts for top longitudinal conventional reinforcement in Cow Creek deck panel.

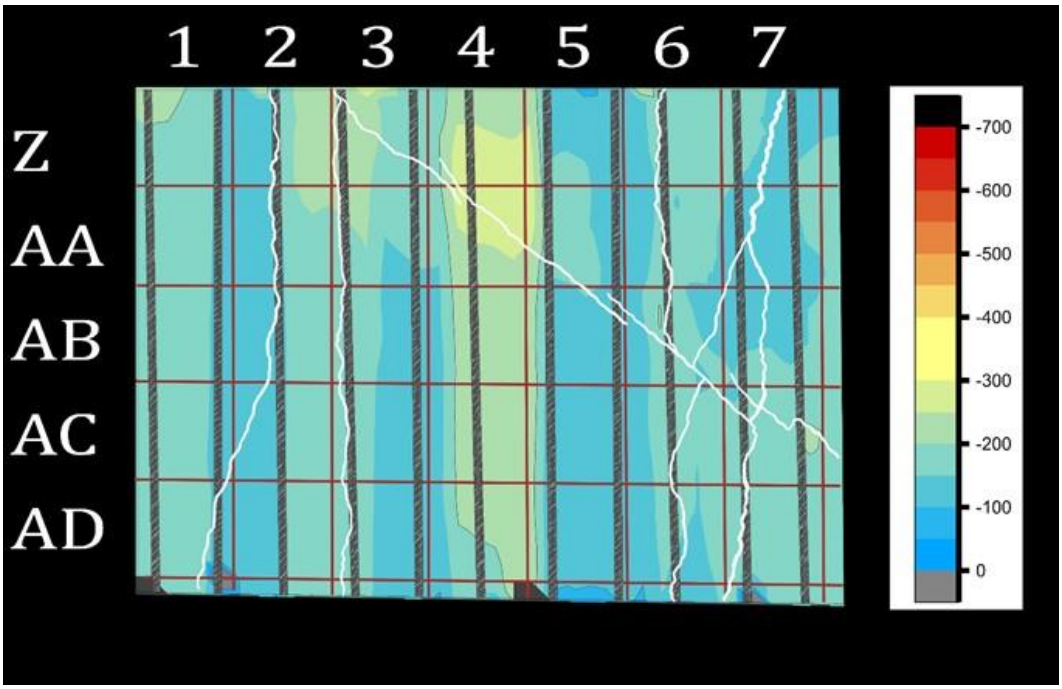

Figure 3.78: Half-cell potential in millivolts for top transverse conventional reinforcement in Cow Creek deck panel.

Figures 3.79 and 3.80 show the half-cell potential contour plots for the top longitudinal and transverse reinforcement, respectively, from one of the Cow Creek deck panels with ECR. As for the panels with conventional reinforcement, similar results were obtained for all three slabs evaluated. Half-cell potentials were generally more negative than those observed for the panels with conventional reinforcement, with values ranging from –0.120 to –0.640 V vs. CSE. This is not unexpected; the epoxy coating prevents oxygen from reaching the steel, which results in a more negative corrosion potential reading even in the absence of corrosion.

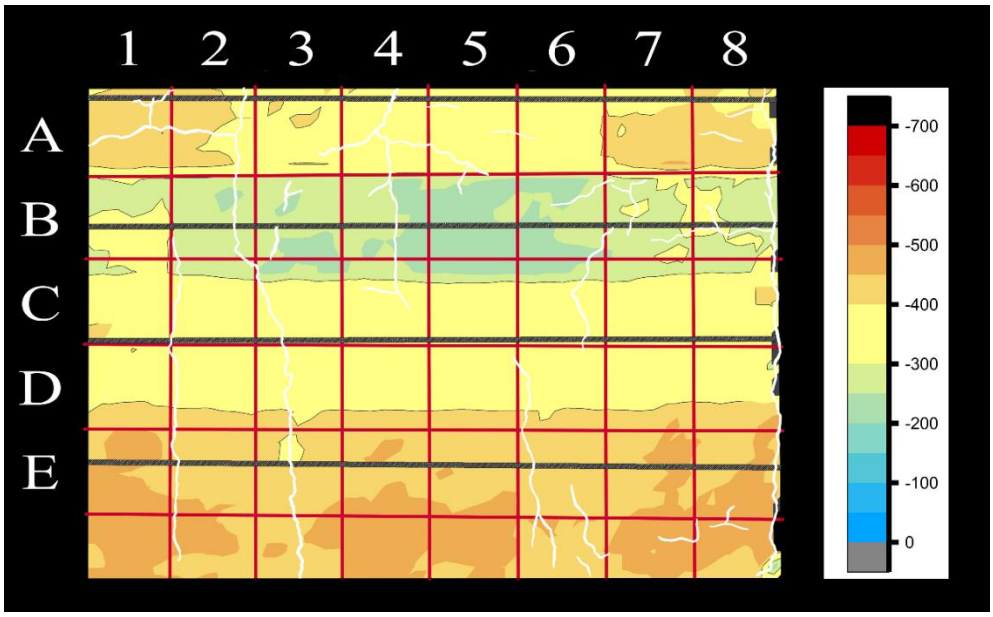

Figure 3.79: Half-cell potential in millivolts for top longitudinal ECR in Cow Creek deck panel.

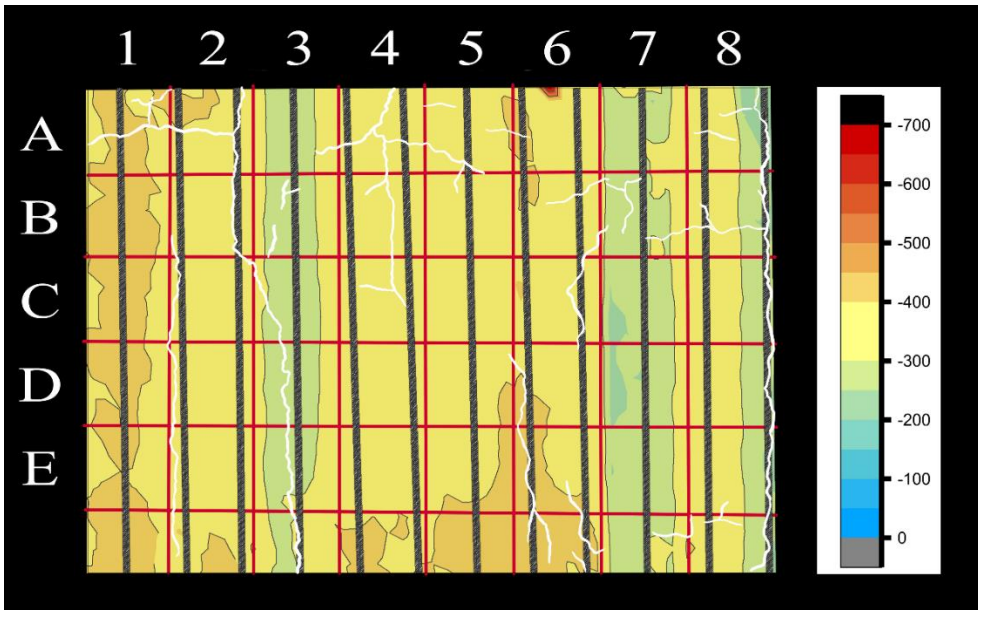

Figure 3.80: Half-cell potential in millivolts for top transverse ECR in Cow Creek deck panel.

3.4.4 Electrical Resistivity Testing

Figure 3.81 shows the average bulk resistivity for cores taken from panels with conventional reinforcement. The error bars give the range of values obtained. The overlay was removed from cores containing conventional reinforcement and analyzed separately. Overlays from all three panels exhibited very high bulk resistivities, exceeding 100 kΩ-cm. The concrete beneath the overlay exhibited a much lower bulk resistivity, approximately 20 kΩ-cm.

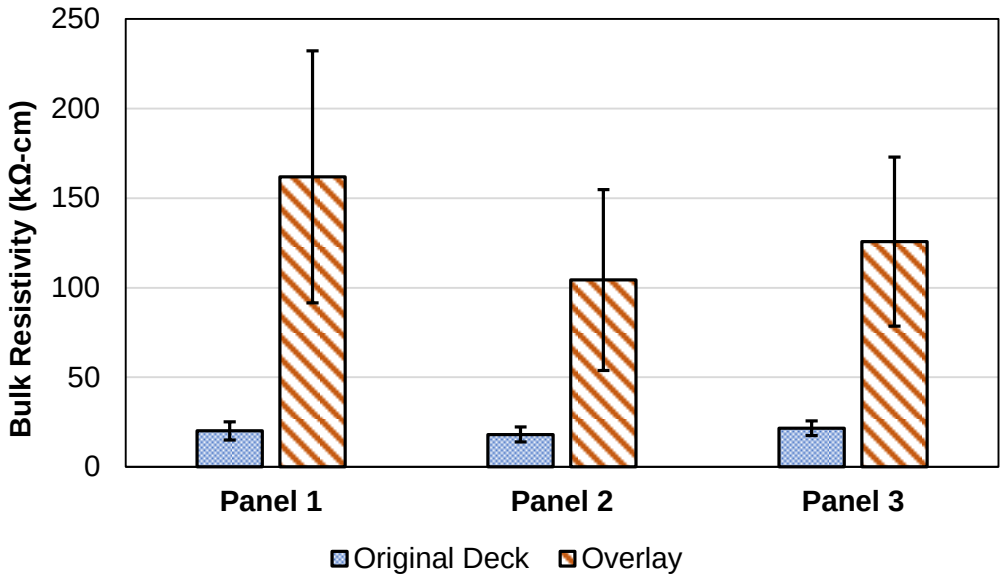

Figure 3.81: Bulk resistivity from cores from panels with conventional reinforcement for original deck and overlay

Figure 3.82 shows the average bulk resistivity for cores taken from panels with conventional reinforcement (original deck) and ECR. The error bars give the range of values obtained. Cores were classified as passive, intermediate, or active based on the corrosion activity of nearby reinforcement, as determined by half-cell potential measurements. As would be expected, the silane treatment applied to the panels with conventional reinforcement resulted in a doubling in average bulk resistivity (19-25 kΩ-cm) compared to ECR (9-10 kΩ-cm). A drop in the average value of resistivity is observed with an increase in corrosion activity, but the differences are not statistically significant.

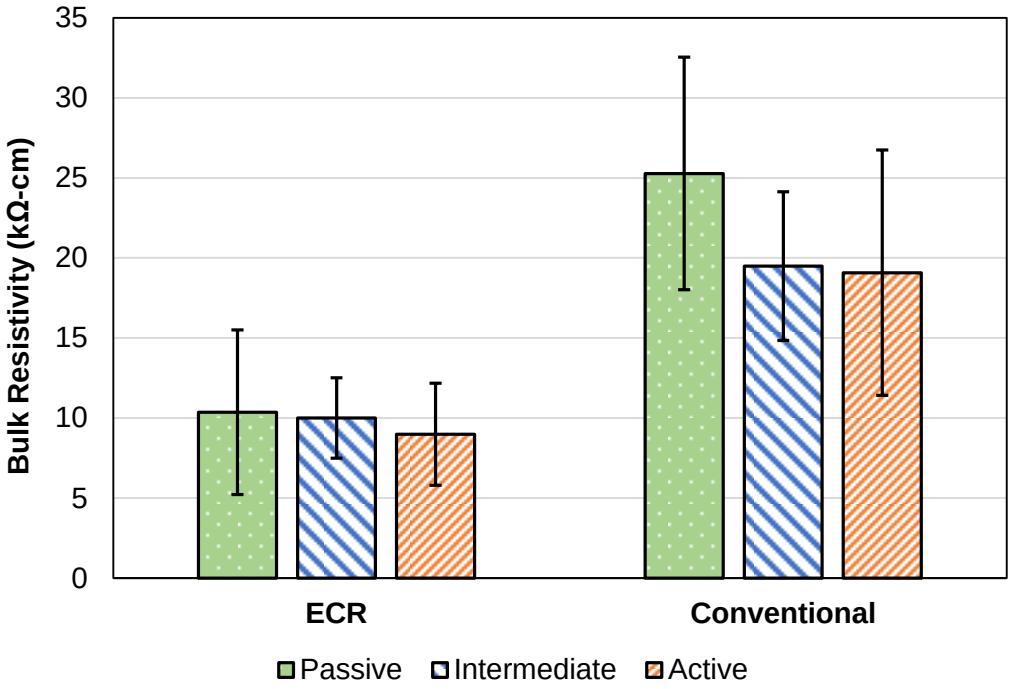

Figure 3.82: Bulk resistivity from cores with ECR and conventional reinforcement.

3.4.5 Ultrasonic Pulse Velocity Testing

Figure 3.83 shows the average ultrasonic pulse velocities for cores taken from panels with conventional reinforcement (original deck) and ECR. The error bars give the range of values obtained. As done for electrical resistivity testing, cores were classified as passive, intermediate, or active based on the corrosion activity of nearby reinforcement as determined by half-cell potential measurements. No real difference in ultrasonic pulse velocity measurements related to corrosion activity or panel type was observed, with all measured values falling between 14,000 and 16,000 ft/s. This is to be expected, as ultrasonic pulse velocity is usually correlated with compressive strength and no statistically significant differences in strength were observed.

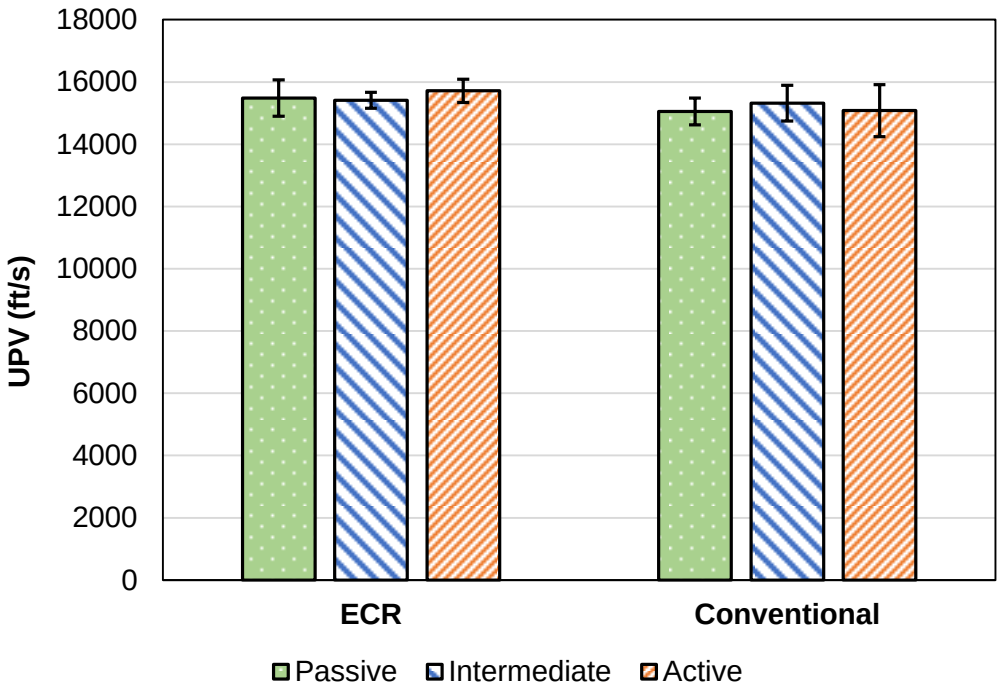

Figure 3.83: Bulk resistivity from cores with ECR and conventional reinforcement.

3.4.6 Linear Polarization Resistance

Linear polarization resistance (LPR) readings were performed on the top and bottom mats of steel from two panels containing conventional reinforcement and two panels containing epoxy-coated reinforcement. For panels with conventional reinforcement, both the top and bottom mats of steel showed corrosion potentials indicative of active corrosion (ranging from –0.283 V to –0.302 V with respect to a copper/copper sulfate electrode (CSE)). The top mats of steel on the two panels tested had estimated corrosion rates of 0.343 and 0.078 µm/yr, respectively. The bottom mats of steel from the two panels had estimated corrosion rates of 0.017 and 0.275 µm/yr, respectively. It should be noted that the panels had been sitting covered for some time at the Perry maintenance facility and that the corrosion rates on the panels were likely higher while they were in service.

Panels with epoxy-coated reinforcement on the top mat had uncoated conventional reinforcement on the bottom mat. The top mats (epoxy) had corrosion potentials of –0.889 and –0.905 V vs. CSE and corrosion rates of 0.004 and 0.036 µm/yr. The corrosion rates are lower than those observed on uncoated reinforcement. These rates, however, were calculated based on the assumption that the entire surface area of the bar was corroding. It is likely that the corrosion was concentrated at damage sites on the epoxy and that the localized corrosion rates were far higher than the values based on the entire surface. The negative corrosion potentials are likely a result of the reduced availability of oxygen on an epoxy-coated bar and do not necessarily indicate a high potential for corrosion. The bottom mats of steel, which contained uncoated conventional reinforcement, had corrosion potentials of –0.355 and –0.437 V and corrosion rates of 0.036 and 1.17 µm/yr, respectively.

3.4.7 Colorimetric Testing of Cores

Colorimetric testing was conducted on six cores from each slab. To ensure the full range of concrete conditions for each panel were represented, one core was taken from each of the following areas:

I. An area with a more negative half-cell potential.
II. An area with a less negative half-cell potential.
III. An area of poor quality concrete (as indicated by visual assessment and rebound hammer measurements) directly over reinforcement.
IV. An area of poor quality concrete away from reinforcement.
V. An area of good quality concrete (as indicated by visual assessment and rebound hammer measurements) directly over reinforcement.
VI. An area of good quality concrete away from reinforcement.

These cores will be referred to using the Roman numerals I-VI above.

Table 3.16 lists the colorimetric testing results from the deck panels with conventional reinforcement. For most cores tested, significant carbonation was noted, with the depth of carbonation from the bottom of any core (ranging from 0 to 1.378 in., with an average of 0.833 in.) exceeding that from the top (ranging from 0 to 0.886 in., with an average of 0.197 in.). This is not surprising, as the deck with conventional reinforcement received an overlay and silane treatment that would reduce carbonation from the top of the panel. The depth of carbonation did not reach the level of reinforcement (2 in.). In cores taken away from cracks, no significant chloride penetration was noted; this is likely due to the indicator used not being sensitive enough to pick up the relatively low chloride contents required to initiate corrosion. At cracks, chloride penetration extended approximately 2 in. into the core. No significant water dye penetration was noted, confirming the presence of silane.

Table 3.16: Colorimetric Testing Results for Deck Panels with Conventional Reinforcement

Panel-Core	Carbonation Depth from Top (in.)	Carbonation Depth from Bottom (in.)	Chloride Penetration (in.)	Water Dye Penetration (in.)
Panel 1-I	0.394	1.378	0	0
Panel 1-II	0.098	0.787	0	0
Panel 1-III	0	0.591	0	0
Panel 1-III (w/ crack)	0.591	0.984	1.772	0.009
Panel 1-IV	0.098	0.984	0	0
Panel 1-V	0.295	0.689	1.969	0
Panel 2-I (w/ crack)	0	0.787	0	0
Panel 2-II	0	0.886	0	0
Panel 2-III	0.098	0.984	0	0
Panel 2-IV	0	0.394	0	0
Panel 2-V	0.591	1.378	0	0
Panel 3-I (w/ crack)	0	1.181	0	0
Panel 3-II	0.098	1.181	0	0
Panel 3-III	0.886	0.787	0	0
Panel 3-IV (w/ crack)	0	0.984	2.165	0
Panel 3-V	0.197	0.197	0	0
Panel 3-VI	0	0	0	0

Table 3.17 lists the colorimetric testing results from the deck panels with ECR. A wider variation in depth of carbonation was observed than was the case for cores from panels with conventional reinforcement, and the maximum depth of carbonation was greater. Carbonation depth from the top of the core ranged from 0 to 1.378 in., with an average of 0.283 in., approximately 50% greater than the depth of carbonation on the cores from panels with conventional reinforcement. This is again expected, as this deck did not receive a silane treatment, as confirmed by the water dye penetration test. Carbonation depth from the bottom of the core ranged from 0 to 1.969 in. The average carbonation depth from the bottom of the core was 0.794 in., comparable to that observed for panels with conventional reinforcement (0.833 in.). Chloride penetration was observed on all cores, in some cases reaching the level of the reinforcement (2 in.) in concentrations high enough to be detected by the indicator.

Table 3.17: Colorimetric Testing Results for Deck Panels with ECR

Panel-Core	Carbonation Depth from Top (in.)	Carbonation Depth from Bottom (in.)	Chloride Penetration (in.)	Water Dye Penetration (in.)
Panel 1-I	0.295	0.787	1.378	0.034
Panel 1-II	0.197	0.984	1.378	0.054
Panel 1-III (w/ crack)	0.098	1.969	1.969	0.038
Panel 1-IV	0.197	0.787	0.984	0.044
Panel 1-V	0	0.400	3.0	0.066
Panel 1-VI	0.591	0.984	1.772	0.032
Panel 2-I	1.378	0.591	0.394	0.026
Panel 2-II (w/ crack)	0	1.378	1.575	0.031
Panel 2-III (w/ crack)	0.098	0	2.362	0.064
Panel 2-IV	0	1.181	0.197	0.059
Panel 2-V	0.098	0.197	1.181	0.049
Panel 2-VI	0.197	0	1.575	0.074
Panel 3-I (w/ crack)	0.197	1.476	2.362	0.207
Panel 3-II	0.984	0.197	1.969	0.192
Panel 3-III	0.098	0.787	1.083	0.074
Panel 3-V (w/ crack)	0.098	0.984	2.362	0.059

3.4.8 Reinforcement Condition

As described in Section 3.4.7, several cores were taken directly over reinforcement, allowing for an inspection of the reinforcement to be performed. Figures 3.84 and 3.85 show conventional reinforcement obtained from cores taken in cracked and uncracked concrete, respectively. At cracks, conventional reinforcement showed clear signs of corrosion, whereas reinforcement in uncracked concrete was free of corrosion products. These results show that the conventional reinforcement performed well in uncracked concrete, while the inevitable formation of cracks resulted in corrosion, even with the silane treatment. Similar trends were observed for ECR (Figures 3.86 and 3.87), though it should be noted that the extent of corrosion on the ECR was much less than that observed on the conventional reinforcement. Under any circumstances, the presence of cracks in the decks had a deleterious effect on the corrosion performance of both uncoated and epoxy-coated reinforcement and demonstrated in large-scale field studies (Darwin et al. 2011).

Figure 3.84: Conventional reinforcement from Cow Creek deck panel. Core taken at a crack location.

Figure 3.85: Conventional reinforcement from Cow Creek deck panel. Core taken in uncracked concrete.

Figure 3.86: ECR from Cow Creek deck panel. Core taken at a crack location.

Figure 3.87: ECR from Cow Creek deck panel. Core taken in uncracked concrete.

CHAPTER 4: DESIGN LIFE AND COST EFFECTIVENESS

This chapter presents the anticipated time to first repair based on the laboratory results presented in Chapter 3 and the predicted cost to achieve a 100-year design life from each system is also presented.

4.1 Predicted Time to Repair

Predicting the time to repair requires that the time to corrosion initiation, the time from initiation to cracking of the concrete due to corrosion, and the time from cracking to repair or replacement be determined. Time to repair is not predicted for undamaged ECR, as it is unrealistic to expect ECR to be handled and placed without sustaining some damage. Undamaged galvanized reinforcement did not exhibit significantly different corrosion performance than damaged galvanized reinforcement, so undamaged galvanized reinforcement is also not considered separately. The methodology for predicting each of these stages based on laboratory data is outlined below.

4.1.1 Time to Corrosion Initiation

The critical chloride corrosion threshold (CCCT) for the types of reinforcement were obtained from samples taken from Southern Exposure specimens and are presented in Chapter 3. To obtain an equivalent time to initiation in a bridge deck, work by Lindquist (2005) and Miller (2000) is used. These studies sampled concrete at varying depths on Kansas bridge decks, both at cracks and away from cracks. Figure 4.1 shows the relationship between the chloride content at crack locations at a depth of 2.5 in., the cover typically specified for the top layer of reinforcement in bridge decks in Oklahoma, versus age for bridges with an average annual daily traffic (AADT) greater than 7,500 (relatively high traffic bridges). In this analysis, a cover of 2.5 and 3.0 in. will be compared.

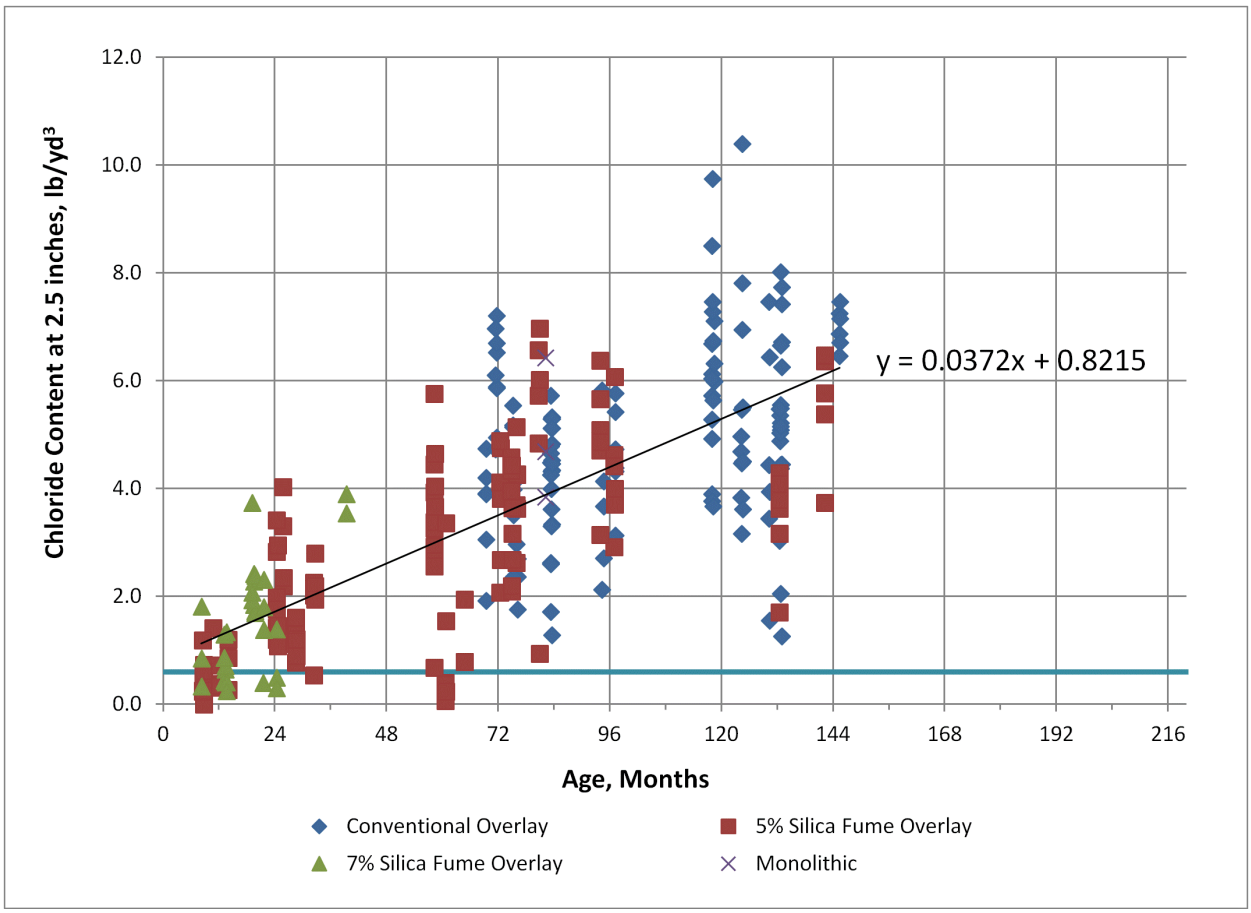

Figure 4.1: Chloride content taken at cracks interpolated at a depth of 2.5 in. versus age for bridges with an AADT greater than 7,500 (Lindquist 2005)

Equation (4.1) gives the average time *T* (x in Figure 4.1) in months to reach a specific chloride content *C* at a depth of 2.5 in., and is obtained by solving the best-fit equation from Figure 4.1 for time *T*.

$$T = \frac{C - 0.8215}{0.0372} \tag{4.1}$$

Based on the work by Lindquist (2005) and Miller (2000), a similar equation for the time to reach a specific chloride content at a depth of 3.0 in. is:

$$T = \frac{C - 0.7440}{0.0315} \tag{4.2}$$

Table 4.1 presents the average initiation age for corrosion initiation in months for the reinforcement in this study. The difference in critical chloride corrosion thresholds between Conv-A and Conv-C is not statistically significant, whereas the difference between those heats and Conv-B is. The three heats of steel will be considered separately to demonstrate the inherit variability in corrosion. For the A767 and A1094 bars, the average CCCT among all specimens was used, as the differences between the two types of bar are not statistically significant. As neither Ipanex nor Xypex altered the CCCT, CCCT values are taken as identical to those for the reinforcement cast in concrete without an inhibitor.

The low chloride threshold for Conv-B reinforcement resulted in a very low or negative initiation age based on Eq. (4.1); in this case, a minimum age of initiation of 6 months is used reflect an approximate time between casting of the concrete and the first salt application. As shown in Table 4.1, conventional reinforcement would be expected to initiate corrosion in 25.2 months or less; ECR has an initiation age over twice as long, 58.3 months. UV exposure did not alter the age of initiation for ECR, as discussed in Chapter 3. A767 and A1094 reinforcement have initiation ages comparable to conventional reinforcement. This is likely a conservative assumption; Darwin at al. (2009) found a higher critical chloride corrosion threshold for galvanized reinforcement than obtained in this study. A1035 reinforcement exhibited the highest time to initiation of any reinforcement in this study, 83.4 months. The Ipanex or Xypex do not alter the critical chloride corrosion threshold for either A1035 or conventional reinforcement.

Table 4.1: Equivalent Initiation Age (Months) For Reinforcement

System	CCCT, lb/yd^3	Equivalent Initiation Age (2.5 in. Cover), Months	Equivalent Initiation Age (3.0 in. Cover), Months
Conv-A	1.36	14.5	19.5
Conv-B	0.65	6.0*	6.0*
Conv-C	1.54	19.2	25.2
ECR	2.58	47.3	58.3
ECR-UV-1000	2.58	47.3	58.3
A767	1.48	17.7	23.4
A1094	1.48	17.7	23.4
A1035	3.37	68.6	83.4
A1035-Ipanex	3.37	68.6	83.4
A1035-Xypex	3.37	68.6	83.4
Conv-B-Ipanex	0.65	6.0*	6.0*
Conv-B-Xypex	0.65	6.0*	6.0*

*Minimum of 6 months assumed.

4.1.2 Time from Initiation to Cracking

The time from initiation of corrosion to cracking of the concrete depends on the corrosion rate of the reinforcement and the corrosion loss required to cause cracking. These factors are discussed in Sections 4.1.2.1 and 4.1.2.2, respectively.

4.1.2.1 Average Corrosion Rates after Initiation

The average corrosion rate after initiation is established for each system in this study based on the LPR corrosion losses in the cracked beam test, because corrosion-related damage is a function of total corrosion loss and the overwhelming majority of bridge decks exhibit cracking due to settlement or shrinkage of concrete. The average corrosion rate after

initiation is determined as follows:

1. The LPR corrosion loss at corrosion initiation based on total area, L_i, and the age of the specimen at corrosion initiation in weeks, W_i, are recorded.
2. The LPR corrosion loss at the end of testing based on total area, L_f, and the age of the specimen at the end of testing, W_f, are recorded.
3. The average corrosion rate after initiation based on losses is calculated for each specimen using Eq. (4.3).

$$R = \frac{L_f - L_i}{W_f - W_i} \times 52 \,\text{weeks}/\text{year} \tag{4.3}$$

The resulting average corrosion rates based on losses are shown in Table 4.2. The trends generally match those for the corrosion rates and losses shown in Chapter 3. Conventional reinforcement exhibited the highest corrosion rates of any system in this study. Conv-B, with an average rate of 24.6 µm/yr, exceeded those of Conv-A (19.8 µm/yr) or Conv-C (14.9 µm/yr), differences that are statistically significant; the difference in rates between Conv-A and Conv-C is not statistically significant (p = 0.22). ECR exhibited the lowest corrosion rate based on total area, 0.330 µm/yr, although its performance was significantly worsened (10 times higher) after prolonged UV exposure (p = 0.0003). In addition to corrosion rates based on total area, Table 4.2 also includes average corrosion rates expressed in terms of exposed area for the damaged epoxy-coated bars. These values are about 190 times those expressed in terms of total area, A767 and A1094 reinforcement exhibited similar corrosion rates (11.5 and 10.8 µm/yr, respectively); because this difference in rates is not statistically significant, an average value of 11.2 µm/yr is used for both types of reinforcement. Ipanex did not significantly alter the corrosion rate of conventional reinforcement. In contrast, Xypex resulted in a 48.7% reduction in the corrosion rate of Conv-B (p = 0.00004). Xypex was not tested with Conv-A or Conv-C; for the purpose of estimating cost effectiveness, it will be assumed that a similar reduction in rate would have occurred with these heats of conventional reinforcement. This is being done to ensure Xypex is not penalized for being paired with the poorest performing heat of conventional reinforcement. Specimens with A1035 reinforcement and Ipanex exhibited a corrosion rate (11.4 µm/yr) higher than A1035 reinforcement alone (7.41 µm/yr), a difference that is statistically significant (p=0.004); this behavior was not observed with conventional reinforcement.

Table 4.2: Average Corrosion Rates Based on Losses

	Average Corrosion Rate (µm/yr, Total Area) Based on Losses						Average	Std. Dev
	1	2	3	4	5	6		
Conv-A	25.8	21.1	24.0	14.8	20.7	12.7	19.8	5.14
Conv-B	21.6	23.9	30.0	23.1			24.6	3.70
Conv-C	12.4	21.1	11.2				14.9	5.39
ECR	0.037	0.536	0.683	0.063			0.330	0.329
ECR-UV-1000	2.68	3.66	3.56				3.301	0.543
A767	8.25	12.7	15.3	4.73	9.84	18.4	11.5	4.95
A1094	7.70	18.1	6.89	7.05	10.3	14.6	10.8	4.63
A1035	9.10	8.03	7.88	6.09	9.73	3.66	7.41	2.22
A1035-Ipanex	12.0	11.9	10.1	9.50	13.9	11.2	11.4	1.54
A1035-Xypex	6.76	10.2	8.26	8.25	8.31	6.96	8.11	1.22
Conv-B-Ipanex	22.4	33.3	27.4	18.7	20.9	22.2	24.1	5.30
Conv-B-Xypex	12.6	12.3	13.3	12.1	12.3	13.1	12.6	0.494
	Average Corrosion Rate (µm/yr, Exposed Area) Based on Losses						Avg.	Std. Dev
	1	2	3	4	5	6		
ECR	7.18	103	131	12.1			63.3	63.1
ECR-UV-1000	514	703	684				634	104

4.1.2.2 Equivalent Field Test Corrosion Rates

The cracked beam test is an accelerated test method, and the corrosion rates obtained under this test method are typically higher than what would be expected in the field. Darwin et al. (2011) evaluated identical corrosion protection systems using both laboratory and field specimens to establish a correlation between laboratory and field test specimen performance. Laboratory corrosion rates from cracked beam specimens are used, as prior studies (and the crack survey performed as part of the current study) have found that in bridge decks, cracks almost always form over the reinforcement due to settlement of plastic concrete and shrinkage of the hardened concrete. Darwin et al. (2011) found that, on average, bare reinforcement exhibited a corrosion rate in the field equal to 0.134 times that of the same reinforcement in the lab. Darwin et al. also noted that corrosion typically occurred only over approximately 40% of the bar surface area in the field, as opposed to nearly 100% of the bar area in the cracked beam test. These factors are used to convert the cracked beam corrosion rate into an equivalent field corrosion rate over the effective corroding area. For ECR, corrosion is assumed to be localized to the damaged area of the bar, 0.521% of the total area based on the damage pattern used in the cracked beam test (Chapter 2), and occurring at the rate based on the exposed area in the cracked beam specimens. That is, the corrosion rates for ECR are based on exposed area. The cracked beam corrosion rates and equivalent field corrosion rates are shown in Table 4.3, in the

following section.

4.1.2.3 Corrosion Loss to Cause Concrete Cracking and Time to Cracking

Table 4.3 also shows the corrosion loss to cause cracking for each system in this study, and the equivalent time from initiation to cracking in years. Based on work by Darwin et al. (2011), the corrosion loss in μm required to cause cracks in concrete is:

$$x_{crit} = 13.5\left(\frac{C^{2-A_f}}{D^{0.38}L_f^{\ 0.1}A_f^{\ 0.6}} + 0.6\right) \times 3^{A_f - 1} \quad (4.4)$$

where

x_{crit} = corrosion loss at crack initiation, μm

C = cover, in.

D = bar diameter, in.

L_f = fractional length of bar corroding, $L_{corroding}/L_{bar}$

A_f = fractional surface area of bar corroding, $A_{corroding}/A_{bar}$

For a No. 5 uncoated conventional steel bars with a concrete cover of 2.5 in., $L_f = A_f =$ 0.4 (since 40% of the surface area corrodes in field specimens), the value of x_{crit} is 72 μm. For the same bar with 3.0 in. cover, x_{crit} is 94 μm. O'Reilly et al. (2018) found that galvanized reinforcement requires approximately twice the corrosion loss to cause cracking for conventional reinforcement, giving x_{crit} values of 144 μm and 188 μm for 2.5 in. and 3.0 in. cover, respectively. For a No. 5 epoxy-coated bar with a damage pattern equal to that used for the field test specimens (1/8-in. diameter holes spaced at 4.9 in. on each side of the bar), the fractional length of exposed bar L_f is 0.024, the fractional area of exposed bar A_f is 0.0023, and the value of x_{crit} is 1826 μm. For the same bar with 3.0 in. cover, the value of x_{crit} is 2627 μm.

The corrosion losses to cause cracking are divided by the equivalent field corrosion rate to obtain the time from initiation to cracking, shown in Table 4.3. For decks with 2.5-in. cover, ECR-UV-1000 exhibited the lowest time to cracking after corrosion initiation, 2.9 years. It should be noted that the equivalent field rate for ECR with UV exposure is likely somewhat lower than reported. As shown in Chapter 3, ECR-UV bars exhibited significant blistering and cracking; thus, the corroding area of bar is likely somewhat greater than just the areas of intentional damage; this would result in a lower effective field rate and therefore a longer time to cracking. This area cannot be accurately determined; regardless, the detrimental effect of prolonged UV exposure on ECR is clear. ECR without UV exposure has a time to cracking after corrosion initiation 28.7 years

For conventional reinforcement, the time to cracking ranged from 8.7 to 14.4 years with 2.5-in. cover. The use of Xypex increased this time from 8.7 to 17.1 years for Conv-B reinforcement. A1035 reinforcement exhibited a time to first cracking of 29 years, and galvanized reinforcement exhibited the longest time to cracking, 38.4 years. Increasing the concrete cover to 3.0 in. extended the time to cracking for all systems, as expected.

Table 4.3: Effective Field Corrosion Rates and Time from Initiation to Cracking

	Cracked Beam-Average Rate, μm/yr	Equivalent Effective Field Rate**, μm/yr	Loss to Cause Cracking (2.5 in. Cover), μm	Time from Initiation to Cracking (2.5 in. Cover), years	Loss to Cause Cracking (3.0 in. Cover), μm	Time from Initiation to Cracking (3.0 in. Cover), years
Conv-A	19.8	6.6	72.0	10.8	94.0	14.1
Conv-B	24.6	8.3	72.0	8.7	94.0	11.4
Conv-C	14.9	5.0	72.0	14.4	94.0	18.9
ECR	0.33	63.3	1816.0	28.7	2627.0	41.5
ECR-UV-1000	3.3	633.7	1816.0	2.9	2627.0	4.1
A767	11.2	3.8	144.0	38.4	188.0	50.1
A1094	11.2	3.8	144.0	38.4	188.0	50.1
A1035	7.4	2.5	72.0	29.0	94.0	37.8
A1035-Ipanex	11.4	3.8	72.0	18.8	94.0	24.5
A1035-Xypex	7.4	2.5	72.0	29.0	94.0	37.9
Conv-B-Ipanex	24.6	8.3	72.0	8.7	94.0	11.4
Conv-B-Xypex	12.6	4.2	72.0	17.1	94.0	22.3
Conv-A-Xypex*	10.2	3.4	72.0	21.2	94.0	27.6
Conv-C-Xypex*	7.62	2.6	72.0	28.2	94.0	36.8

*Assumed value
**Based on exposed area for ECR and equivalent corroding area for other bars.

4.1.3 Time to First Repair

The time to first repair for each system is the sum of the time to corrosion initiation, the time to initial cracking of the concrete after corrosion initiation, and the time from first cracking to the time when the deck is repaired. The latter period is assumed to be 10 years, during which a series of short-term temporary repairs are conducted.

Tables 4.4 and 4.5 show the estimated time to repair for each system in bridge decks with 2.5 and 3.0 in. cover, respectively. For bridge decks with 2.5-in. cover, conventional reinforcement has times to first repair ranging from 19.2 to 26.1 years. The use of Xypex extends these values to 27.6 to 39.8 years. ECR has a predicted time to first repair of 42.6 years, provided it is protected from excessive UV exposure. Galvanized bars have a time to first repair of 49.9, largely due to the increased corrosion losses required to crack the concrete. A1035 reinforcement has an estimated time to first repair of 44.7 years. Increasing the cover to 3.0 in. extends the time to first repair of all systems, but notably, no system evaluated in this study is able to reach 100 years without repair.

Table 4.4: Estimated Time to First Repair in Years-Bridge Decks with 2.5 in. Cover

	Time to Initiation	Time from Initiation to Cracking	Time from Cracking to Repair	Predicted Time to First Repair
Conv-A	1.2	10.8	10.0	22.0
Conv-B	0.5	8.7	10.0	19.2
Conv-C	1.6	14.4	10.0	26.1
ECR	3.9	28.7	10.0	42.6
ECR-UV-1000	3.9	2.9	10.0	16.8
A767	1.5	38.4	10.0	49.9
A767-ND	1.5	38.4	10.0	49.9
A1094	1.5	38.4	10.0	49.9
A1094-ND	1.5	38.4	10.0	49.9
A1035	5.7	29.0	10.0	44.7
A1035-Ipanex	5.7	18.8	10.0	34.5
A1035-Xypex	5.7	29.0	10.0	44.8
Conv-B-Ipanex	0.5	8.7	10.0	19.2
Conv-B-Xypex	0.5	17.1	10.0	27.6
Conv-A-Xypex*	1.2	21.2	10.0	32.4
Conv-C-Xypex*	1.6	28.2	10.0	39.8

*Assumed values

Table 4.5: Estimated Time to First Repair in Years-Bridge Decks with 3.0 in. Cover

	Time to Initiation	Time from Initiation to Cracking	Time from Cracking to Repair	Predicted Time to First Repair
Conv-A	1.6	14.1	10.0	25.8
Conv-B	0.5	11.4	10.0	21.9
Conv-C	2.1	18.9	10.0	31.0
ECR	4.9	41.5	10.0	56.3
ECR-UV-1000	4.9	4.1	10.0	19.0
A767	1.9	50.1	10.0	62.1
A767-ND	1.9	50.1	10.0	62.1
A1094	1.9	50.1	10.0	62.1
A1094-ND	1.9	50.1	10.0	62.1
A1035	7.0	37.8	10.0	54.8
A1035-Ipanex	7.0	24.5	10.0	41.5
A1035-Xypex	7.0	37.9	10.0	54.9
Conv-B-Ipanex	0.5	11.4	10.0	21.9
Conv-B-Xypex	0.5	22.3	10.0	32.8
Conv-A-Xypex*	1.6	27.6	10.0	39.3
Conv-C-Xypex*	2.1	36.8	10.0	48.9

*Assumed values

4.2 100-year Cost Analysis

A 100-year economic life is used to compare the costs of each system for a typical bridge deck. A 150-ft-long, 42.2-ft-wide, 8-in.-thick bridge deck with concrete cover of 2.5 in. is used for this analysis. Reinforcing steel costs were obtained from the manufacturers; all other costs are based on winning bids for new construction and full-deck replacements in Oklahoma.

4.2.1 Initial cost

Table 4.6 presents the base cost for all types of reinforcement used in this study. A placement cost of $0.69/lb is used for all reinforcement with the exception of ECR, where a placement cost of $0.89/lb is used. A steel reinforcement density of 64.9 lb/yd^2 is used, based on the average quantity of steel used in bridge decks constructed in Oklahoma. The in-place cost for each type of reinforcement is the sum of the base and placement costs of the reinforcement, multiplied by the estimated steel quantity per square yard of deck, and is also presented in Table 4.6.

Table 4.6: In-place Reinforcement Costs

	Base Cost ($/lb)	Placement Cost ($/lb)	Total Cost ($/lb)	Steel Quantity (lb/yd^2)	In-Place Cost ($/yd^2)
Conv	$0.28	$0.69	$0.97	64.9	$62.95
ECR	$0.36	$0.89	$1.25	64.9	$81.13
A767	$0.71	$0.69	$1.40	64.9	$90.86
A1094	$0.58	$0.69	$1.27	64.9	$82.42
A1035	$1.03	$0.69	$1.72	64.9	$111.63

An in-place cost of concrete of $508.60/yd^3 is used in this study is based on costs for new bridge decks let in 2020 in Oklahoma. Assuming an 8-in.-thick bridge deck, 0.222 yd^3 of concrete are required per 1 yd^2 surface area of deck. Assuming an 8.5-in.-thick bridge deck, 0.236 yd^3 of concrete are required per 1 yd^2 surface area of deck. The concrete cost per square yard is then the cost per cubic yard multiplied by the concrete requirements listed above. Representatives from Xypex quoted the admixture cost as $19.44/yd^3; cost estimates for Ipanex were not available, so a similar cost is assumed. These costs are added to the cubic yard concrete costs given above.

The total initial costs, equal to the sum of reinforcement and concrete costs-for each system, are shown in Tables 4.7 and 4.8 for 8-in. (2.5-in. cover) and 8.5-in. (3.0-in. cover) decks, respectively. For bridge decks with a 2.5-in. cover, conventional reinforcement has the lowest initial cost, $175.95/yd^2. ECR comes in at a slightly higher initial cost, $194.13. A1035 is the most expensive reinforcement in terms of initial cost, $224.63. The addition of Ipanex or Xypex slightly increases initial costs, as does increasing cover to 3.0 in. (Table 4.8)

Table 4.7: Initial Costs–8-in. Deck, 2.5-in. Cover

	In-Place Cost	Concrete Cost ($/yd^2)	Total Cost ($/yd^2)
Conv	$62.95	$113.00	$175.95
ECR	$81.13	$113.00	$194.13
A767	$90.86	$113.00	$203.86
A1094	$82.42	$113.00	$195.42
A1035	$111.63	$113.00	$224.63
A1035-Ipanex	$111.63	$117.31	$228.94
A1035-Xypex	$111.63	$117.31	$228.94
Conv-Ipanex	$62.95	$117.31	$180.26
Conv-Xypex	$62.95	$117.31	$180.26

Table 4.8: Initial Costs–8.5-in. Deck, 3.0-in. Cover

	In-Place Cost	Concrete Cost ($/yd^2)	Total Cost ($/yd^2)
Conv	$62.95	$120.10	$183.05
ECR	$81.13	$120.10	$201.23
A767	$90.86	$120.10	$210.96
A1094	$82.42	$120.10	$202.52
A1035	$111.63	$120.10	$231.73
A1035-Ipanex	$111.63	$124.96	$236.59
A1035-Xypex	$111.63	$124.96	$236.59
Conv-Ipanex	$62.95	$124.96	$187.91
Conv-Xypex	$62.95	$124.96	$187.91

4.2.2 Repair Costs Over a 100-year Design Life

The repair costs for the bridge deck are based on full deck replacement costs in Oklahoma, as full deck replacement is the most commonly used means of repair in Oklahoma. These data only include the repair of bridge decks with conventional reinforcement; it is assumed these costs will not vary with reinforcement type. A cost of $323.18 is assumed and is limited to costs associated with mobilization, traffic control, removal of the existing deck, and related work. This cost does not include the cost of a new deck; those costs are summarized in Section 4.2.1 and must be added to the $323.18 to get the total cost of rehabilitation. This total cost is shown in Table 4.9. As expected, the repair costs are much greater than the initial cost of the deck.

The total cost of each type of reinforcement over a 100-year design life is calculated using the time to first repair for systems in cracked concrete listed in Tables 4.3 and 4.4. Cost effectiveness is based on the initial cost of the deck and the present value of future repair costs. The present value is calculated as shown Eq. (4.5), where *P* is the present value, *F* is the future cost of a repair, *i* is the discount rate, and n is the time to repair.

$$P = F\left(1+i\right)^{-n} \tag{4.5}$$

For this study, a discount rate of 2 percent is used, as it is representative of what is assumed by most state governments. Tables 4.10 and 4.11 show the estimated 100-year design life costs for 8- and 8.5-in. bridge decks with 2.5 and 3.0-in. cover, respectively. For ECR-UV bars, it is assumed repairs are performed with ECR that has been protected from UV exposure. A discussion of these results follows.

Table 4.9: Total Repair Cost, $/yd^2

	8-in. Deck, 2.5-in. Cover	8.5-in. Deck, 3.0-in. Cover
Conv-A	$499.13	$506.23
Conv-B	$499.13	$506.23
Conv-C	$499.13	$506.23
ECR	$517.31	$524.41
ECR-UV-1000	$517.31	$524.41
A767	$527.04	$534.14
A1094	$518.60	$525.70
A1035	$547.81	$554.91
A1035-Ipanex	$549.14	$556.31
A1035-Xypex	$549.14	$556.31
Conv-B-Ipanex	$503.44	$511.09
Conv-B-Xypex	$503.44	$511.09
Conv-A-Xypex	$503.44	$511.09
Conv-C-Xypex	$503.44	$511.09

The total costs over a 100-year design life are given in Tables 4.10 and 4.11 for 8-in. decks with a 2.5-in. cover and 8.5-in. decks with a 3.0-in. cover, respectively. The costs for decks initially constructed with UV exposed ECR are based on the assumption that repairs are made with epoxy-coated bars that have not had extended UV exposure.

Table 4.10: 100-year Design Life Costs–8-in. Deck, 2.5-in. Cover

	Initial Cost, $/yd^2	Time to Repair, Years					Repair Cost, $/yd^2	Total Present Cost, $/yd^2
		1	2	3	4	5		
Conv-A	$175.95	22.0	44.1	66.1	88.2		$499.13	$929
Conv-B	$175.95	19.2	38.4	57.7	76.9	96.1	$499.13	$1,093
Conv-C	$175.95	26.1	52.1	78.2			$499.13	$758
ECR	$194.13	42.6	85.2				$517.31	$512
ECR-UV-1000	$194.13	16.8	59.4				$517.31	$725
A767	$203.86	49.9	99.7				$527.04	$473
A1094	$195.42	49.9	99.7				$518.60	$461
A1035	$224.63	44.7	89.4				$547.81	$544
A1035-Ipanex	$225.96	34.5	69.0				$549.14	$643
A1035-Xypex	$225.96	44.8	89.5				$549.14	$546
Conv-B-Ipanex	$180.26	19.2	38.4	57.7	76.9	96.1	$503.44	$1,105
Conv-B-Xypex	$180.26	27.6	55.1	82.7			$503.44	$739
Conv-A-Xypex	$180.26	32.4	64.7	97.1			$503.44	$659
Conv-C-Xypex	$180.26	39.8	79.6				$503.44	$513

Table 4.11: 100-year Design Life Costs–8.5-in. Deck, 3.0-in. Cover

	Initial Cost, $/yd^2	Time to Repair, Years					Repair Cost, $/yd^2	Total Present Cost, $/yd^2
		1	2	3	4	5		
Conv-A	$183.05	25.8	51.5	77.3			$506.23	$779
Conv-B	$183.05	21.9	43.8	65.7	87.5		$506.23	$951
Conv-C	$183.05	31.0	61.9	92.9			$506.23	$686
ECR	$201.23	56.3					$524.41	$373
ECR-UV-1000	$201.23	19.0	75.3				$524.41	$679
A767	$210.96	62.1					$534.14	$367
A1094	$202.52	62.1					$525.70	$356
A1035	$231.73	54.8					$554.91	$419
A1035-Ipanex	$233.13	41.5	83.0				$556.31	$585
A1035-Xypex	$233.13	54.9					$556.31	$421
Conv-B-Ipanex	$187.91	21.9	43.8	65.7	87.5		$511.09	$964
Conv-B-Xypex	$187.91	32.8	65.5	98.3			$511.09	$667
Conv-A-Xypex	$187.91	39.3	78.5				$511.09	$531
Conv-C-Xypex	$187.91	48.9	97.9	-			$511.09	$455

4.2.3 Discussion

Decks constructed with conventional reinforcement, as expected, had the highest costs over the 100-year design life. The three different heats of steel in this study exhibit a wide range in 100-year design life costs, ranging from $758 to $1093. This variation highlights the difficulties in precisely predicting design life and costs, as slight changes in steel chemistry or production result in drastically different outcomes. Using conventional reinforcement with Xypex was effective at reducing total costs over a 100-year design life, although even the best-performing heat of conventional reinforcement with Xypex gave a 100-year cost comparable with ECR in a 2.5-in. cover deck and worse than ECR with a 3.0-in. cover. Ipanex will not be effective in reducing the 100-year design life costs.

Decks with epoxy-coated reinforcement with UV exposure exhibited about twice the cost of decks with ECR without UV exposure because of the shortened time to first repair. As previously discussed, however, the time to first repair for decks containing ECR with UV damage is very likely underestimated; furthermore, it is unlikely that ECR would sit for one year exposed to the elements (the equivalent of 1000 hours of UV exposure under ASTM G154). Nevertheless, rapid macrocell test results (Chapter 3) suggest even 100 hours of UV exposure under ASTM G154, equivalent to just over a month of exposure and within the guidelines of ASTM D3963, result in reduced corrosion protection. When protected from UV exposure, ECR exhibits one of the lowest 100-year costs in this study–$512for 8-in. decks with a 2.5-in. cover.

Decks with either A767 or A1094 reinforcement exhibited low 100-year costs, and those with A1094 reinforcement exhibited the lowest costs in this study for both 8-in. decks and 8.5-in. decks (2.5-in. and 3.0-in. cover, respectively). These values should be viewed with some caution, however. As described in Chapter 3, significant portions of the coatings of both A767 and A1094 showed corrosion of the zinc coating–even on the bottom mat, in the absence of chlorides. This suggests the bars may exhibit corrosion from the moment the concrete is placed, lowering the design life somewhat. Furthermore, although prior research (O'Reilly et al. 2018) found galvanized reinforcement required twice the corrosion loss to crack concrete as conventional reinforcement, this research was performed on laboratory-scale specimens and may not be directly applicable on a larger scale. In addition, the performance of galvanized reinforcement will depend on the application of zinc over the full bar surface, not universally achieved in bars delivered for use in this study. Further research is needed, particularly on the relative performance of A767 and A1094 bars and effect of bends on the corrosion performance of both (Table 3.12). Both, however, show promise as a cost-effective corrosion protection system.

Decks containing A1035 reinforcement exhibited costs slightly higher than those containing ECR, but better than those with any heat of conventional reinforcement in this study. Unlike conventional reinforcement, however, A1035 reinforcement did not appear to benefit from the addition of Xypex. This may be due to the lower corrosion rate of A1035 reinforcement. Xypex claims to reduce the permeability of concrete, and therefore slows oxygen and moisture transport to the cathode in a corroding bar. This reduction in permeability may inhibit corrosion on a bar with low corrosion resistance, where the cathode reaction would run quickly and rapidly consume water and oxygen, but may not impact corrosion on a more corrosion-resistant material, where the slower corrosion rate would result in less demand for oxygen and moisture at the cathode.

In all cases, even with the higher initial and repair costs, increasing the deck thickness from 8 to 8.5 in, obtained by increasing the cover from 2.5 to 3.0 in., significantly reduced total costs over a 100-year design life. This reduction in cost is tied to the increase in corrosion losses needed to crack the concrete with greater cover, resulting in longer time to repair. With the increased cover, several corrosion protection systems (ECR, galvanized, and A1035) achieve a 100-year design life with only a single repair, as opposed to two repairs with a 2.5-in. cover.

The values presented in this report should not be viewed as absolute; the results in Chapter 3 show that each system exhibited significant variations in performance, variations that will certainly affect field performance. The analysis demonstrates that ECR, galvanized, and A1035 reinforcement are viable and cost-effective corrosion protection systems and should be considered for use.

CHAPTER 5: SUMMARY AND CONCLUSIONS

5.1 Summary

This study evaluated the corrosion resistance of conventional, epoxy-coated, galvanized ASTM A767 and A1094 reinforcement, and ASTM A1035 reinforcement containing a nominal chromium content of 9% using the rapid macrocell, Southern Exposure, and cracked beam tests. Coated bars were evaluated with coatings in both an undamaged condition and with damage simulating that which would occur during handling and placing. Selected epoxy-coated bars were exposed to an accelerated weathering program under ultraviolet light, simulating outdoor exposure. Galvanized reinforcement is evaluated after bending, was well as straight. Two waterproofing admixtures, Ipanex and Xypex, were also evaluated. Field observations of an in-service bridge deck on I-35 over Chikaskia River containing A1035 reinforcement with Ipanex were conducted, and deck panels containing conventional and epoxy-coated reinforcement from a bridge on I -35 over Cow Creek were evaluated. The results from the laboratory data and prior field results, combined with construction costs, were used to determine the cost of each system over a 100-year design life.

5.2 Conclusions

The following conclusions are based on the research presented in this report.

1. Epoxy-coated reinforcement (ECR) without UV exposure exhibited a significant increase in corrosion resistance compared to conventional reinforcement across all laboratory tests. Undamaged ECR exhibited no significant corrosion activity under any test conditions.
2. After as few as 100 hours of UV exposure under ASTM G154 Cycle 1 conditions (equivalent to approximately 1.2 months of outdoor exposure), the corrosion resistance of ECR was drastically reduced, with UV-exposed ECR exhibiting corrosion rates several times higher than ECR without UV exposure.
3. A767 and A1094 reinforcement exhibited similar performance in terms of corrosion resistance. Corrosion losses were generally slightly less than that of conventional reinforcement both with and without damage to the coating; however, corrosion losses increased when the bars were bent.
4. In concrete, A1035 reinforcement exhibited corrosion losses lower than conventional reinforcement, but higher than ECR. The corrosion resistance of A1035 reinforcement was not improved by the addition of Ipanex or Xypex.
5. Ipanex was not effective in improving the corrosion resistance of conventional reinforcement; however, conventional reinforcement with Xypex showed significant reductions in corrosion losses in both uncracked and cracked concrete.
6. Crack surveys of the deck on the Chikaskia River bridge showed significant shrinkage and settlement cracking, though no signs of corrosion damage. Based on the analyses presented in this report and given the age of the deck, no signs of damage would be expected.
7. Examination of the Cow Creek deck panels found that concrete was effective in protecting the reinforcement from corrosion if uncracked, but not if cracked.
8. The cost analysis over a 100-year design life found that ECR, galvanized, and

A1035 reinforcement were all cost-effective corrosion protection systems.

9. Increasing cover from 2.5 to 3 in. decreased the costs over a 100-year design life for every reinforcement system in this study.

5.3 Recommendations

1. Conventional reinforcement is not a cost-effective corrosion protection system and should not be used on bridge deck components exposed to chlorides.
2. ECR should be stored in a manner that protects it from UV exposure. The existing guidelines in ASTM D3963 limiting unprotected exposure to two months are not sufficient to protect the coating from damage, and limiting exposure to one month or less should be required.
3. ASTM A767 and A1094 reinforcement exhibited similar corrosion resistance and can be used interchangeably.
4. Additional research is needed on the corrosion loss to crack concrete in large-scale structures with galvanized reinforcement, particularly A1094 reinforcement for which there is no data. Research is also needed on the effect of bends on the corrosion performance of both types of galvanized reinforcement and the type of repair(s) needed if bends are shown to consistently reduce the corrosion performance of either A767 or A1094 bars.
5. Increasing the concrete cover from 2.5 to 3.0 in. should be considered as a means of reducing costs over the design life of a bridge deck.

CHAPTER 6: REFERENCES

201.1R-08 (2008). “Guide for Conducting a Visual Inspection of Concrete in Service,“ American Concrete Institute, Farmington Hills, Michigan, 16 pp.

ACI 364.1-19 (2019). “Guide for Assessment of Concrete Structures Before Rehabilitation,” American Concrete Institute, Farmington Hills, Michigan, 19 pp.

Andrade, M., and Macias, A. (1988). “Galvanized Reinforcements in Concrete,” *Surface Coatings—2*, Springer, pp. 137-182.

ASTM A615-20 (2020). “Standard Specification for Deformed and Plain Carbon-Steel Bars for Concrete Reinforcement,” American Society for Testing and Materials, West Conshohocken, PA, 8 pp.

ASTM A767-19 (2019). “Standard Specification for Zinc-Coated (Galvanized) Steel Bars for Concrete Reinforcement,” American Society for Testing and Materials, West Conshohocken, PA, 6 pp.

ASTM A775-19 (2019). “Standard Specification for Epoxy-Coated Steel Reinforcing Bars,” American Society for Testing and Materials, West Conshohocken, PA, 11 pp.

ASTM A955-19 (2019). “Standard Specification for Deformed and Plain Stainless Steel Bars for Concrete Reinforcement,” American Society for Testing and Materials, West Conshohocken, PA, 16 pp.

ASTM A1035-19 (2019). “Standard Specification for Deformed and Plain, Low-Carbon, Chromium, Steel Bars for Concrete Reinforcement,” American Society for Testing and Materials, West Conshohocken, PA, 7 pp.

ASTM A1094-18 (2018). “Standard Specification for Continuous Hot-Dip Galvanized Steel Bars for Concrete Reinforcement,” American Society for Testing and Materials, West Conshohocken, PA, 5 pp.

ASTM C39-20 (2020). “Standard Test Method for Compressive Strength of Cylindrical Concrete Specimens,” American Society for Testing and Materials, West Conshohocken, PA, 8 pp.

ASTM C42-20 (2020). “Standard Test Method for Obtaining and Testing Drilled Cores and Sawed Beams of Concrete,” American Society for Testing and Materials, West Conshohocken, PA, 7 pp.

ASTM C469-14 (2014). “Standard Test Method for Static Modulus of Elasticity and Poisson's Ratio of Concrete in Compression,” American Society for Testing and Materials, West Conshohocken, PA, 5 pp.

ASTM C496-17 (2017). “Standard Test Method for Splitting Tensile Strength of Cylindrical Concrete Specimens,” American Society for Testing and Materials, West Conshohocken, PA, 5 pp.

ASTM C805-18 (2018). “Standard Test Method for Rebound Number of Hardened Concrete,” American Society for Testing and Materials, West Conshohocken, PA, 4 pp.

ASTM C876-15 (2015). “Standard Test Method for Corrosion Potentials of Uncoated Reinforcing Steel in Concrete,” American Society for Testing and Materials, West Conshohocken, PA, 8 pp.

ASTM C1218-20 (2020). “Standard Test Method for Water-Soluble Chloride in Mortar and Concrete,” American Society for Testing and Materials, West Conshohocken, PA, 3 pp.

ASTM D3963-15 (2015). “Standard Specification for Fabrication and Jobsite Handling of Epoxy-Coated Steel Reinforcing Bars,” American Society for Testing and Materials, West Conshohocken, PA, 3 pp.

ASTM G154-16 (2016). “Standard Practice for Operating Fluorescent Ultraviolet (UV) Lamp Apparatus for Exposure of Nonmetallic Materials,” American Society for Testing and Materials, West Conshohocken, PA, 11 pp.

Bertolini, L., Elsener, B., Pedeferri, P., Redaelli, E., and Polder, R. (2013). “Corrosion of Steel in Concrete: Prevention, Diagnosis, Repair,” *Wiley Online Library*.

Broomfield, J. P. (2003). “Corrosion of Steel in Concrete: Understanding, Investigation and Repair,” *CRC Press*.

“Cement Chemistry Systems”. https://www.ipanex.com Accessed March 29, 2020.

Cetiner, M., Singh, P., Abes, J., and Gilroy-Scott, A. (2000). UV Degradation of Fusion Bonded Epoxy Coating in Stockpiled Pipes,” Paper presented at *The International Pipeline Conference*.

“ChromX”. https://www.cmc.com/en/americas/our-businesses/mill-products/chromx Accessed August 25 2020.

Darwin, D., Browning, J., Van Nguyen, T., and Locke Jr, C. E. (2002). “Mechanical and Corrosion Properties of a High-strength, High Chromium Reinforcing Steel for Concrete,” *SM Report* No. 66*,* Lawrence, KS, University of Kansas Center for Research, 142 pp.

Darwin, D., Browning, J., O’Reilly, M., Xing, L., and Jianxin, J. (2009). “Critical Chloride Corrosion Threshold of Galvanized Reinforcing Bars,” *ACI Materials Journal,* Vol. 106, No 2, pp. 176-183.

Darwin, D., O'Reilly, M., Farshadfar, O., Browning, J., and Locke Jr, C. (2018). “Corrosion-Induced Concrete Cracking for Uncoated and Galvanized Reinforcing Bars,” *ACI Materials Journal,* Vol. 115, No 6, pp. 825-832.

Draper, J., Darwin, D., Browning, J. P., Locke, C. E. (2009). “Evaluation of Multiple Corrosion Protection Systems for Reinforced Concrete Bridge Decks,” *SM Report* No. 96*,* Lawrence, KS, University of Kansas Center for Research, 429 pp.

Engle, E. (1999). “Effect of Waterproofing Admixture Ipanex on Concrete Durability,” Iowa Department of Transportation Report MLR-98-2, Ames, IA, 22 pp.

Fedor, G. R., and Brennan, P. J. (2011). “Comparison Between Natural Weathering and Fluorescent UV Exposures,” *Durability Testing of Nonmetallic Materials,* 15 pp.

Gong, L., Darwin, D., Browning, J. P., and Locke Jr, C. E. (2002). “Evaluation of Mechanical and Corrosion Properties of MMFX Reinforcing Steel for Concrete,” *SM Report* No. 70, University of Kansas Center for Research, 113 pp.

Hisey, J. (2004). “Investigation of MMFX Reinforcing Steel and the Admixture IPANEX for Use in Bridge Decks,” Oklahoma State University, 130 pp.

Ji, J., Darwin, D., and Browning, J. (2005). “Corrosion Resistance of Duplex Stainless Steels and MMFX Microcomposite Steel for Reinforced Concrete Bridge Decks,” *SM Report* No. 80, University of Kansas Center for Research, 453 pp.

Kamde, D., and Pillai, R. (2020). “Effect of Sunlight/Ultraviolet Exposure on The Corrosion of Fusion Bonded-Epoxy (FBE) Coated Steel Rebars in Concrete,” *Corrosion,* Vol. 76, No. 9, pp. 843-860.

Koch, G. H., Brongers, M. P., Thompson, N. G., Virmani, Y. P., and Payer, J. H. (2002). “Corrosion Cost and Preventive Strategies in the United States,” United States. Federal Highway Administration, 786 pp.

Kotnarowska, D. (1999). “Influence of Ultraviolet Radiation And Aggressive Media on Epoxy Coating Degradation,” *Progress in Organic Coatings,* Vol. 37, No 3-4, pp. 149-159.

Lindquist, W.; Darwin, D.; and Browning, J. (2005) “Cracking and Chloride Contents in Reinforced Concrete Bridge Decks,” *SM Report* No. 78, University of Kansas Center for Research, Lawrence, KS, Feb., 453 pp.

Lindquist, W., Darwin, D., Browning, J., and Miller, G. G. (2006). “Effect of Cracking on Chloride Content in Concrete Bridge Decks,” *American Concrete Institute,* Vol. 103, No 6, pp. 467-473.

Lindquist, W.; Darwin, D.; and Browning, J. (2008) “Development and Construction of Low-Cracking High Performance Concrete (LC-HPC) Bridge Decks: Free Shrinkage, Mixture Optimization, and Concrete Production” *SM Report* No. 92, University of Kansas Center for Research, Lawrence, KS, Nov., 540 pp.

Miller, G.G. and Darwin, D., “Performance and Constructability of Silica Fume Bridge Deck Overlays,” *SM Report* No. 57, The University of Kansas Center for Research, Lawrence, Kansas, January 2000, 423 pp.

Ogunsanya, I. (2017). “Evaluation of the Behaviour of Continuously Galvanized Rebar,” University of Waterloo, 96 pp.

O’Reilly, M., Darwin, D., Browning, J., and Locke, C. E. J. (2011). “Evaluation of Multiple Corrosion Protection Systems for Reinforced Concrete Bridge Decks,” *SM Report* No. 100, Lawrence, KS, University of Kansas Center for Research, 487 pp.

Poursaee, A. (2016). “Corrosion of Steel in Concrete Structures,” in *Corrosion of Steel in Concrete*

Structures, *Elsevier*, pp. 19-33.

Torres-Acosta, A. A., and Sagues, A. A. (2004). “Concrete Cracking by Localized Steel Corrosion--Geometric Effects,” *ACI Materials Journal,* Vol. 101, No 6, pp. 501-507.

Treadaway, K. W. J., Cox, R. N., and Brown, B. L. (1989). “Durability of corrosion resisting steels in concrete,” *Proceedings of the Institution of Civil Engineers,* Vol. 86, No 2, pp. 305-331.

Verbeck, G. J. (1975). “Mechanisms of corrosion of steel in concrete,” *Special Publication,* Vol. 49, American Concrete Insitute, Farmington Hills, MI, No, pp. 21-38.

Weyers, R. E., Pyc, W., and Sprinkel, M. M. (1998). “Estimating the Service Life of Epoxy Coated Reinforcing Steel,” *ACI Materials Journal,* Vol. 95, No 5, pp. 546-557.

“XYPEX”. https://www.xypex.com Accessed March 29, 2020.

APPENDIX A: INDIVIDUAL SPECIMEN CORROSION RATES AND POTENTIALS

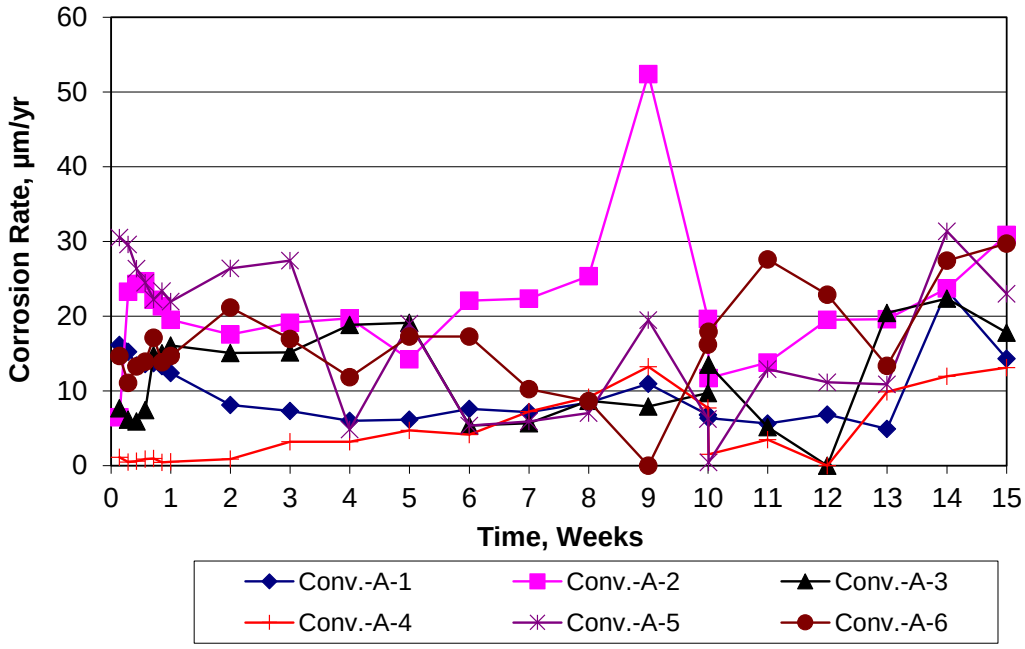

Figure A.1: Rapid macrocell test. Corrosion rate of Conv-A reinforcement.

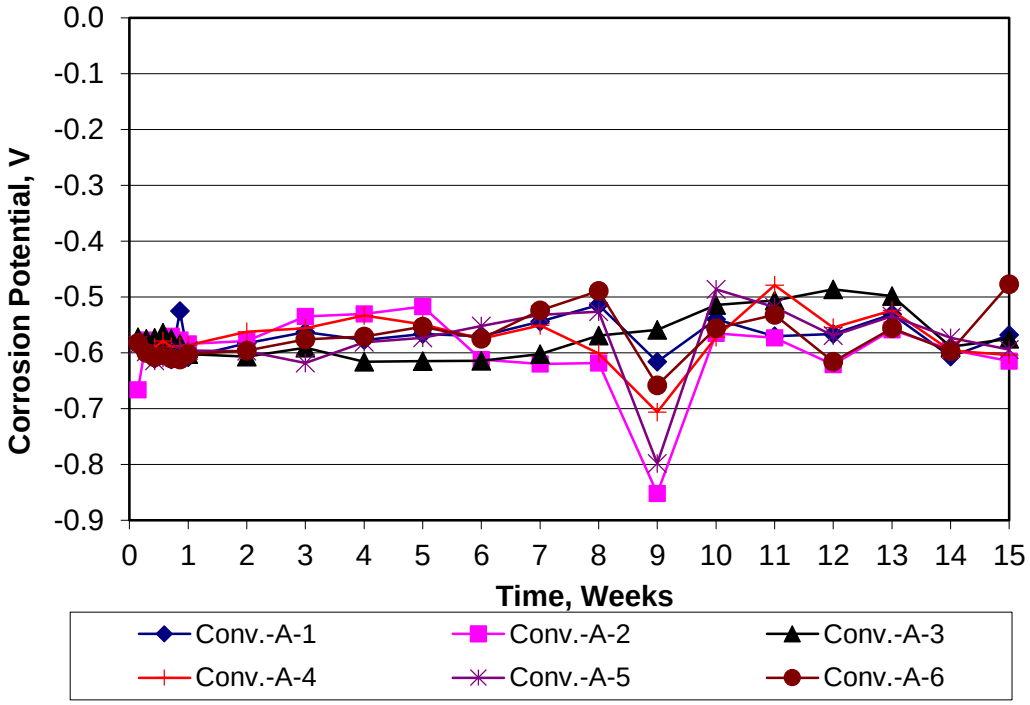

Figure A.2: Rapid macrocell test. Corrosion potential of Conv-A reinforcement.

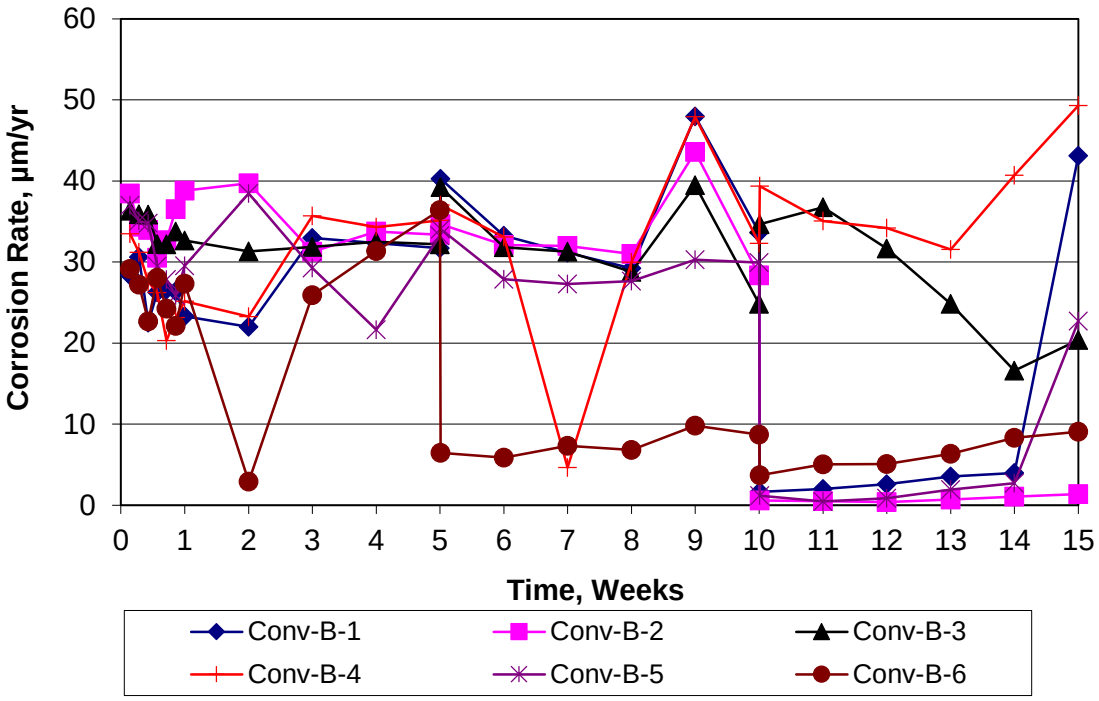

Figure A.3: Rapid macrocell test. Corrosion rate of Conv-B reinforcement.

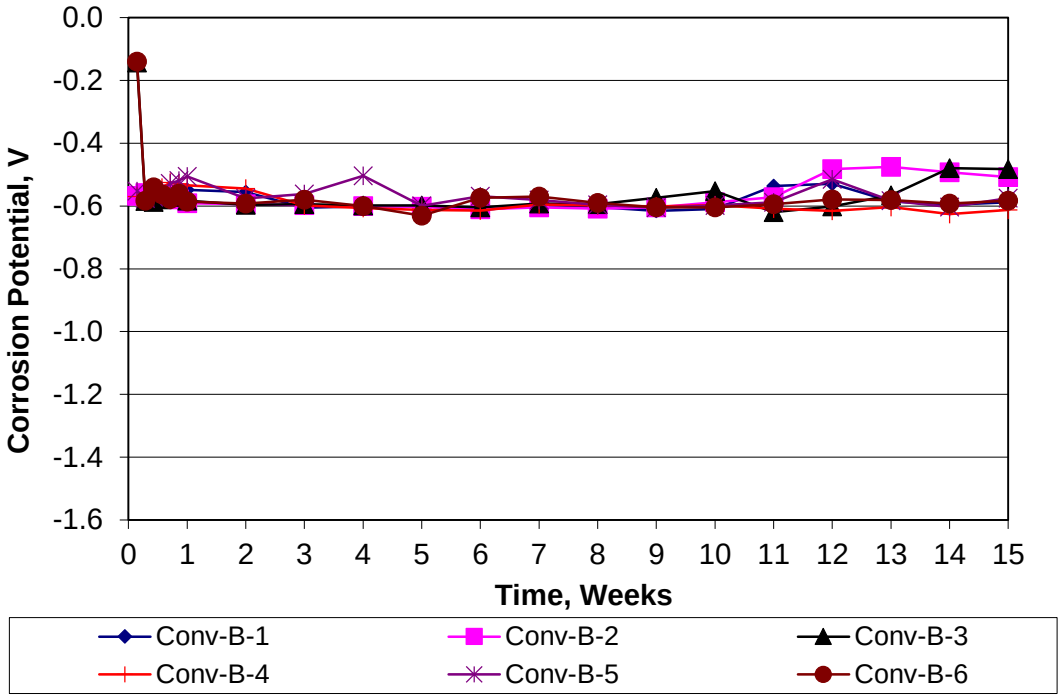

Figure A.4: Rapid macrocell test. Corrosion potential of Conv-B reinforcement.

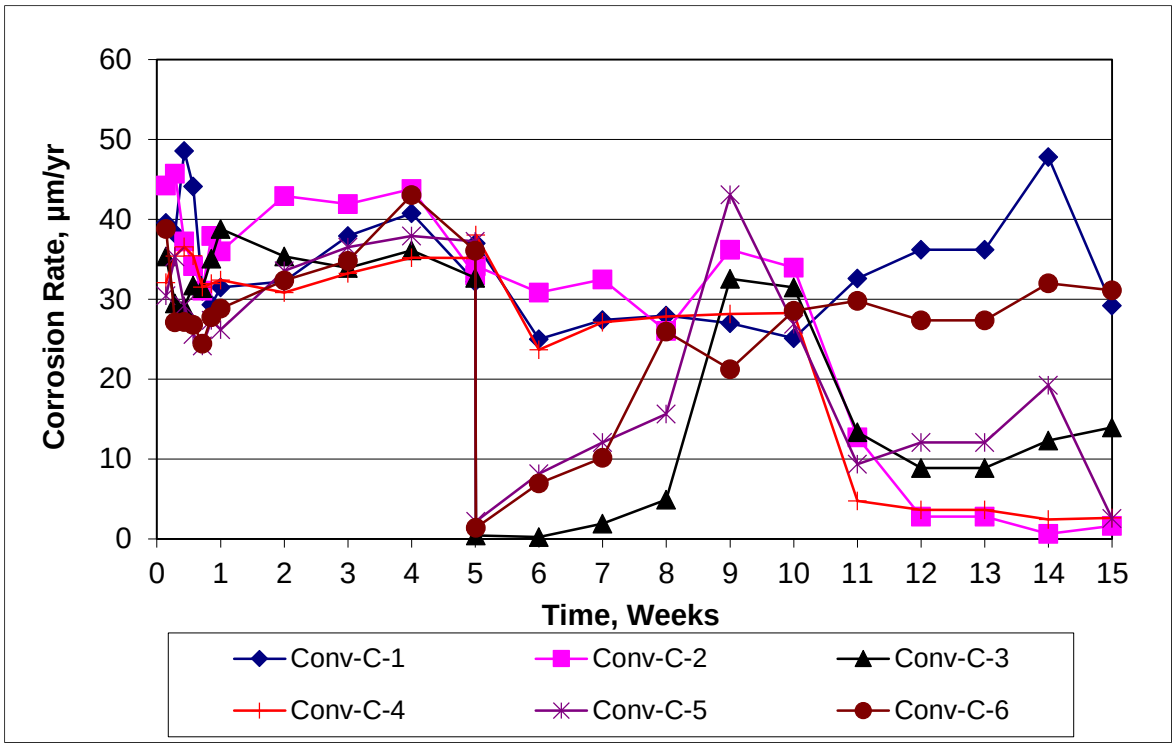

Figure A.5: Rapid macrocell test. Corrosion rate of Conv-C reinforcement.

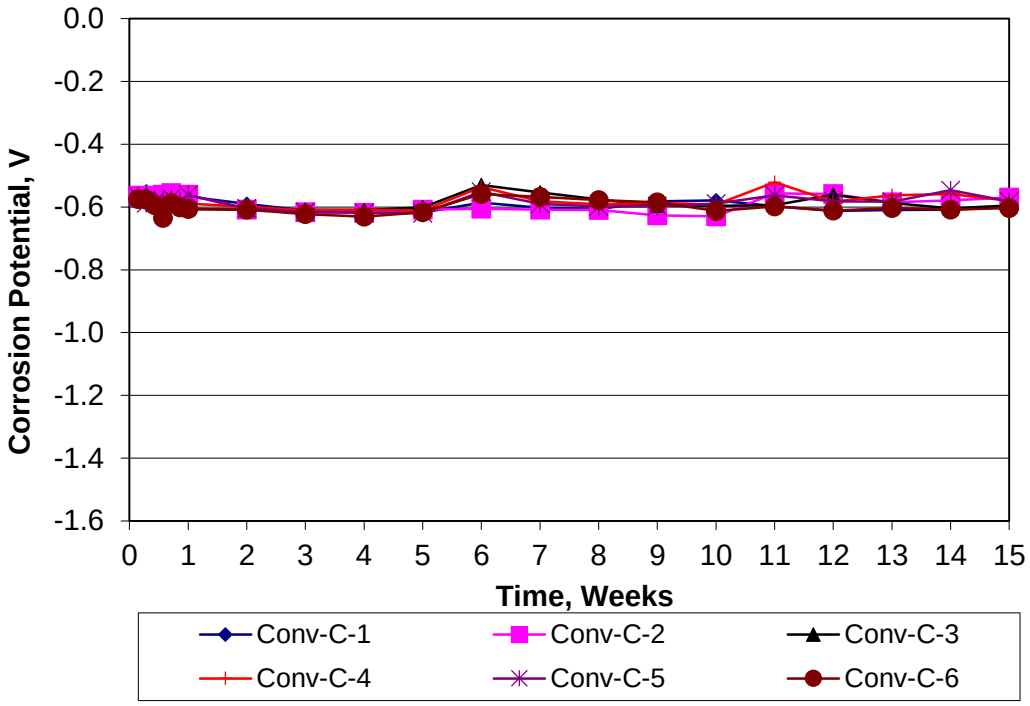

Figure A.6: Rapid macrocell test. Corrosion potential of Conv-C reinforcement.

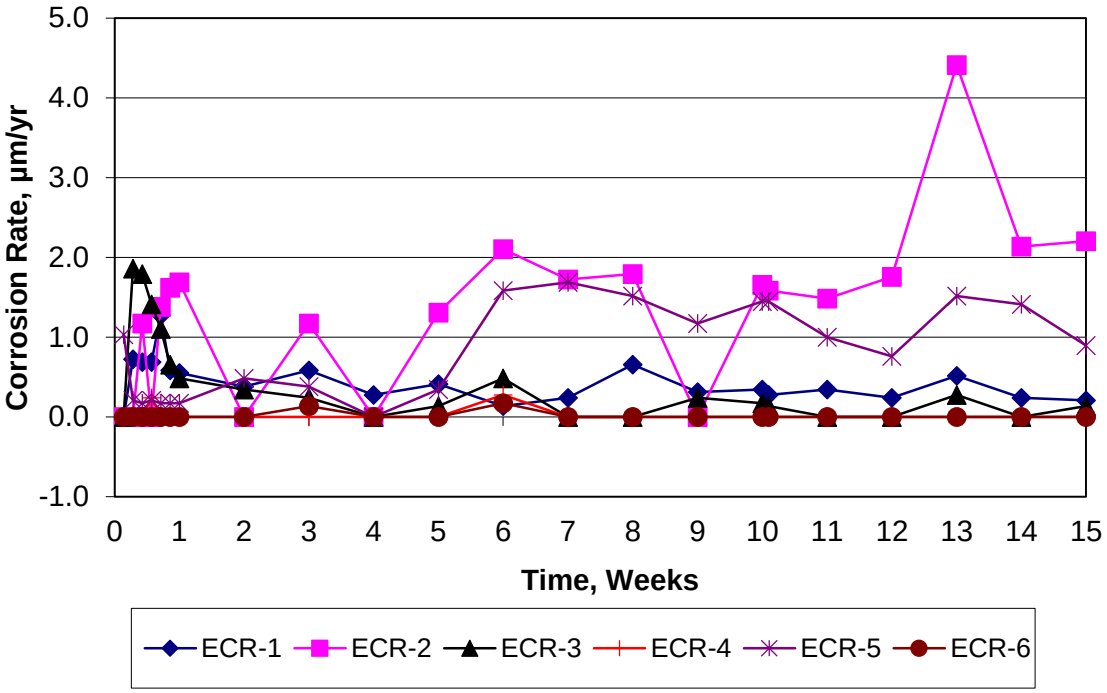

Figure A.7: Rapid macrocell test. Corrosion rate of ECR.

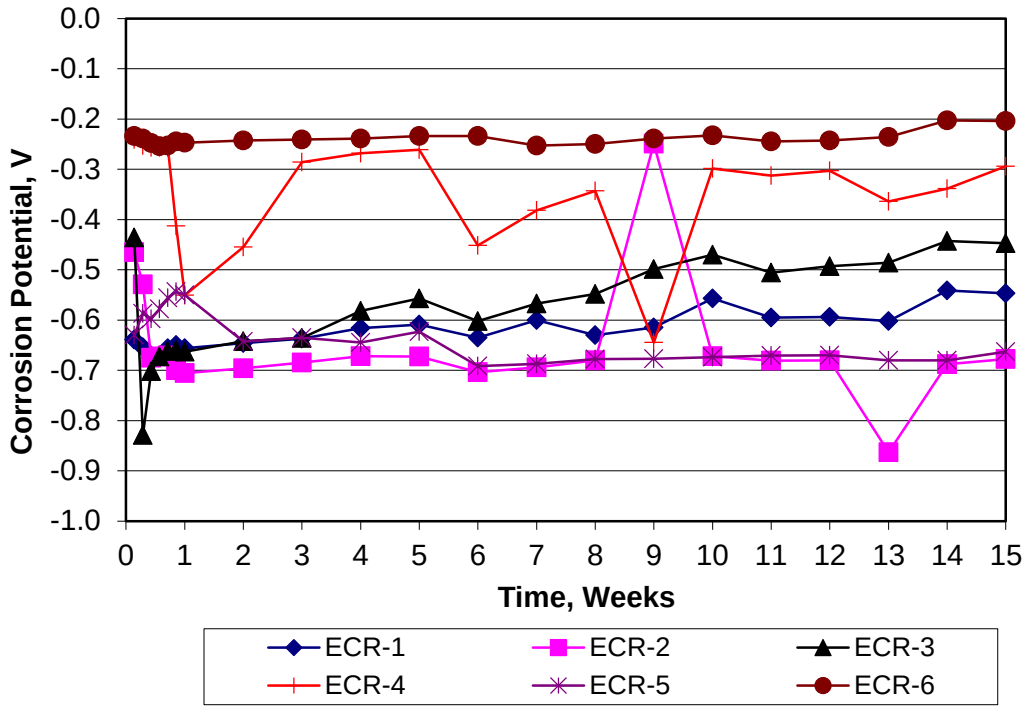

Figure A.8: Rapid macrocell test. Corrosion potential of ECR.

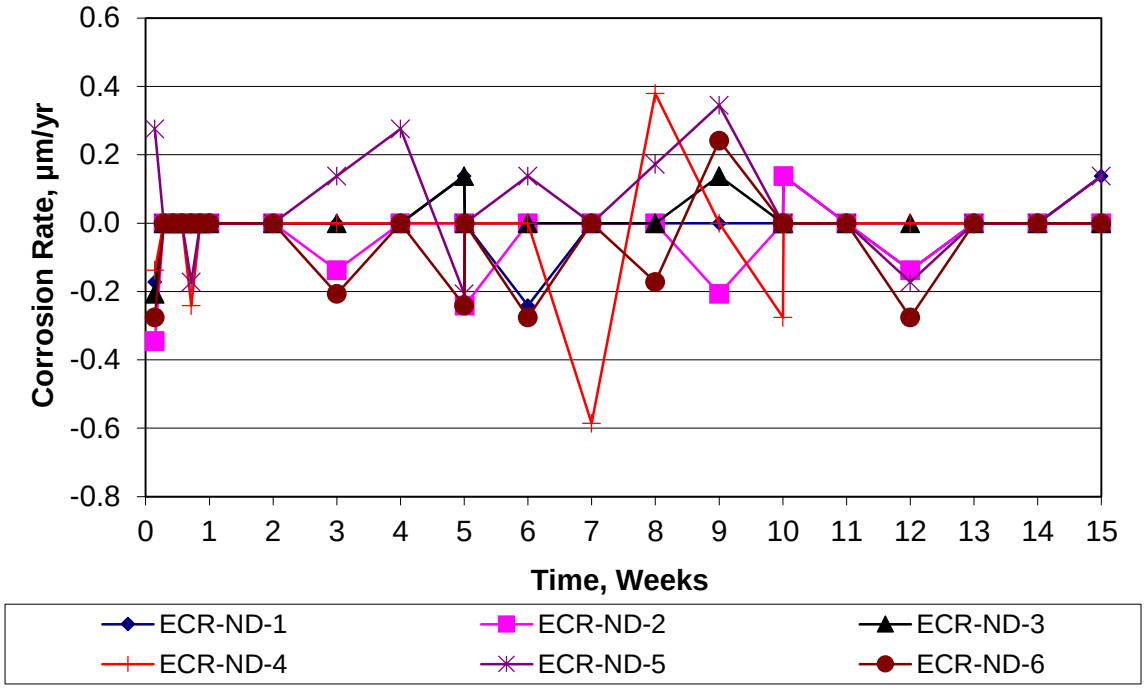

Figure A.9: Rapid macrocell test. Corrosion rate of ECR-ND.

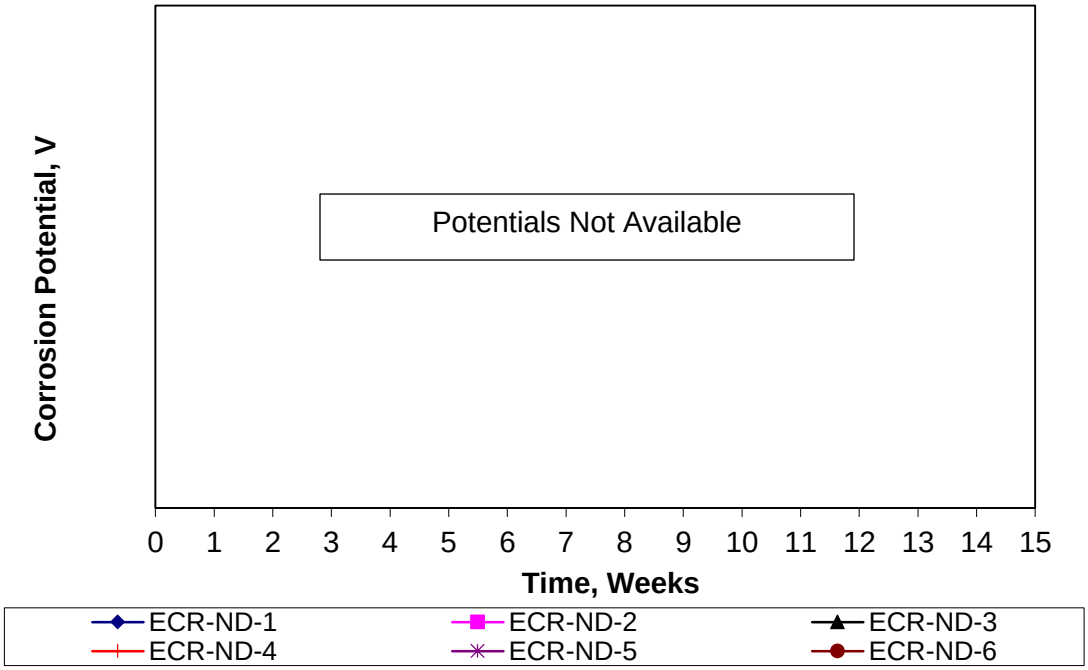

Figure A.10: Rapid macrocell test. Corrosion potential of ECR-ND.

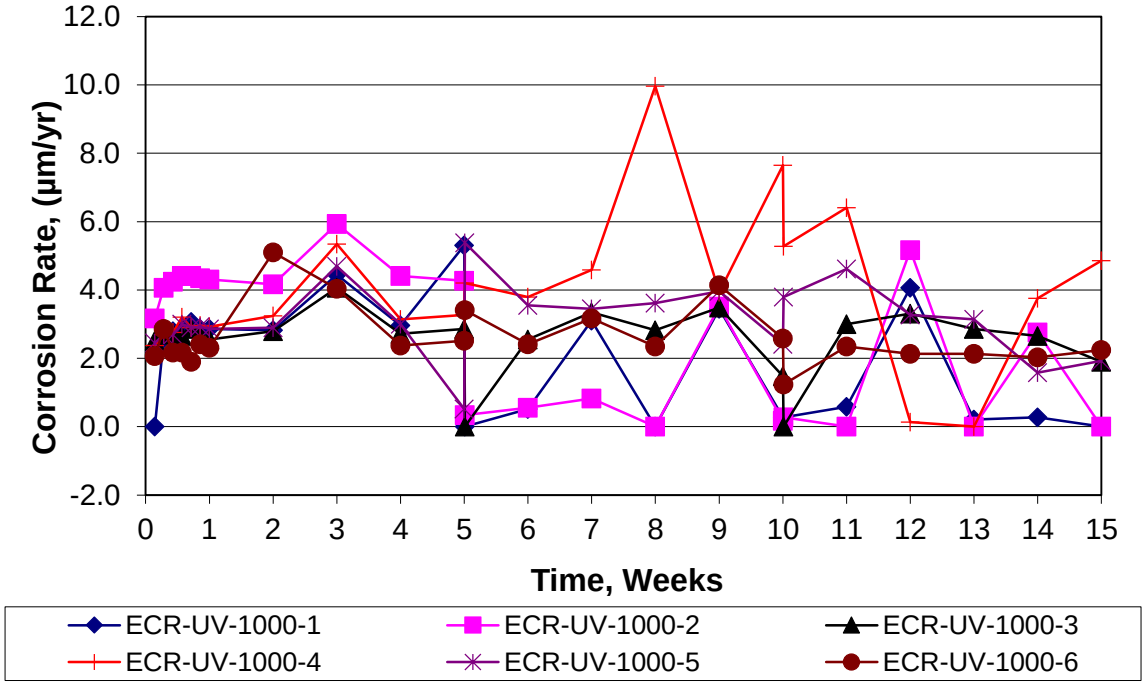

Figure A.11: Rapid macrocell test. Corrosion rate of ECR-UV-1000.

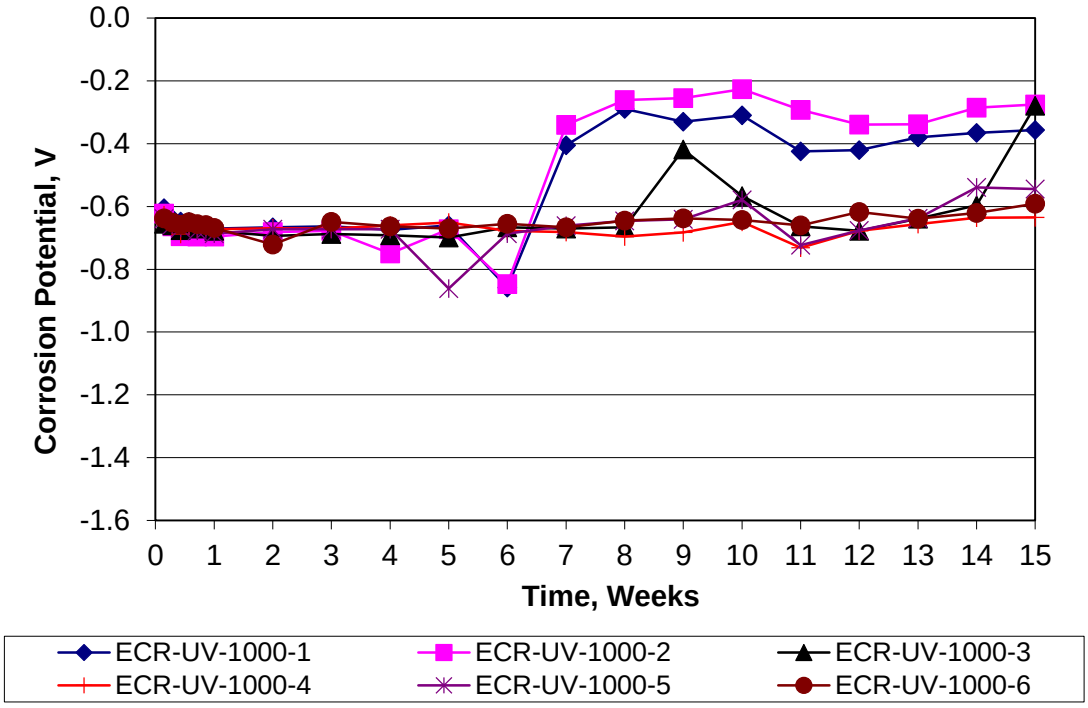

Figure A.12: Rapid macrocell test. Corrosion potential of ECR-UV-1000.

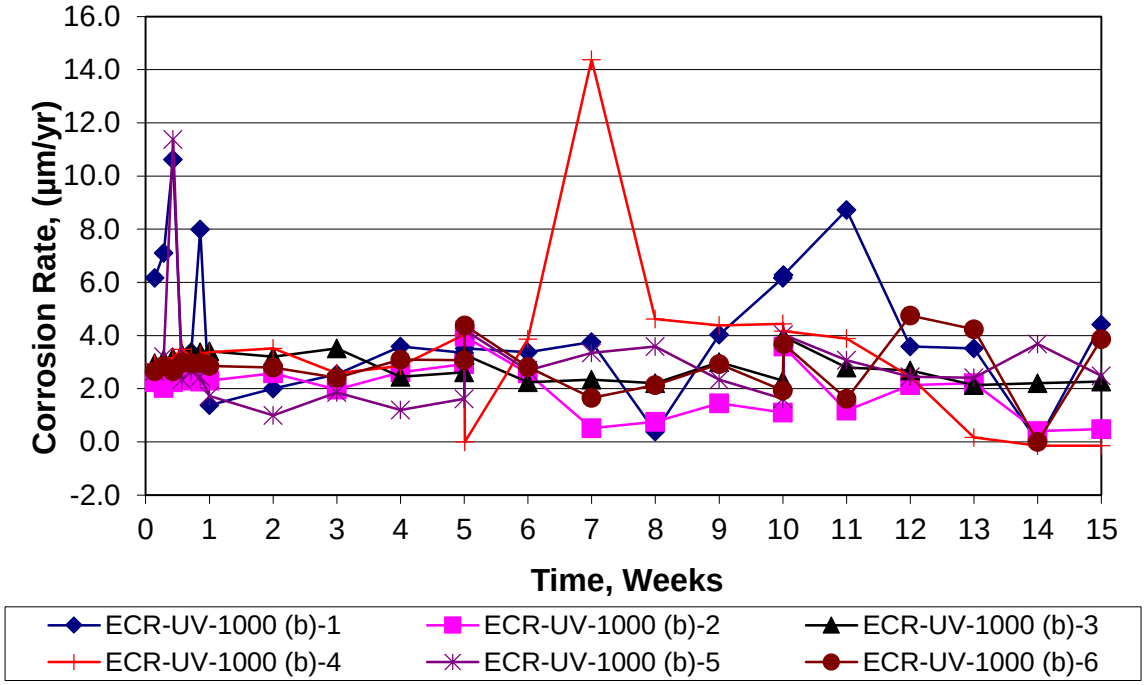

Figure A.13: Rapid macrocell test. Corrosion rate of ECR-UV-1000 (b).

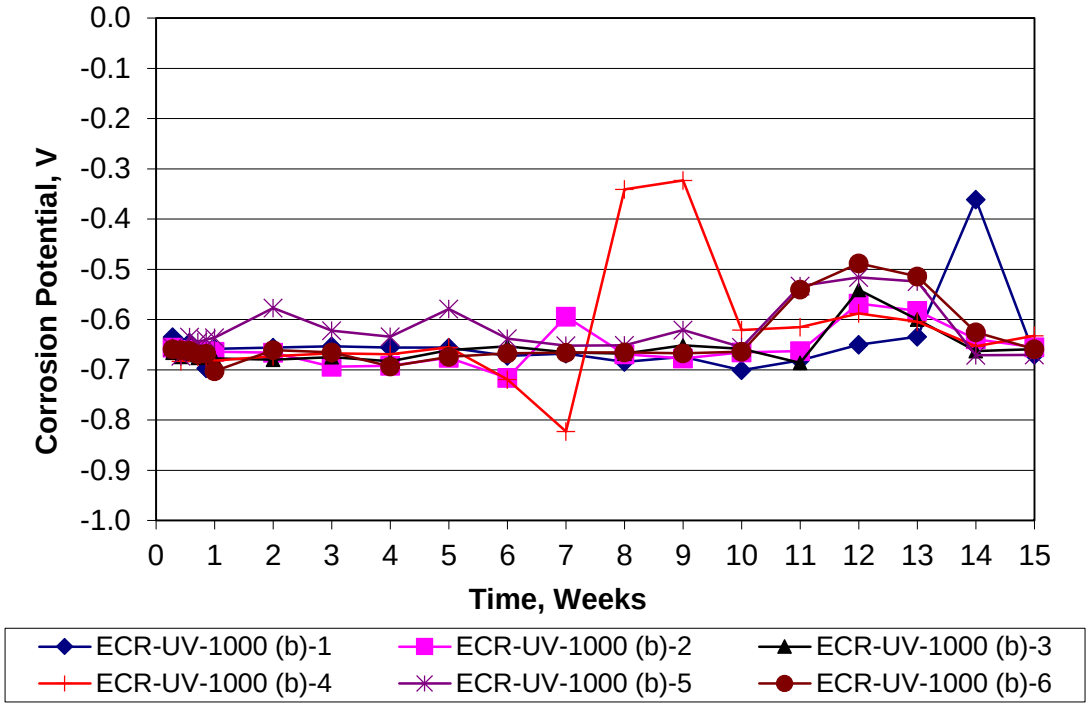

Figure A.14: Rapid macrocell test. Corrosion potential of ECR-UV-1000 (b).

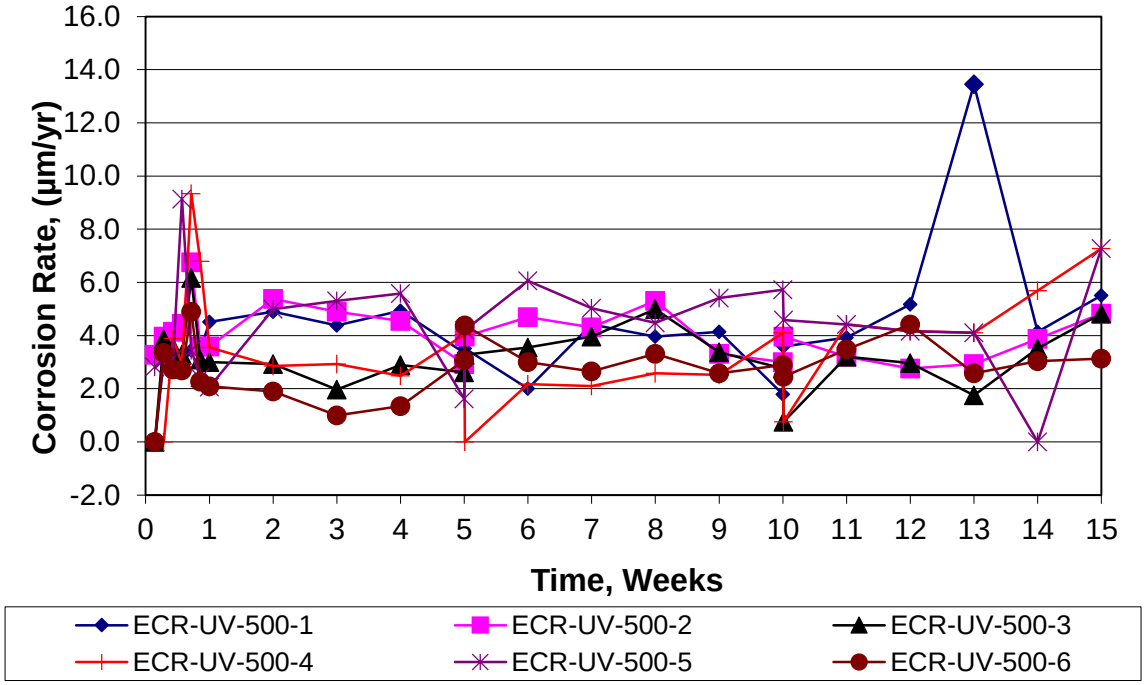

Figure A.15: Rapid macrocell test. Corrosion rate of ECR-UV-500.

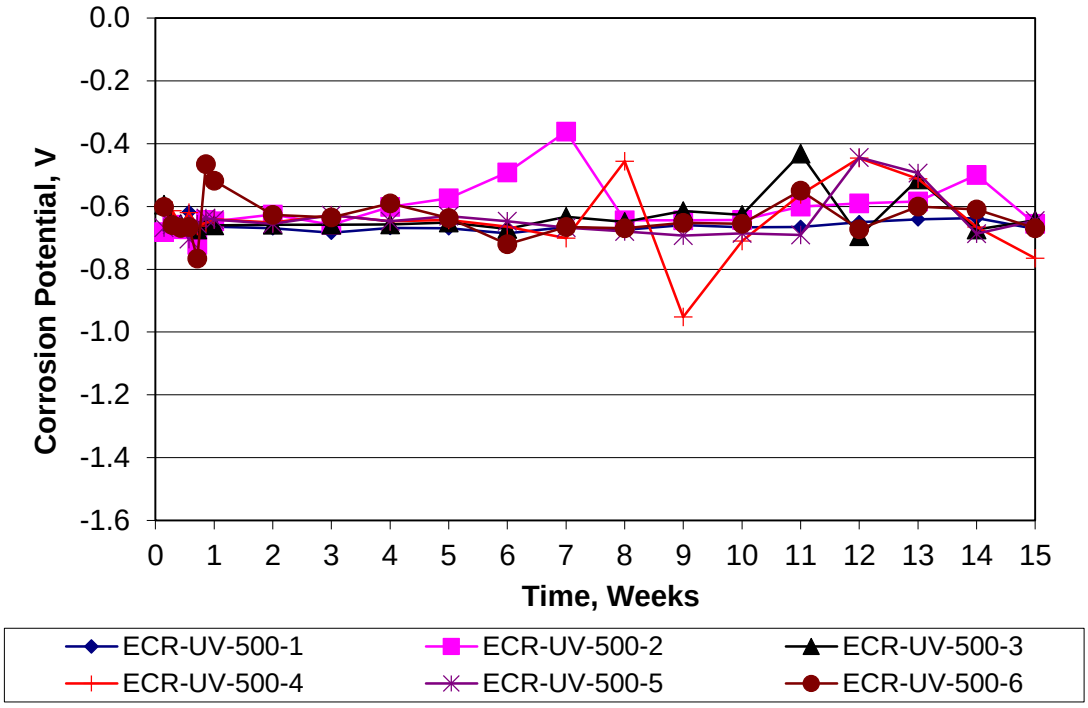

Figure A.16: Rapid macrocell test. Corrosion potential of ECR-UV-500.

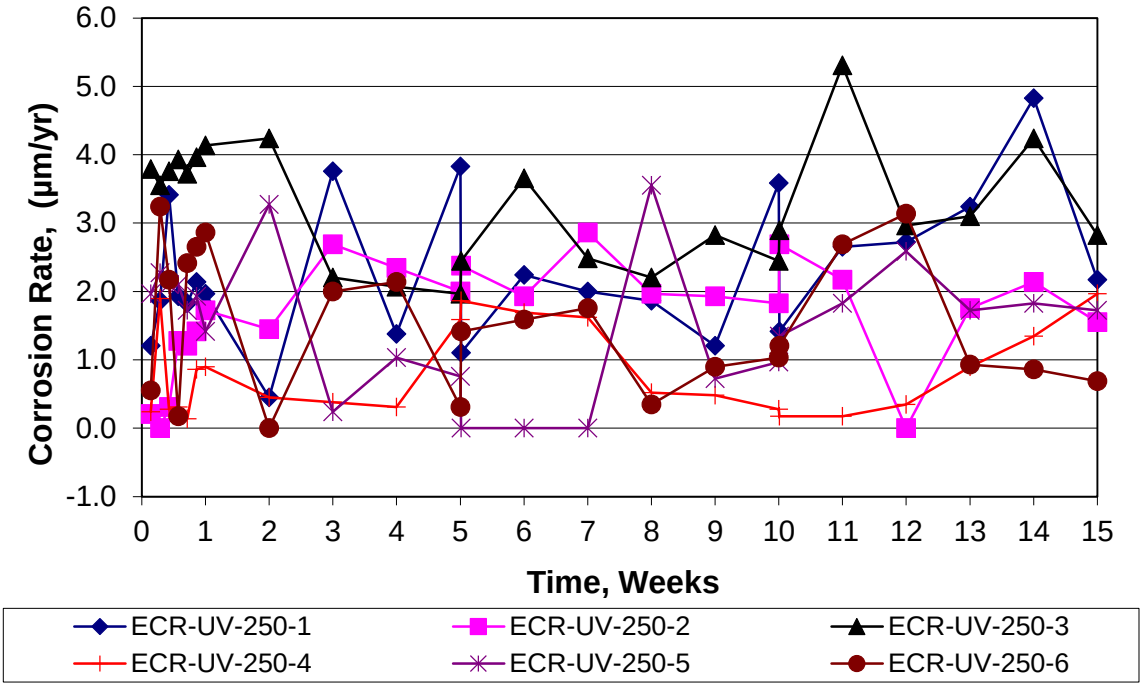

Figure A.17: Rapid macrocell test. Corrosion rate of ECR-UV-250.

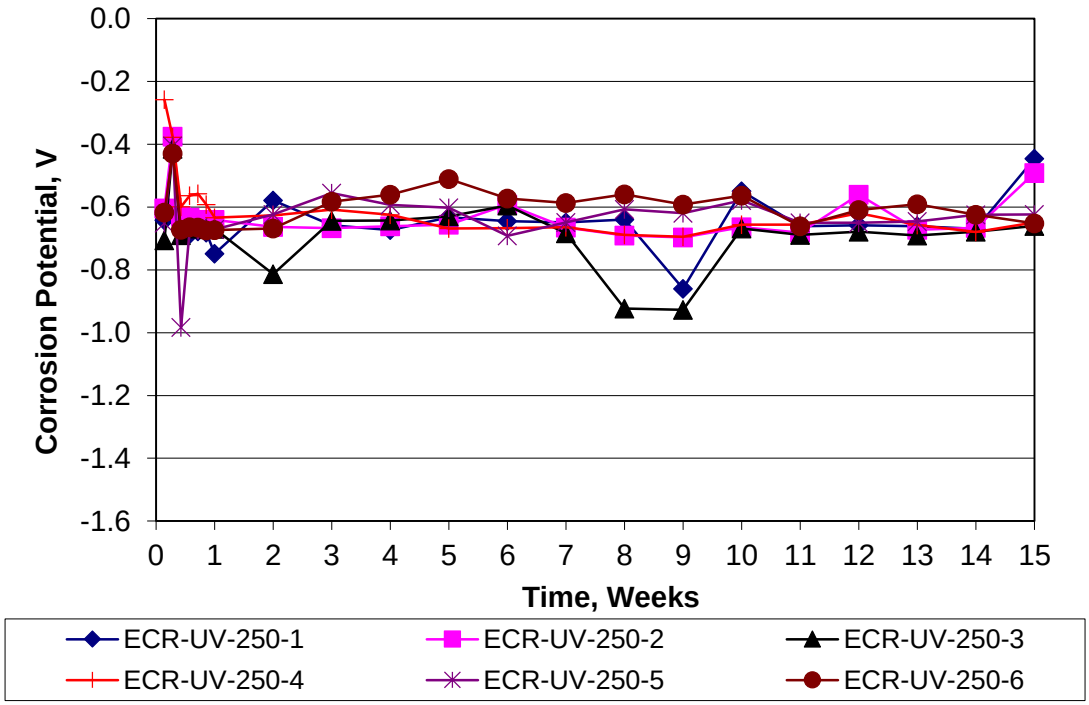

Figure A.18: Rapid macrocell test. Corrosion potential of ECR-UV-250.

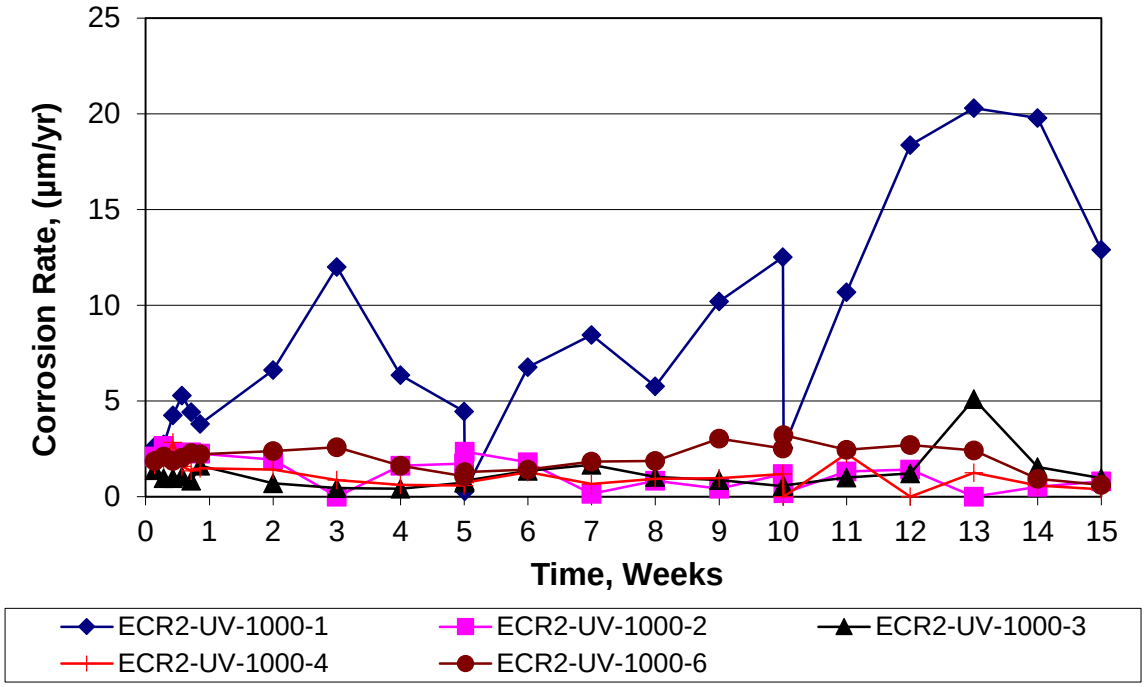

Figure A.19: Rapid macrocell test. Corrosion rate of ECR2-UV-1000.

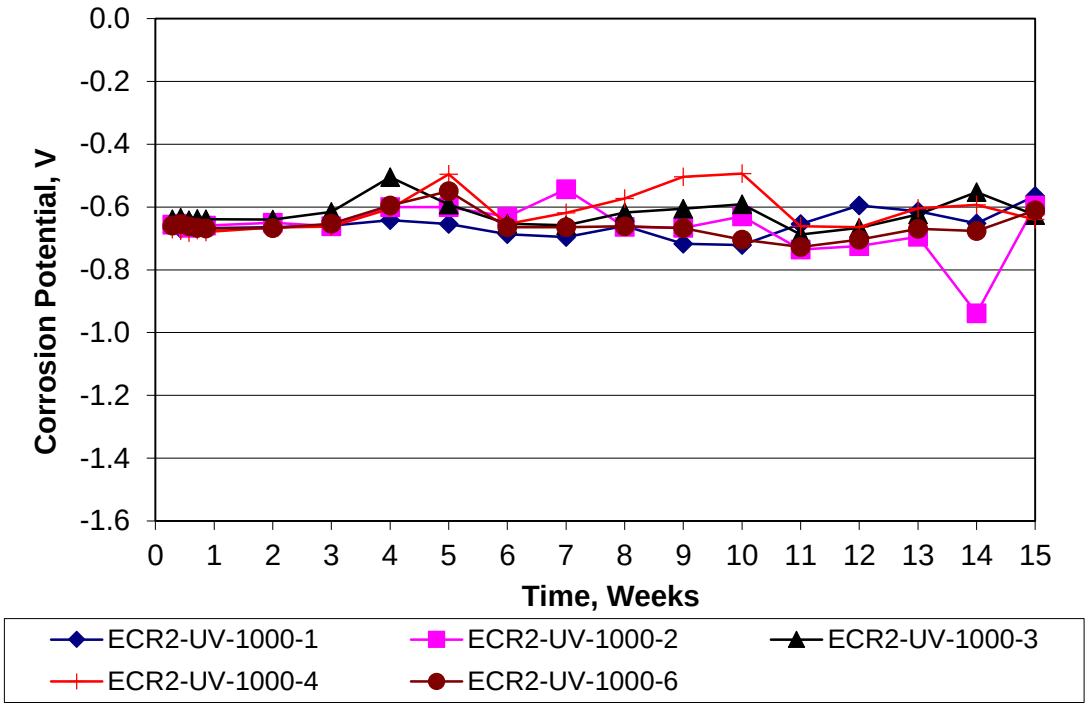

Figure A.20: Rapid macrocell test. Corrosion potential of ECR2-UV-1000.

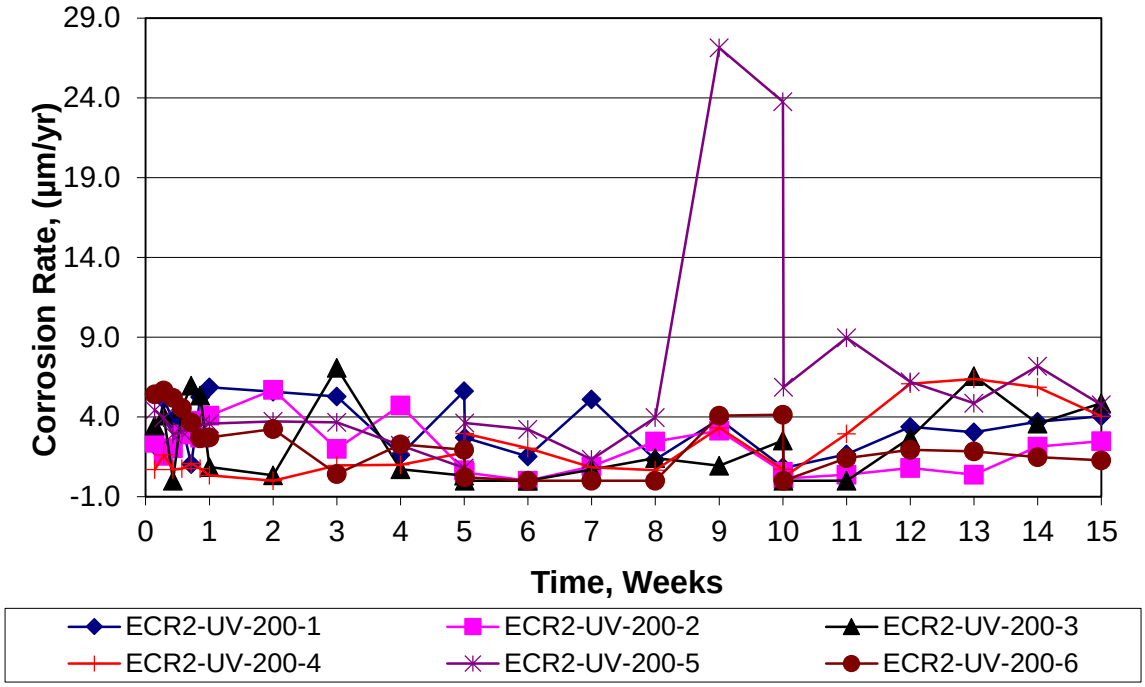

Figure A.21: Rapid macrocell test. Corrosion rate of ECR2-UV-200.

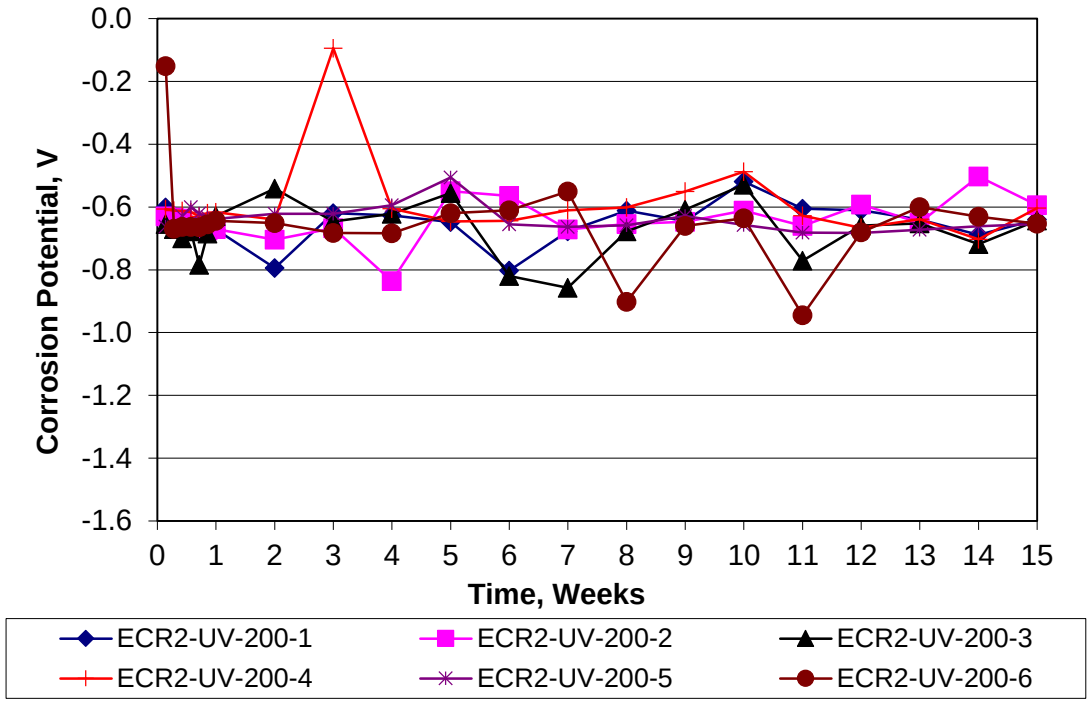

Figure A.22: Rapid macrocell test. Corrosion potential of ECR2-UV-200.

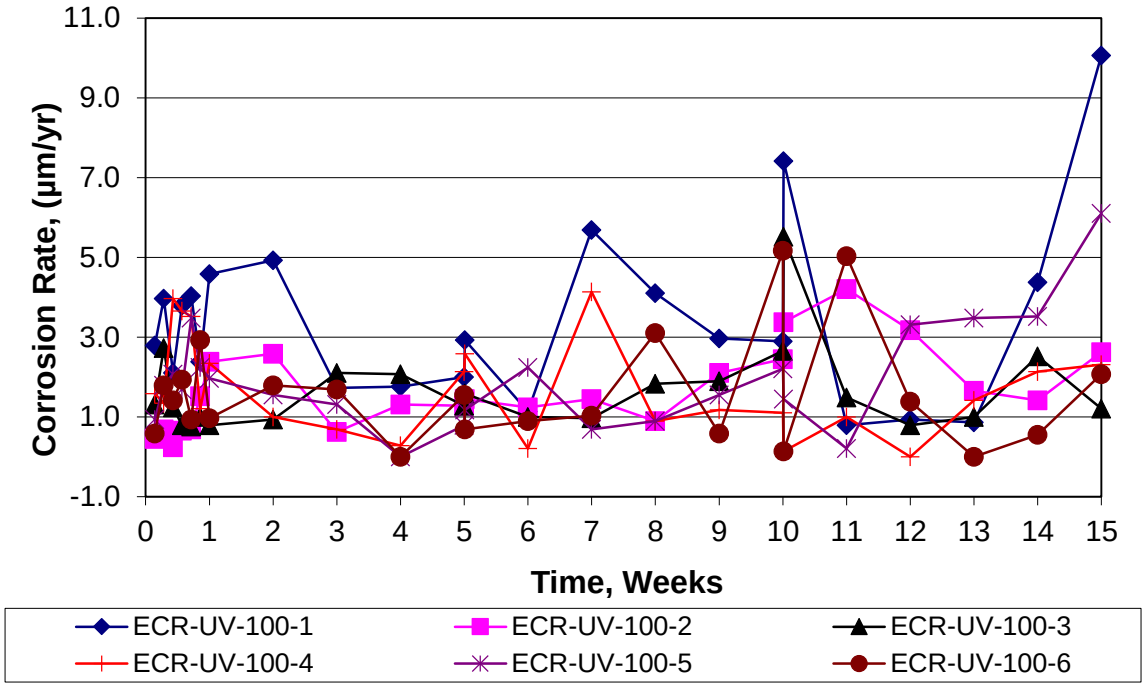

Figure A.23: Rapid macrocell test. Corrosion rate of ECR2-UV-100.

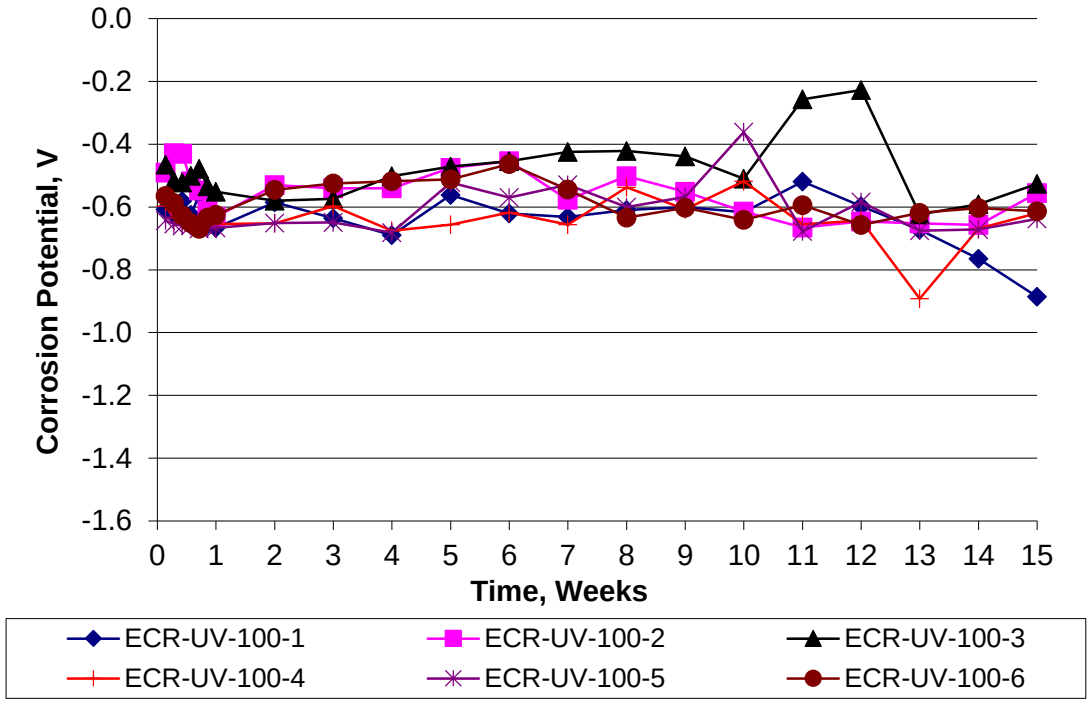

Figure A.24: Rapid macrocell test. Corrosion potential of ECR2-UV-100.

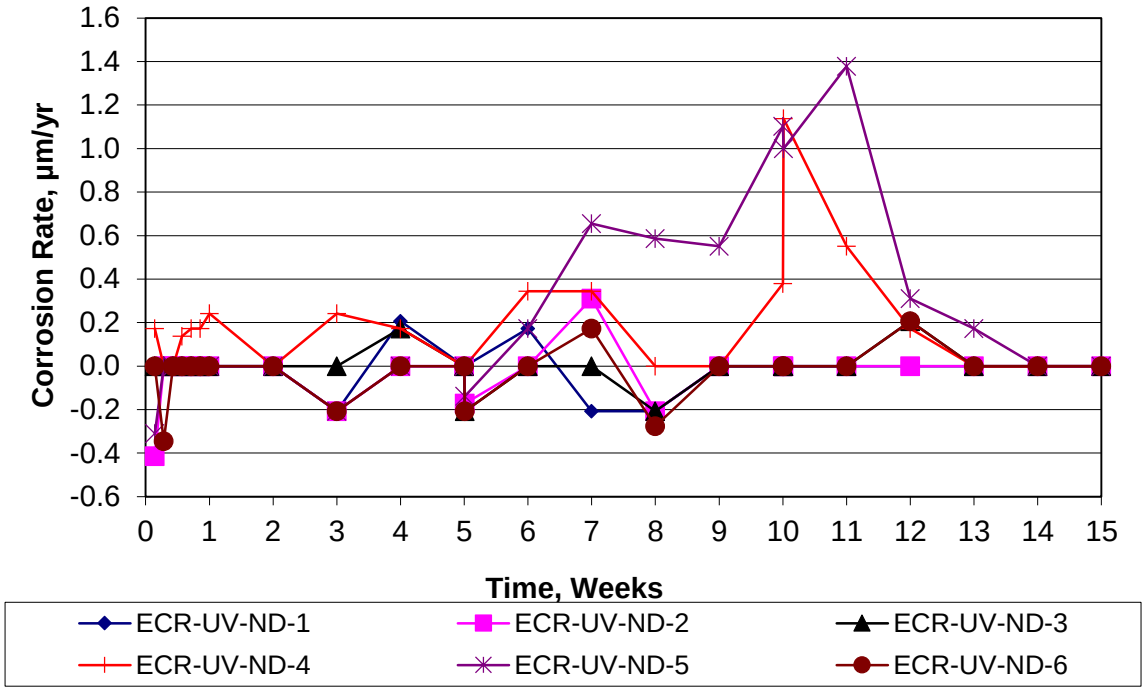

Figure A.25: Rapid macrocell test. Corrosion rate of ECR-UV-1000-ND.

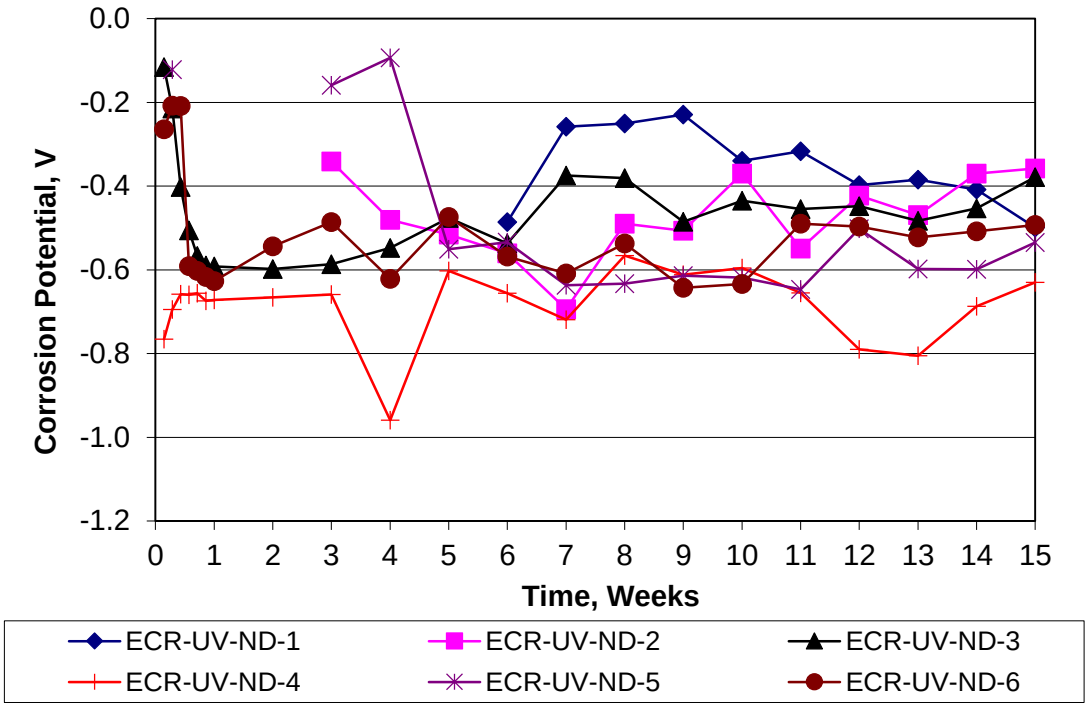

Figure A.26: Rapid macrocell test. Corrosion potential of ECR-UV-1000-ND.

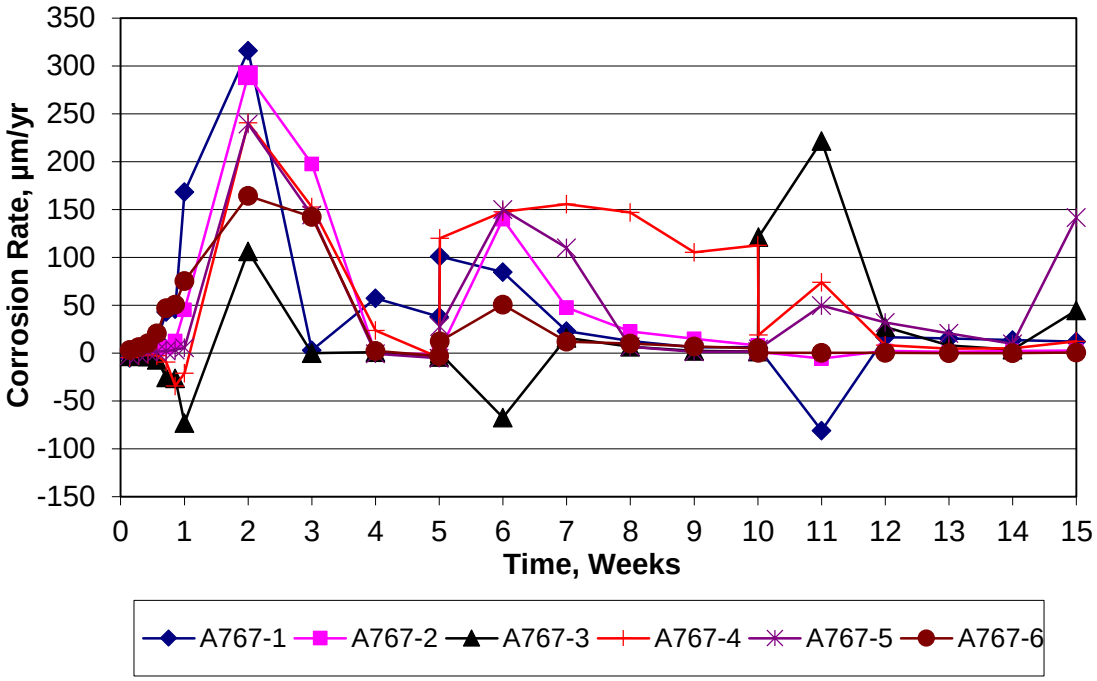

Figure A.27: Rapid macrocell test. Corrosion rate of A767 reinforcement.

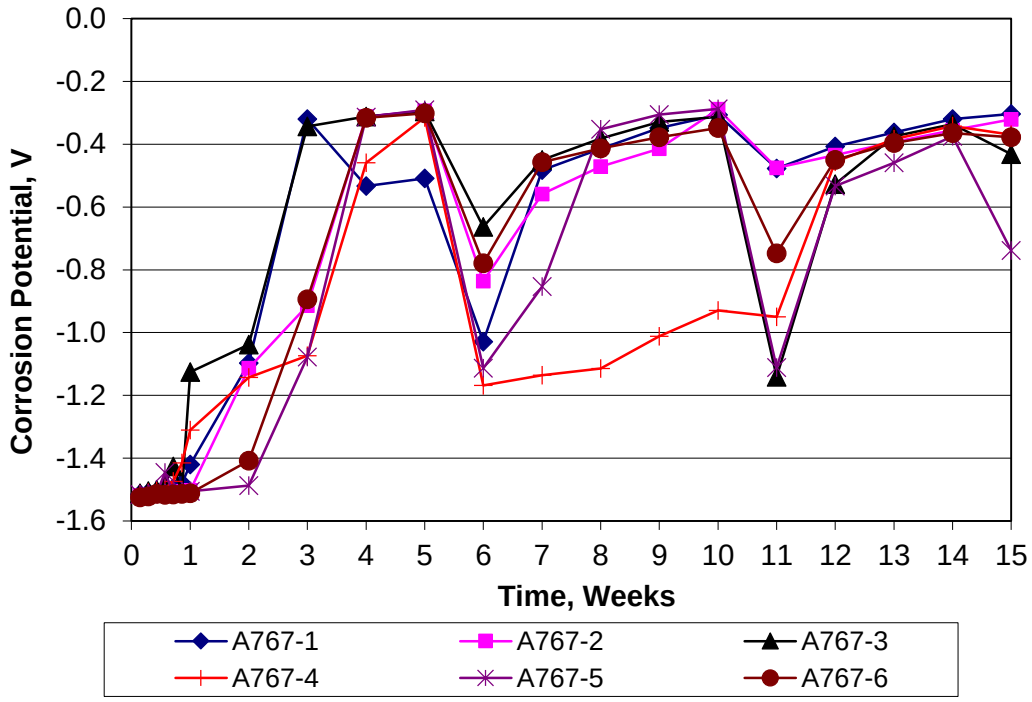

Figure A.28: Rapid macrocell test. Corrosion potential of A767 reinforcement.

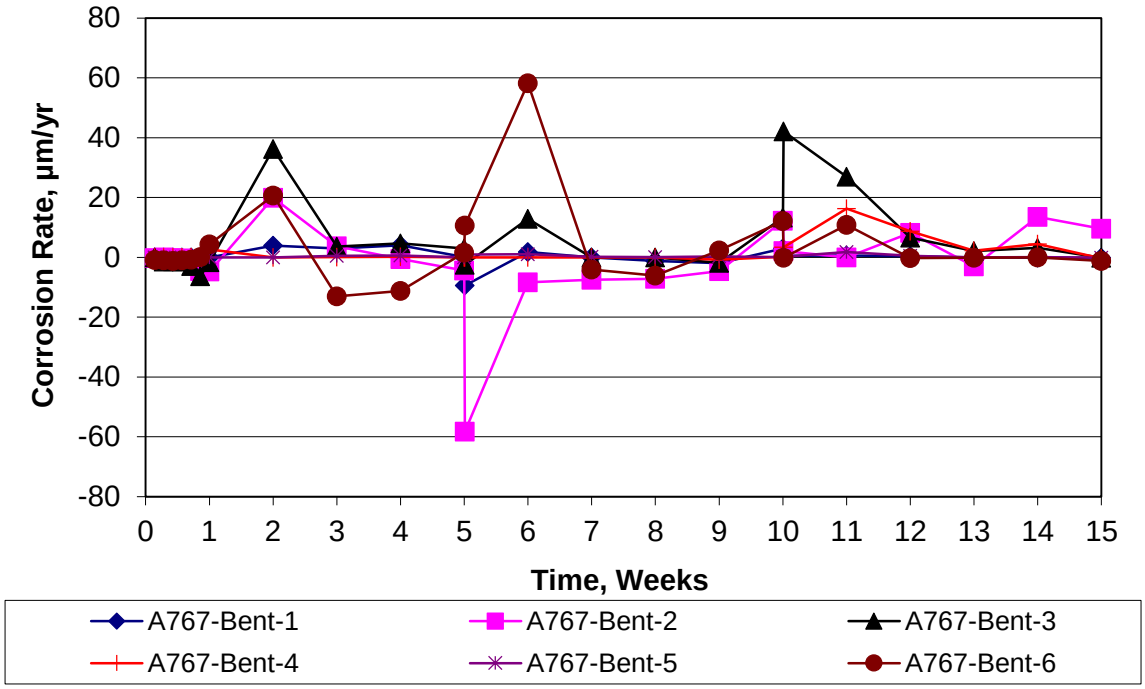

Figure A.29: Rapid macrocell test. Corrosion rate of A767-Bent reinforcement.

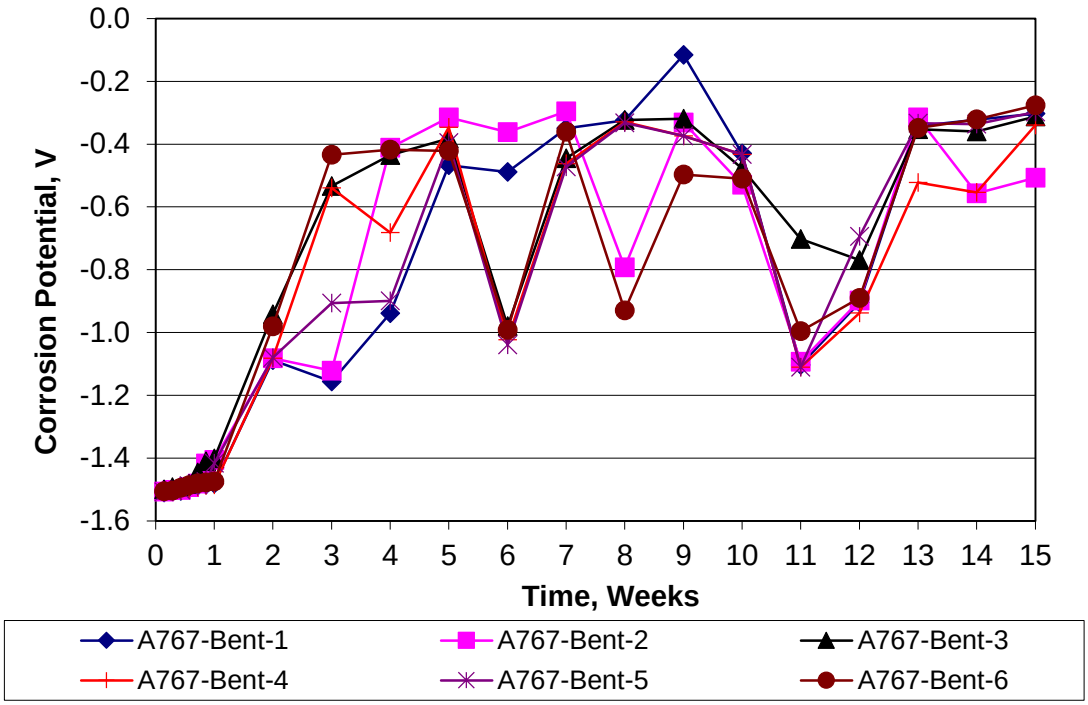

Figure A.30: Rapid macrocell test. Corrosion potential of A767-Bent reinforcement.

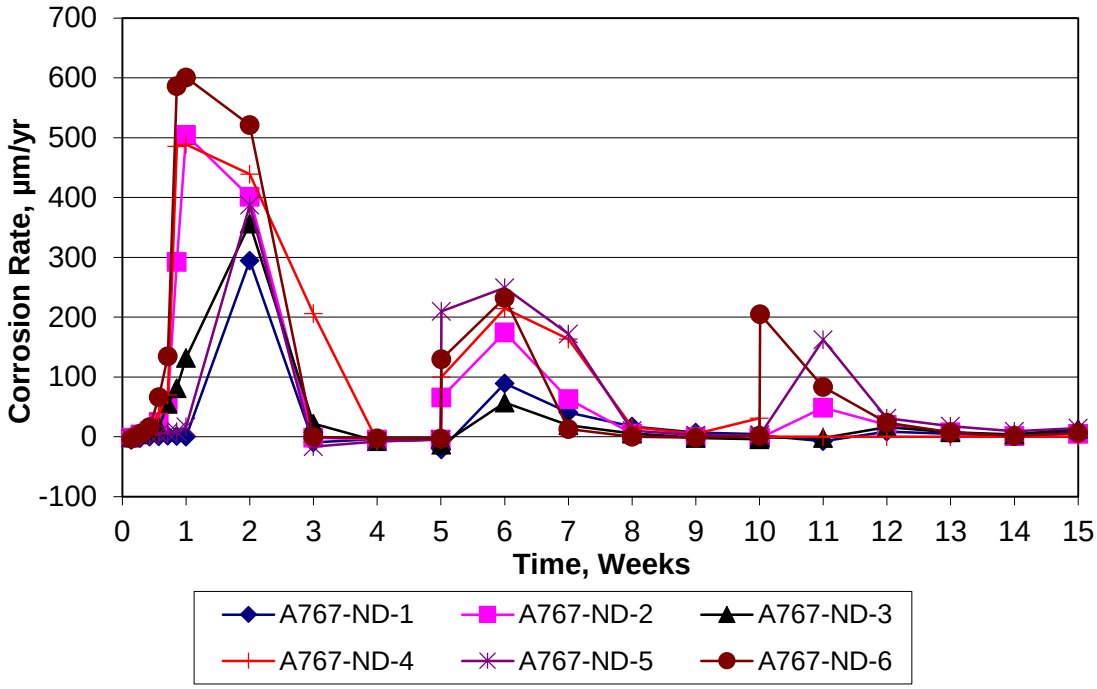

Figure A.31: Rapid macrocell test. Corrosion rate of A767-ND reinforcement.

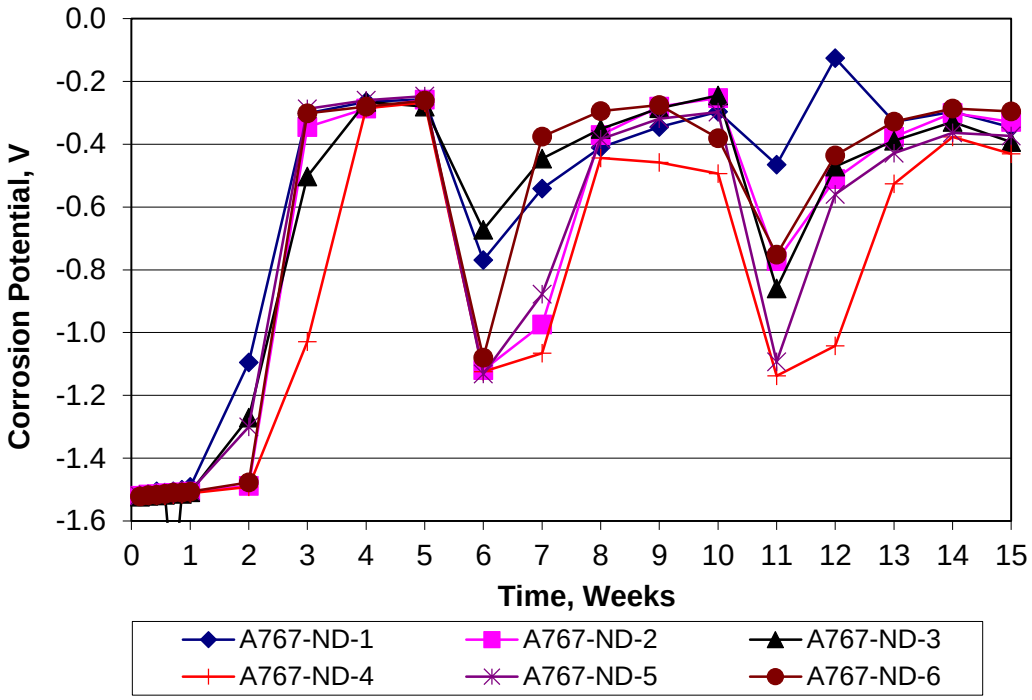

Figure A.32: Rapid macrocell test. Corrosion potential of A767-ND reinforcement.

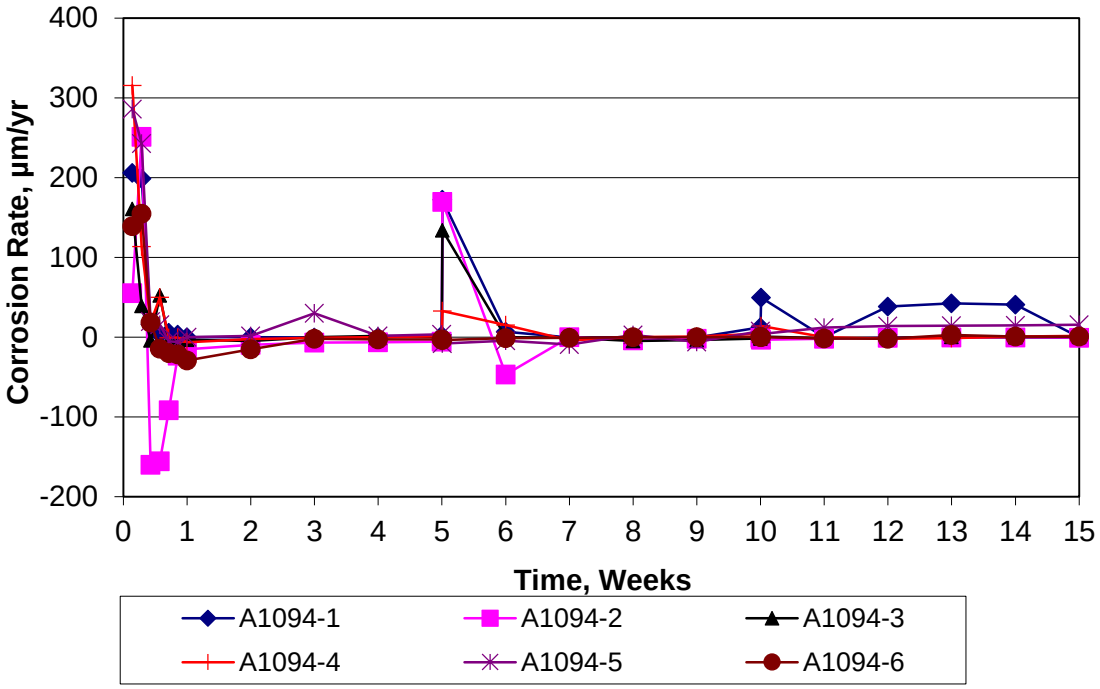

Figure A.33: Rapid macrocell test. Corrosion rate of A1094 reinforcement.

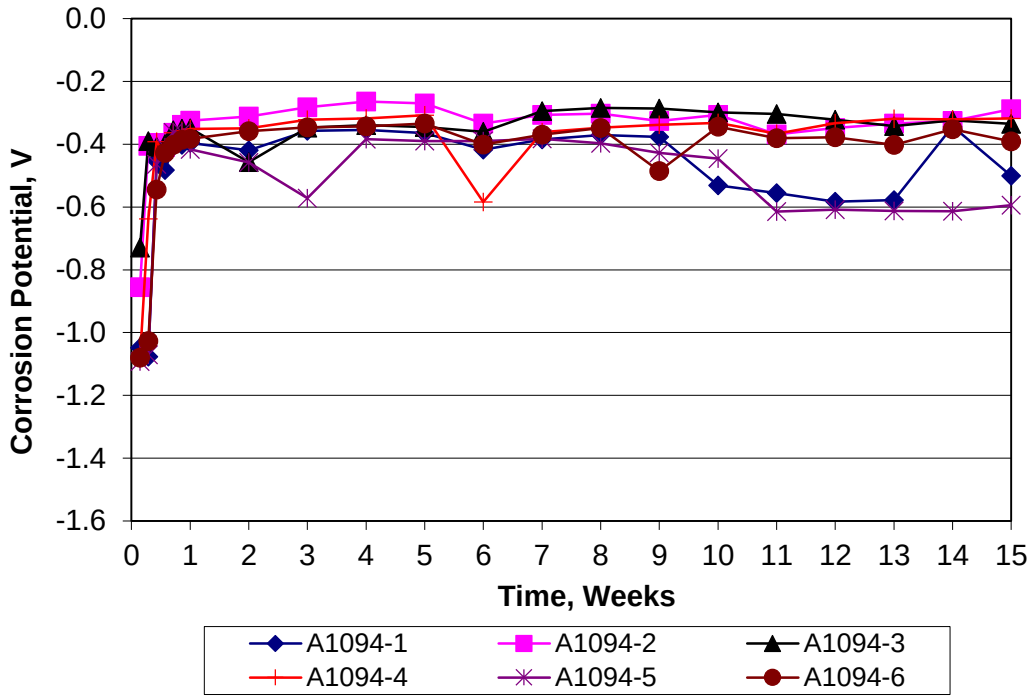

Figure A.34: Rapid macrocell test. Corrosion potential of A1094 reinforcement.

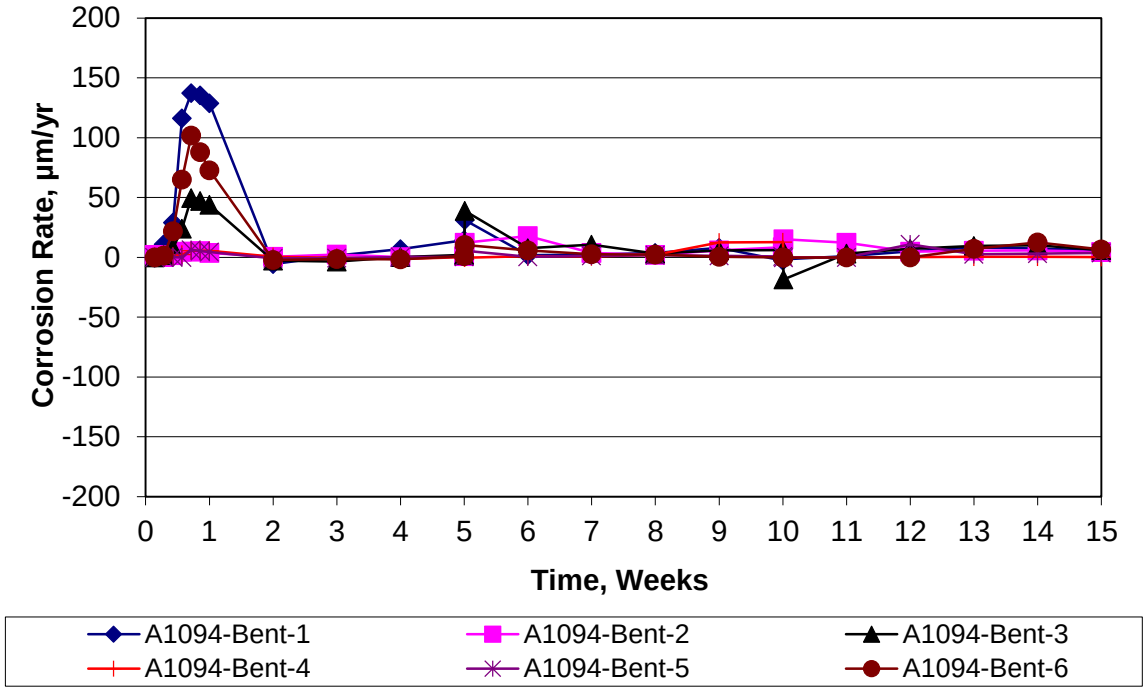

Figure A.35: Rapid macrocell test. Corrosion rate of A1094-Bent reinforcement.

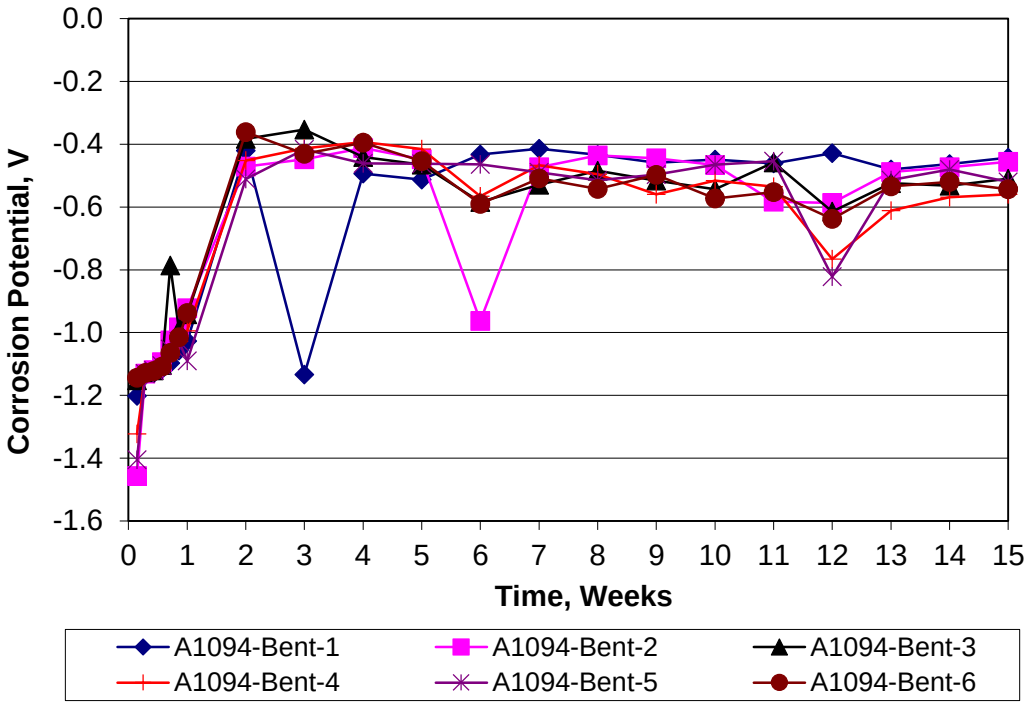

Figure A.36: Rapid macrocell test. Corrosion potential of A1094-Bent reinforcement.

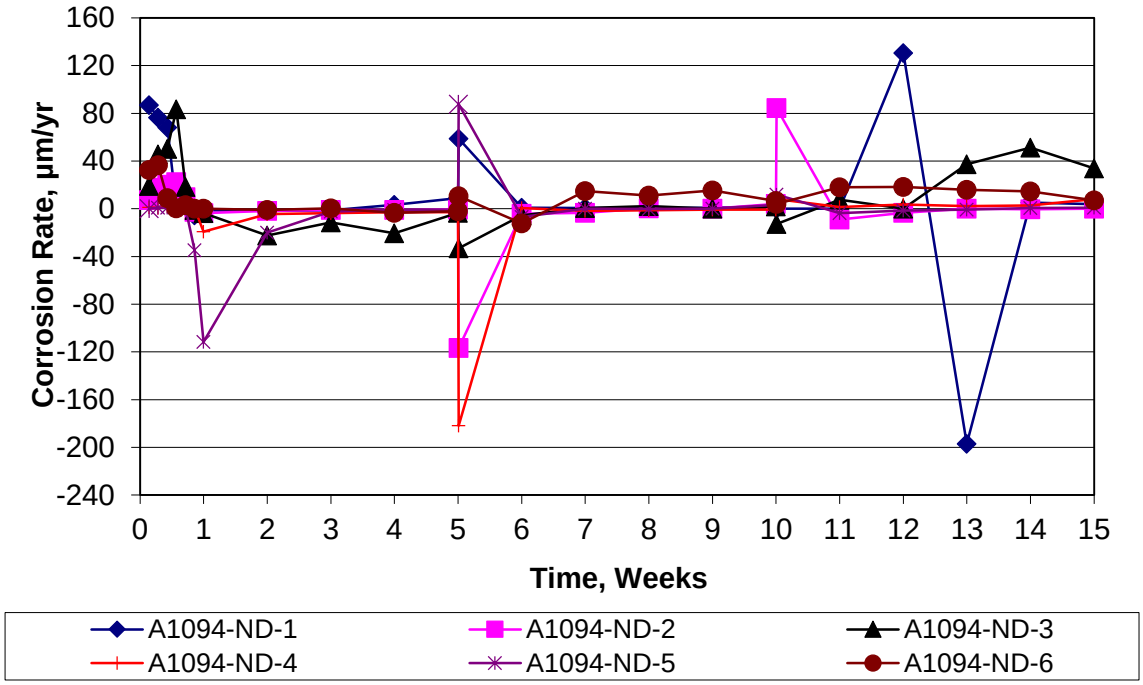

Figure A.37: Rapid macrocell test. Corrosion rate of A1094-ND reinforcement.

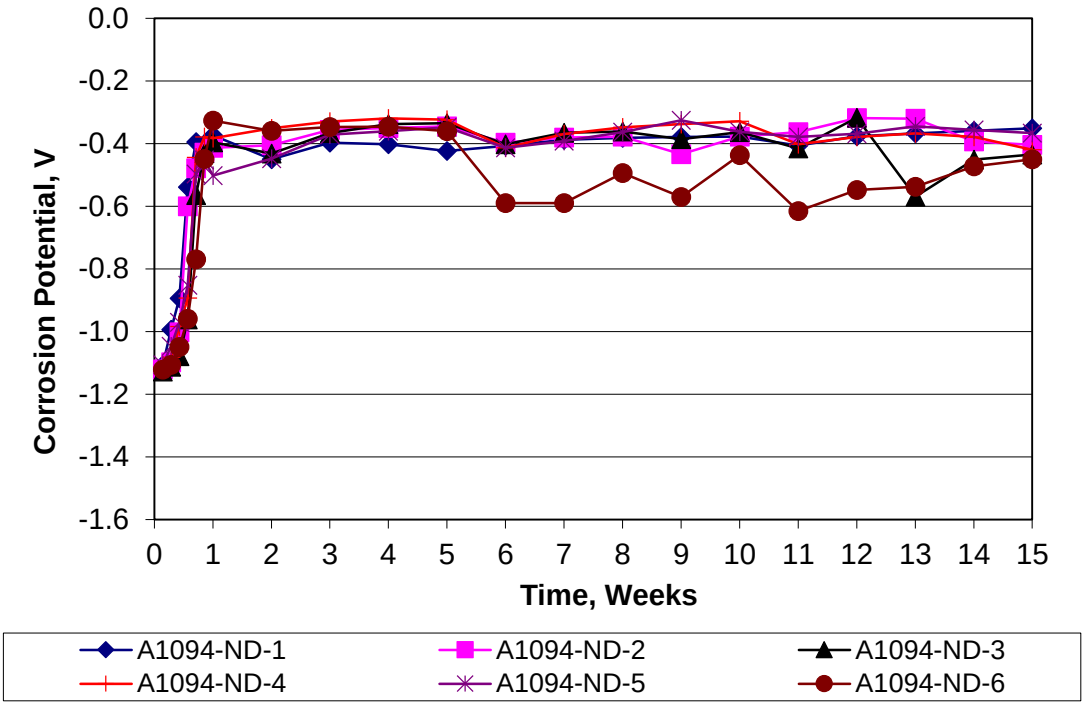

Figure A.38: Rapid macrocell test. Corrosion potential of A1094-ND reinforcement.

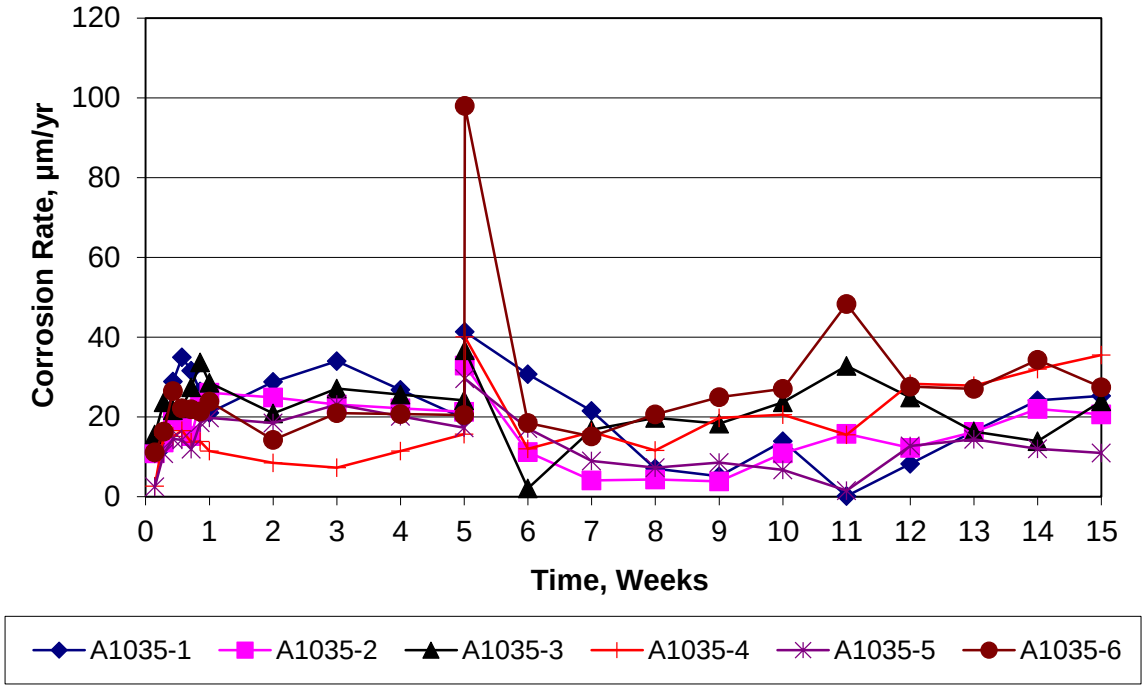

Figure A.39: Rapid macrocell test. Corrosion rate of A1035 reinforcement.

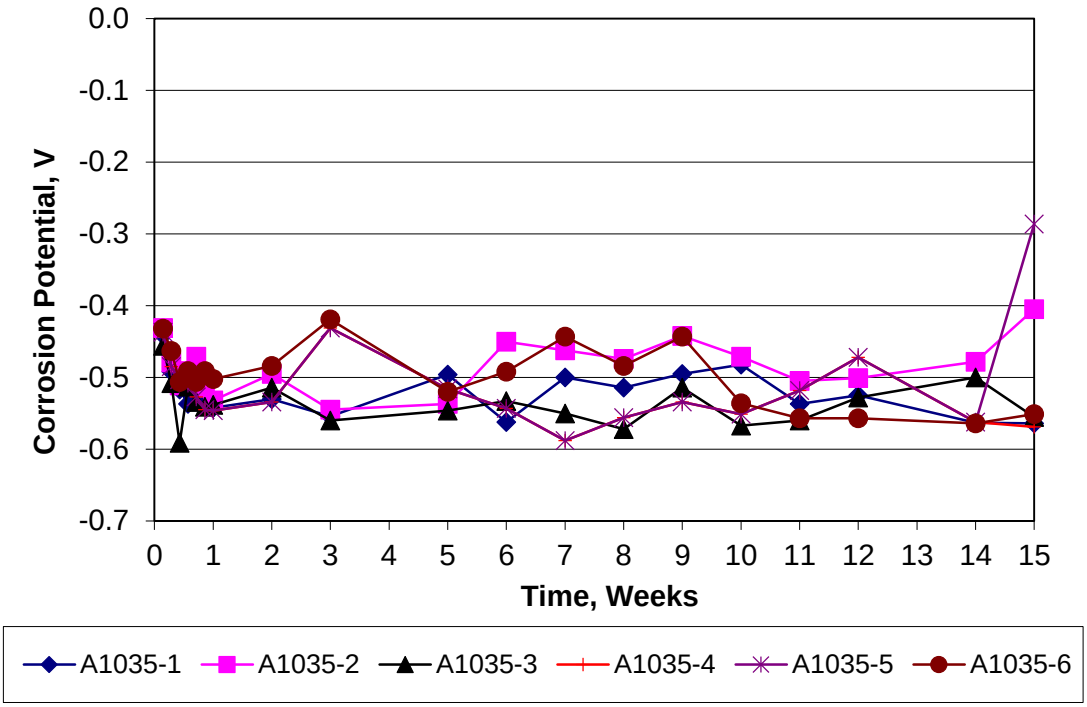

Figure A.40: Rapid macrocell test. Corrosion potential of A1035 reinforcement.

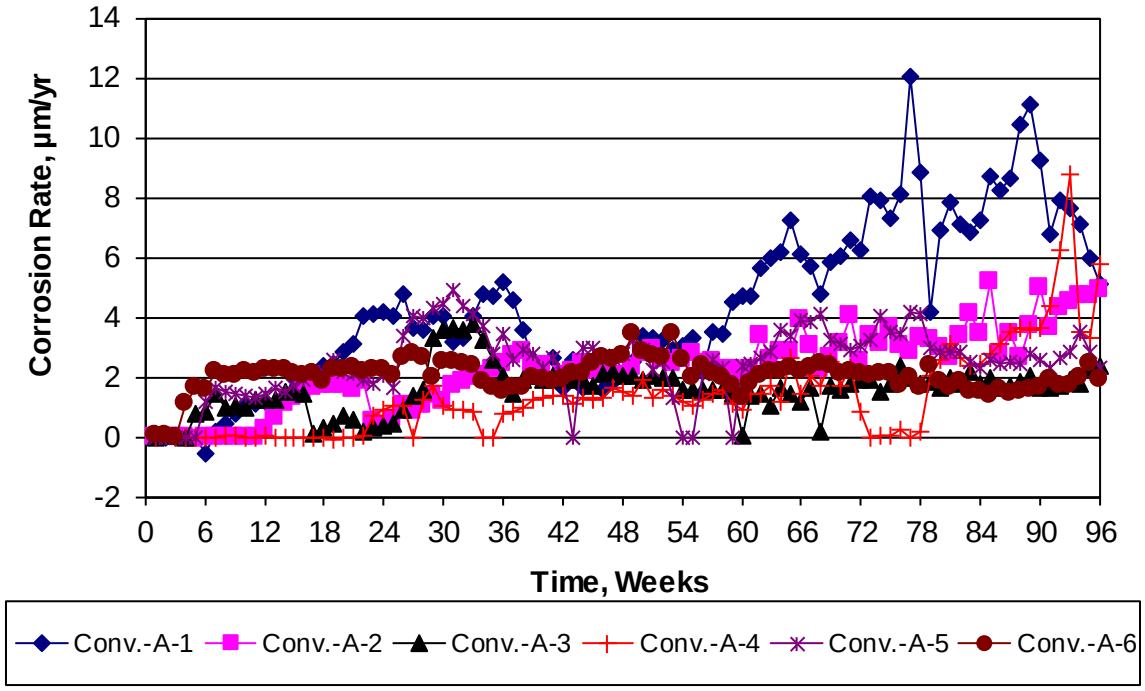

Figure A.41: Southern Exposure test. Corrosion rate of Conv-A reinforcement.

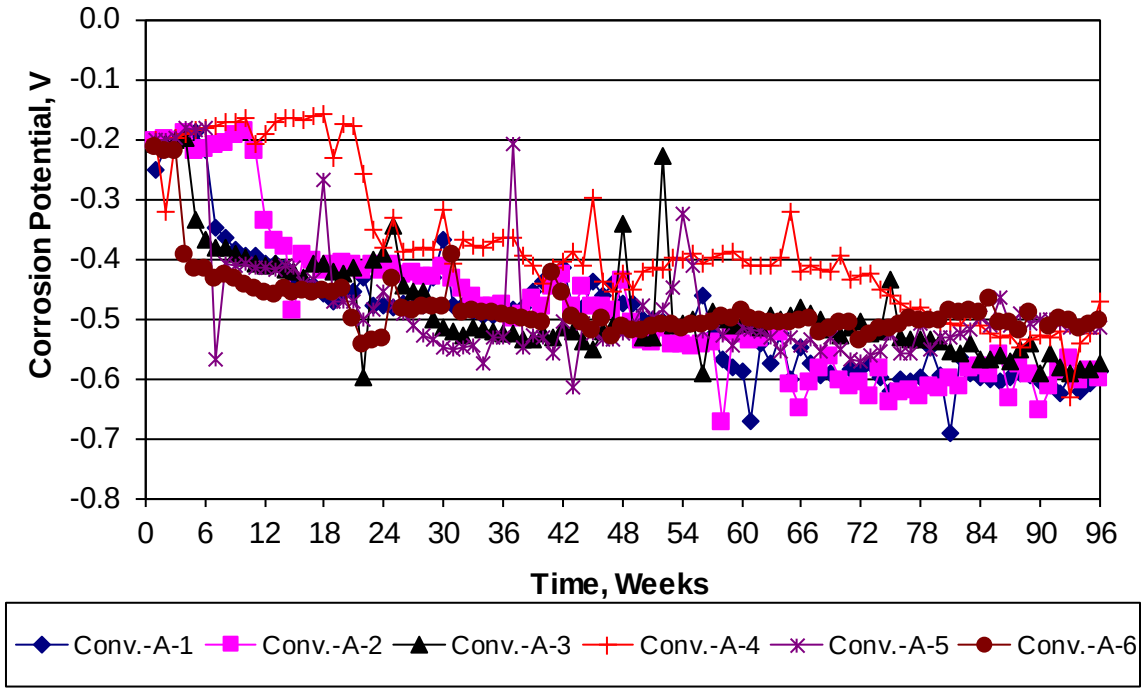

Figure A.42: Southern Exposure test. Corrosion potential of Conv-A reinforcement.

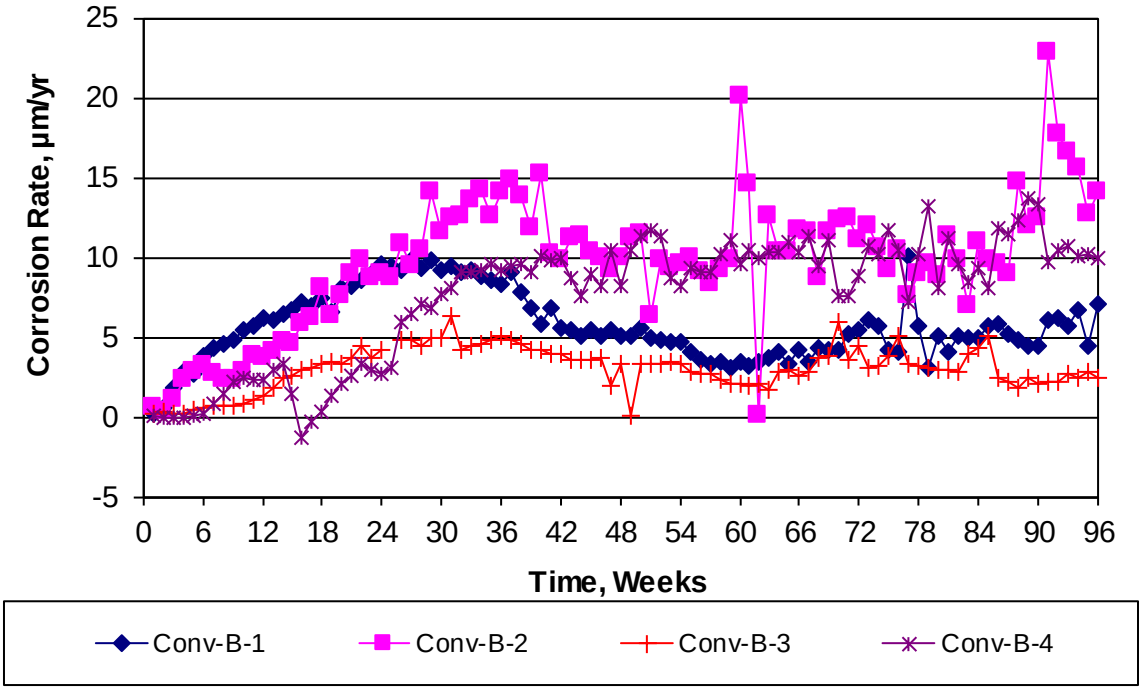

Figure A.43: Southern Exposure test. Corrosion rate of Conv-B reinforcement.

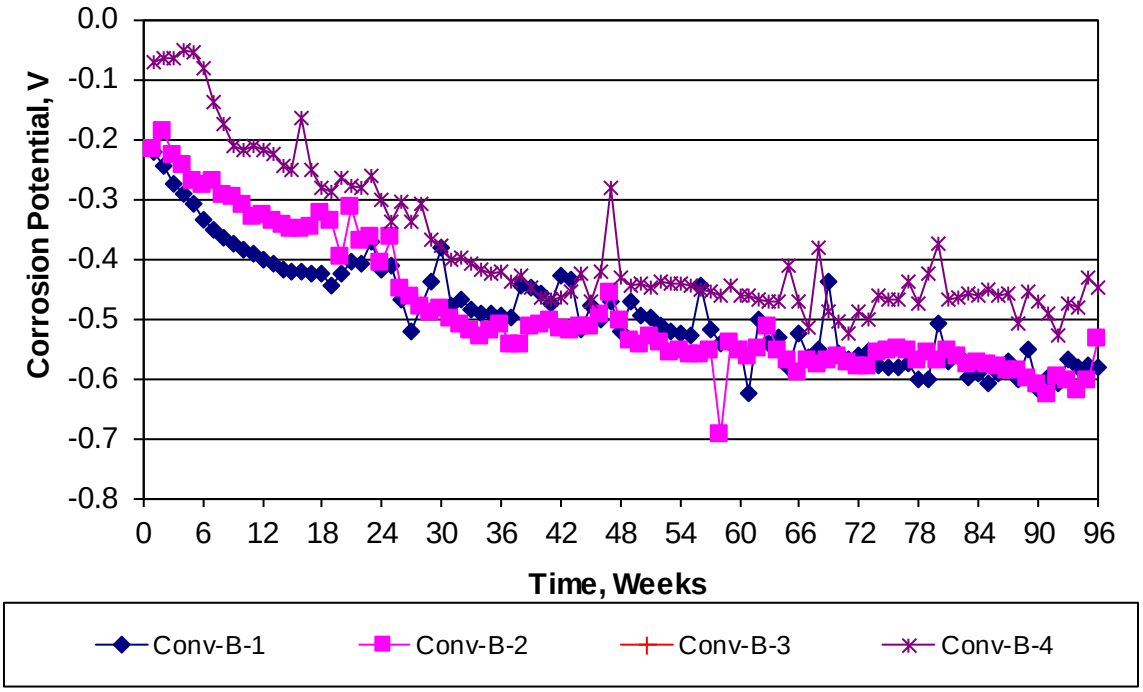

Figure A.44: Southern Exposure test. Corrosion potential of Conv-B reinforcement.

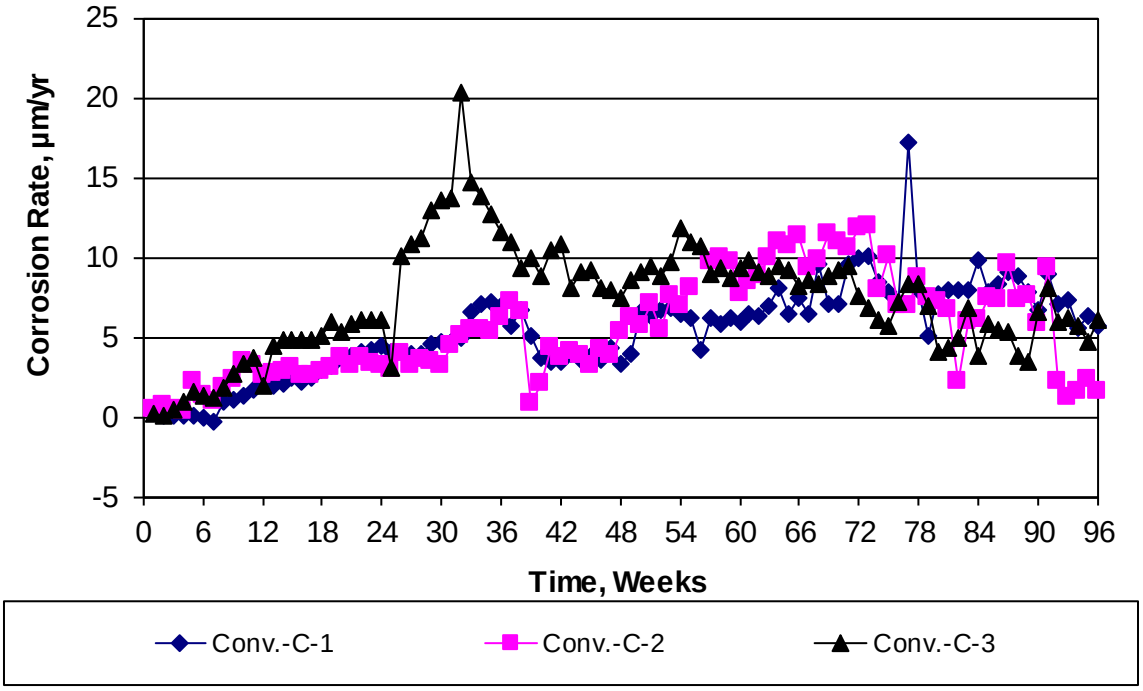

Figure A.45: Southern Exposure test. Corrosion rate of Conv-C reinforcement.

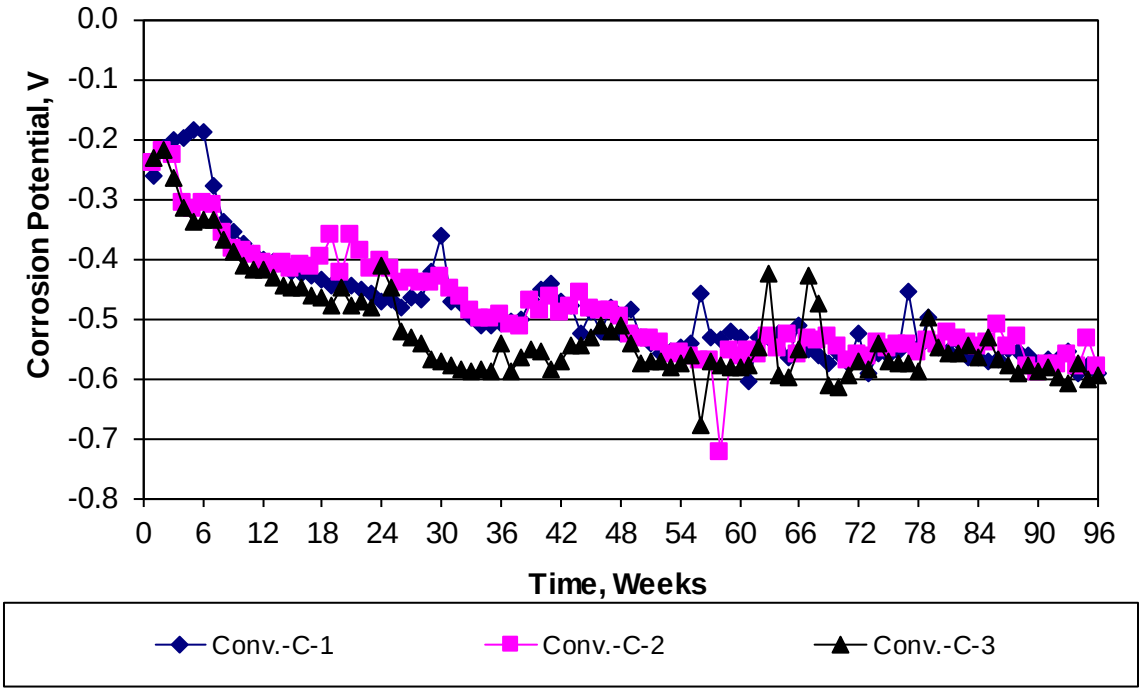

Figure A.46: Southern Exposure test. Corrosion potential of Conv-C reinforcement.

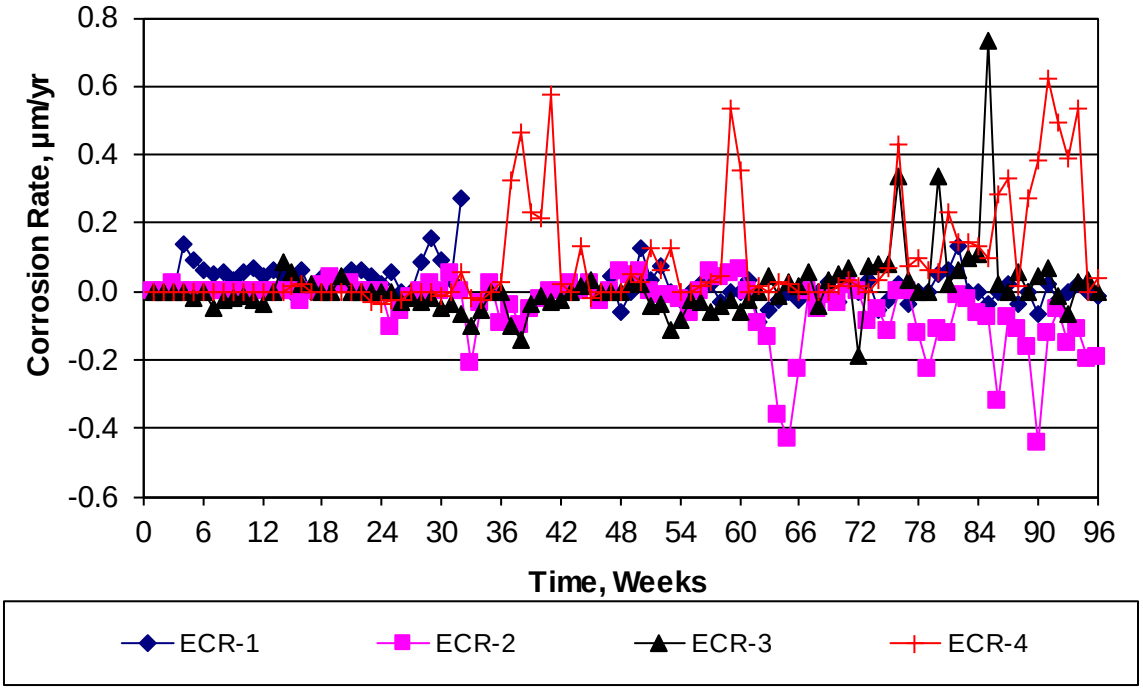

Figure A.47: Southern Exposure test. Corrosion rate of ECR.

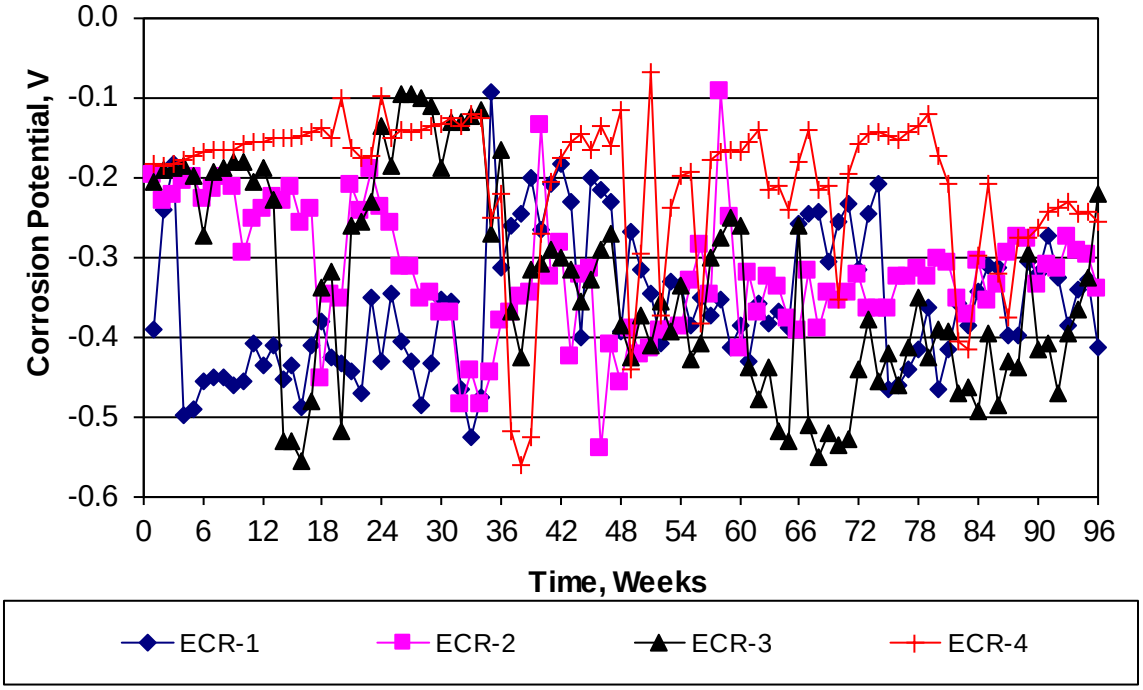

Figure A.48: Southern Exposure test. Corrosion potential of ECR.

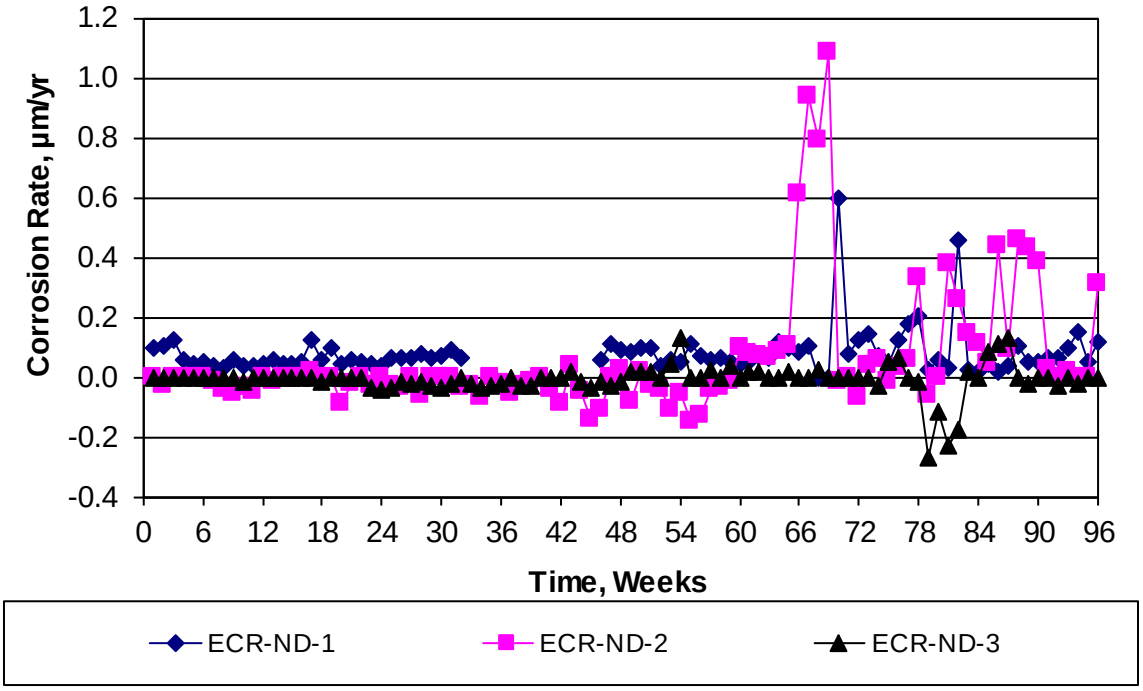

Figure A.49: Southern Exposure test. Corrosion rate of ECR-ND.

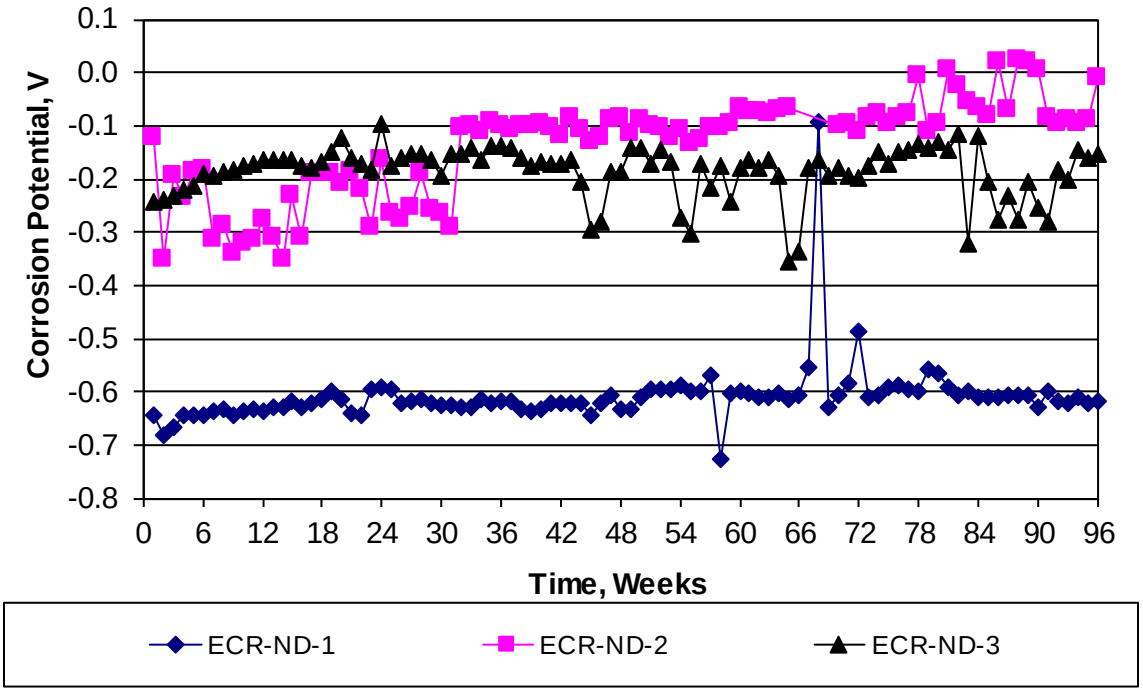

Figure A.50: Southern Exposure test. Corrosion potential of ECR-ND.

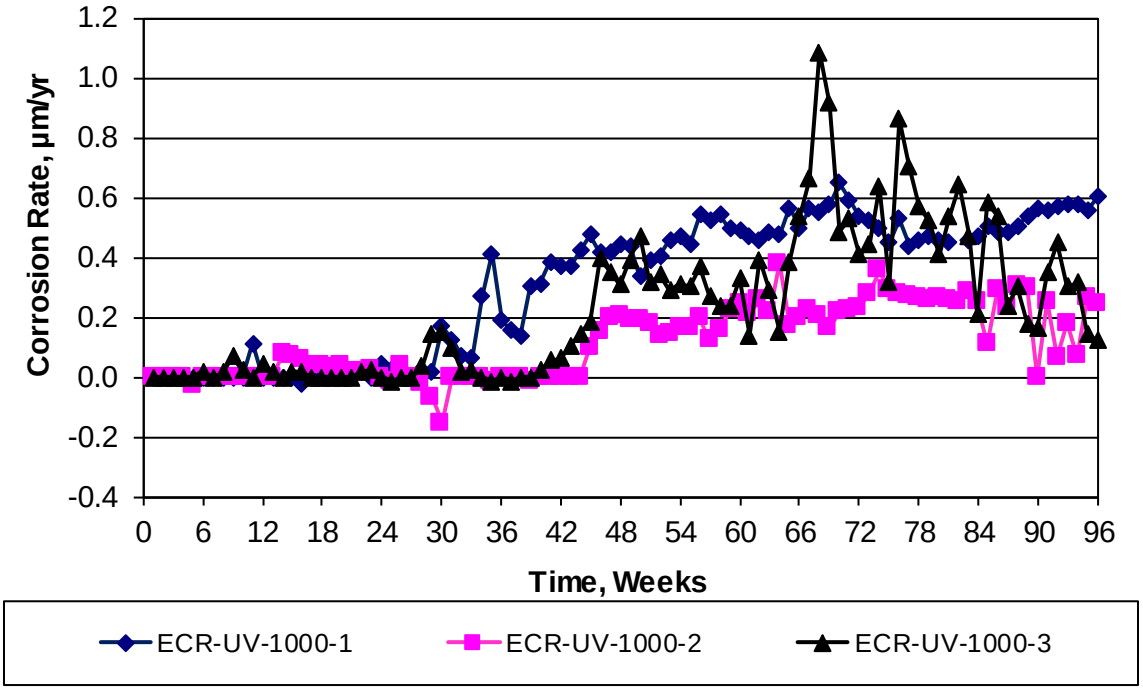

Figure A.51: Southern Exposure test. Corrosion rate of ECR-UV-1000.

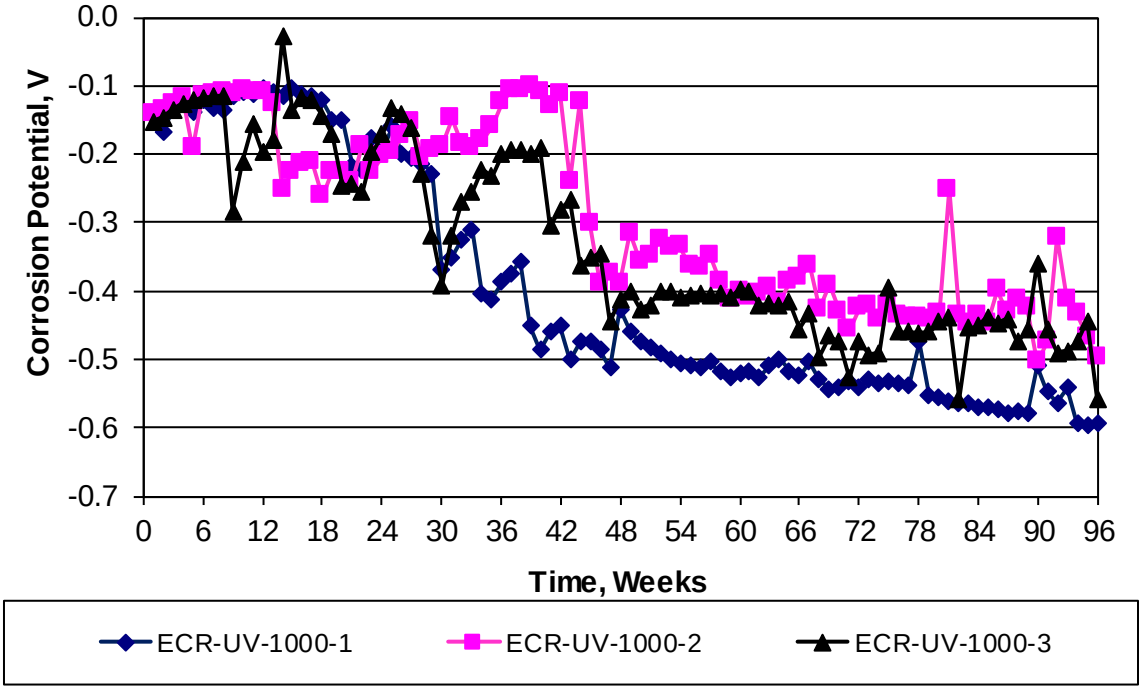

Figure A.52: Southern Exposure test. Corrosion potential of ECR-UV-1000.

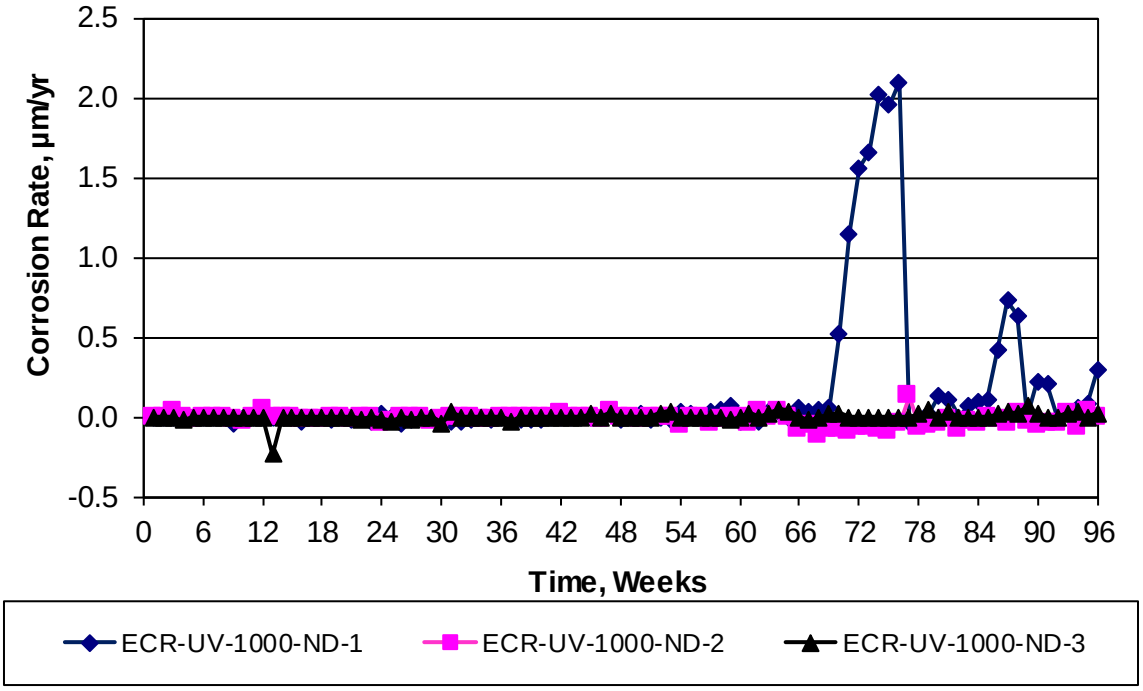

Figure A.53: Southern Exposure test. Corrosion rate of ECR-UV-1000-ND.

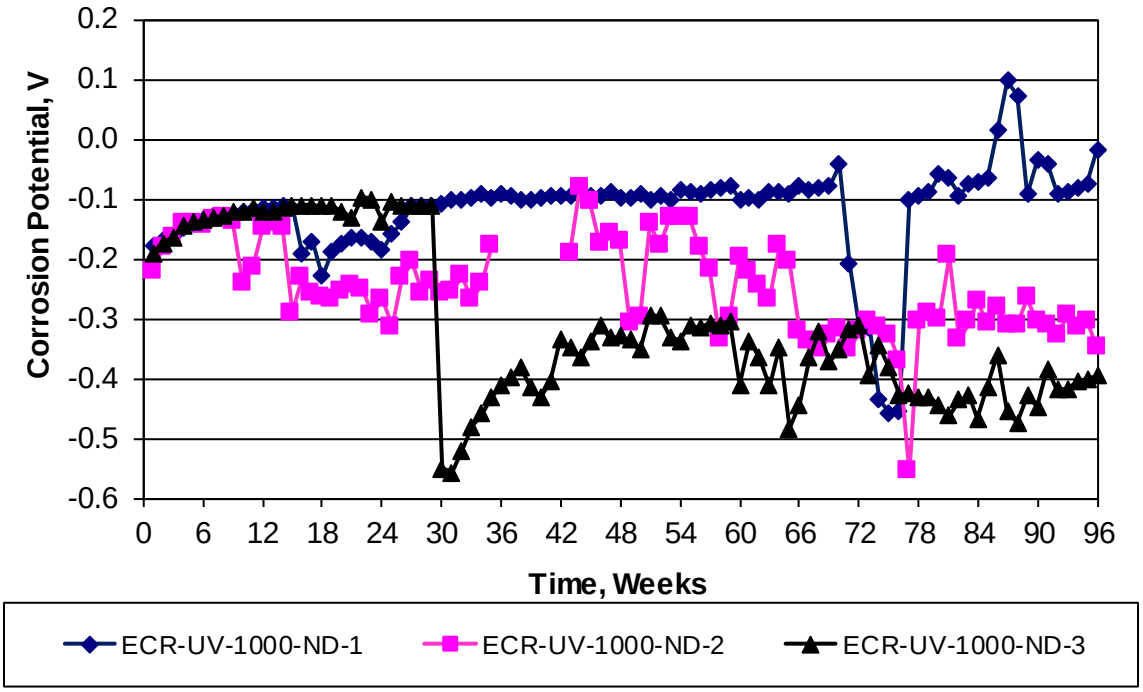

Figure A.54: Southern Exposure test. Corrosion potential of ECR-UV-1000-ND.

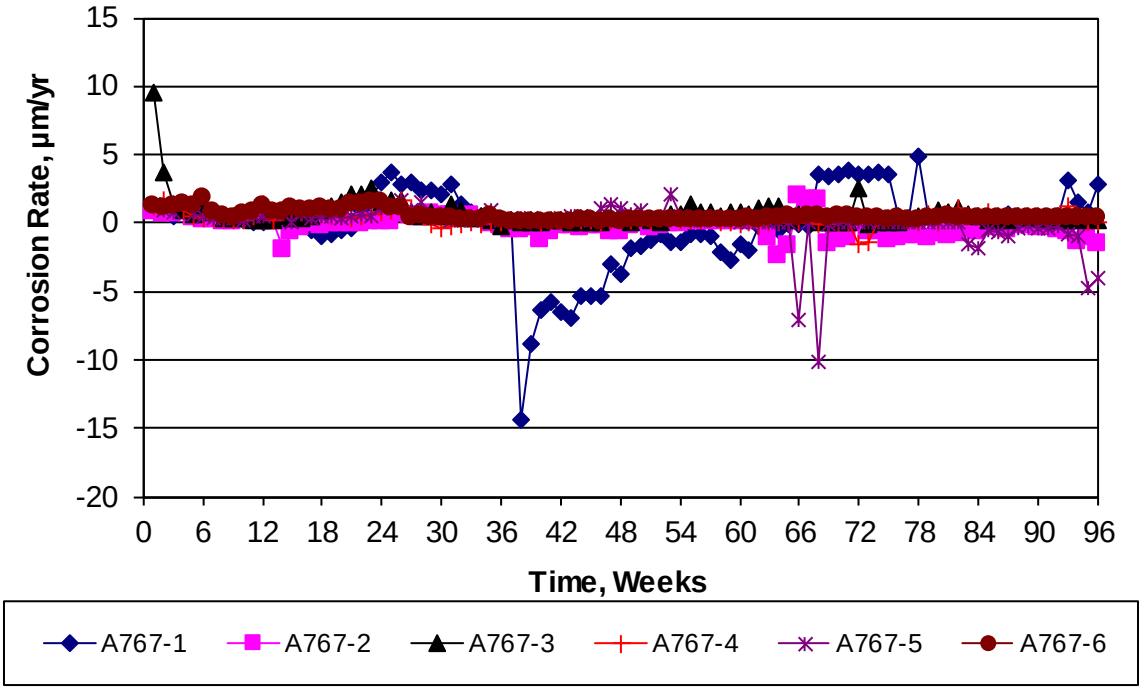

Figure A.55: Southern Exposure test. Corrosion rate of A767 reinforcement.

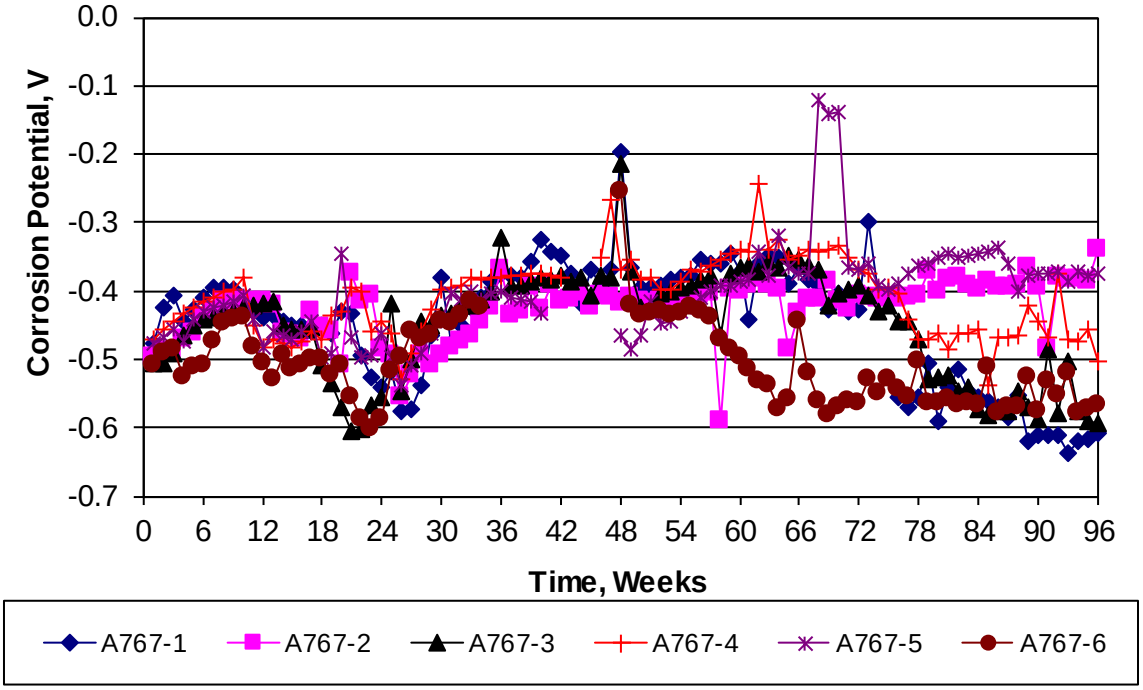

Figure A.56: Southern Exposure test. Corrosion potential of A767 reinforcement.

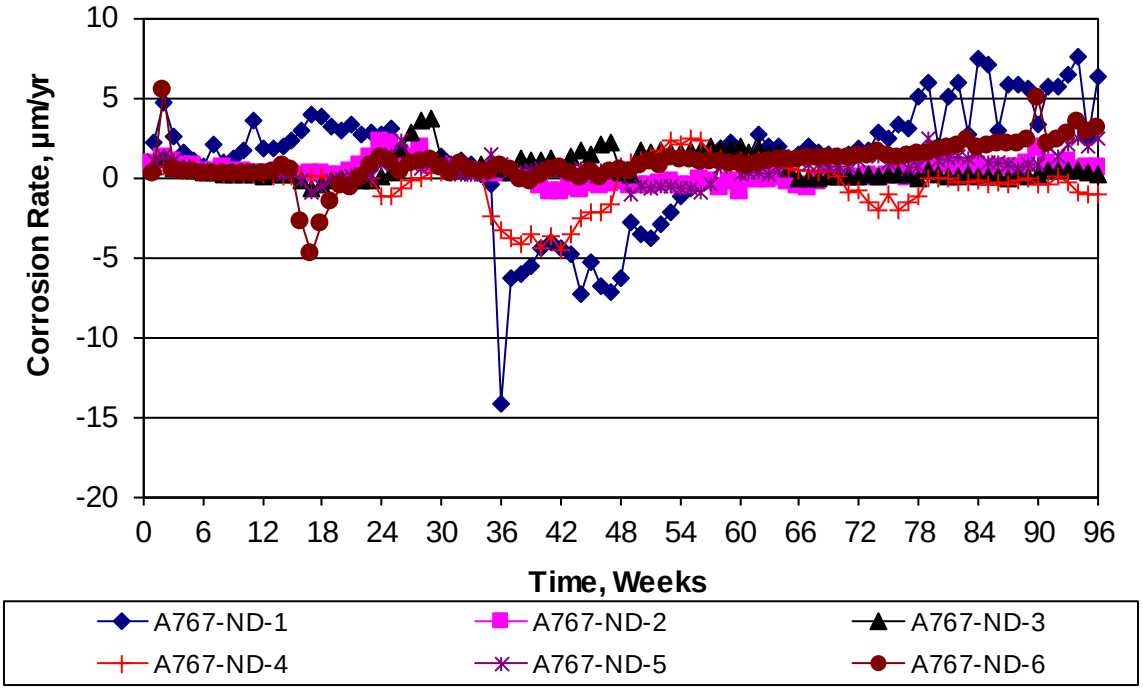

Figure A.57: Southern Exposure test. Corrosion rate of A767-ND reinforcement.

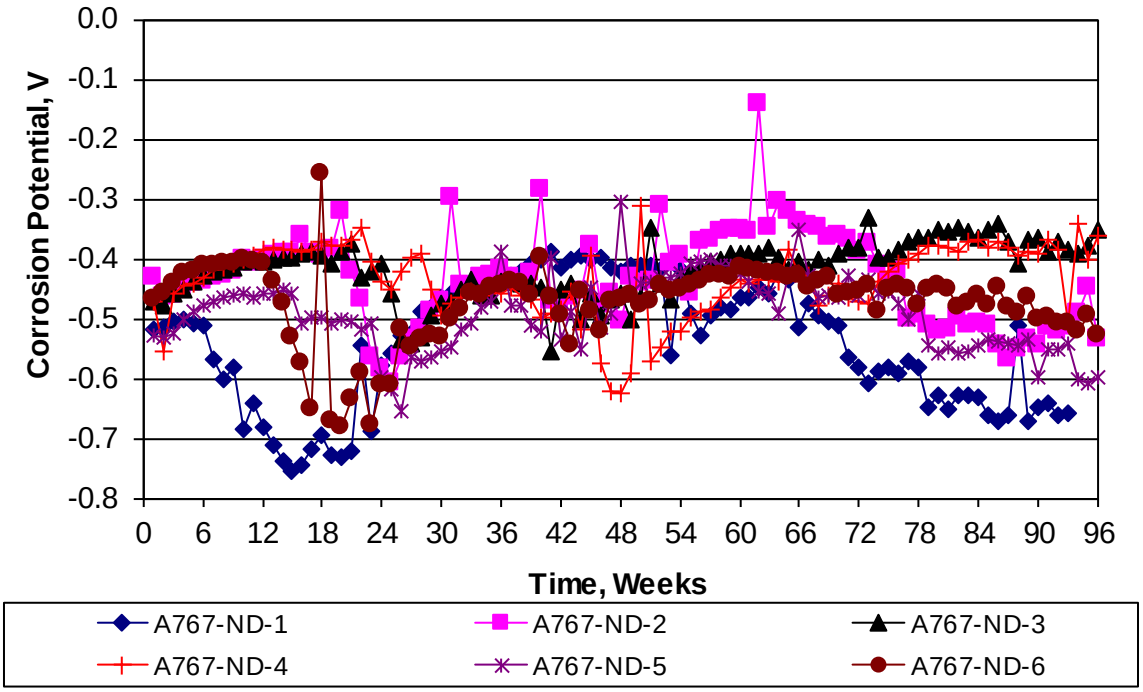

Figure A.58: Southern Exposure test. Corrosion potential of A767-ND reinforcement.

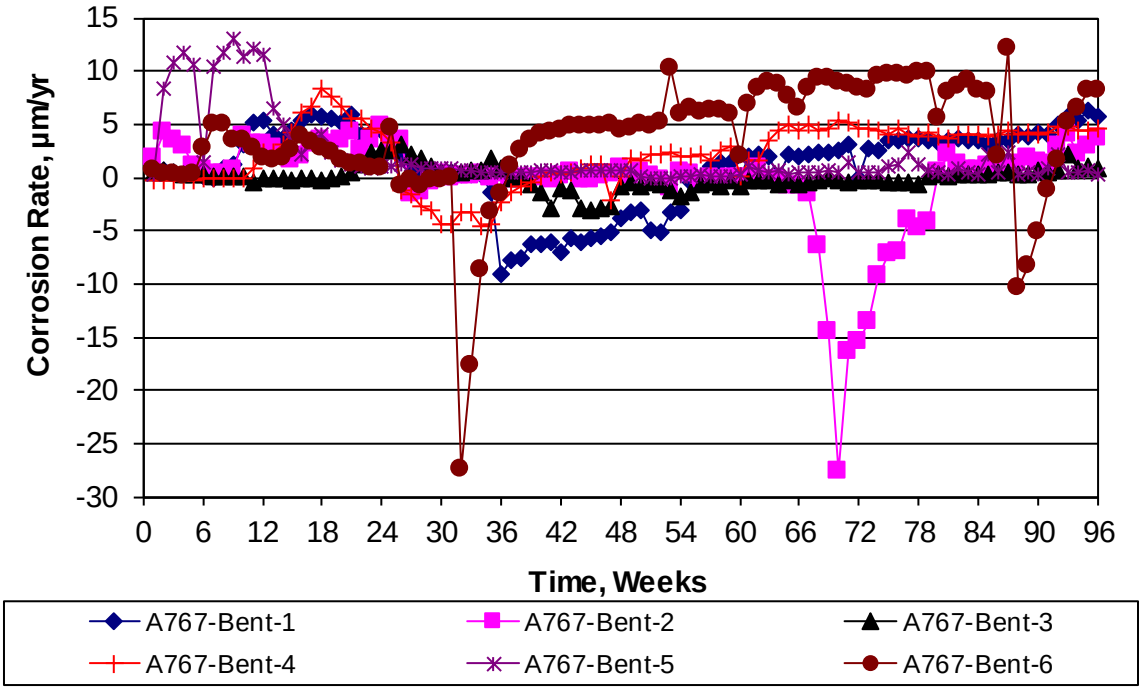

Figure A.59: Southern Exposure test. Corrosion rate of A767-Bent reinforcement.

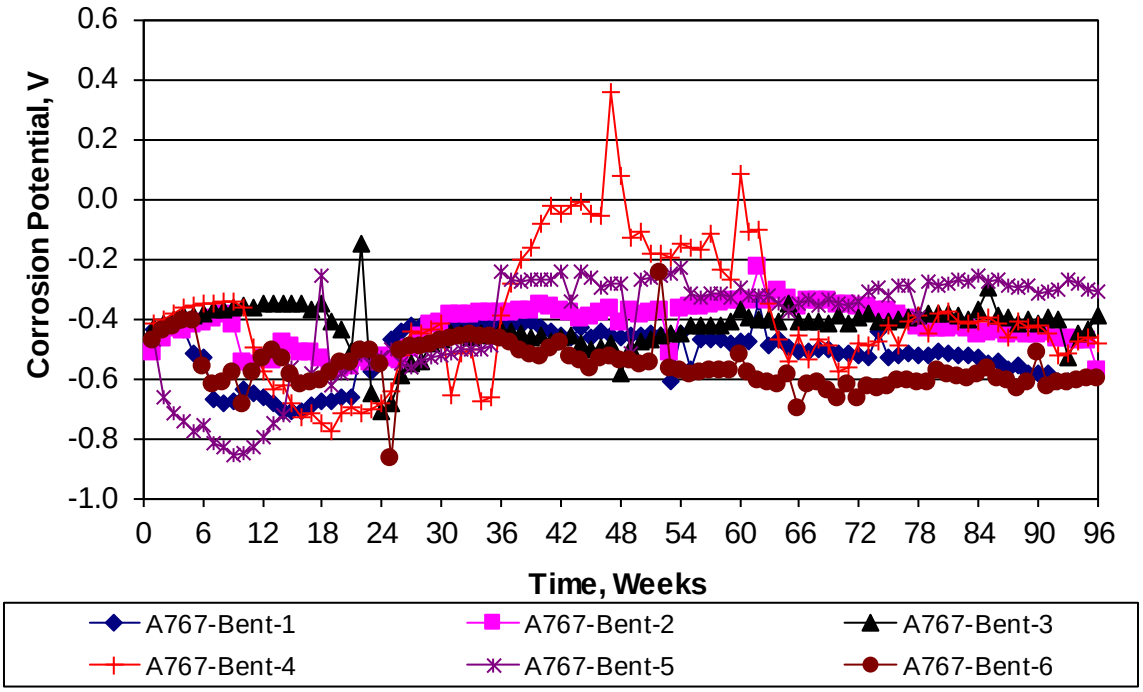

Figure A.60: Southern Exposure test. Corrosion potential of A767-Bent reinforcement.

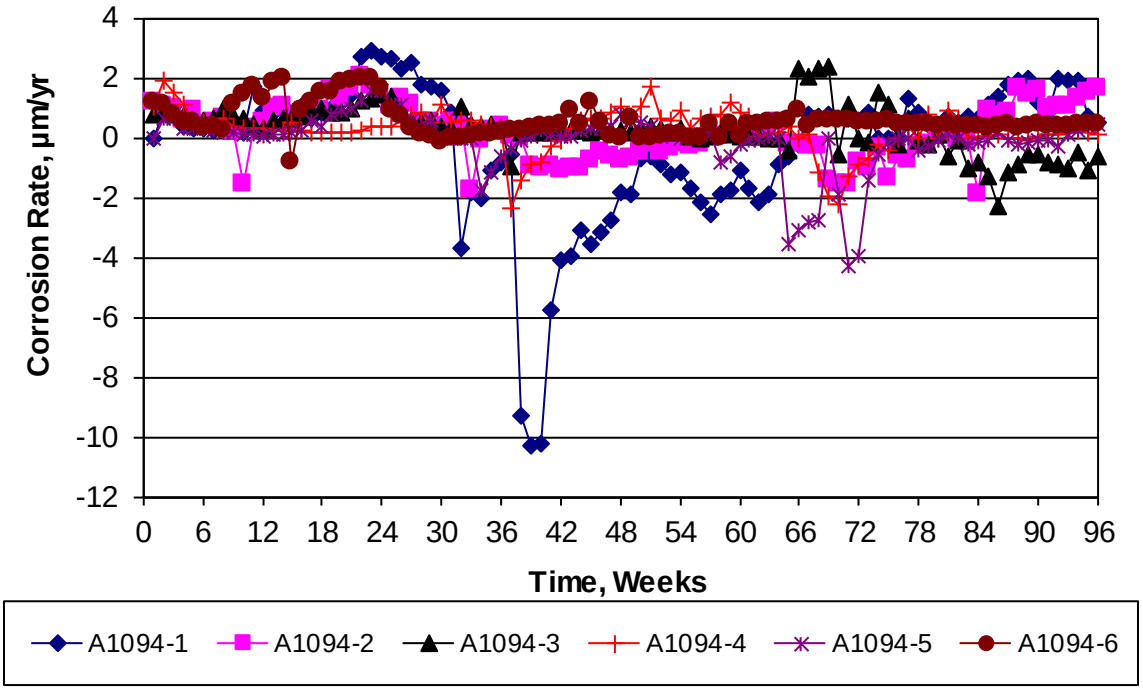

Figure A.61: Southern Exposure test. Corrosion rate of A1094 reinforcement.

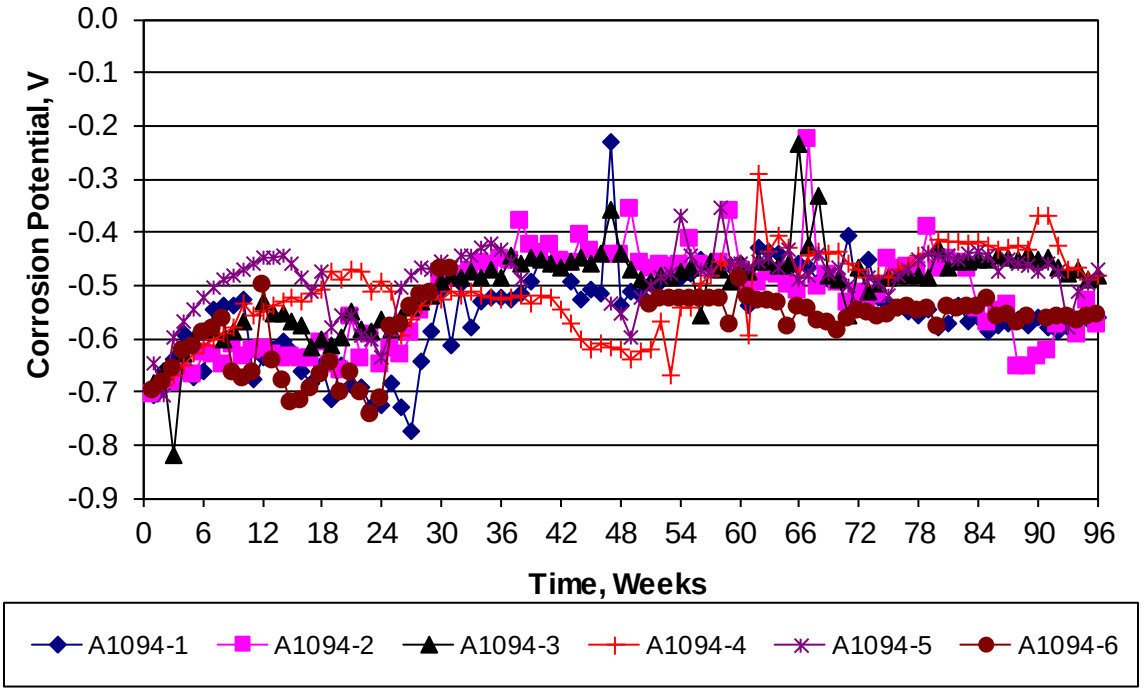

Figure A.62: Southern Exposure test. Corrosion potential of A1094 reinforcement.

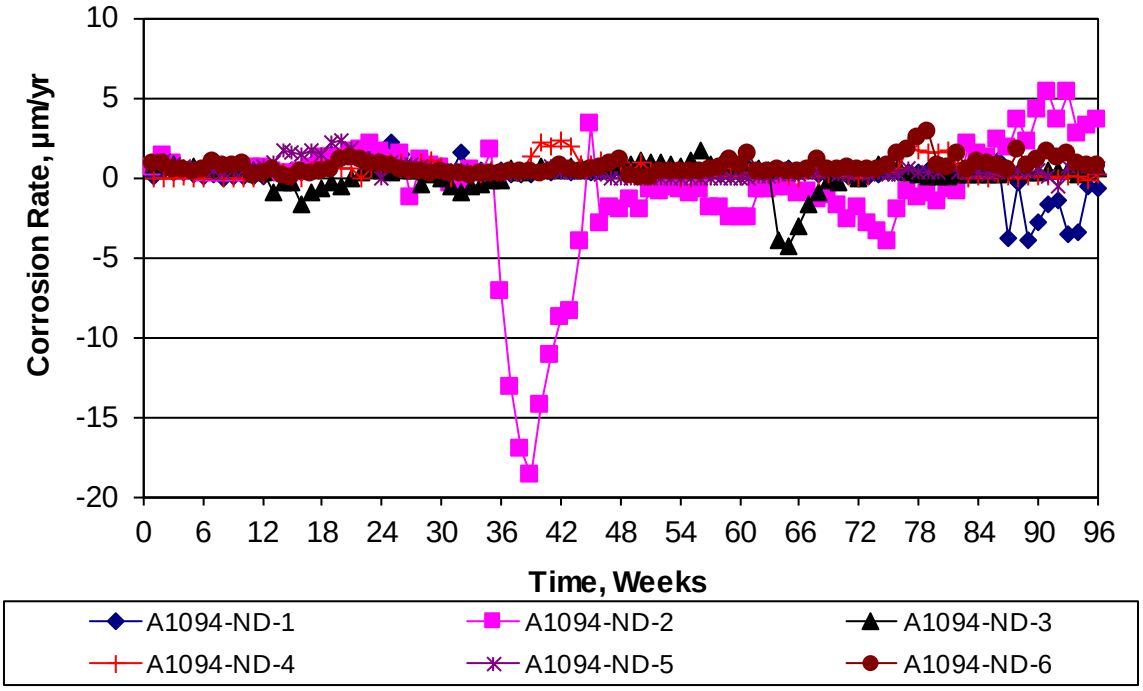

Figure A.63: Southern Exposure test. Corrosion rate of A1094-ND reinforcement.

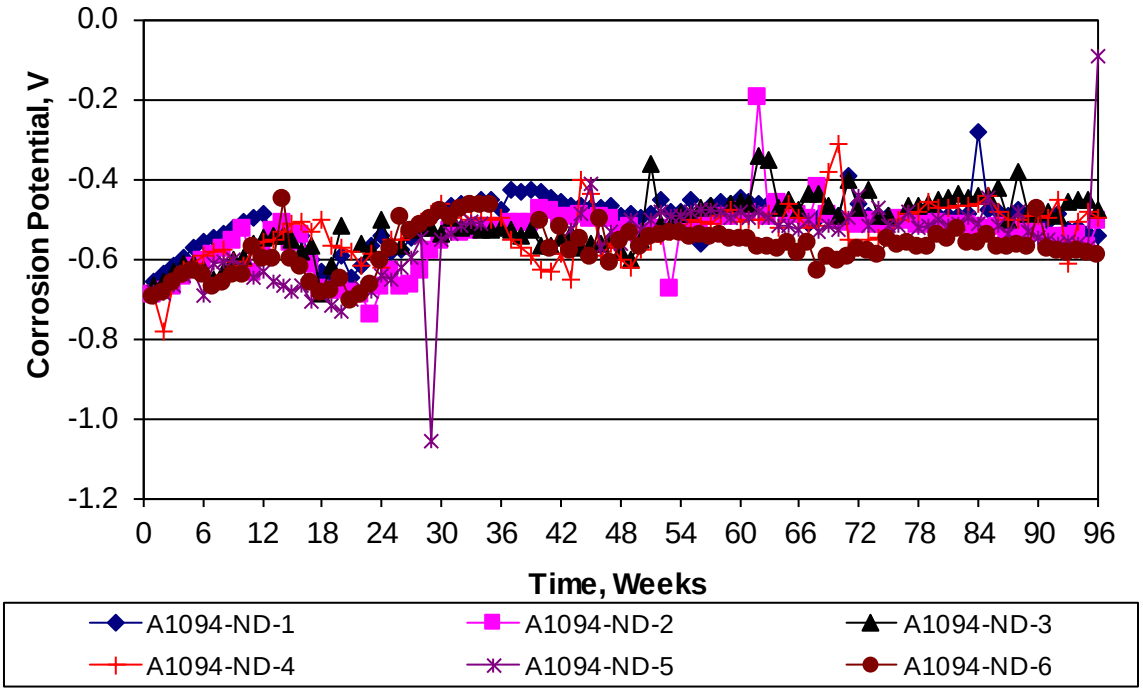

Figure A.64: Southern Exposure test. Corrosion potential of A1094-ND reinforcement.

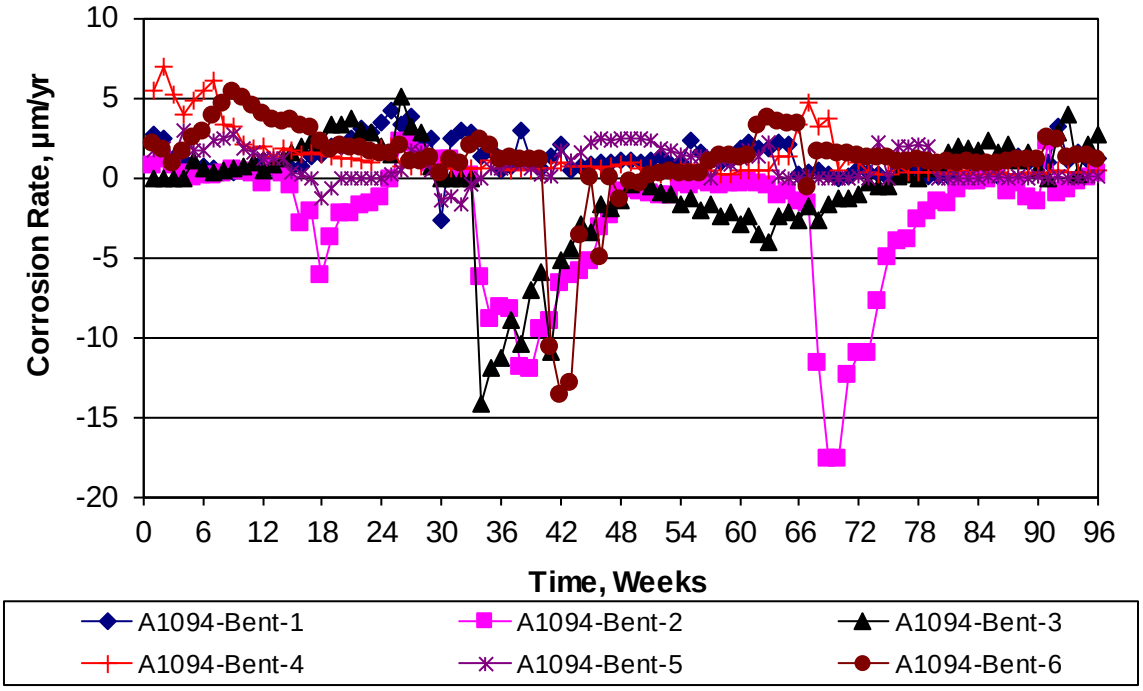

Figure A.65: Southern Exposure test. Corrosion rate of A1094-Bent reinforcement.

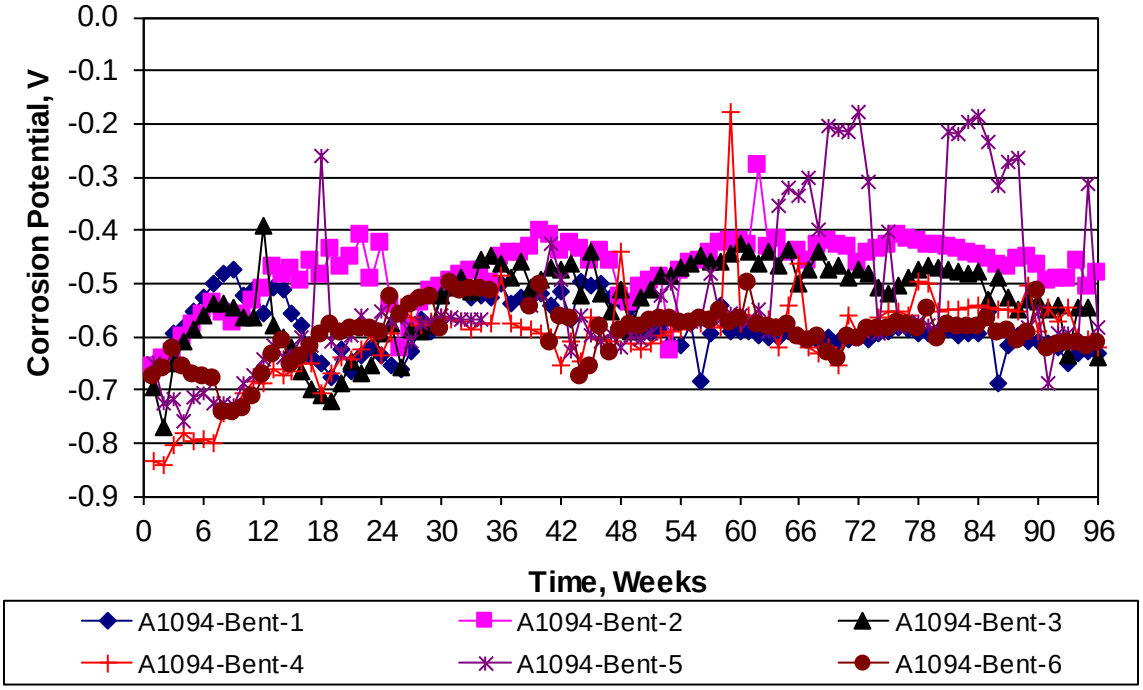

Figure A.66: Southern Exposure test. Corrosion potential of A1094-Bent reinforcement.

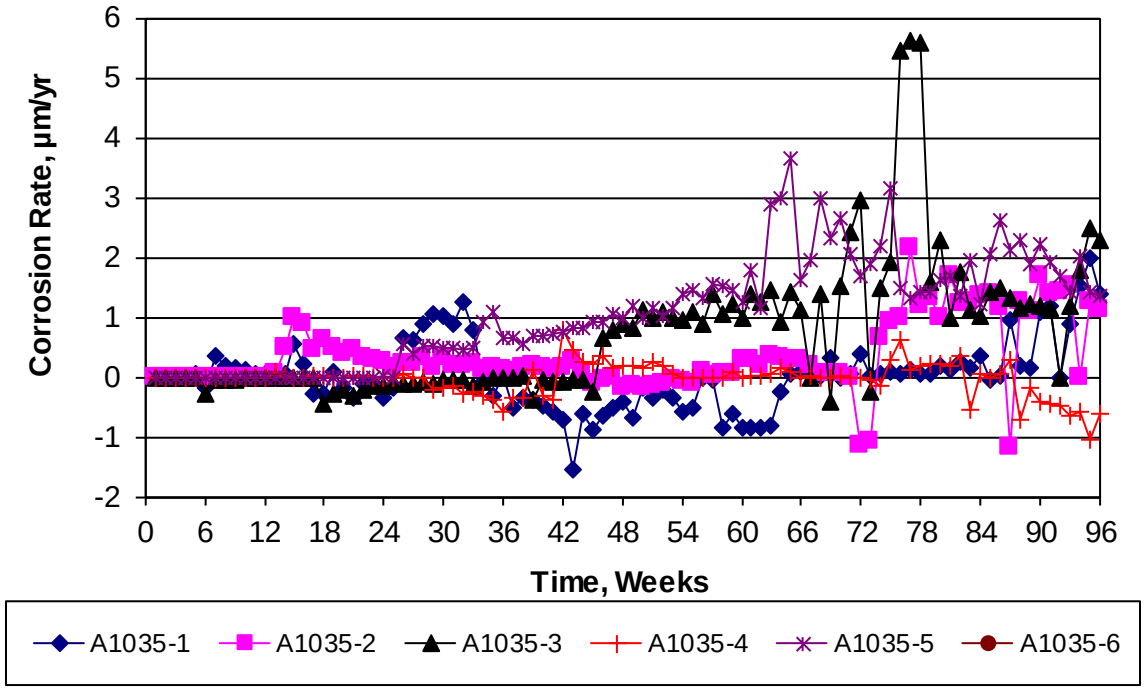

Figure A.67: Southern Exposure test. Corrosion rate of A1035 reinforcement.

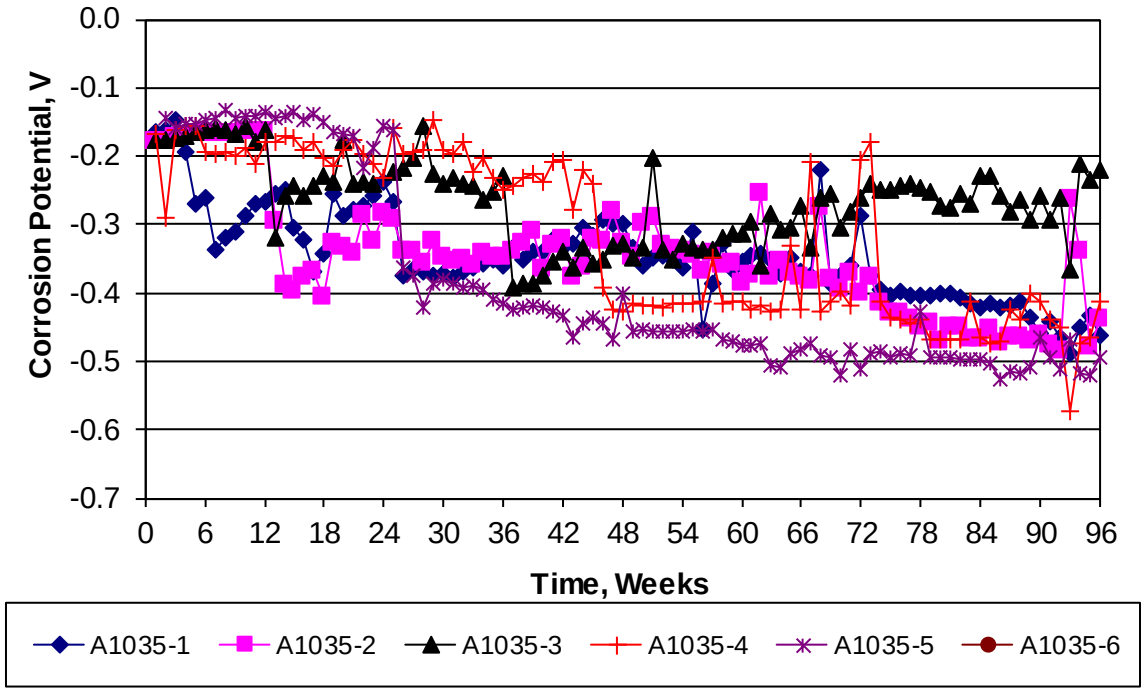

Figure A.68: Southern Exposure test. Corrosion potential of A1035 reinforcement.

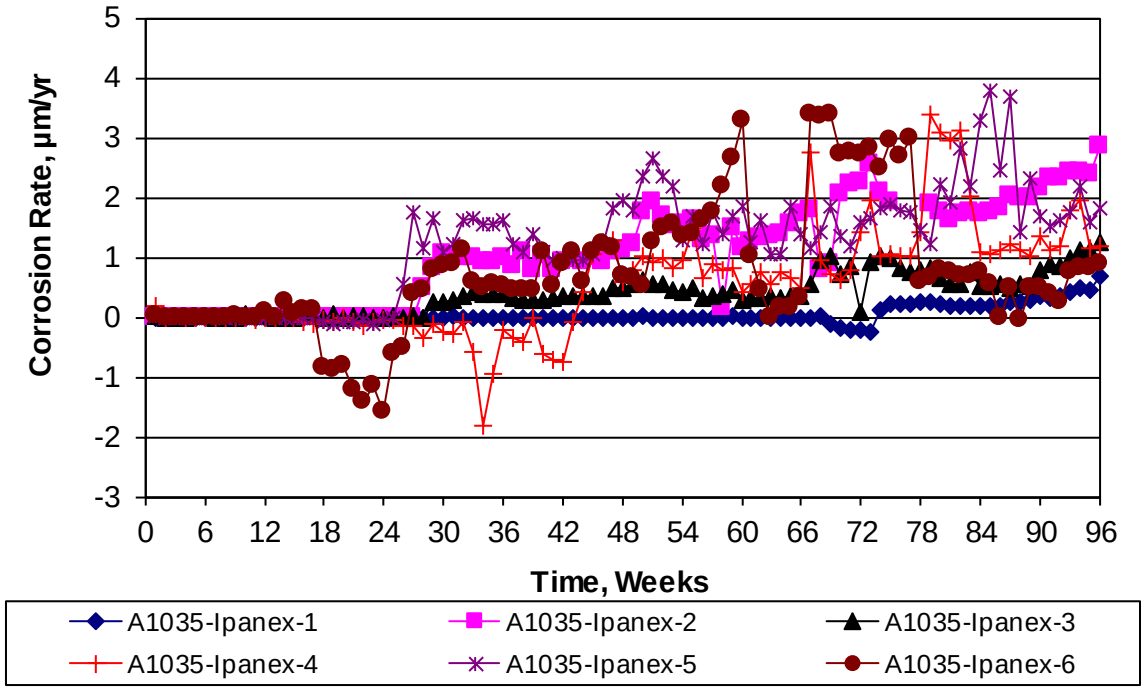

Figure A.69: Southern Exposure test. Corrosion rate of A1035-Ipanex reinforcement.

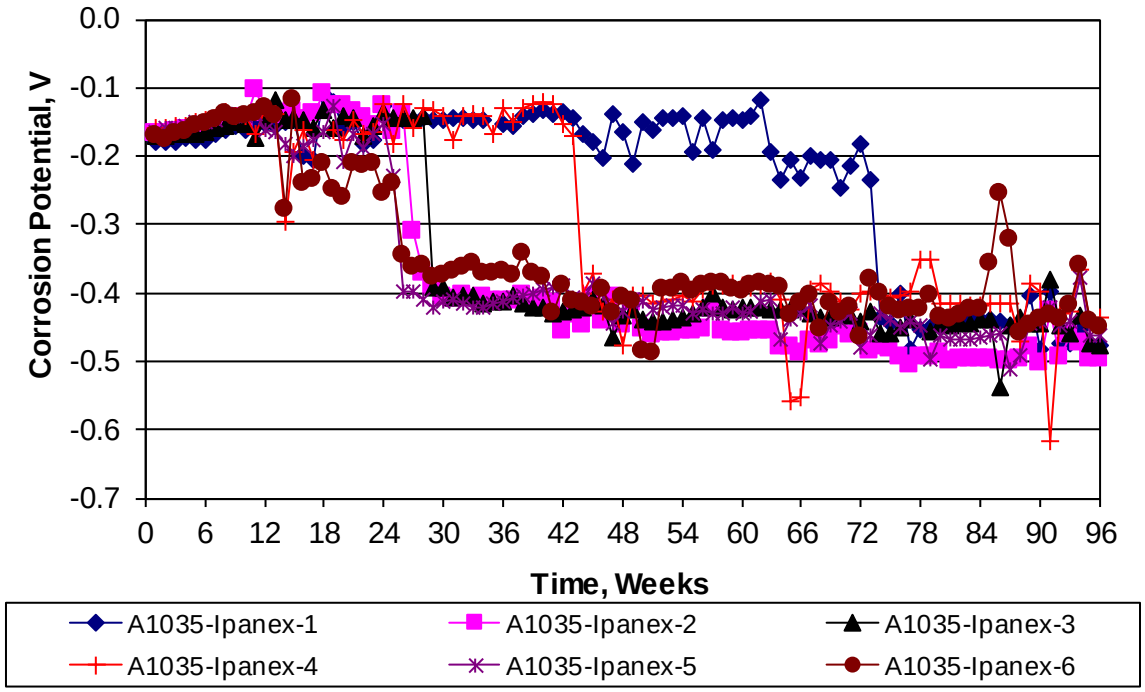

Figure A.70: Southern Exposure test. Corrosion potential of A1035-Ipanex reinforcement.

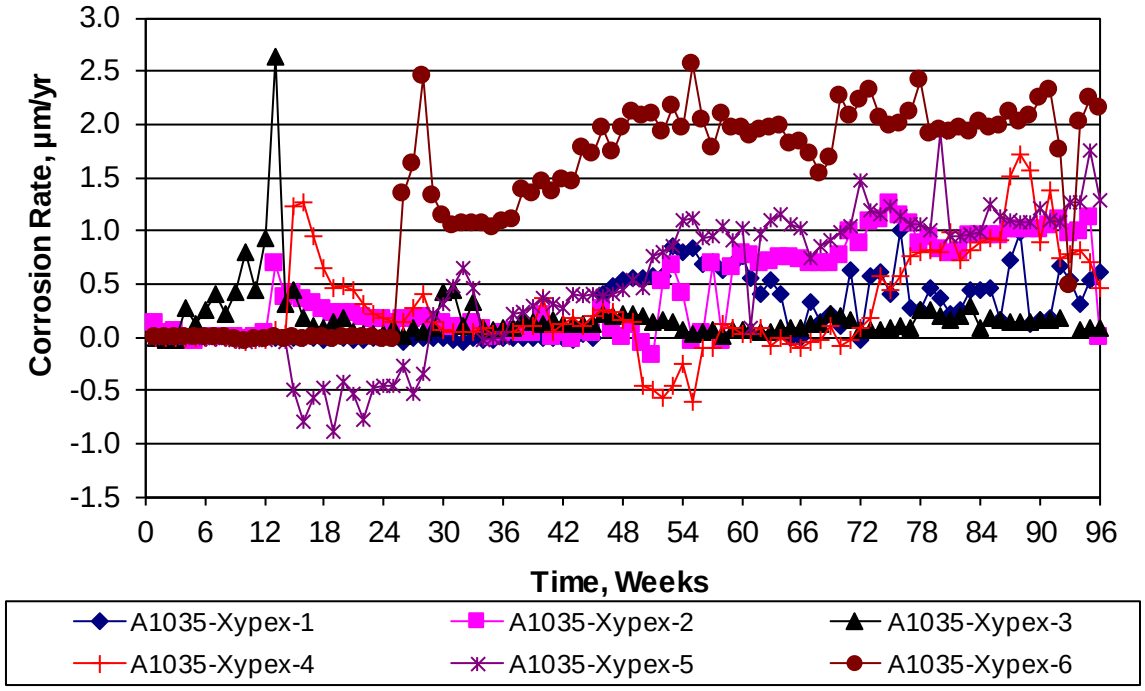

Figure A.71: Southern Exposure test. Corrosion rate of A1035-Xypex reinforcement.

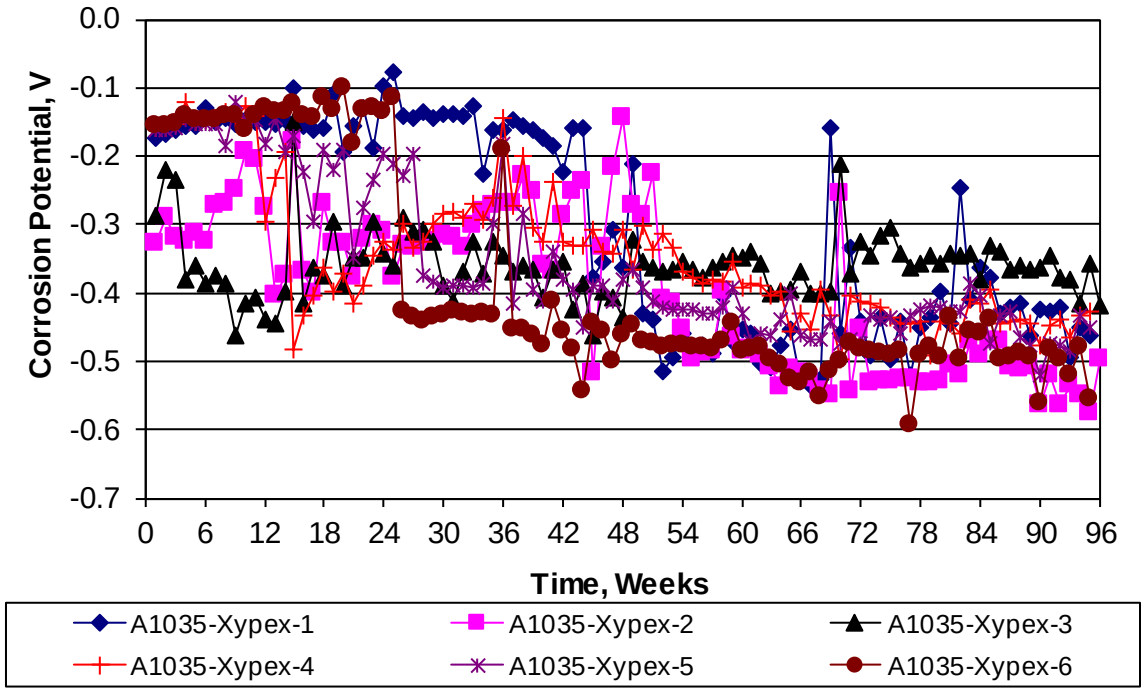

Figure A.72: Southern Exposure test. Corrosion potential of A1035-Xypex reinforcement.

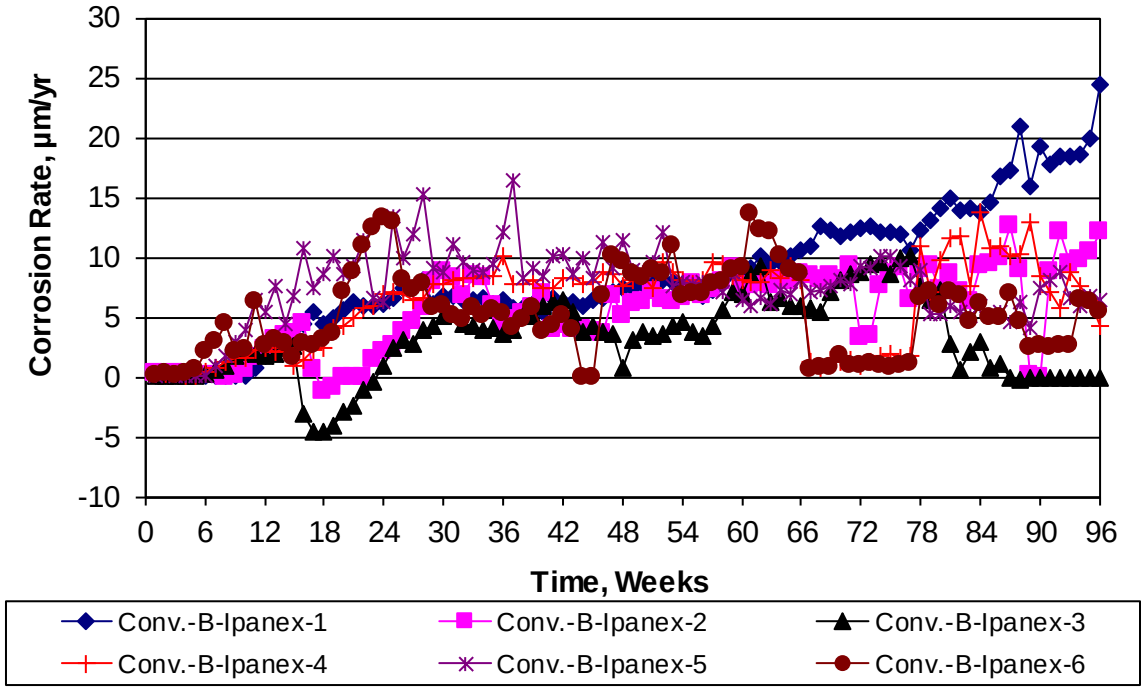

Figure A.73: Southern Exposure test. Corrosion rate of Conv-B-Ipanex reinforcement.

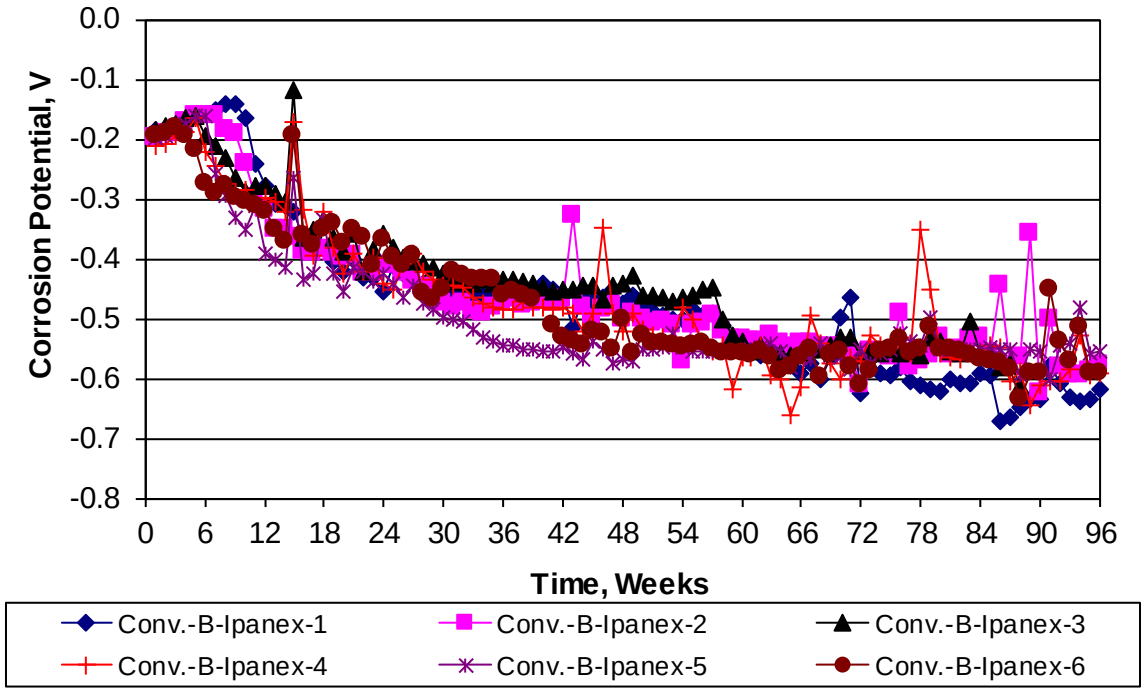

Figure A.74: Southern Exposure test. Corrosion potential of Conv-B-Ipanex reinforcement.

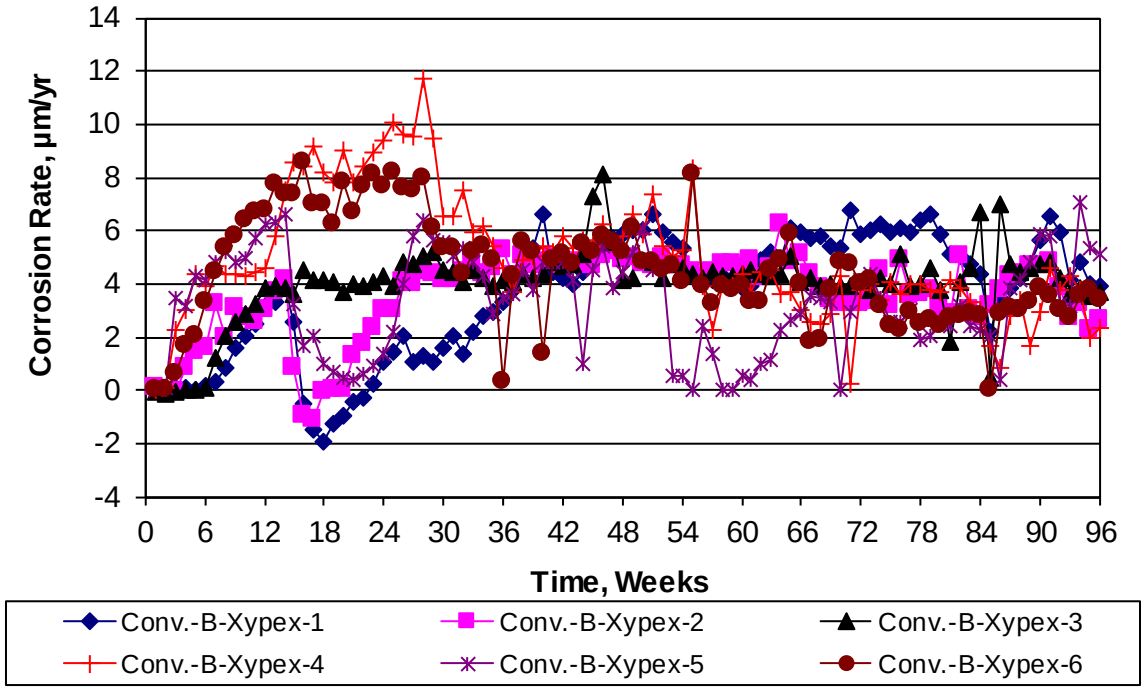

Figure A.75: Southern Exposure test. Corrosion rate of Conv-B-Xypex reinforcement.

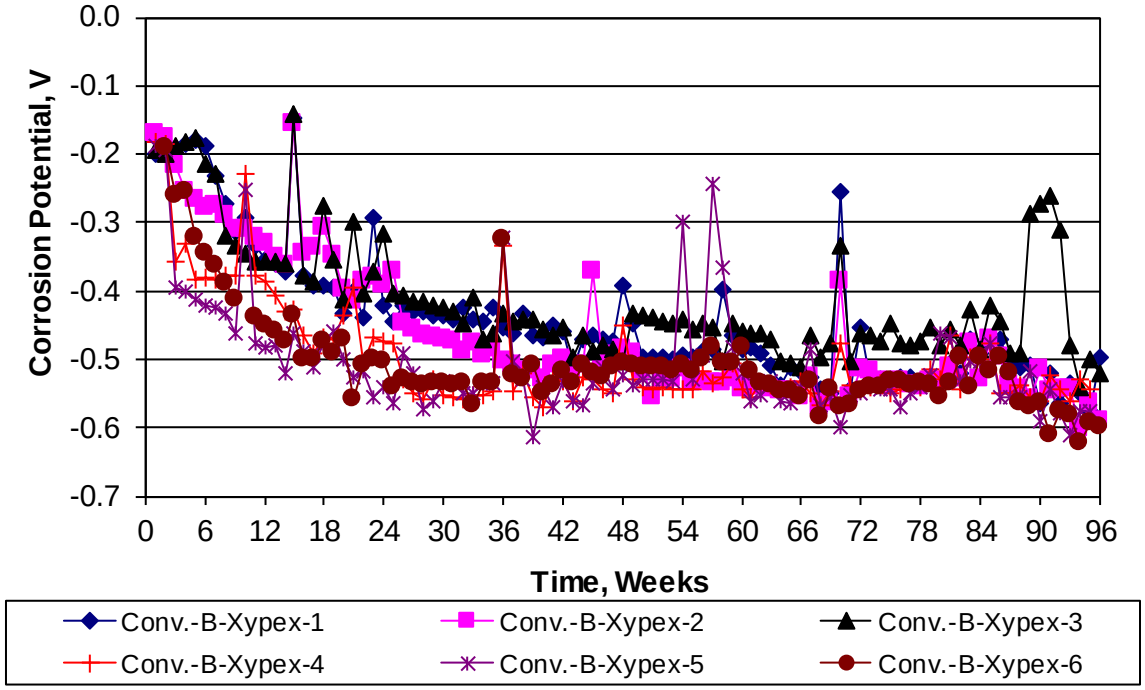

Figure A.76: Southern Exposure test. Corrosion potential of Conv-B-Xypex reinforcement.

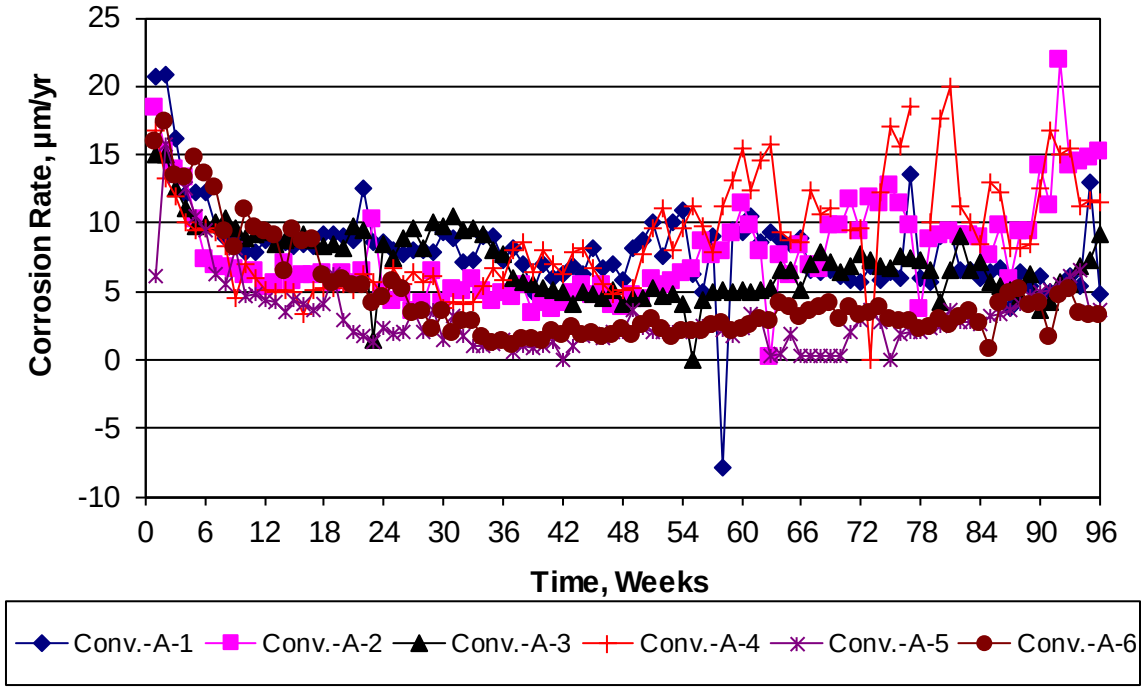

Figure A.77: Cracked beam test. Corrosion rate of Conv-A reinforcement.

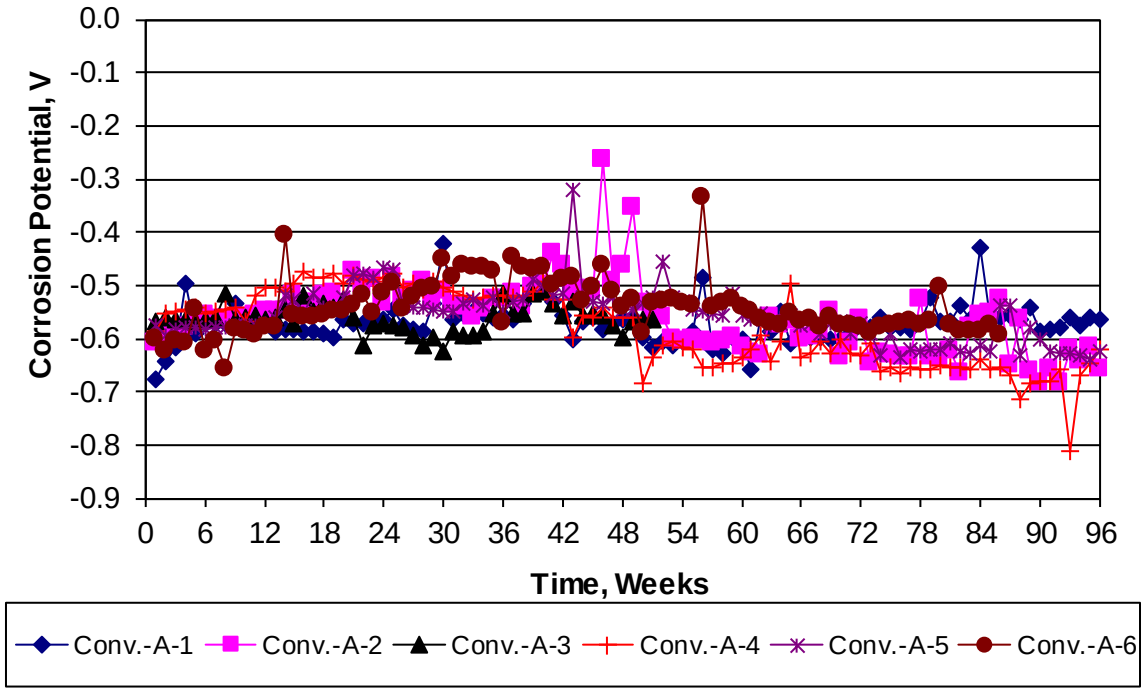

Figure A.78: Cracked beam test. Corrosion potential of Conv-A reinforcement.

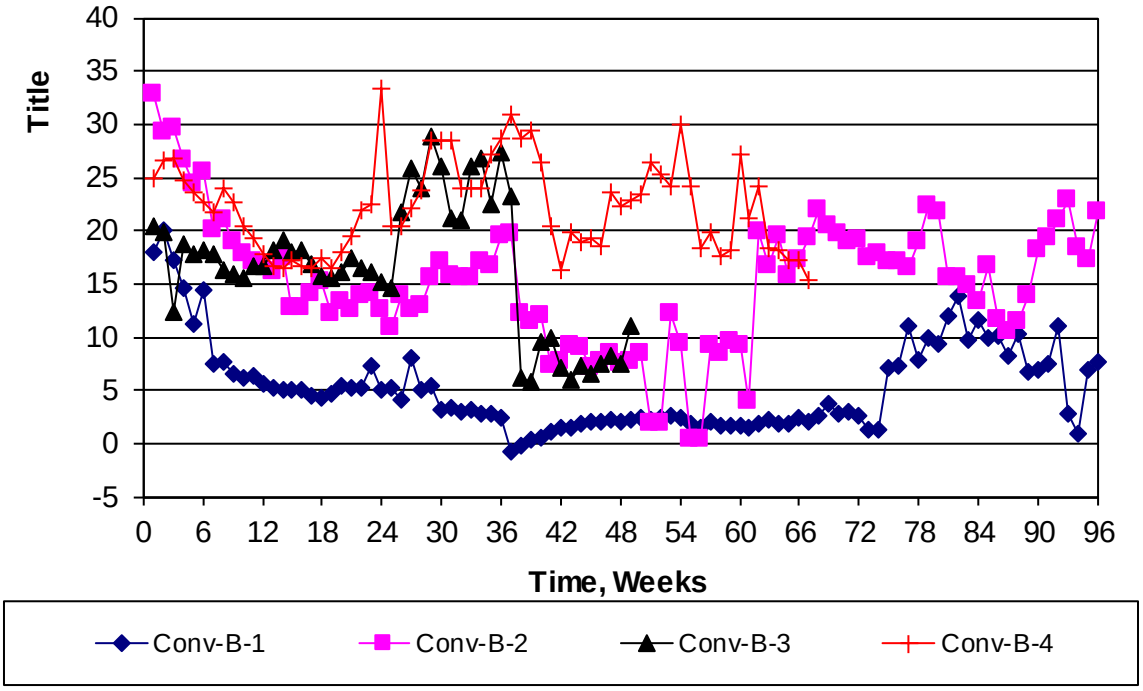

Figure A.79: Cracked beam test. Corrosion rate of Conv-B reinforcement.

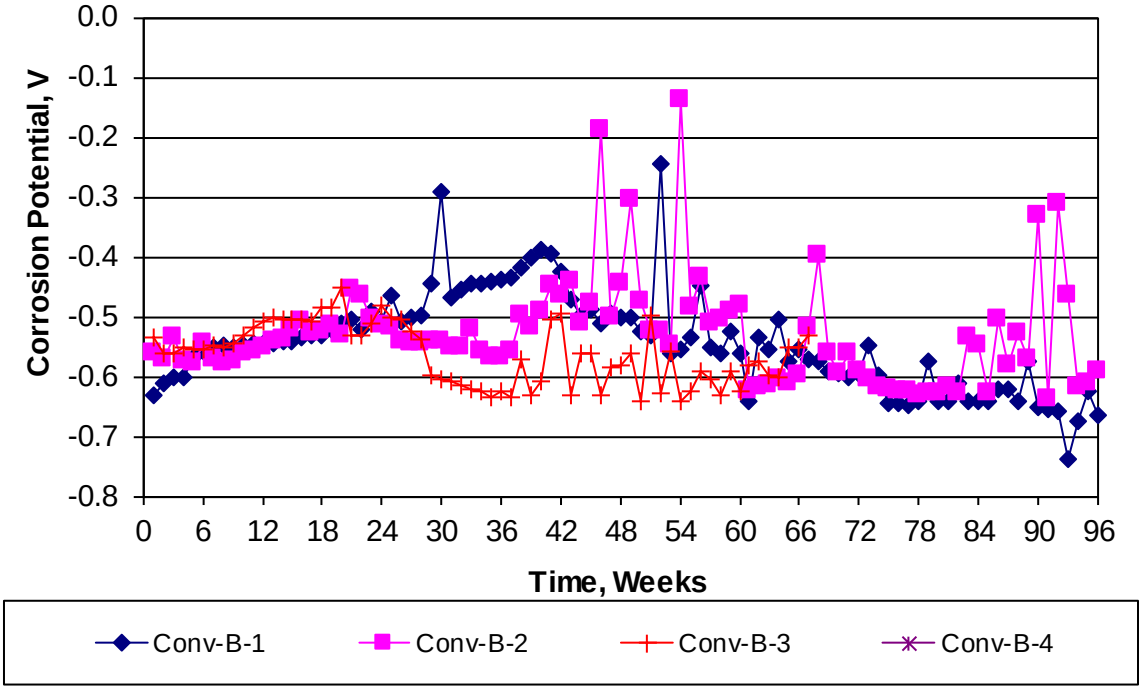

Figure A.80: Cracked beam test. Corrosion potential of Conv-B reinforcement.

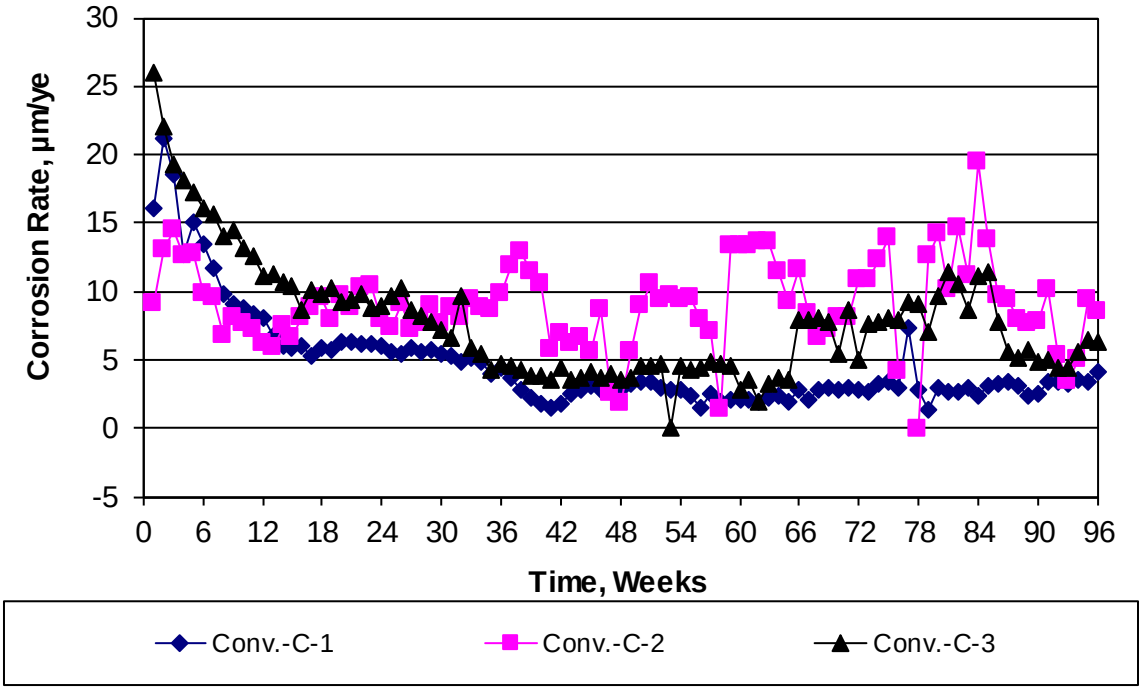

Figure A.81: Cracked beam test. Corrosion rate of Conv-C reinforcement.

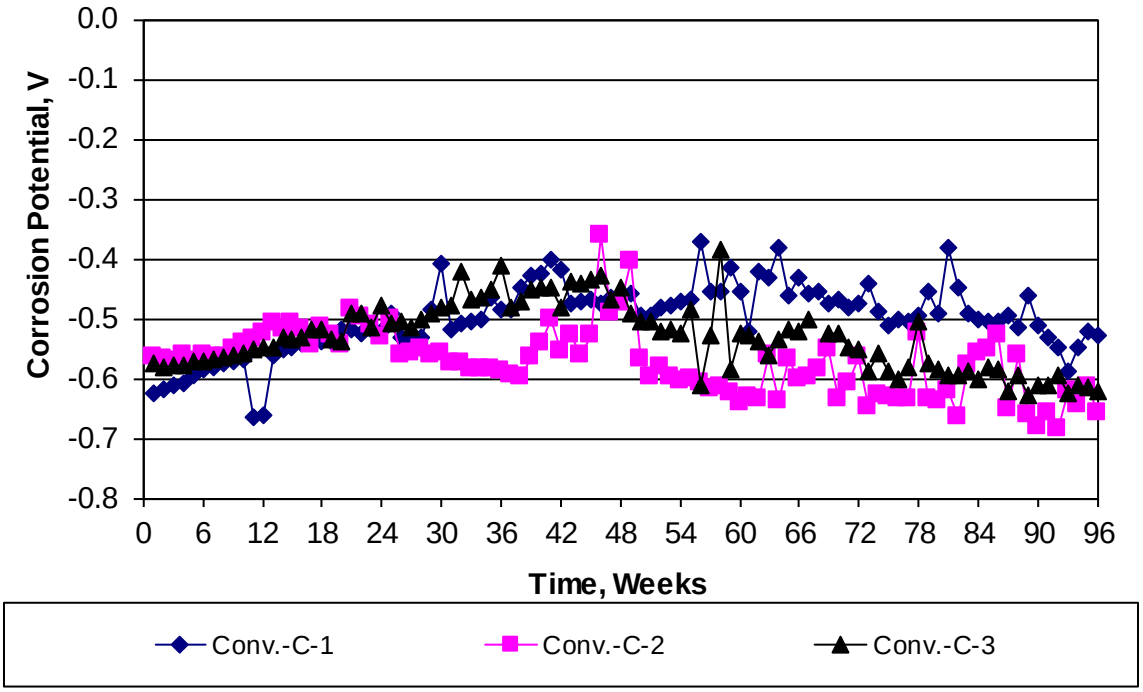

Figure A.82: Cracked beam test. Corrosion potential of Conv-C reinforcement.

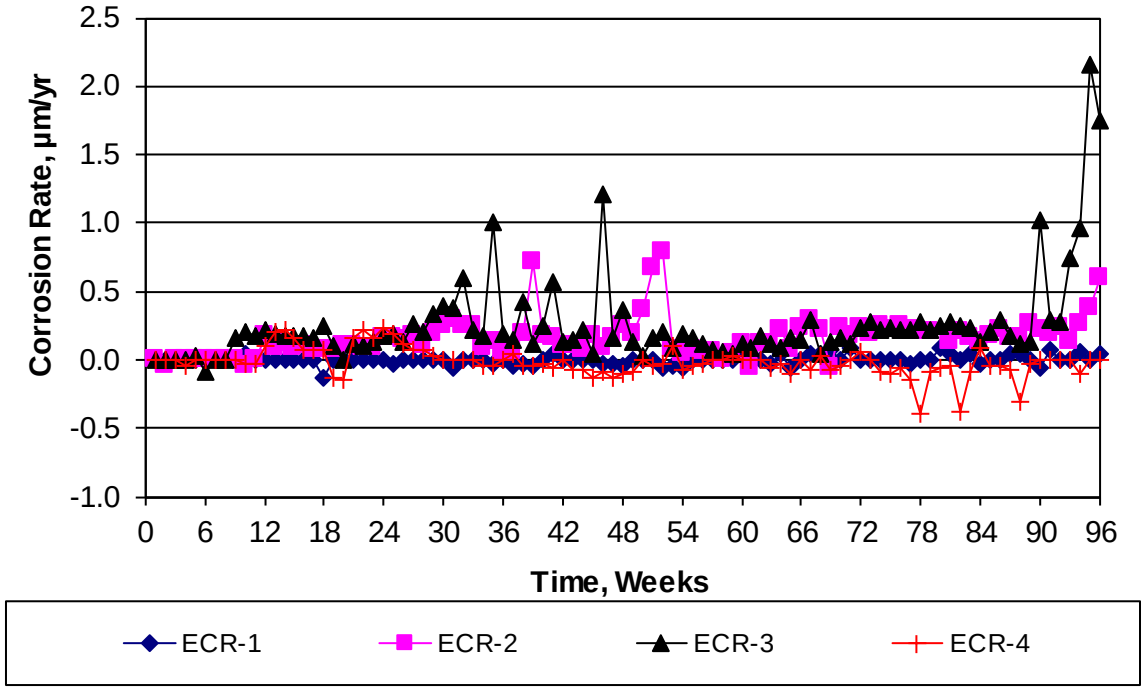

Figure A.83: Cracked beam test. Corrosion rate of ECR.

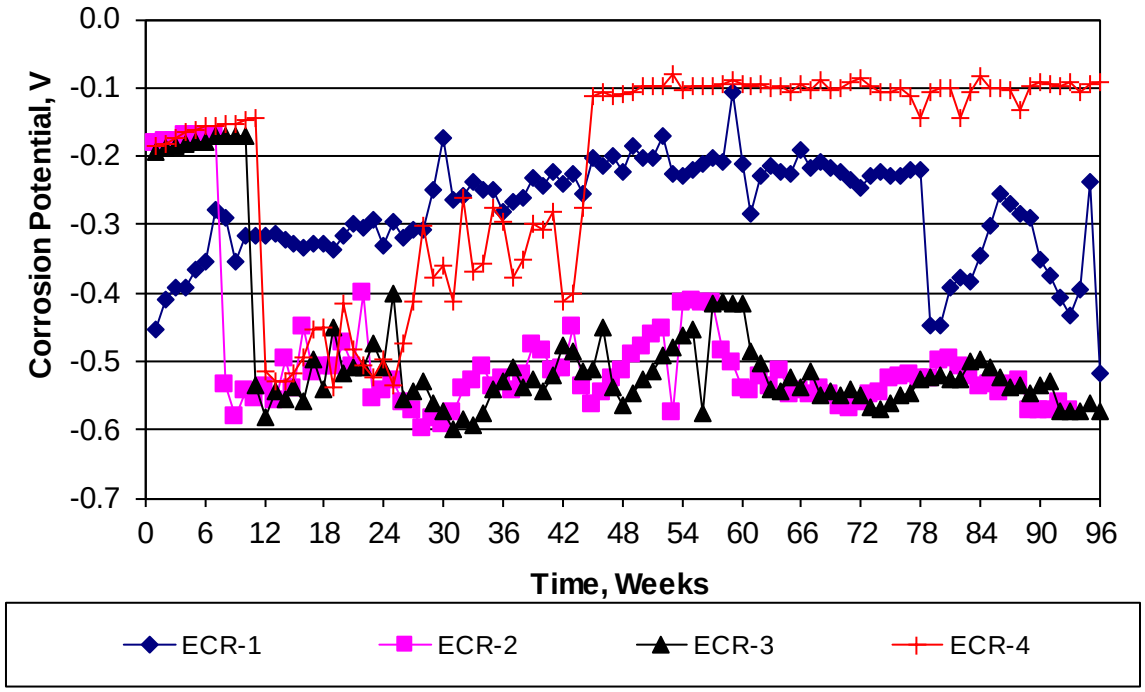

Figure A.84: Cracked beam test. Corrosion potential of ECR.

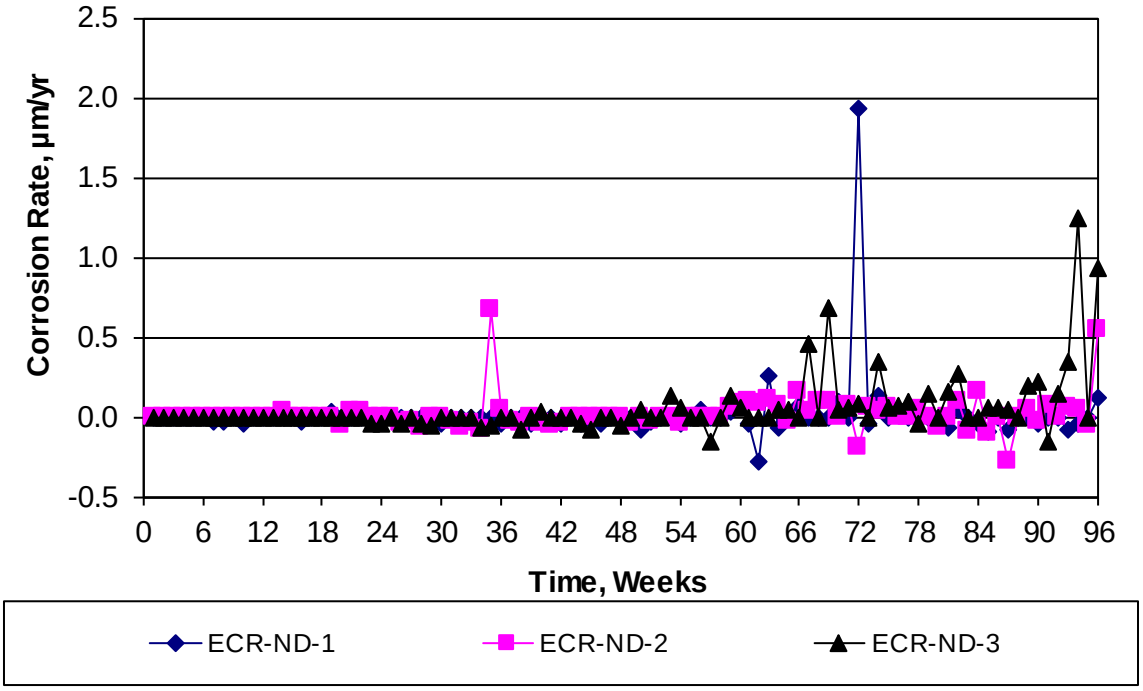

Figure A.85: Cracked beam test. Corrosion rate of ECR-ND.

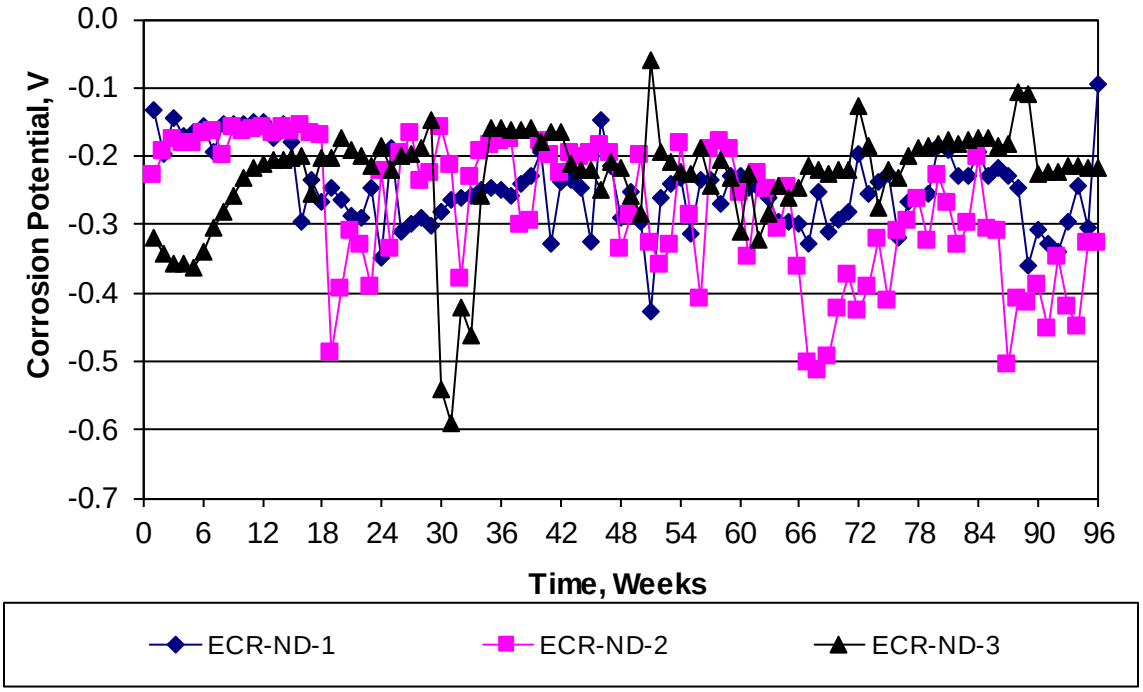

Figure A.86: Cracked beam test. Corrosion potential of ECR-ND.

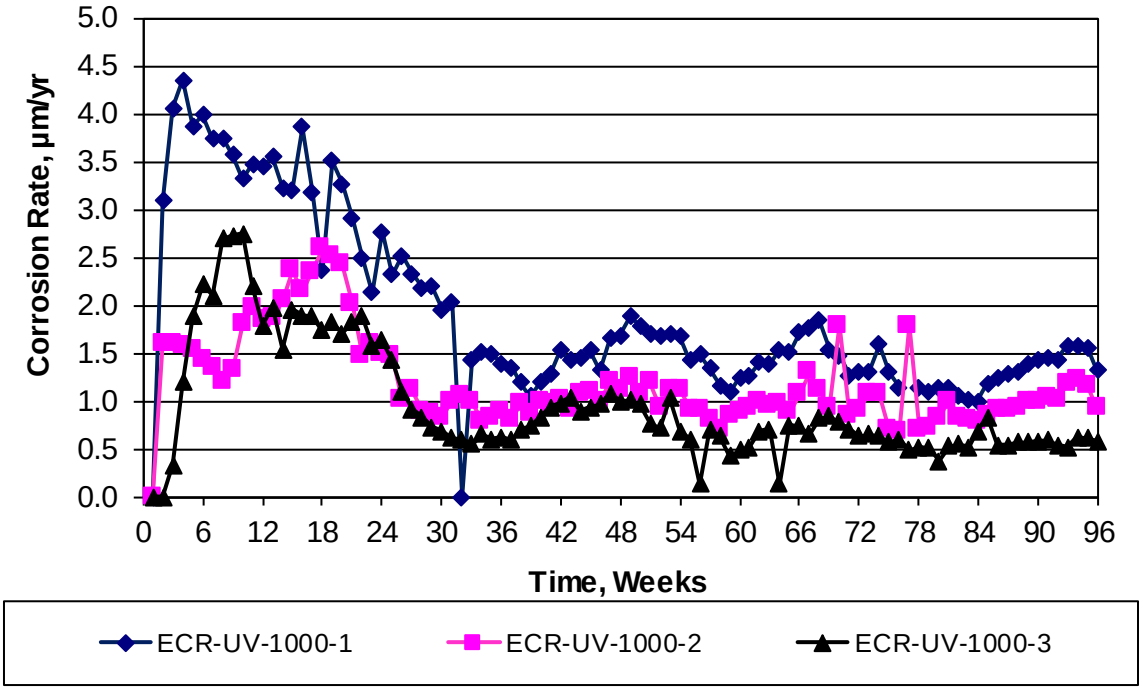

Figure A.87: Cracked beam test. Corrosion rate of ECR-UV-1000.

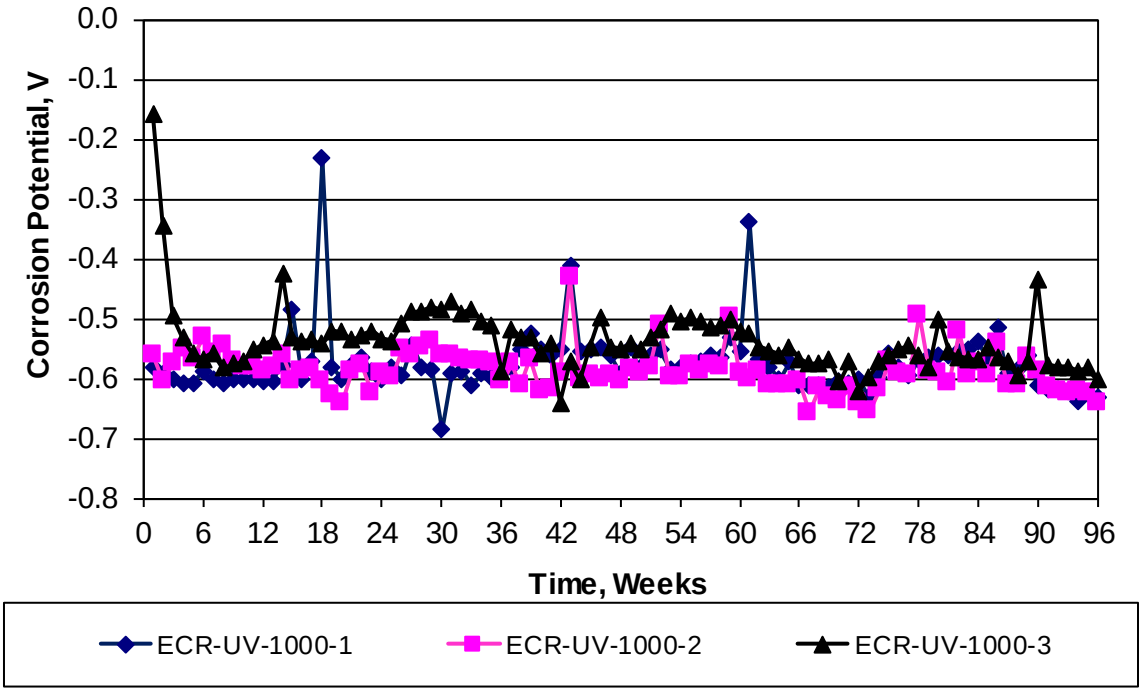

Figure A.88: Cracked beam test. Corrosion potential of ECR-UV-1000.

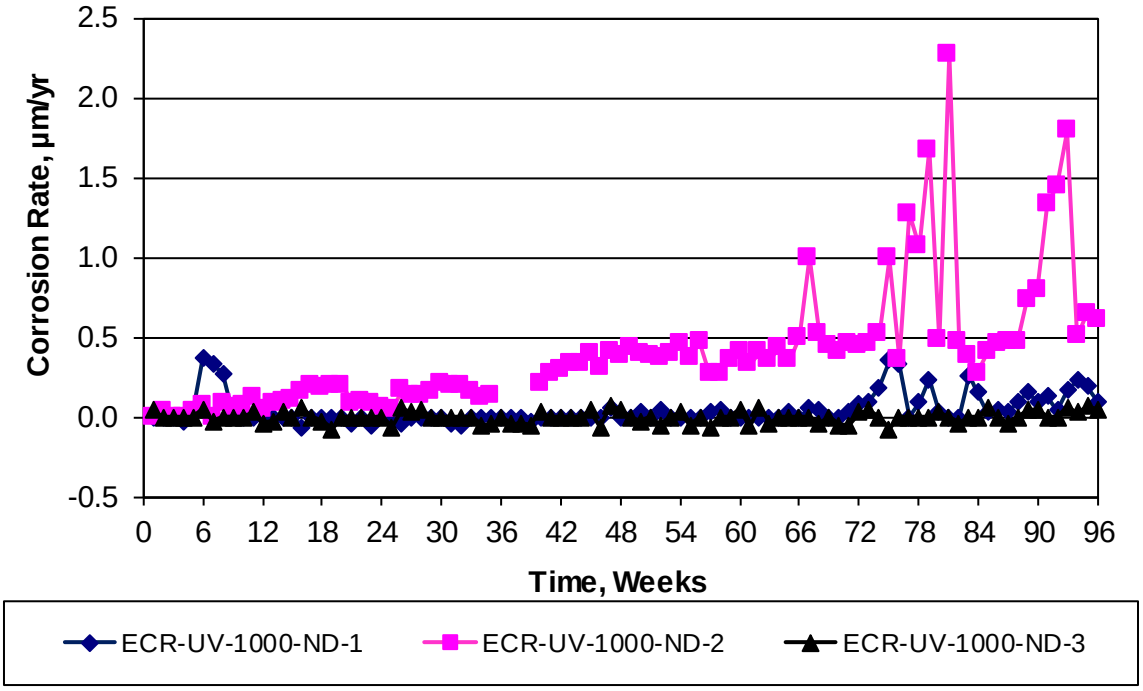

Figure A.89: Cracked beam test. Corrosion rate of ECR-UV-1000-ND.

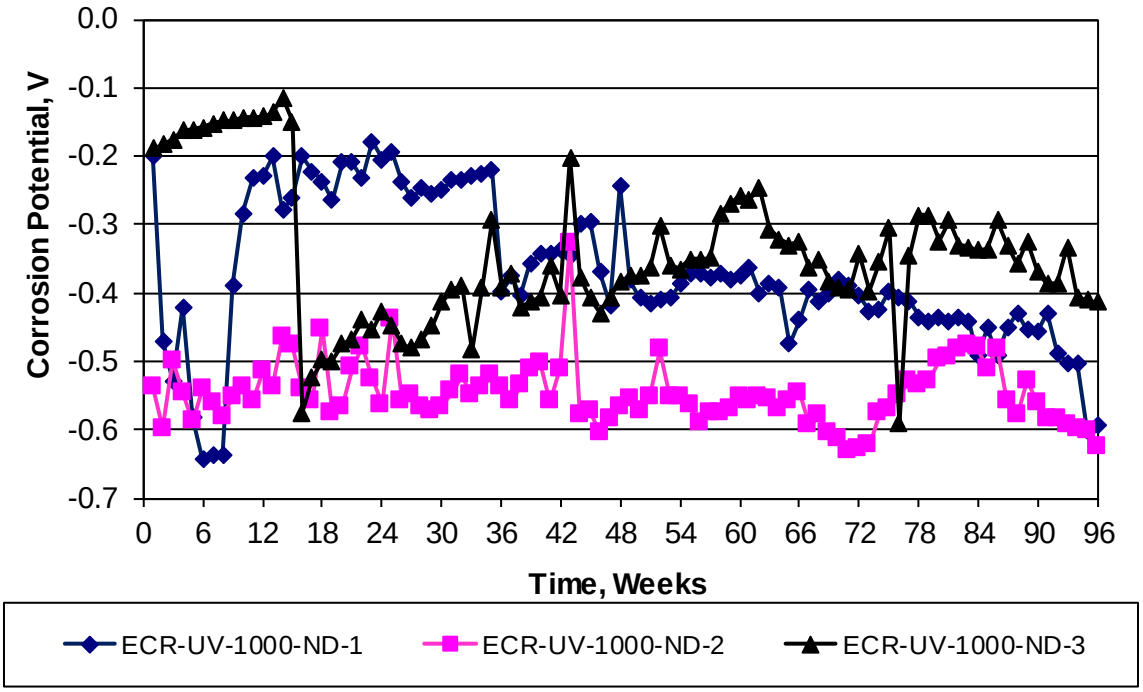

Figure A.90: Cracked beam test. Corrosion potential of ECR-UV-1000-ND.

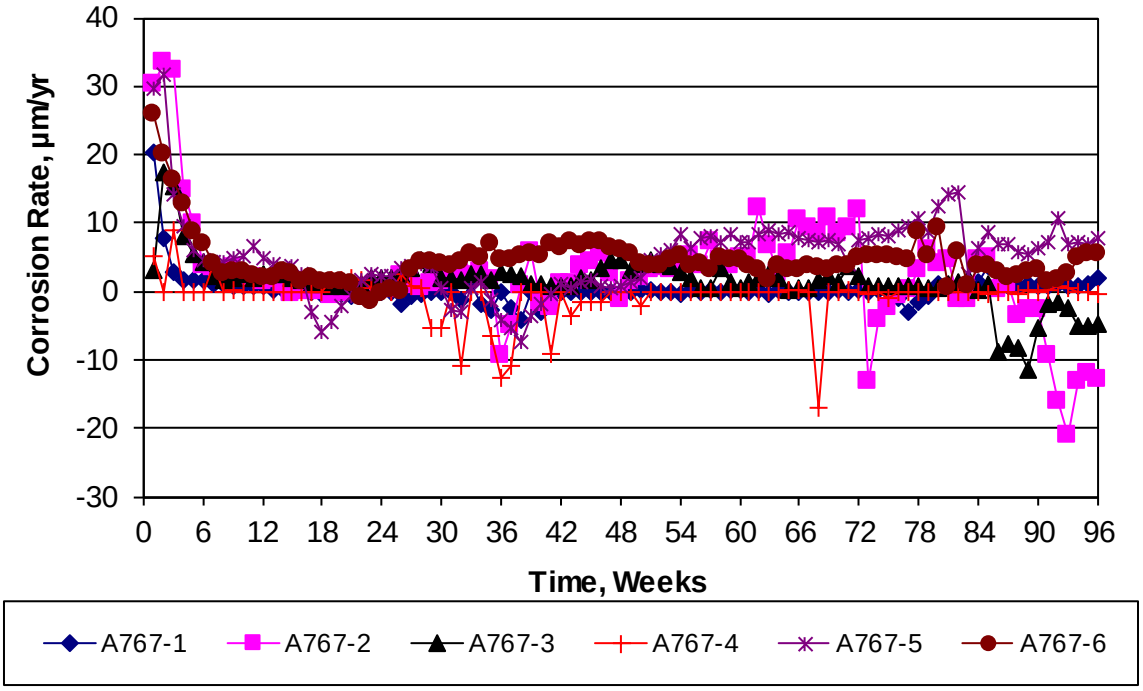

Figure A.91: Cracked beam test. Corrosion rate of A767 reinforcement.

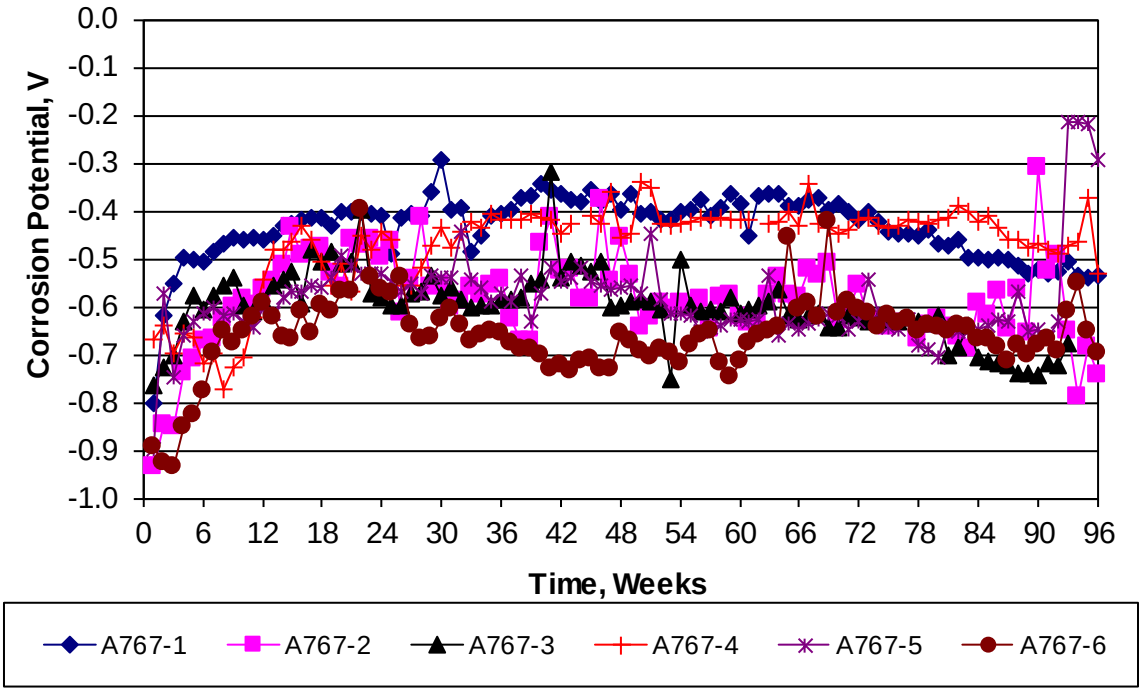

Figure A.92: Cracked beam test. Corrosion potential of A767 reinforcement.

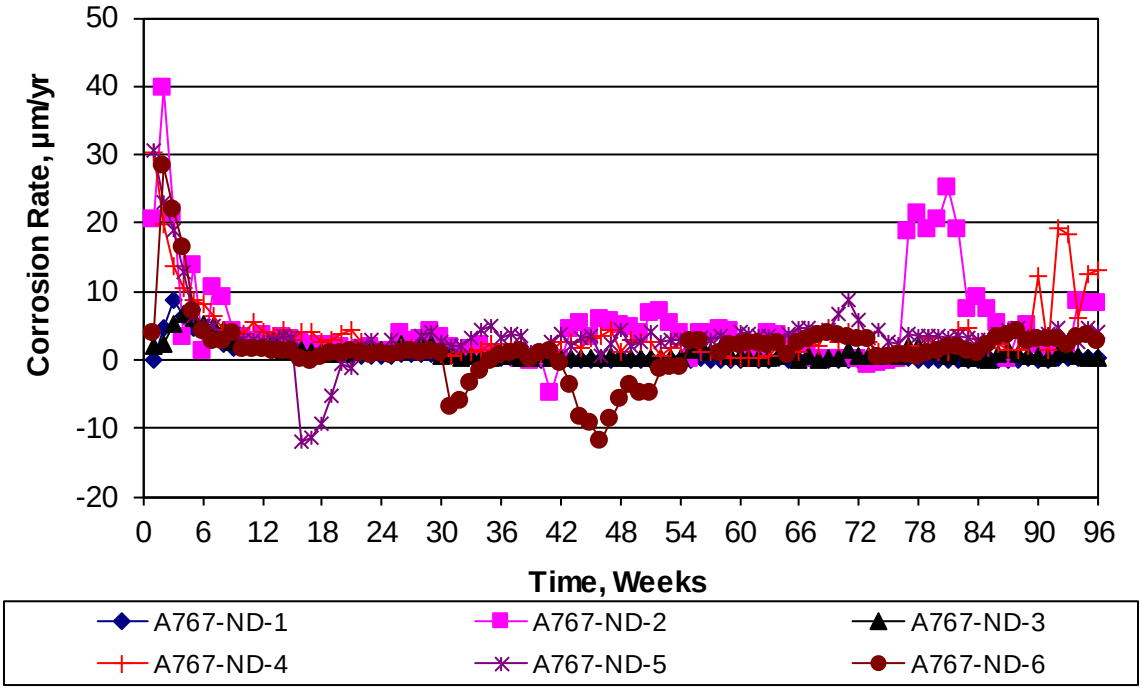

Figure A.93: Cracked beam test. Corrosion rate of A767-ND reinforcement.

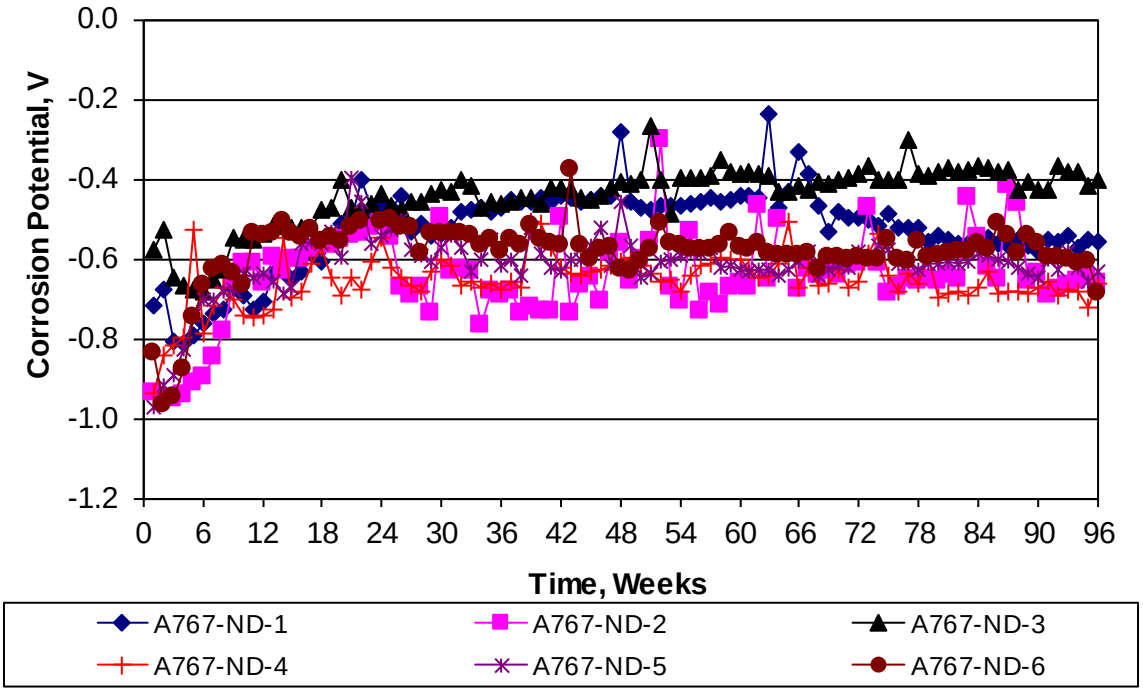

Figure A.94: Cracked beam test. Corrosion potential of A767-ND reinforcement.

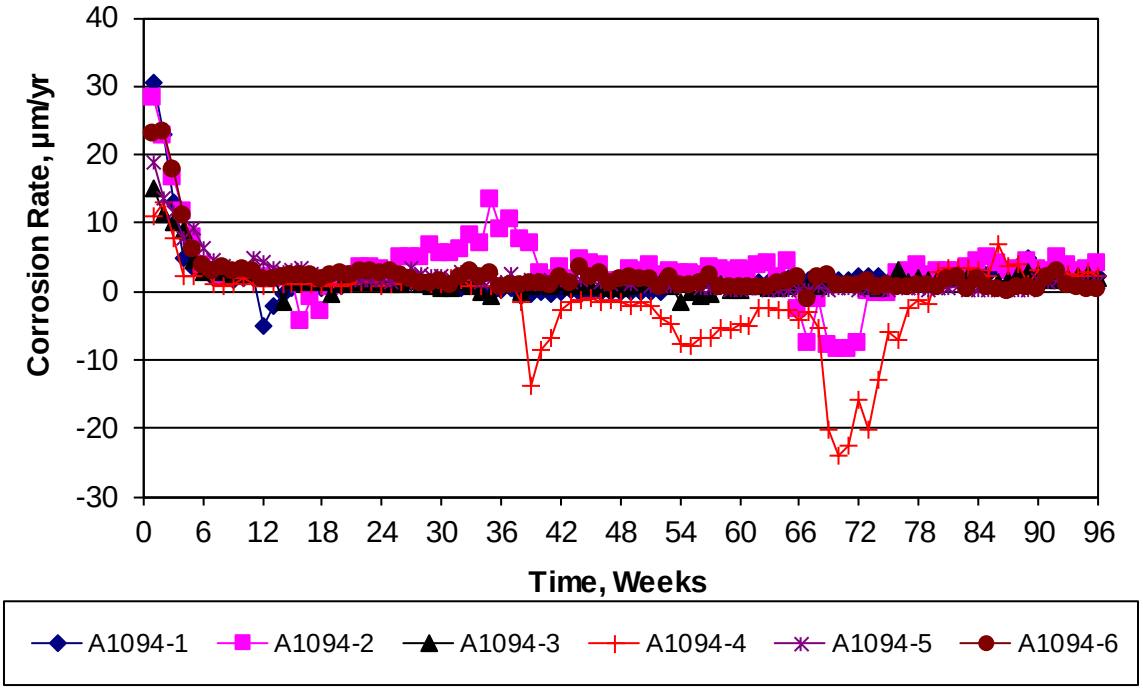

Figure A.95: Cracked beam test. Corrosion rate of A1094 reinforcement.

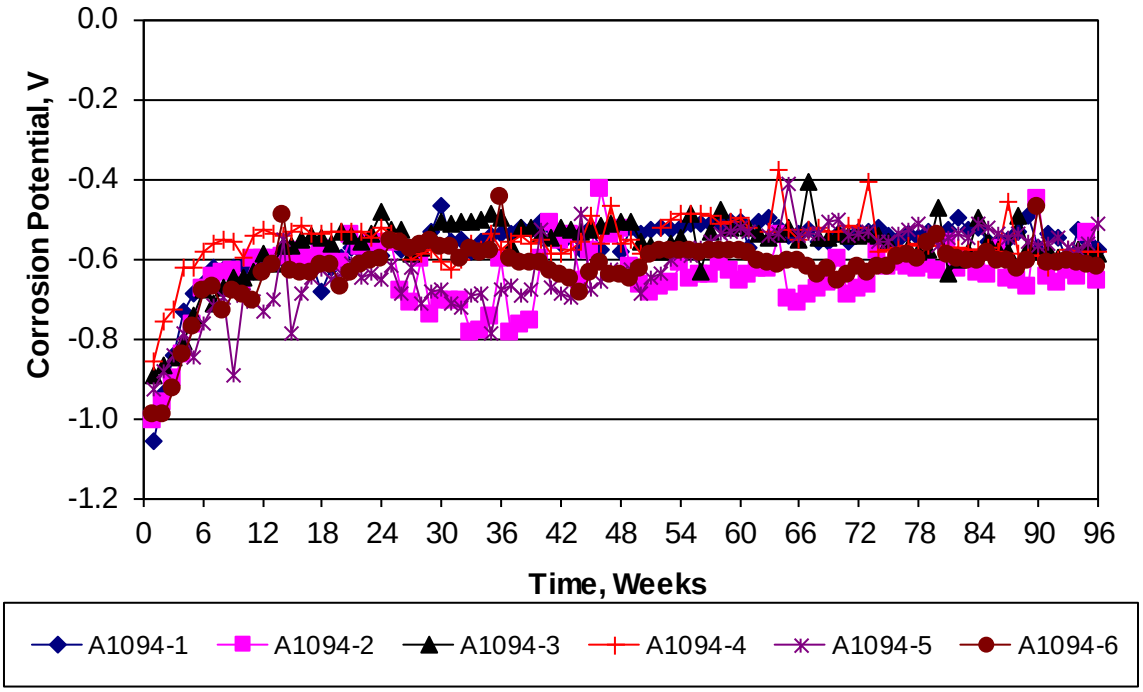

Figure A.96: Cracked beam test. Corrosion potential of A1094 reinforcement.

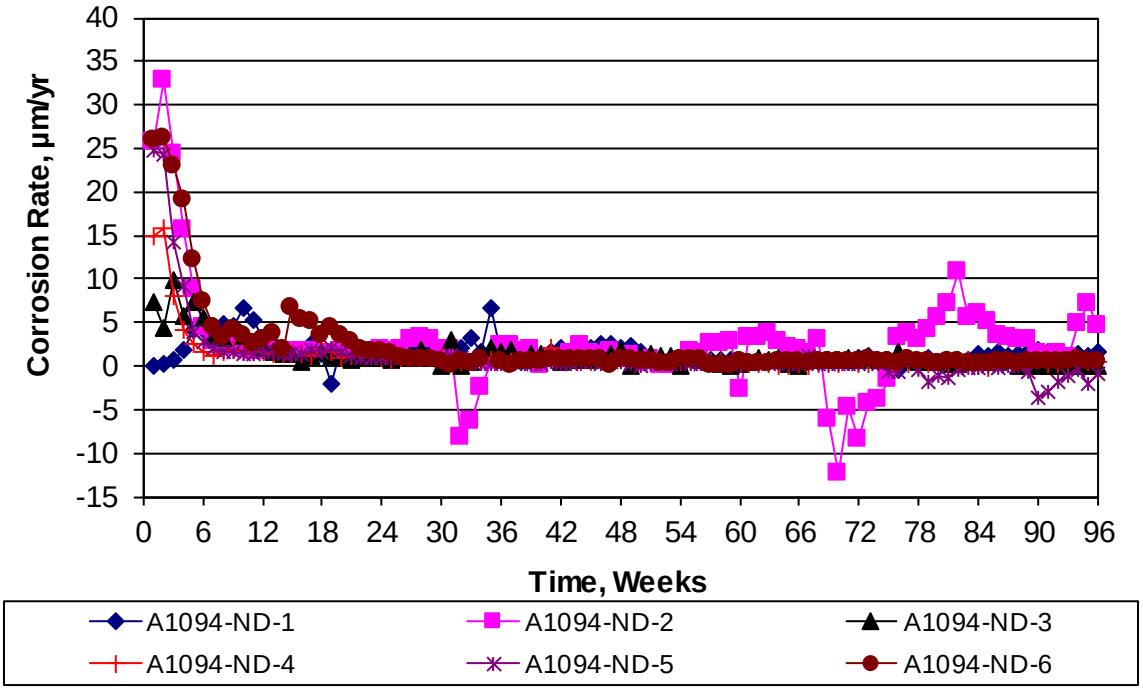

Figure A.97: Cracked beam test. Corrosion rate of A1094-ND reinforcement.

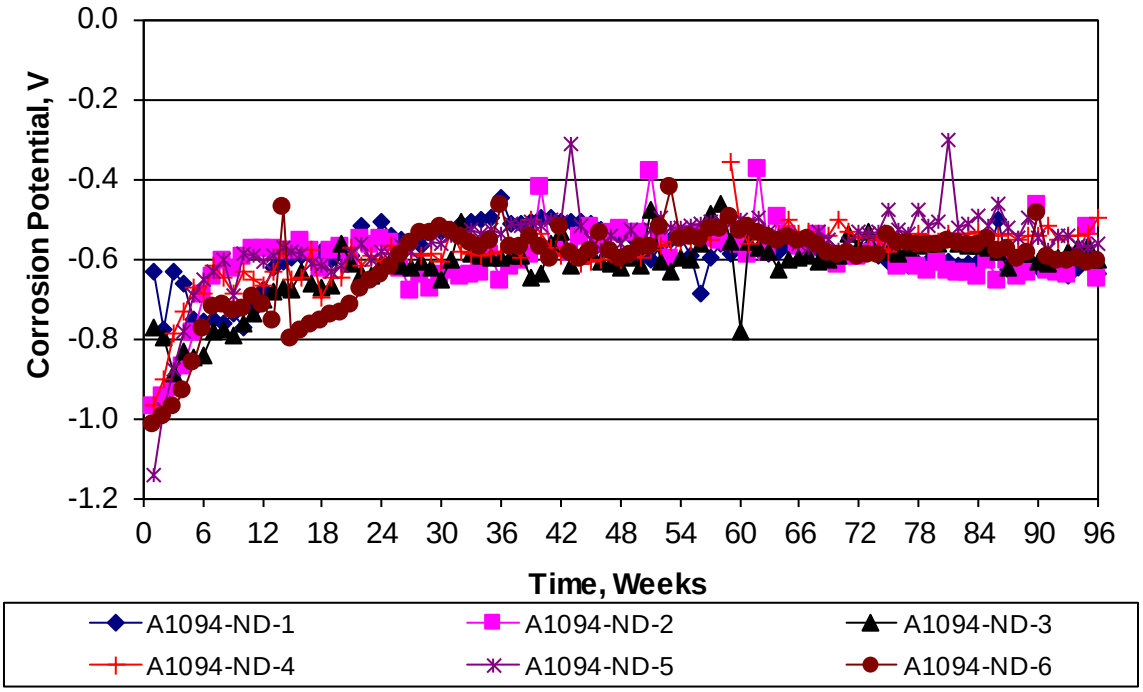

Figure A.98: Cracked beam test. Corrosion potential of A1094-ND reinforcement.

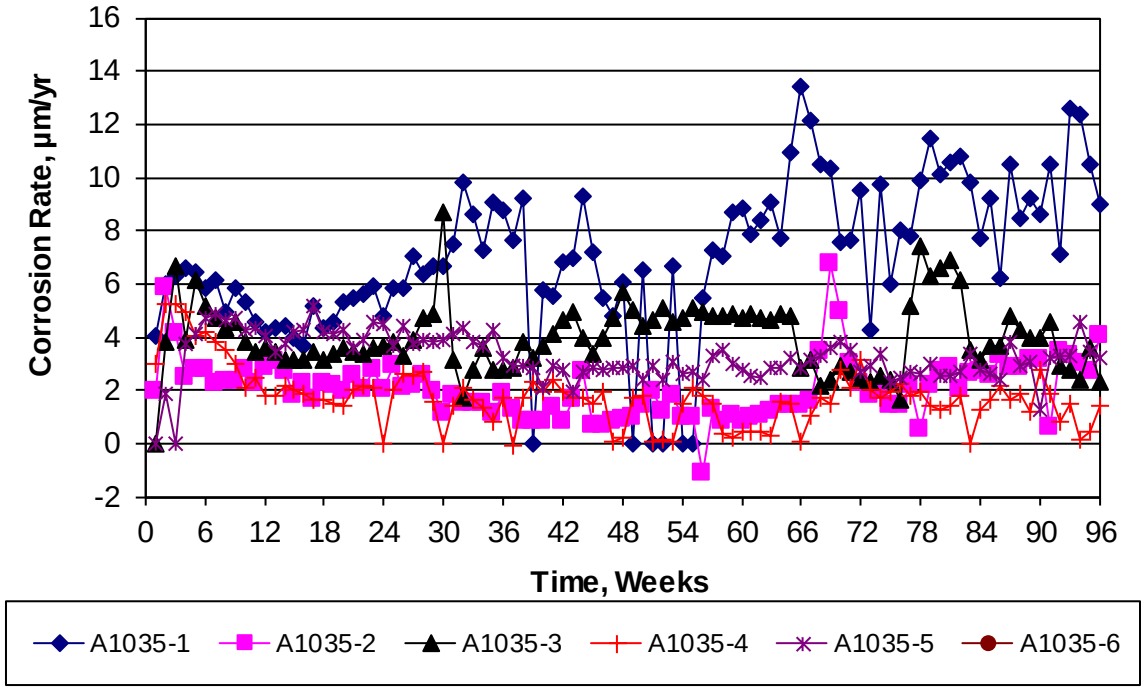

Figure A.99: Cracked beam test. Corrosion rate of A1035 reinforcement.

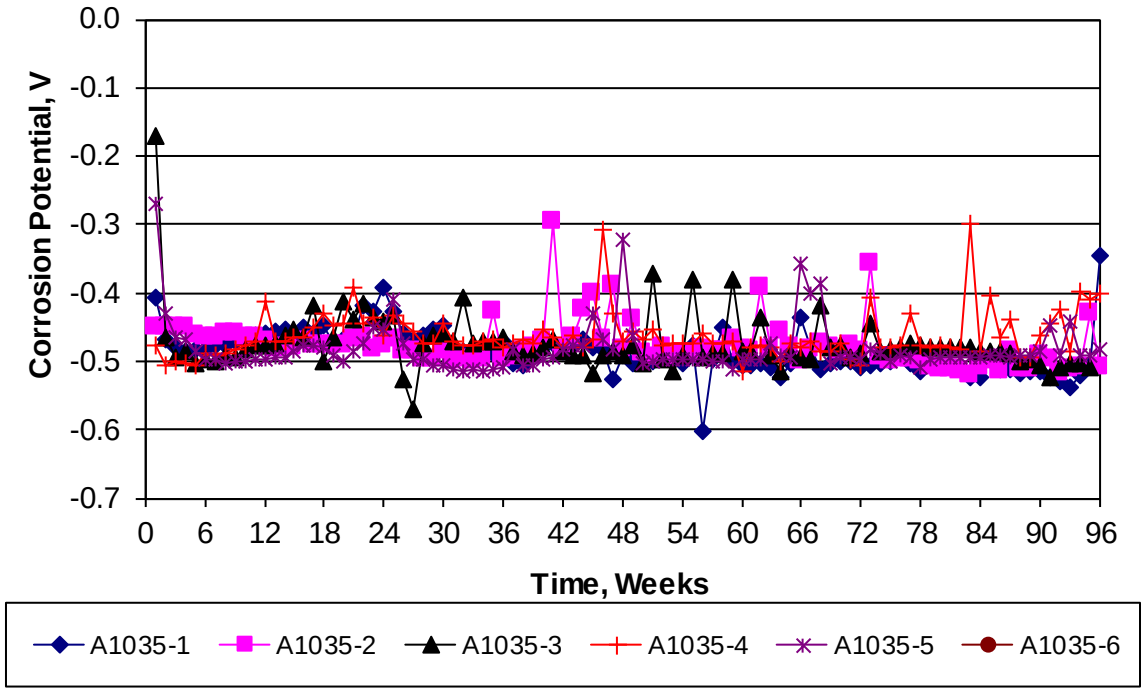

Figure A.100: Cracked beam test. Corrosion potential of A1035 reinforcement.

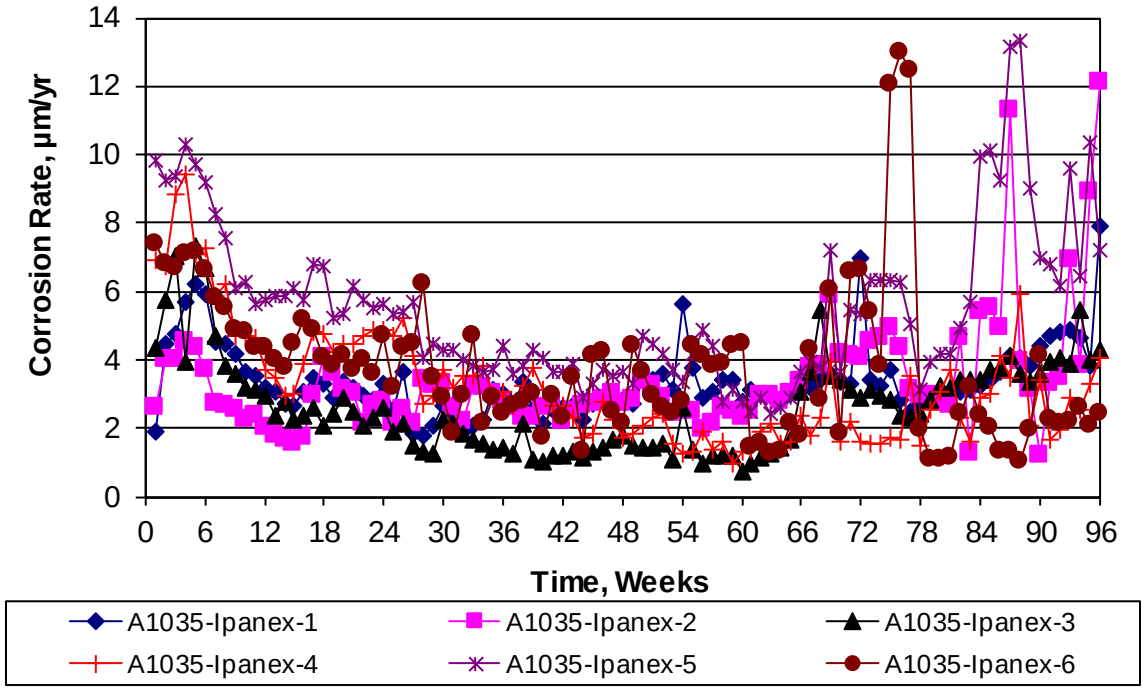

Figure A.101: Cracked beam test. Corrosion rate of A1035-Ipanex reinforcement.

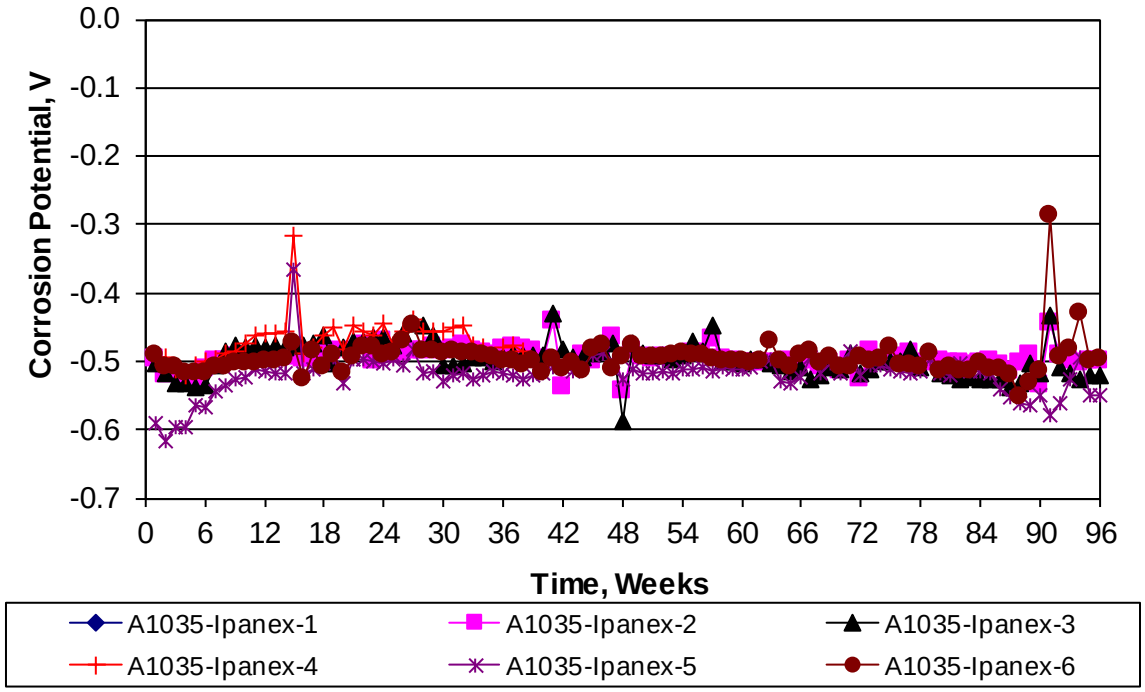

Figure A.102: Cracked beam test. Corrosion potential of A1035-Ipanex reinforcement.

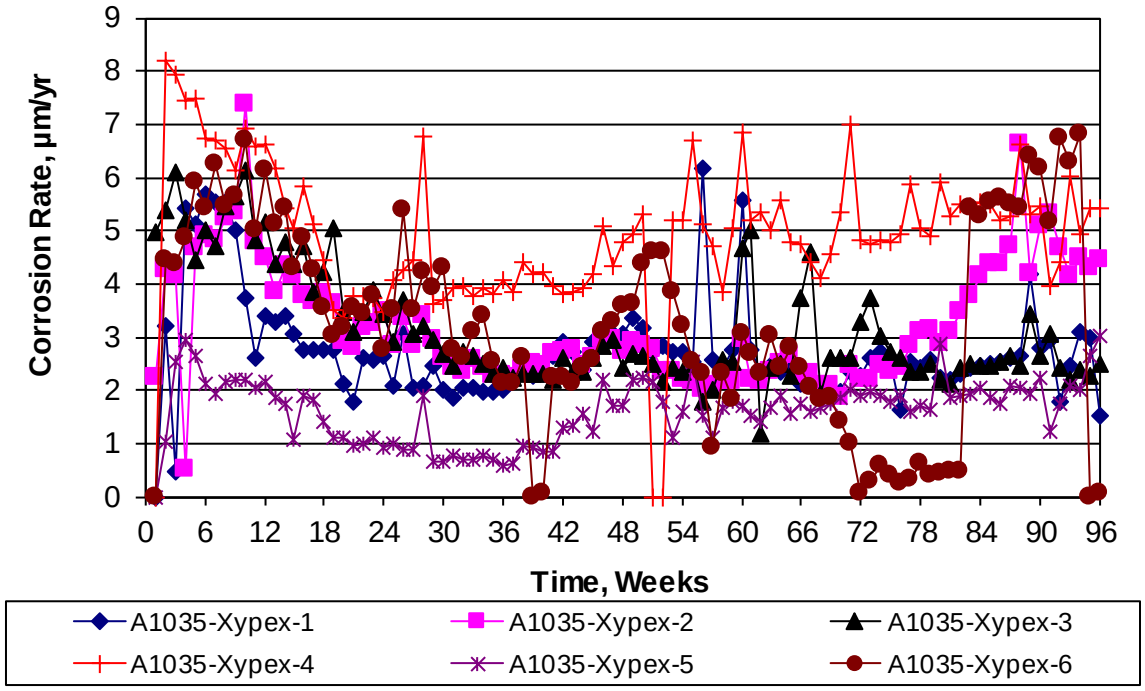

Figure A.103: Cracked beam test. Corrosion rate of A1035-Xypex reinforcement.

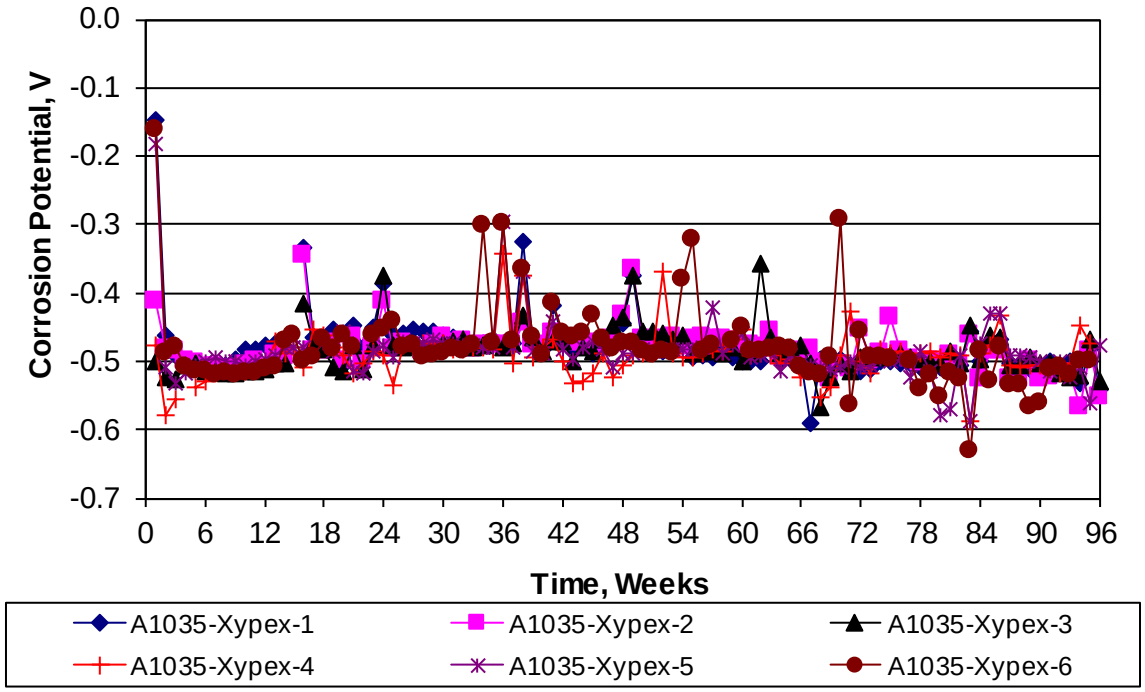

Figure A.104: Cracked beam test. Corrosion potential of A1035-Xypex reinforcement.

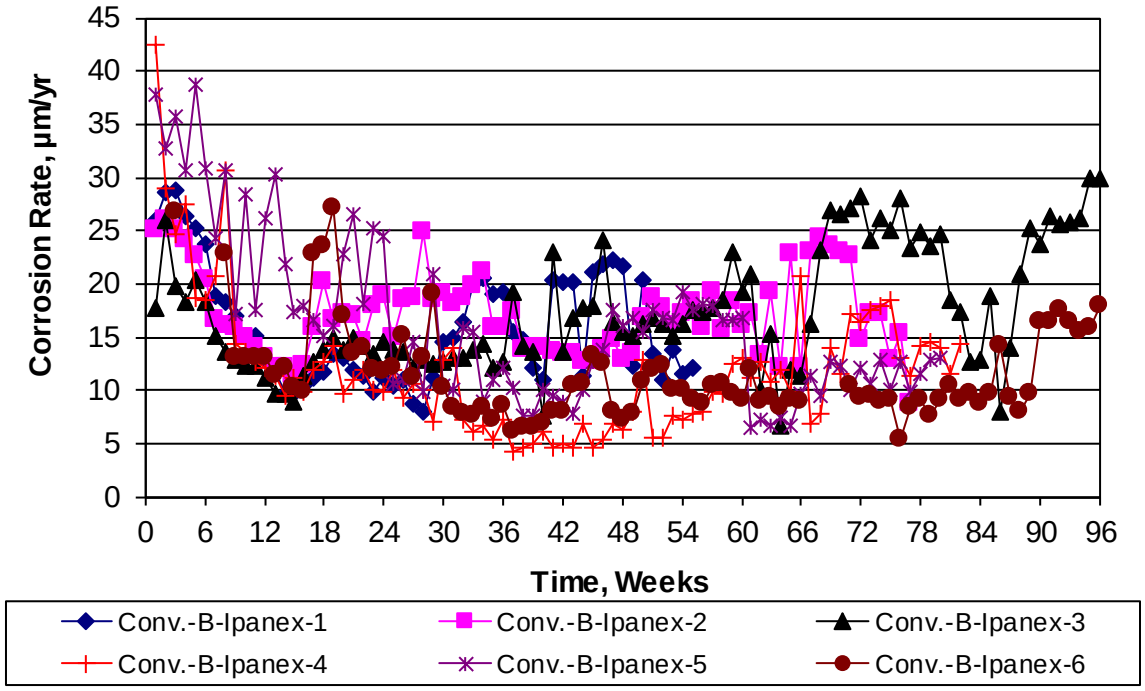

Figure A.105: Cracked beam test. Corrosion rate of Conv-B-Ipanex reinforcement.

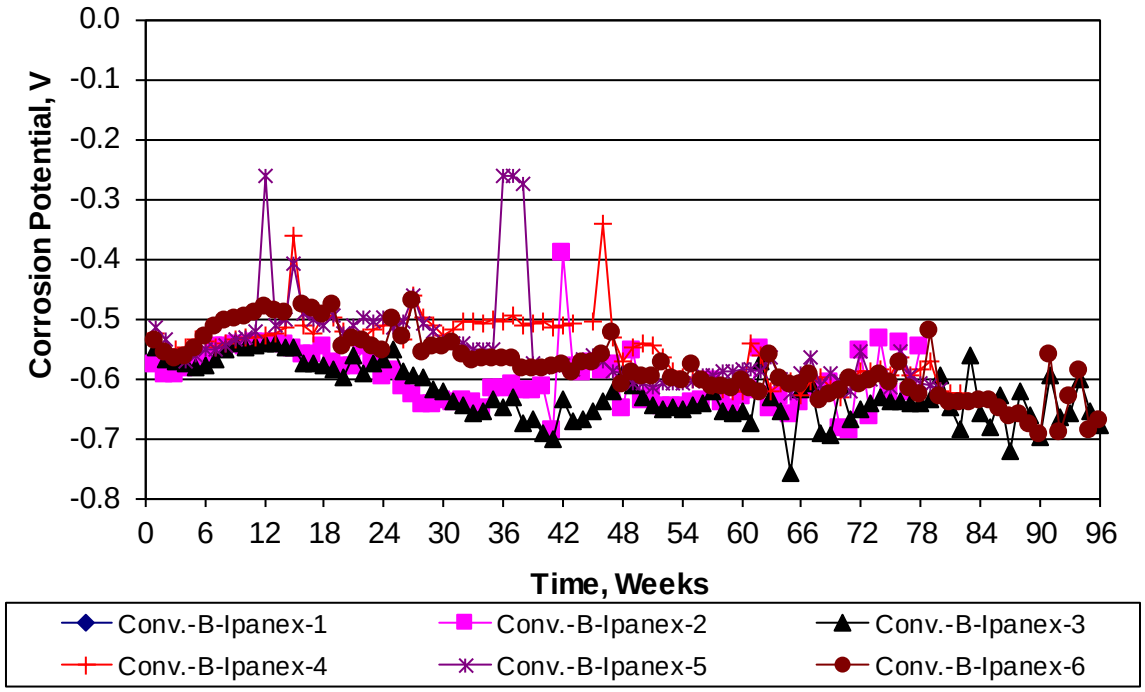

Figure A.106: Cracked beam test. Corrosion potential of Conv-B-Ipanex reinforcement.

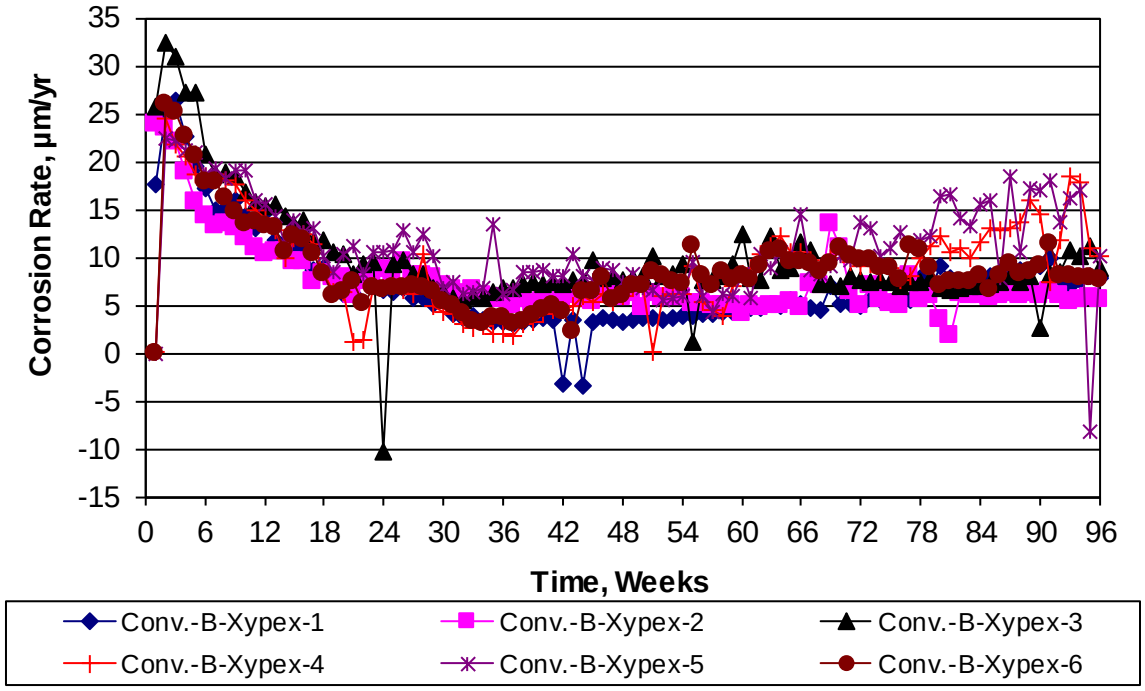

Figure A.107: Cracked beam test. Corrosion rate of Conv-B-Xypex reinforcement.

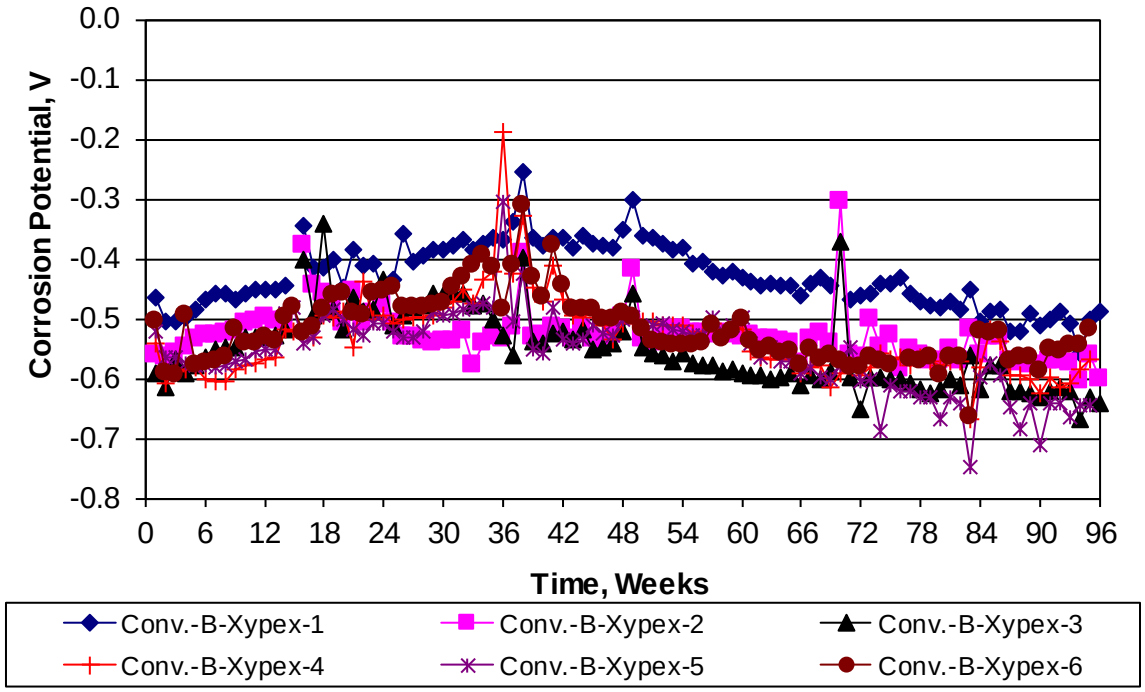

Figure A.108: Cracked beam test. Corrosion potential of Conv-B-Xypex reinforcement.

APPENDIX B: STUDENT'S T-TEST RESULTS

Table B.1: Rapid Macrocell Test. Student's T-Test Comparisons for Macrocell Corrosion Losses at 15 Weeks

	Conv-A	Conv-B	Conv-C	ECR	ECR-ND	ECR-UV-1000	ECR-UV-1000 (b)	ECR-UV-500	ECR-UV-250	ECR2-UV-1000	ECR2-UV-200	ECR2-UV-100	ECR-UV-1000-ND	A767	A767-Bent	A767-ND	A1094	A1094-Bent	A1094-ND	A1035
Conv-A	1	0.019	0.005	3E-04	2E-04	0.001	0.001	0.002	6E-04	0.006	0.002	6E-04	2E-04	0.005	0.002	6E-04	0.036	0.008	0.002	0.142
Conv-B	0.019	1	0.847	8E-06	7E-06	2E-05	2E-05	3E-05	1E-05	2E-04	3E-05	1E-05	7E-06	0.036	4E-05	0.004	8E-04	9E-05	6E-05	0.113
Conv-C	0.005	0.847	1	2E-07	2E-07	6E-07	6E-07	1E-06	4E-07	1E-05	1E-06	4E-07	2E-07	0.037	2E-06	0.004	2E-04	5E-06	6E-06	0.033
ECR	3E-04	8E-06	2E-07	1	0.057	1E-04	2E-04	7E-06	0.009	0.167	0.01	0.002	0.109	3E-04	0.056	6E-05	0.268	0.003	0.582	9E-07
ECR-ND	2E-04	7E-06	2E-07	0.057	1	2E-06	4E-06	2E-07	2E-04	0.092	0.003	2E-05	0.189	3E-04	0.022	5E-05	0.208	0.001	0.411	7E-07
ECR-UV-1000	0.001	2E-05	6E-07	1E-04	2E-06	1	0.837	0.055	0.047	0.937	0.739	0.042	4E-06	5E-04	0.992	8E-05	0.683	0.099	0.506	4E-06
ECR-UV-1000 (b)	0.001	2E-05	6E-07	2E-04	4E-06	0.837	1	0.04	0.068	0.984	0.664	0.064	6E-06	5E-04	0.944	8E-05	0.663	0.087	0.535	3E-06
ECR-UV-500	0.002	3E-05	1E-06	7E-06	2E-07	0.055	0.04	1	0.002	0.505	0.478	9E-04	2E-07	6E-04	0.418	9E-05	0.9	0.332	0.265	6E-06
ECR-UV-250	6E-04	1E-05	4E-07	0.009	2E-04	0.047	0.068	0.002	1	0.567	0.16	0.826	4E-04	4E-04	0.385	7E-05	0.474	0.023	0.887	2E-06
ECR2-UV-1000	0.006	2E-04	1E-05	0.167	0.092	0.937	0.984	0.505	0.567	1	0.814	0.604	0.101	0.001	0.954	3E-04	0.709	0.277	0.652	9E-05
ECR2-UV-200	0.002	3E-05	1E-06	0.01	0.003	0.739	0.664	0.478	0.16	0.814	1	0.178	0.003	5E-04	0.824	8E-05	0.756	0.218	0.449	9E-06
ECR2-UV-100	6E-04	1E-05	4E-07	0.002	2E-05	0.042	0.064	9E-04	0.826	0.604	0.178	1	3E-05	4E-04	0.422	7E-05	0.491	0.024	0.847	2E-06
ECR-UV-1000-ND	2E-04	7E-06	2E-07	0.109	0.189	4E-06	6E-06	2E-07	4E-04	0.101	0.003	3E-05	1	3E-04	0.025	5E-05	0.217	0.001	0.436	7E-07
A767	0.005	0.036	0.037	3E-04	3E-04	5E-04	5E-04	6E-04	4E-04	0.001	5E-04	4E-04	3E-04	1	5E-04	0.364	1E-03	7E-04	5E-04	0.01
A767-Bent	0.002	4E-05	2E-06	0.056	0.022	0.992	0.944	0.418	0.385	0.954	0.824	0.422	0.025	5E-04	1	8E-05	0.695	0.201	0.561	1E-05
A767-ND	6E-04	0.004	0.004	6E-05	5E-05	8E-05	8E-05	9E-05	7E-05	3E-04	8E-05	7E-05	5E-05	0.364	8E-05	1	2E-04	1E-04	8E-05	0.001
A1094	0.036	8E-04	2E-04	0.268	0.208	0.683	0.663	0.9	0.474	0.709	0.756	0.491	0.217	1E-03	0.695	2E-04	1	0.823	0.488	0.002
A1094-Bent	0.008	9E-05	5E-06	0.003	0.001	0.099	0.087	0.332	0.023	0.277	0.218	0.024	0.001	7E-04	0.201	1E-04	0.823	1	0.148	5E-05
A1094-ND	0.002	6E-05	6E-06	0.582	0.411	0.506	0.535	0.265	0.887	0.652	0.449	0.847	0.436	5E-04	0.561	8E-05	0.488	0.148	1	5E-05
A1035	0.142	0.113	0.033	9E-07	7E-07	4E-06	3E-06	6E-06	2E-06	9E-05	9E-06	2E-06	7E-07	0.01	1E-05	0.001	0.002	5E-05	5E-05	1

Table B.2: Rapid Macrocell Test. Student's T-Test Comparisons for Total Corrosion Losses at 15 Weeks

	Conv-A	Conv-B	Conv-C	ECR	ECR-ND	ECR-UV-1000	ECR-UV-1000 (b)	ECR-UV-500	ECR-UV-250	ECR2-UV-1000	ECR2-UV-200	ECR2-UV-100	ECR-UV-1000-ND	A767	A767-Bent	A767-ND	A1094	A1094-Bent	A1094-ND	A1035
Conv-A	1	0.069	0.039	5E-06	5E-07	0.046	6E-06	2E-05	3E-06	9E-06	2E-06	2E-06	8E-07	0.001	2E-04	0.04	0.062	0.444	3E-04	1E-04
Conv-B	0.069	1	0.165	0.005	0.002	0.016	0.004	0.004	0.003	0.007	0.003	0.003	0.002	0.001	6E-04	0.042	0.025	0.052	0.007	0.008
Conv-C	0.039	0.165	1	1E-07	9E-09	0.006	7E-08	3E-07	5E-08	2E-07	3E-08	4E-08	1E-08	0.001	2E-04	0.041	0.002	0.119	8E-06	2E-06
ECR	5E-06	0.005	1E-07	1	0.032	0.138	6E-05	0.013	0.144	0.017	0.198	0.348	0.507	0.002	3E-04	0.06	8E-04	0.058	0.011	2E-04
ECR-ND	5E-07	0.002	9E-09	0.032	1	0.075	2E-07	0.001	0.01	2E-05	0.006	0.036	0.058	1E-03	9E-05	0.039	2E-04	0.029	0.002	2E-05
ECR-UV-1000	0.046	0.016	0.006	0.138	0.075	1	0.337	0.333	0.163	0.209	0.14	0.139	0.092	0.001	1E-04	0.039	0.364	0.43	0.668	0.816
ECR-UV-1000 (b)	6E-06	0.004	7E-08	6E-05	2E-07	0.337	1	0.904	0.011	0.001	0.001	0.004	4E-06	1E-03	1E-04	0.039	0.003	0.102	0.184	0.009
ECR-UV-500	2E-05	0.004	3E-07	0.013	0.001	0.333	0.904	1	0.093	0.094	0.038	0.048	0.004	1E-03	1E-04	0.039	0.004	0.102	0.214	0.028
ECR-UV-250	3E-06	0.003	5E-08	0.144	0.01	0.163	0.011	0.093	1	0.888	0.624	0.626	0.05	1E-03	1E-04	0.039	8E-04	0.054	0.025	7E-04
ECR2-UV-1000	9E-06	0.007	2E-07	0.017	2E-05	0.209	0.001	0.094	0.888	1	0.399	0.477	0.002	0.002	3E-04	0.06	0.002	0.081	0.035	8E-04
ECR2-UV-200	2E-06	0.003	3E-08	0.198	0.006	0.14	0.001	0.038	0.624	0.399	1	0.942	0.058	1E-03	1E-04	0.039	5E-04	0.048	0.014	3E-04
ECR2-UV-100	2E-06	0.003	4E-08	0.348	0.036	0.139	0.004	0.048	0.626	0.477	0.942	1	0.157	1E-03	1E-04	0.039	6E-04	0.047	0.016	4E-04
ECR-UV-1000-ND	8E-07	0.002	1E-08	0.507	0.058	0.092	4E-06	0.004	0.05	0.002	0.058	0.157	1	1E-03	9E-05	0.039	2E-04	0.034	0.004	4E-05
A767	0.001	0.001	0.001	0.002	1E-03	0.001	1E-03	1E-03	1E-03	0.002	1E-03	1E-03	1E-03	1	0.003	0.498	0.001	0.001	0.001	0.001
A767-Bent	2E-04	6E-04	2E-04	3E-04	9E-05	1E-04	1E-04	1E-04	1E-04	3E-04	1E-04	1E-04	9E-05	0.003	1	0.059	2E-04	2E-04	1E-04	1E-04
A767-ND	0.04	0.042	0.041	0.06	0.039	0.039	0.039	0.039	0.039	0.06	0.039	0.039	0.039	0.498	0.059	1	0.04	0.04	0.039	0.039
A1094	0.062	0.025	0.002	8E-04	2E-04	0.364	0.003	0.004	8E-04	0.002	5E-04	6E-04	2E-04	0.001	2E-04	0.04	1	0.844	0.037	0.043
A1094-Bent	0.444	0.052	0.119	0.058	0.029	0.43	0.102	0.102	0.054	0.081	0.048	0.047	0.034	0.001	2E-04	0.04	0.844	1	0.209	0.257
A1094-ND	3E-04	0.007	8E-06	0.011	0.002	0.668	0.184	0.214	0.025	0.035	0.014	0.016	0.004	0.001	1E-04	0.039	0.037	0.209	1	0.611
A1035	1E-04	0.008	2E-06	2E-04	2E-05	0.816	0.009	0.028	7E-04	8E-04	3E-04	4E-04	4E-05	0.001	1E-04	0.039	0.043	0.257	0.611	1

Table B.3: Southern Exposure Test. Student's T-Test Comparisons for Corrosion Initiation Age

	Conv-A	Conv-B	Conv-C	ECR	ECR-ND	ECR-UV-1000	ECR-UV-1000-ND	A767	A767-ND	A767-Bent	A1094	A1094-ND	A1094-Bent	A1035	A1035-Ipanex	A1035-Xypex	Conv-B-Ipanex	Conv-B-Xypex
Conv-A	1	0.739	0.407	3E-04	-	0.008	-	0.01	2E-04	1E-04	3E-04	0.015	0.006	0.004	0.005	0.01	0.919	0.224
Conv-B	0.739	1	0.271	5E-04	-	0.012	-	0.028	1E-03	8E-04	0.001	0.036	0.016	0.007	0.013	0.019	0.426	0.157
Conv-C	0.407	0.271	1	0.002	-	0.022	-	0.044	0.003	0.002	0.004	0.056	0.028	0.011	0.021	0.027	0.069	0.916
ECR	3E-04	5E-04	0.002	1	-	0.262	-	0.969	0.487	0.289	0.402	0.982	0.82	0.215	0.6	0.227	3E-05	1E-05
ECR-ND	-	-	-	-	-	-	-	-	-	-	-	-	-	-	-	-	-	-
ECR-UV-1000	0.008	0.012	0.022	0.262	-	1	-	0.488	0.127	0.078	0.118	0.537	0.544	0.995	0.672	0.902	0.003	1E-03
ECR-UV-1000-ND	-	-	-	-	-	-	-	-	-	-	-	-	-	-	-	-	-	-
A767	0.01	0.028	0.044	0.969	-	0.488	-	1	0.594	0.371	0.518	0.95	0.823	0.377	0.612	0.308	0.009	0.005
A767-ND	2E-04	1E-03	0.003	0.487	-	0.127	-	0.594	1	0.614	0.828	0.556	0.382	0.064	0.197	0.051	1E-04	5E-05
A767-Bent	1E-04	8E-04	0.002	0.289	-	0.078	-	0.371	0.614	1	0.794	0.353	0.224	0.032	0.097	0.024	9E-05	4E-05
A1094	3E-04	0.001	0.004	0.402	-	0.118	-	0.518	0.828	0.794	1	0.49	0.33	0.057	0.169	0.047	2E-04	8E-05
A1094-ND	0.015	0.036	0.056	0.982	-	0.537	-	0.95	0.556	0.353	0.49	1	0.879	0.431	0.679	0.361	0.013	0.007
A1094-Bent	0.006	0.016	0.028	0.82	-	0.544	-	0.823	0.382	0.224	0.33	0.879	1	0.454	0.793	0.396	0.004	0.002
A1035	0.004	0.007	0.011	0.215	-	0.995	-	0.377	0.064	0.032	0.057	0.431	0.454	1	0.603	0.875	0.002	5E-04
A1035-Ipanex	0.005	0.013	0.021	0.6	-	0.672	-	0.612	0.197	0.097	0.169	0.679	0.793	0.603	1	0.514	0.004	0.002
A1035-Xypex	0.01	0.019	0.027	0.227	-	0.902	-	0.308	0.051	0.024	0.047	0.361	0.396	0.875	0.514	1	0.007	0.002
Conv-B-Ipanex	0.919	0.426	0.069	3E-05	-	0.003	-	0.009	1E-04	9E-05	2E-04	0.013	0.004	0.002	0.004	0.007	1	0.02
Conv-B-Xypex	0.224	0.157	0.916	1E-05	-	1E-03	-	0.005	5E-05	4E-05	8E-05	0.007	0.002	5E-04	0.002	0.002	0.02	1

Table B.4: Southern Exposure Test. Student's T-Test Comparisons for Critical Chloride Corrosion Threshold

	Conv-A	Conv-B	Conv-C	ECR	ECR-ND	ECR-UV-1000	ECR-UV-1000-ND	A767	A767-ND	A767-Bent	A1094	A1094-ND	A1094-Bent	A1035	A1035-Ipanex	A1035-Xypex	Conv-B-Ipanex	Conv-B-Xypex
Conv-A	1	0.161	0.795	0.098	-	-	-		0.977			0.984		0.048	0.400	0.064	0.253	0.287
Conv-B	0.161	1	0.005	0.010	-	-	-		0.001			0.096		0.027	0.083	0.044	0.464	0.641
Conv-C	0.795	0.005	1	0.243	-	-	-		0.105			0.766		0.258	0.660	0.306	0.118	0.201
ECR	0.098	0.010	0.243	1	-	-	-		0.049			0.109		0.534	0.559	0.565	0.008	0.020
ECR-ND	-	-	-	-	-	-	-		-			-		-	-	-	-	-
ECR-UV-1000	-	-	-	-	-	-	-		-			-		-	-	-	-	-
ECR-UV-1000-ND	-	-	-	-	-	-	-		-			-		-	-	-	-	-
A767																		
A767-ND	0.977	0.001	0.105	0.049	-	-	-		1			0.995		0.075	0.355	0.114	0.080	0.140
A767-Bent																		
A1094																		
A1094-ND	0.984	0.096	0.766	0.109	-	-	-		0.995			1		0.090	0.434	0.122	0.210	0.261
A1094-Bent																		
A1035	0.048	0.027	0.143	0.534	-	-	-		0.075			0.090		1	0.323	0.972	0.012	0.023
A1035-Ipanex	0.400	0.083	0.660	0.559	-	-	-		0.355			0.434		0.323	1	0.353	0.082	0.124
A1035-Xypex	0.064	0.044	0.306	0.565	-	-	-		0.114			0.122		0.972	0.353	1	0.022	0.036
Conv-B-Ipanex	0.253	0.464	0.118	0.008	-	-	-		0.080			0.210		0.012	0.082	0.022	1	0.914
Conv-B-Xypex	0.287	0.641	0.201	0.020	-	-	-		0.140			0.261		0.023	0.124	0.036	0.914	1

Table B.5: Southern Exposure Test. Student's T-Test Comparisons for Macrocell Corrosion Loss at 96 Weeks

	Conv-A	Conv-B	Conv-C	ECR	ECR-ND	ECR-UV-1000	ECR-UV-1000-ND	A767	A767-ND	A767-Bent	A1094	A1094-ND	A1094-Bent	A1035	A1035-Ipanex	A1035-Xypex	Conv-B-Ipanex	Conv-B-Xypex
Conv-A	1	0.011	0.002	0.003	0.009	0.013	0.009	9E-04	0.004	0.236	5E-04	0.001	0.017	0.006	0.006	0.003	3E-04	0.075
Conv-B	0.011	1	0.837	0.004	0.013	0.014	0.013	6E-04	9E-04	0.006	5E-04	6E-04	0.002	0.002	0.001	8E-04	0.921	0.064
Conv-C	0.002	0.837	1	9E-05	7E-04	8E-04	7E-04	5E-06	1E-05	0.002	4E-06	1E-05	6E-04	5E-05	1E-05	9E-06	0.601	0.027
ECR	0.003	0.004	9E-05	1	0.51	0.017	0.639	0.356	0.088	0.11	0.965	0.649	0.875	0.096	0.018	0.06	4E-05	5E-04
ECR-ND	0.009	0.013	7E-04	0.51	1	0.05	0.987	0.5	0.161	0.176	0.87	0.756	0.917	0.175	0.045	0.121	2E-04	0.002
ECR-UV-1000	0.013	0.014	8E-04	0.017	0.05	1	0.085	0.935	0.351	0.233	0.364	0.868	0.937	0.394	0.122	0.318	3E-04	0.003
ECR-UV-1000-ND	0.009	0.013	7E-04	0.639	0.987	0.085	1	0.501	0.162	0.176	0.874	0.755	0.916	0.176	0.046	0.123	2E-04	0.002
A767	9E-04	6E-04	5E-06	0.356	0.5	0.935	0.501	1	0.231	0.088	0.379	0.884	0.932	0.294	0.065	0.226	2E-06	7E-05
A767-ND	0.004	9E-04	1E-05	0.088	0.161	0.351	0.162	0.231	1	0.214	0.07	0.271	0.572	0.878	0.594	0.906	4E-06	2E-04
A767-Bent	0.236	0.006	0.002	0.11	0.176	0.233	0.176	0.088	0.214	1	0.053	0.09	0.186	0.23	0.294	0.191	2E-04	0.017
A1094	5E-04	5E-04	4E-06	0.965	0.87	0.364	0.874	0.379	0.07	0.053	1	0.604	0.837	0.092	0.015	0.058	1E-06	5E-05
A1094-ND	0.001	6E-04	1E-05	0.649	0.756	0.868	0.755	0.884	0.271	0.09	0.604	1	0.983	0.348	0.11	0.28	3E-06	1E-04
A1094-Bent	0.017	0.002	6E-04	0.875	0.917	0.937	0.916	0.932	0.572	0.186	0.837	0.983	1	0.649	0.428	0.599	5E-05	0.001
A1035	0.006	0.002	5E-05	0.096	0.175	0.394	0.176	0.294	0.878	0.23	0.092	0.348	0.649	1	0.486	0.959	2E-05	5E-04
A1035-Ipanex	0.006	0.001	1E-05	0.018	0.045	0.122	0.046	0.065	0.594	0.294	0.015	0.11	0.428	0.486	1	0.475	4E-06	3E-04
A1035-Xypex	0.003	8E-04	9E-06	0.06	0.121	0.318	0.123	0.226	0.906	0.191	0.058	0.28	0.599	0.959	0.475	1	3E-06	2E-04
Conv-B-Ipanex	3E-04	0.921	0.601	4E-05	2E-04	3E-04	2E-04	2E-06	4E-06	2E-04	1E-06	3E-06	5E-05	2E-05	4E-06	3E-06	1	0.005
Conv-B-Xypex	0.075	0.064	0.027	5E-04	0.002	0.003	0.002	7E-05	2E-04	0.017	5E-05	1E-04	0.001	5E-04	3E-04	2E-04	0.005	1

Table B.6: Southern Exposure Test. Student's T-Test Comparisons for Total Corrosion Loss at 96 Weeks

	Conv-A	Conv-B	Conv-C	ECR	ECR-ND	ECR-UV-1000	ECR-UV-1000-ND	A767	A767-ND	A767-Bent	A1094	A1094-ND	A1094-Bent	A1035	A1035-Ipanex	A1035-Xypex	Conv-B-Ipanex	Conv-B-Xypex
Conv-A	1	0.063	0.006	3E-04	0.001	0.002	0.001	0.787	0.058	0.138	0.446	0.345	0.282	0.009	9E-04	0.002	0.046	0.01
Conv-B	0.063	1	0.125	8E-05	5E-04	7E-04	5E-04	0.175	0.002	0.712	0.069	0.05	0.803	0.001	5E-05	2E-04	0.927	0.254
Conv-C	0.006	0.125	1	8E-06	1E-04	1E-04	1E-04	0.057	3E-04	0.727	0.02	0.015	0.292	4E-04	6E-06	3E-05	0.181	0.985
ECR	3E-04	8E-05	8E-06	1	0.513	0.022	0.244	0.026	0.002	0.007	0.027	0.03	0.005	0.087	0.009	0.02	7E-05	2E-04
ECR-ND	0.001	5E-04	1E-04	0.513	1	0.071	0.994	0.054	0.007	0.019	0.055	0.062	0.013	0.147	0.024	0.046	4E-04	8E-04
ECR-UV-1000	0.002	7E-04	1E-04	0.022	0.071	1	0.064	0.073	0.014	0.024	0.078	0.088	0.017	0.256	0.081	0.11	5E-04	0.001
ECR-UV-1000-ND	0.001	5E-04	1E-04	0.244	0.994	0.064	1	0.054	0.007	0.019	0.055	0.061	0.013	0.147	0.024	0.046	4E-04	8E-04
A767	0.787	0.175	0.057	0.026	0.054	0.073	0.054	1	0.341	0.148	0.723	0.626	0.287	0.107	0.048	0.07	0.105	0.027
A767-ND	0.058	0.002	3E-04	0.002	0.007	0.014	0.007	0.341	1	0.026	0.545	0.658	0.036	0.144	0.03	0.079	0.001	7E-04
A767-Bent	0.138	0.712	0.727	0.007	0.019	0.024	0.019	0.148	0.026	1	0.081	0.066	0.562	0.014	0.005	0.007	0.696	0.666
A1094	0.446	0.069	0.02	0.027	0.055	0.078	0.055	0.723	0.545	0.081	1	0.888	0.151	0.152	0.069	0.105	0.035	0.009
A1094-ND	0.345	0.05	0.015	0.03	0.062	0.088	0.061	0.626	0.658	0.066	0.888	1	0.119	0.185	0.087	0.132	0.024	0.007
A1094-Bent	0.282	0.803	0.292	0.005	0.013	0.017	0.013	0.287	0.036	0.562	0.151	0.119	1	0.014	0.004	0.006	0.723	0.22
A1035	0.009	0.001	4E-04	0.087	0.147	0.256	0.147	0.107	0.144	0.014	0.152	0.185	0.014	1	0.796	0.976	6E-04	5E-04
A1035-Ipanex	9E-04	5E-05	6E-06	0.009	0.024	0.081	0.024	0.048	0.03	0.005	0.069	0.087	0.004	0.796	1	0.7	4E-05	6E-05
A1035-Xypex	0.002	2E-04	3E-05	0.02	0.046	0.11	0.046	0.07	0.079	0.007	0.105	0.132	0.006	0.976	0.7	1	1E-04	1E-04
Conv-B-Ipanex	0.046	0.927	0.181	7E-05	4E-04	5E-04	4E-04	0.105	0.001	0.696	0.035	0.024	0.723	6E-04	4E-05	1E-04	1	0.225
Conv-B-Xypex	0.01	0.254	0.985	2E-04	8E-04	0.001	8E-04	0.027	7E-04	0.666	0.009	0.007	0.22	5E-04	6E-05	1E-04	0.225	1

Table B.7: Cracked Beam Test. Student's T-Test Comparisons for Macrocell Corrosion Loss at 96 Weeks

	Conv-A	Conv-B	Conv-C	ECR	ECR-ND	ECR-UV-1000	ECR-UV-1000-ND	A767	A767-ND	A1094	A1094-ND	A1035	A1035-Ipanex	A1035-Xypex	Conv-B-Ipanex	Conv-B-Xypex
Conv-A	1	0.242	0.791	5E-04	0.002	0.007	0.002	0.007	0.006	0.001	4E-04	0.029	0.016	0.009	0.023	0.01
Conv-B	0.067	1	0.186	0.011	0.028	0.045	0.03	0.015	0.013	0.007	0.004	0.028	0.019	0.015	0.408	0.016
Conv-C	0.791	0.449	1	5E-04	0.002	0.006	0.003	0.014	0.008	0.002	2E-04	0.033	0.007	0.005	0.104	0.005
ECR	5E-04	0.011	5E-04	1	0.278	0.004	0.741	0.11	0.023	0.1	0.001	0.008	5E-04	5E-04	0.003	4E-04
ECR-ND	0.002	0.028	0.002	0.278	1	0.009	0.323	0.152	0.04	0.134	0.003	0.018	5E-04	0.002	0.014	0.001
ECR-UV-1000	0.007	0.045	0.006	0.004	0.009	1	0.018	0.564	0.282	0.782	0.53	0.102	0.007	0.027	0.019	0.021
ECR-UV-1000-ND	0.002	0.03	0.003	0.741	0.323	0.018	1	0.178	0.05	0.168	0.005	0.021	6E-04	0.002	0.014	0.002
A767	0.007	0.015	0.014	0.11	0.152	0.564	0.178	1	0.749	0.641	0.569	0.289	0.167	0.314	0.003	0.277
A767-ND	0.006	0.013	0.008	0.023	0.04	0.282	0.05	0.749	1	0.356	0.23	0.374	0.194	0.413	0.002	0.358
A1094	0.001	0.007	0.002	0.1	0.134	0.782	0.168	0.641	0.356	1	0.981	0.093	0.024	0.068	0.001	0.055
A1094-ND	4E-04	0.004	2E-04	0.001	0.003	0.53	0.005	0.569	0.23	0.981	1	0.041	0.001	0.009	4E-04	0.006
A1035	0.029	0.028	0.033	0.008	0.018	0.102	0.021	0.289	0.374	0.093	0.041	1	0.871	0.775	0.003	0.845
A1035-Ipanex	0.016	0.019	0.007	5E-04	5E-04	0.007	6E-04	0.167	0.194	0.024	0.001	0.871	1	0.514	0.001	0.598
A1035-Xypex	0.009	0.015	0.005	5E-04	0.002	0.027	0.002	0.314	0.413	0.068	0.009	0.775	0.514	1	0.001	0.896
Conv-B-Ipanex	0.023	0.408	0.104	0.003	0.014	0.019	0.014	0.003	0.002	0.001	4E-04	0.003	0.001	0.001	1	0.001
Conv-B-Xypex	0.01	0.016	0.005	4E-04	0.001	0.021	0.002	0.277	0.358	0.055	0.006	0.845	0.598	0.896	0.001	1

Table B.8: Cracked Beam Test. Student's T-Test Comparisons for Total Corrosion Loss at 96 Weeks

	Conv-A	Conv-B	Conv-C	ECR	ECR-ND	ECR-UV-1000	ECR-UV-1000-ND	A767	A767-ND	A1094	A1094-ND	A1035	A1035-Ipanex	A1035-Xypex	Conv-B-Ipanex	Conv-B-Xypex
Conv-A	1	0.481	0.219	7E-05	3E-04	0.001	4E-04	0.017	0.007	0.009	0.001	3E-04	0.003	3E-04	0.264	0.006
Conv-B	0.481	1	0.152	6E-06	1E-04	2E-04	1E-04	0.024	0.008	0.014	4E-04	1E-04	1E-04	9E-06	0.547	4E-06
Conv-C	0.219	0.152	1	0.003	0.009	0.021	0.01	0.387	0.248	0.276	0.077	0.019	0.172	0.017	0.114	0.312
ECR	7E-05	6E-06	0.003	1	0.175	2E-04	0.996	0.002	7E-04	0.002	5E-05	2E-04	5E-06	2E-06	1E-04	6E-11
ECR-ND	3E-04	1E-04	0.009	0.175	1	5E-04	0.147	0.006	0.002	0.006	2E-04	8E-04	5E-06	1E-05	0.001	1E-09
ECR-UV-1000	0.001	2E-04	0.021	2E-04	5E-04	1	8E-04	0.027	0.015	0.031	0.003	0.018	6E-05	4E-04	0.002	3E-08
ECR-UV-1000-ND	4E-04	1E-04	0.01	0.996	0.147	8E-04	1	0.007	0.003	0.007	3E-04	0.001	6E-06	1E-05	0.001	2E-09
A767	0.017	0.024	0.387	0.002	0.006	0.027	0.007	1	0.816	0.791	0.431	0.092	0.963	0.131	0.014	0.612
A767-ND	0.007	0.008	0.248	7E-04	0.002	0.015	0.003	0.816	1	0.958	0.531	0.088	0.771	0.128	0.005	0.325
A1094	0.009	0.014	0.276	0.002	0.006	0.031	0.007	0.791	0.958	1	0.621	0.139	0.75	0.202	0.009	0.362
A1094-ND	0.001	4E-04	0.077	5E-05	2E-04	0.003	3E-04	0.431	0.531	0.621	1	0.114	0.161	0.173	4E-04	0.014
A1035	3E-04	1E-04	0.019	2E-04	8E-04	0.018	0.001	0.092	0.088	0.139	0.114	1	0.004	0.513	2E-04	2E-04
A1035-Ipanex	0.003	1E-04	0.172	5E-06	5E-06	6E-05	6E-06	0.963	0.771	0.75	0.161	0.004	1	0.002	2E-04	0.109
A1035-Xypex	3E-04	9E-06	0.017	2E-06	1E-05	4E-04	1E-05	0.131	0.128	0.202	0.173	0.513	0.002	1	4E-05	8E-06
Conv-B-Ipanex	0.264	0.547	0.114	1E-04	0.001	0.002	0.001	0.014	0.005	0.009	4E-04	2E-04	2E-04	4E-05	1	8E-05
Conv-B-Xypex	0.006	4E-06	0.312	6E-11	1E-09	3E-08	2E-09	0.612	0.325	0.362	0.014	2E-04	0.109	8E-06	8E-05	1

Table B.9: Cracked Beam Test. Student's T-Test Comparisons for Average Corrosion Rate Based on Loss

	Conv-A	Conv-B	Conv-C	ECR	ECR-UV-1000	A767	A767-ND	A1094	A1094-ND	A1035	A1035-Ipanex	A1035-Xypex	Conv-B-Ipanex	Conv-B-Xypex
Conv-A	1	0.148	0.22	7E-05	0.001	0.017	0.007	0.009	0.001	3E-04	0.003	3E-04	0.183	0.006
Conv-B	0.148	1	0.035	1E-05	2E-04	0.002	0.001	0.001	5E-05	1E-05	6E-06	6E-06	0.875	4E-05
Conv-C	0.22	0.035	1	0.003	0.021	0.383	0.245	0.272	0.075	0.018	0.168	0.017	0.043	0.305
ECR	7E-05	1E-05	0.003	1	3E-04	0.002	8E-04	0.002	5E-05	3E-04	7E-07	2E-06	3E-04	9E-11
ECR-UV-1000	0.001	2E-04	0.021	3E-04	1	0.027	0.015	0.031	0.003	0.018	6E-05	4E-04	3E-04	3E-08
A767	0.017	0.002	0.383	0.002	0.027	1	0.816	0.791	0.431	0.092	0.963	0.131	0.002	0.612
A767-ND	0.007	6E-04	0.245	8E-04	0.015	0.816	1	0.958	0.531	0.088	0.131	0.128	6E-04	0.325
A1094	0.009	0.001	0.272	0.002	0.031	0.791	0.958	1	0.621	0.139	0.75	0.202	9E-04	0.362
A1094-ND	0.001	5E-05	0.075	5E-05	0.003	0.431	0.531	0.621	1	0.114	0.161	0.173	1E-04	0.014
A1035	3E-04	1E-05	0.018	3E-04	0.018	0.092	0.088	0.139	0.114	1	0.004	0.513	3E-05	2E-04
A1035-Ipanex	0.003	5E-05	0.168	7E-07	6E-05	0.963	0.771	0.75	0.161	0.004	1	0.002	2E-04	0.109
A1035-Xypex	3E-04	6E-06	0.017	2E-06	4E-04	0.131	0.128	0.202	0.173	0.513	0.002	1	3E-05	8E-06
Conv-B-Ipanex	0.183	0.875	0.043	3E-04	3E-04	0.002	6E-04	9E-04	1E-04	3E-05	2E-04	3E-05	1	3E-04
Conv-B-Xypex	0.006	4E-05	0.305	9E-11	3E-08	0.612	0.325	0.362	0.014	2E-04	0.109	8E-06	3E-04	1